[redacted]

# AEC RESEARCH AND DEVELOPMENT REPORT

ORNL-1302
Progress

MARTIN MARIETTA ENERGY SYSTEMS LIBRARIES
3 4456 0353039 2

LABORATORY RECORDS
1954

Classification Cancelled
Or Changed To
By Authority Of
By Date

## METALLURGY DIVISION

## QUARTERLY PROGRESS REPORT

FOR PERIOD ENDING APRIL 30, 1952

OAK RIDGE NATIONAL LABORATORY
CENTRAL RESEARCH LIBRARY
CIRCULATION SECTION
4500N ROOM 175
LIBRARY LOAN COPY
DO NOT TRANSFER TO ANOTHER PERSON
If you wish someone else to see this report, send in name with report and the library will arrange a loan.
UCN-7969 (3 9-77)

OAK RIDGE NATIONAL LABORATORY

CARBID

CLASSIFICATION CANCELLED
David R. Hamrin 9/6/2013
ADD Signature Date
Single review of CCRP-declassified documents was authorized by DOE Office of Declassification memo of August 22, 1994.

[redacted]

[redacted]

ORNL-1302

This document consists of 168 pages.
Copy 8 of 146 copies. Series A.

Contract No. W-7405-eng-26

# METALLURGY DIVISION

# QUARTERLY PROGRESS REPORT

## for Period Ending April 30, 1952


J. H. Frye, Jr., Director

EDITED BY

W. H. Bridges


DATE ISSUED

SEP 2 1952


OAK RIDGE NATIONAL LABORATORY
operated by
CARBIDE AND CARBON CHEMICALS COMPANY
A Division of Union Carbide and Carbon Corporation
Post Office Box P
Oak Ridge, Tennessee



MARTIN MARIETTA ENERGY SYSTEMS LIBRARIES

3 4456 0353039 2


[redacted]

[redacted]

ORNL-1302
Progress

*INTERNAL DISTRIBUTION*

1. G. T. Felbeck (C&CCC)
2-3. Chemistry Library
4. Physics Library
5. Biology Library
6. Health Physics Library
7. Metallurgy Library
8-9. Training School Library
10. Reactor Experimental Engineering Library
11-14. Central Files
15. C. E. Center
16. C. E. Larson
17. W. B. Humes (K-25)
18. L. B. Emlet (Y-12)
19. A. M. Weinberg
20. E. H. Taylor
21. E. J. Murphy
22. E. D. Shipley
23. J. H. Frye, Jr.
24. F. C. VonderLage
25. R. C. Briant
26. J. A. Swartout
27. S. C. Lind
28. F. L. Steahly
29. A. H. Snell
30. A. Hollaender
31. M. T. Kelley
32. K. Z. Morgan
33. J. S. Felton
34. A. S. Householder
35. C. S. Harrill
36. C. E. Winters
37. D. S. Billington
38. D. W. Cardwell
39. E. M. King
40. A. J. Miller
41. D. D. Cowen
42. P. M. Reyling
43. W. H. Bridges
44. A. G. H. Andersen
45. L. K. Jetter
46. E. J. Boyle
47. W. D. Manly
48. C. D. Susano
49. W. W. Parkinson
50. R. J. Gray
51. B. S. Borie
52. D. C. Vreeland
53. D. E. Hamby
54. E. E. Stansbury
55. G. P. Smith
56. J. E. Cunningham
57. Anton Brasunas
58. R. S. Crouse
59. R. E. Adams
60. J. H. Erwin
61. J. O. Betterton, Jr.
62. L. D. Dyer
63. G. M. Adamson
64. E. S. Bomar
65. F. H. Eckert
66. R. B. Day
67. T. W. Fulton
68. W. J. Fretague
69. R. B. Oliver
70. P. Patriarca
71. J. T. Howe
72. T. H. Blewitt
73. W. E. Taylor
74. J. H. Crawford, Jr.
75. A. F. Cohen
76. J. C. Wilson
77. H. W. Savage
78. E. E. Hoffman
79. W. J. Leonard
80. J. A. Miller
81. J. M. Warde
82-85. Central Files (O.P.)

[redacted]

[redacted]

[redacted]

*EXTERNAL DISTRIBUTION*

86-93. Argonne National Laboratory
94-101. Atomic Energy Commission, Washington
102. Battelle Memorial Institute
103-106. Brookhaven National Laboratory
107-110. Carbide and Carbon Chemicals Company (Y-12)
111-112. Knolls Atomic Power Laboratory
113-114. General Electric Company, Richland
115-117. General Electric Company (ANPP)
118. Hanford Operations Office
119-122. Los Alamos
123. Massachusetts Institute of Technology (Kaufmann)
124-125. New York Operations Office
126. Patent Branch, Washington
127. Savannah River Operations Office, Wilmington
128-142. Technical Information Service, Oak Ridge
143-146. University of California Radiation Laboratory

[redacted]

[redacted]

Reports previously issued in this series are as follows:

| | |
|---|---|
| ORNL-28 | Period Ending March 1, 1948 |
| ORNL-69 | Period Ending May 31, 1948 |
| ORNL-407 | Period Ending July 31, 1949 |
| ORNL-511 | Period Ending October 31, 1949 |
| ORNL-583 | Period Ending January 31, 1950 |
| ORNL-754 | Period Ending April 30, 1950 |
| ORNL-827 | Period Ending July 31, 1950 |
| ORNL-910 | Period Ending October 31, 1950 |
| ORNL-987 | Period Ending January 31, 1951 |
| ORNL-1033 | Period Ending April 30, 1951 |
| ORNL-1108 | Period Ending July 31, 1951 |
| ORNL-1161 | Period Ending October 31, 1951 |
| ORNL-1267 | Period Ending January 31, 1952 |

[redacted]

[redacted]

## TABLE OF CONTENTS


| | PAGE |
|---|---|
| SUMMARY | 1 |
| THORIUM RESEARCH | 5 |
| Alloy Development | 5 |
| Mechanical Properties of Thorium and Thorium Alloys | 11 |
| Fabrication of Thorium | 16 |
| Recrystallization of Thorium | 16 |
| Radiation Damage of Thorium | 19 |
| PREFERRED ORIENTATION OF URANIUM | 21 |
| ANP PROGRAM | 39 |
| Static Corrosion | 39 |
| Dynamics Corrosion | 50 |
| Physical Metallurgy of Corrosion | 56 |
| Physical Chemistry of Corrosion | 59 |
| Mechanical Testing | 67 |
| Fabrication | 71 |
| Brazing | 78 |
| Welding | 87 |
| CERAMICS LABORATORY | 91 |
| Organization | 91 |
| Research Program | 91 |
| Design and Building of Equipment | 91 |
| Hafnia Research | 91 |
| Ceramic Coatings | 92 |
| Radiation Damage Studies | 92 |
| Lithium-Glass Diffusion Barrier | 92 |
| Reports | 92 |
| Service Work | 92 |
| HOMOGENEOUS REACTOR PROGRAM | 95 |
| Corrosion | 95 |
| Welding of Stainless Steel | 95 |
| Nondestructive Testing | 95 |


[redacted]

[redacted]


| | PAGE |
|---|---|
| Radiation Damage Studies | 95 |
| HRE Control Plates | 95 |
| Titanium Welding | 98 |
| Properties of Titanium and Zirconium | 99 |
| X-RAY LABORATORY | 101 |
| Crystal Structure of NiOOH | 101 |
| Crystal Structure of $NaNiO_2$ | 104 |
| METALLOGRAPHIC LABORATORY | 105 |
| Metallographic Examination of Thorium and Thorium Alloys | 107 |
| EXPERIMENTAL PLATE-CLADDING PROGRAM | 121 |
| Cladding of Uranium with Zirconium | 121 |
| Cladding of Thorium with Zirconium | 134 |
| Edge Closure by Welding | 146 |
| Cladding of Thorium with Aluminum | 149 |
| Ceramics Protective Coatings | 152 |
| Experimental Welding of Uranium, Thorium, and Zirconium | 153 |
| FUEL AND CONTROL ELEMENT FABRICATION | 157 |
| MTR Fuel and Control Rod Elements | 157 |
| Experimental CP-5 Fuel Units | 158 |
| LITR Fuel Units | 160 |
| Bulk Shielding Facility Fuel and Control Elements | 160 |
| Fuel Units for Chemical Processing | 160 |
| Service Work | 160 |


[redacted]

# METALLURGY DIVISION QUARTERLY PROGRESS REPORT

## SUMMARY

Results of the thorium alloy development work indicate that carbon is a potent hardening addition. Additions of 0.2% carbon produce threefold increases in strength without severe loss of ductility. Beryllium and oxygen have only minor effects when added to thorium in amounts in the range found in normal Ames material. Chromium additions to thorium produce substantial increases in strength and hardness and offer some promise of improving corrosion resistance.

Marked differences in mechanical properties have been observed in in thorium extruded at two different rates of speed. Material extruded at a low rate (1 ft/min) has strength about double that of material extruded at a fast rate (600 ft/min). Rod extruded at the slow rate shows a major [111] texture with a minor [110] texture. A single [114] texture is observed in material extruded at the fast rate.

The effect of elevated-temperature heat treatment on the impact strength of thorium at room temperature has been determined. A sharp transition in impact strength has been noted between anneals at temperatures from 800 to 1100°C and those at 1200 to 1600°C; the material treated at 1200°C and above showed very much lower impact strength.

Isothermal recrystallization curves have been determined for 80% cold-worked iodide and Ames thorium. It appears that the start of recrystallization occurs at about 520°C for the Ames thorium and at about 510°C for the iodide thorium.

Some preliminary, qualitative data have been obtained on possible changes in dimensions and hardness of thorium as a result of radiation damage. Examination of slugs irradiated at Hanford for 93 days at a flux of $0.7 \times 10^{13}$ neutrons/cm$^2$·sec has shown no significant dimensional changes. There is some possibility that a slight amount of hardening has taken place.

The examination of alpha-extruded uranium rods by the spherical x-ray-diffraction technique has been completed. The textures are summarized and correlated with the fabricating conditions of recrystallization. It appears that the recrystallization texture developed in extruded uranium rod is dependent upon the mode of induction of the recrystallization.

The Division has contributed consultation and service assistance to the Homogeneous Reactor Project on corrosion problems, welding specifications, and fabrication of HRE safety plates. The cooperative work with the Y-12 Nondestructive Test Group and the ORNL Solid State Division on homogeneous reactor problems, continues. Progress has been made in the initial stages of investigations of titanium and zirconium fabrication for application to homogeneous reactors.

High-temperature brazing alloys have been studied for possible use in the Aircraft Nuclear Propulsion Program. The tests conducted on these brazing alloys include flowability, corrosion, and physical properties. It was found that the

60% Pd-40% Ni alloy was the best brazing material to use in contact with fluoride mixtures. Additional experiments have been conducted on cone-arc welding techniques to obtain an understanding of the variables of this process. Some work has been completed on practical application of the cone-arc welding technique to actual fabrication of the tube-to-header joints in heat exchangers.

An additional method for the production of solid fuel elements has been studied that involves loose-powder sintering of uranium-bearing mixture to a solid backing plate. The following variables have been investigated: sintering temperature, sintering time, fuel component particle size, cold working and resintering, surface preparation, and sintering under load. Powder mixtures of boron carbide and 20% by volume of iron have been hot pressed to make slugs for the safety rod of the ARE. Hot-pressed mixtures of aluminum oxide and boron carbide are being studied for possible use in the regulating rod of the ARE.

Dynamic corrosion tests in thermal convection loops have been conducted with uranium-bearing and nonuranium-bearing fluoride mixtures to find a suitable container for the fluoride fuels to be used in the aircraft reactor experiment. Approximately 30 loops have been run with fluoride as a circulating medium. The container materials studied have been the 300- and 400-series stainless steels, Nimonic, and Inconel. The stainless steel loops operated only a short period of time before plugging; whereas the Inconel loops operated for 500 and 1000 hr successfully. However, the Inconel suffered severe corrosion to a depth of 10 to 15 mils because of leaching of chromium from the metallic solid solution. Static and modified dynamic tests are being used for the development of a possible inhibitor for fluoride corrosion. Additions of sodium, potassium, manganese, and calcium have been shown to be quite beneficial in minimizing the corrosive action of the fluorides on the container material.

Other static and modified dynamic tests were conducted to find a possible corrosion and/or mass transfer inhibitor for the metal-hydroxide systems. Preliminary experiments have shown that the corrosion and mass transfer usually associated with the metal-hydroxide systems can be appreciably reduced by the removal of oxygen from the system with purified hydrogen. In the study of the reaction products of container materials with the hydroxides a new compound has been found that is believed to be $NaNiO_2$. This is the first time that $NaNiO_2$ has been shown to exist. A similar, previously reported compound, $NaFeO_2$, has also been found as a reaction product of iron with sodium hydroxide.

The crystal structure of NiOOH has been worked out by x-ray diffraction methods. The unit cell is rhombohedral, $a$ = 7.17 Å and $\alpha$ = 22.84 degrees, and is believed to contain three formula weights. Work has started on the determination of the crystal structure of $NaNiO_2$.

The apparatus for two simplified methods of studying dynamic corrosion have been developed. This equipment was used successfully in preliminary tests for studying the metal-hydroxide mass-transfer phenomenon.

Various cleaning procedures for container materials such as 300- and 400-series stainless steels and Inconel are being investigated, since it was found that oxide scale had an appreciable effect on the corrosion of the container materials by the fluorides. The complicated configuration of the ARE makes it impossible to use hydrogen

firing as a method for removal of the oxide scale, so the pickling method must be substituted. Successful cleaning procedures have been found for the various container materials.

The main effort of the Ceramic Laboratory during the past quarter has been the design and installation of equipment. A research program was laid out and work commenced on the ceramic coating, hafnia, and radiation-damage phases. An investigation of a lithium-glass diffusion barrier was started.

For the determination of ferromagnetic areas in nonferromagnetic alloys, the magnetic-etch method has been used. Colloidal iron is coated on the specimen and a magnetic field is used to attract the iron to the ferromagnetic areas. Microscopic examination then reveals the affected areas.

Reliable techniques have been developed for cladding pure uranium with zirconium by rolling. The important factors of billet preparation, jacket design, method of evacuation and sealing, rolling temperature, and amount of reduction required have been studied.

Uranium can be bonded metallurgically to zirconium by hot rolling at 1175°F with a reduction of 10 to 1. Shear strengths as high as 60,000 psi have been measured. Clad samples have successfully withstood bombardment in the Y-12 calutron under a heat load of 1 kw/in.$^2$ for a 24-hr test period. Also, quenching directly from 720°C into room temperature water (beta heat treatment) has failed to destroy the bond.

Because of its high chemical activity and melting point, thorium is somewhat more difficult to clad with zirconium than uranium. Unfortunately, the formation of a low-melting-point phase in the zirconium-iron diagram limits the rolling temperature to 1650°F or lower. A technique of hot rolling at 1500°F, followed by an 1800°F heat treatment after stripping the steel can, has resulted in good bonding. Thus far, a low-carbon grade of titanium-deoxidized steel has proved to be the best canning material found to protect these active metals during hot working.

Although a simple, cylindrical type of billet design was used with considerable success for the initial phase of this investigation, a new nonframing type of jacket design has been adopted for large-scale production of double-clad plate. Such a design obviates the difficult problem of maintaining perfect alignment during rolling of extra long plates and results in a more uniformly clad plate. One disadvantage is the exposure of the core material along the ends and lateral edges.

Experimental welding work is in progress to close these exposed edges by welding. Preliminary results indicate that the method is definitely feasible. Zirconium filler rod has been used successfully in the welding of thorium core plates; a 3 wt % nickel alloy is used with the uranium core plates.

Developmental work on the problem of cladding of thorium with aluminum for production of $U^{233}$ by irradiation continues. Test samples, prepared by the direct method, have been rolled at 400, 500, and 600°C and evaluated. Alclad plates rolled at 400°C are probably suitable for service in the Materials Testing Reactor. Unfortunately, the metallurgical bond obtained will not withstand the aluminum-silicon brazing treatment, so this method cannot be used for plate assembly.

The possibility of using special ceramic coatings to protect highly active metals like zirconium, thorium, and uranium during hot-working operations is being investigated.

Sixty-six enriched fuel units and eight cadmium shim-safety rods were fabricated for the Materials Testing Reactor and shipped to ARCO. All shipments arrived safely. No trouble was experienced in loading the initial set of 23 fuel and 4 control elements into the reactor for the start-up.

The remainder of the third and all of the fourth pile loading are in various stages of completion. Measures are being taken to step-up production commensurate with the expected increase in demand.

Developmental work was initiated on the fabrication of a modified MTR fuel unit for the CP-5 reactor at Argonne National Laboratory. Three dummy aluminum assemblies were made to determine optimum jig dimensions and develop a brazing cycle that will yield brazed assemblies well within the CP-5 specified tolerances. Inspection results were encouraging. All units, with the possible exception of the first, met specifications. No trouble is anticipated in fabricating the remaining 16 active assemblies that were ordered.

In connection with the proposed power level increase of the LITR from approximately 1 to 1.5 megawatts, two replacement and five additional enriched-fuel assemblies were fabricated.

Five fuel units containing a subnormal amount of $U^{235}$ were prepared for the Bulk Shielding Facility. The units were needed to complete a matched set of cold elements for making gamma-ray spectra measurements on the ANP divided-shield experiment.

Four of the 20 normal-uranium fuel assemblies were completed for American Cyanamid at ARCO for use in conducting the initial dissolving and separation runs at the chemical processing plant.

# THORIUM RESEARCH

E. J. Boyle

## ALLOY DEVELOPMENT

J. A. Milko

The alloy development program was initiated primarily to advance the general metallurgical knowledge of thorium and several of its alloys.[1] The objective of the program is the development of alloys of thorium that have high strength and satisfactory corrosion resistance. Another aim is the determination of solubility of certain elements in pure thorium and their effects on mechanical and physical properties. It is felt that the results of this study will be useful, since the information gained will fill many gaps in the existing knowledge.

A part of the program has been the investigation of the effects of elements such as carbon, oxygen, and beryllium on the properties of pure thorium so that the effects could be evaluated satisfactorily when present in combination in commercial thorium. The effect of chromium was also investigated because of its promise as an alloying addition to improve the corrosion resistance and strength properties of thorium. The results of the partly completed investigation are presented in the following text under appropriate headings.

**Experimental Work.** The method of preparing the alloys was described previously.[1] Conventional techniques were used for the hardness and tensile tests - a crosshead speed of 0.05 in./min was used in the tensile tests.

**Effect of Quenching Temperature on the Hardness of the Thorium-Carbon Alloys.** Hardness values are presented in Table 1 for nine thorium-carbon alloys quenched from the indicated temperatures. From this table it may be observed readily that an increase in the carbon content in thorium-carbon alloys results in a marked increase in the hardness of the alloy. This trend is apparent in the as-arc-cast condition, as well as in the quenched state.

An examination of the data in Table 1 shows that the hardness changed definitely for the 0.07, 0.09, 0.11, 0.20, and 0.26% carbon alloys below the quenching temperature of 1400°C. These changes are suggestive of a solid-solution type of hardening by these amounts of carbon in thorium, in the temperature range of 1400 to 1600°C. Below 1400°C, the hardness decreases progressively, which is somewhat indicative of decreasing solubility of carbon in the thorium with decreasing temperature. These observations will be verified by x-ray-diffraction studies of these alloys.

For the alloys containing carbon in the range of 0.5 to 2.5%, no definite trend of the relationship of carbon content to quenching temperature can be observed. There appears to be a tendency, however, for the hardness values to increase at certain quenching temperatures. Thus, for the 0.5% carbon alloy, higher hardness values were obtained in the quenching temperature range of 1100 to 1400°C than in the range 1400 to 1600°C. This observation is also true for the 1.0 and 2.5% alloys, whereas the 1.4% alloy does not indicate this trend.

(1) *Metallurgy Division Quarterly Progress Report for Period Ending January 31, 1952*, ORNL-1267.

TABLE 1

**Effect of Quenching Temperature and Carbon Content on the Hardness of Thorium-Carbon Alloys***

| ALLOY NO. | CHEMICAL COMPOSITION (%), CARBON | 136° DPH HARDNESS (10-kg load, 16-mm objective) | | | | | | | | | | | |
|---|---|---|---|---|---|---|---|---|---|---|---|---|---|
| | | AS-ARC-CAST AND HOMOGENIZED 24 hr at 950°C | AFTER QUENCHING FROM INDICATED TEMPERATURE | | | | | | | | | | |
| | | | 400°C | 600°C | 800°C | 1000°C | 1100°C | 1200°C | 1300°C | 1400°C | 1500°C | 1600°C |
| F-8 | 0.07 | 78 | 78 | 82 | 80 | 94 | 89 | 100 | 98 | 110 | 123 | 135 |
| F-13 | 0.09 | 88 | 87 | 88 | 84 | 91 | 93 | 98 | 94 | 112 | 123 | 141 |
| F-3 | 0.11 | 107 | 100 | 122 | 110 | 112 | 119 | 120 | 126 | 132 | 146 | 146 |
| F-6 | 0.20 | 129 | 129 | 134 | 138 | 143 | 142 | 142 | 153 | 164 | 175 | 178 |
| F-9 | 0.26 | 156 | 152 | 150 | 160 | 161 | 163 | 171 | 176 | 182 | 186 | 189 |
| F-11 | 0.50 | 205 | 205 | 201 | 218 | 246 | 265 | 259 | 252 | 257 | 244 | 240 |
| F-19 | 1.05 | 276 | 270 | 287 | 280 | 285 | 385 | 359 | 351 | 394 | 370 | 361 |
| F-17 | 1.42 | 309 | 290 | 296 | 325 | 379 | 424 | 415 | 415 | 408 | 418 | 408 |
| F-20 | 2.50 | 358 | 282 | 286 | 393 | 406 | 448 | 430 | 472 | 460 | 441 | 421 |

*Crystal-bar iodide thorium of the following nominal composition, 0.02% C, 0.001% N, 0.08% O, 0.005% Al, 0.001% W, 0.0001% Cu, 0.0002% Mo, 0.0002% As, 0.0003% Zn, 0.0005% Fe, and Be, B, Si, Co, Ni, Mn, Pb, Cr, Cd, Sn, and Mg present only in trace quantities.

These observed changes may be the result of precipitation of a second phase in the temperature range of 1100 to 1400 °C, or they may be effected by inhomogeneities in the test specimens. The changes will be checked by microscopic and x-ray-diffraction studies.

**Effect of Quenching Temperature on the Hardness of Thorium-Oxygen Alloys.** Hardness values are presented in Table 2 for 11 thorium-oxygen alloys quenched from the given temperatures. Since addition of oxygen to thorium increases the hardness only moderately, oxygen does not appear to be a potent alloying addition to thorium to increase the hardness and, perhaps, strength. About 2% oxygen is required to double the hardness of pure thorium.

The data in Table 2 indicate a change in hardness below the quenching temperature of 1500 °C, which may show that a definite amount of oxygen is soluble at temperatures of 1500 to 1600 °C. There appears to be considerably less solubility of oxygen below 1400 °C, as indicated by the rather abrupt change in hardness below this temperature. These observations will be checked by microscopic and x-ray-diffraction studies.

**Effect of Carbon Additions on the Properties of Pure Thorium.** Additions of carbon were made to the relatively pure crystal-bar thorium, which was produced by the decomposition of its tetraiodide. The strength properties and hardness values obtained on seven such alloys are presented in Table 3.

The strength properties and hardness of the relatively pure thorium metal are quite low. An addition of only about 0.05% carbon to the pure thorium more than doubles its yield strength. This amount of carbon has even a more marked effect on the proportional limit; it increases that property about five times. The hardness value (VHN) is increased by 20 points by the addition of this small amount of carbon. Additions of greater amounts of carbon to the pure thorium appear to increase the strength properties and hardness appreciably without detrimental effect on the ductility, as measured by tensile elongation and reduction of area.

Although these trends were obtained on single test specimens, it is felt that carbon is a potent alloying addition to thorium in that it increases its strength and hardness. Preliminary indications are that carbon in amounts up to 0.2% may also improve the corrosion resistance in water solutions and the scaling resistance in air.

**Effect of Carbon Additions on the Properties of Ames Thorium.** The strength properties of 15 thorium-carbon alloys are presented in Table 4. All the alloys were prepared from thorium that had nominal amounts of impurities, such as iron, beryllium, silicon, and aluminum. The carbon content ranged from about 0.03 to 0.14%.

It may be observed from Table 4 that the addition of carbon to Ames thorium increases its strength and hardness. This is the same trend that was observed with the addition of carbon to pure thorium.

Although the alloys listed in Table 4 were prepared in the same manner as those in Table 3, a direct comparison of the properties is not possible. The alloys of Table 4 were annealed (after 85% cold reduction) at 750 °C in order to obtain more complete recrystallization than in the alloys listed in Table 3, which were annealed at 650 °C.

**TABLE 2**

**Effect of Quenching Temperature and Oxygen Content on the Hardness of Thorium-Oxygen Alloys[a]**

| ALLOY NO. | CHEMICAL COMPOSITION (%) | | | 136° DPH HARDNESS (10-kg load, 16-mm objective) | | | | | | | | | |
|---|---|---|---|---|---|---|---|---|---|---|---|---|---|
| | | | | AS-ARC-CAST AND HOMOGENIZED 24 hr at 950 °C | AFTER QUENCHING FROM INDICATED TEMPERATURE | | | | | | | | |
| | O[b] | C | N (by vacuum fusion) | | 400 °C | 600 °C | 800 °C | 1000 °C | 1100 °C | 1200 °C | 1300 °C | 1400 °C | 1500 °C |
| F-34 | 0.006 | 0.025 | 0.008 | 42 | 43 | 41 | 39 | 37 | 47 | 51 | 47 | 65 | 111 |
| F-32 | 0.013 | 0.025 | 0.011, 0.014[c] | 43 | 41 | 39 | 41 | 38 | 47 | 51 | 49 | 63 | 110 |
| F-30 | 0.022 | 0.016 | 0.027 | 43 | 42 | 44 | 42 | 38 | 54 | 55 | 52 | 62 | 117 |
| F-26 | 0.050 | 0.035 | 0.047 | 44 | 44 | 41 | 41 | 42 | 57 | 62 | 59 | 65 | 109 |
| F-36 | 0.080 | 0.021 | 0.07[d] | 43 | 47 | 42 | 39 | 43 | 59 | 57 | 74 | 90 | 107 |
| F-28 | 0.120 | 0.025 | 0.22 | 44 | 45 | 47 | 42 | 49 | 58 | 62 | 79 | 75 | 110 |
| F-38 | 0.240 | 0.024 | 0.077, 0.16[c] | 47 | 50 | 52 | 44 | 49 | 64 | 59 | 78 | 86 | 111 |
| F-40 | 0.440 | 0.030 | 0.14, 0.22, 0.66, 0.16 | 46 | 46 | 48 | 46 | 50 | 66 | 67 | 84 | 96 | 127 |
| F-42 | 0.770 | 0.021 | 0.07, 0.07, 0.25 | 56 | 54 | 57 | 57 | 53 | 64 | 65 | 101 | 91 | 134 |
| F-48 | 1.50 | 0.048 | 0.55, 0.24 | 63 | 75 | 82 | 87 | 83 | 77 | 84 | 101 | 116 | 136 |
| F-24 | 2.00 | 0.053 | 0.036, 0.088, 0.065 | 87 | 80 | 93 | 85 | 101 | 94 | 98 | 116 | 119 | 140 |

[a] Crystal-bar iodide thorium of the following nominal composition, 0.02% C, 0.001% N, 0.08% O, 0.005% Al, 0.001% W, 0.0001% Cu, 0.002% Mo, 0.0002% As, 0.0003% Zn, 0.0005% Fe, and Be, Si, Co, Ni, Mn, Pb, Cr, Cd, Sn, and Mg present only in trace quantities.

[b] Intended amount.

[c] Two values reported.

[d] Average.

## TABLE 3

### Effect of Carbon Additions on the Properties of Pure Thorium

All samples were cold rolled into sheet form, approximately 85% reduction, and annealed at 650 °C for ½ hr

| ALLOY NO. | CHEMICAL COMPOSITION (%) | | | TENSILE STRENGTH (psi) | YIELD STRENGTH AT 0.2% OFFSET (psi) | PROPORTIONAL LIMIT (psi) | MODULUS OF ELASTICITY (million psi)[a] | ELONGATION IN 2 IN. (%) | REDUCTION OF AREA (%) | HARDNESS | | |
|---|---|---|---|---|---|---|---|---|---|---|---|---|
| | C | O | OTHER | | | | | | | ROCKWELL | VHN[b] | 136° DPH[c] |
| F-54 | 0.015 | | 0.15 W[d]<br>0.02 Cu | 18,000 | 7,600 | 2,400 | 12.8 | 27.0[e] | 69.0 | 74 $R_H$ | 40 | 54 |
| F-65 | 0.022 | 0.05 | 0.001 W<br>0.003 Cu | 17,600 | 6,500 | 4,500 | 9.0 | 50.0 | 62.0 | 61 $R_H$ | 34 | 54 |
| F-66 | 0.047 | | 0.001 W<br>0.003 Cu | 26,000 | 16,400 | 11,400 | 9.1 | | 43.0 | 89 $R_H$ | 60 | 72 |
| F-67 | 0.070 | 0.05 | 0.001 W<br>0.003 Cu | 34,400 | 26,900 | 22,300 | 9.4 | 46.0 | 51.0 | 99 $R_H$ | 83 | 93 |
| F-69 | 0.130 | 0.01 | 0.001 W<br>0.004 Cu | 43,900 | 35,100 | 22,400 | 9.0 | 41.0 | 46.0 | 57 $R_B$ | 109 | 113 |
| F-71 | 0.187 | | 0.001 W<br>0.03 Cu | 53,600 | 50,300 | 31,300 | 10.4 | 38.0 | 39.0 | 71 $R_B$ | 125 | 130 |
| F-83 | 0.22 | | 0.001 W<br>0.02 Cu | 60,700 | 50,300 | 32,800 | 9.4 | 30.0 | 39.0 | 83 $R_B$ | 140 | 144 |

[a] Value was not obtained with precision.

[b] 10-kg load and 2/3-in. objective.

[c] 10-kg load and 1/16-mm objective.

[d] Probably introduced during arc melting.

[e] This value appears to be entirely too low; it will be checked.

## TABLE 4

### Effect of Carbon Additions on the Properties of Ames Thorium

All samples were cold rolled into sheet form, approximately 85% reduction, and annealed at 750°C for ½ hr

| ALLOY NO. | CHEMICAL COMPOSITION (%) | | | TENSILE STRENGTH (psi) | YIELD STRENGTH AT 0.2% OFFSET (psi) | PROPORTIONAL LIMIT (psi) | MODULUS OF ELASTICITY (million psi)[a] | ELONGATION IN 2 IN. (%) | REDUCTION OF AREA (%) | HARDNESS | | |
|---|---|---|---|---|---|---|---|---|---|---|---|---|
| | C | Si | Fe | | | | | | | ROCKWELL | VHN[b] | 136° DPH[c] |
| F-60 | 0.030 | 0.35[d] | 0.02[d] | 29,800 | 19,800 | 14,300 | 12.8 | 38.0 | 49.0 | 90 $R_H$ | 67 | 82 |
| F-73 | 0.040 | 0.21[d] | 0.02[d] | 27,400 | 17,200 | 12,200 | 9.7 | 45.0 | 51.0 | 92 $R_H$ | 66 | 95 |
| F-61 | 0.05 | 0.06[d] | 0.02[d] | 26,900 | 15,800 | 8,900 | 12.0 | 44.0 | 53.0 | 86 $R_H$ | 59 | 72 |
| F-62 | 0.05 | 0.16[d] | 0.02[d] | 31,000 | 20,900 | 12,700 | 9.2 | 43.0 | 50.0 | 90 $R_H$ | 68 | 78 |
| F-63 | 0.05 | 0.17[d] | 0.02[d] | 27,000 | 17,000 | 12,300 | 9.8 | 40.0 | 41.0 | 83 $R_H$ | 61 | |
| F-74 | 0.05 | 0.21[d] | 0.02[d] | 27,600 | 17,500 | 11,100 | 11.0 | 47.0 | 40.0 | 90 $R_H$ | 63 | 100 |
| Average | 0.05 | 0.15 | 0.02[d] | 27,900 | 17,800 | 11,300 | 10.5 | 43.0 | 46.0 | 87 $R_H$ | 63 | 83 |
| F-77 | 0.07 | 0.23[d] | 0.016[d] | 33,500 | 25,900 | 15,900 | 10.6 | 47.0 | 42.0 | 101 $R_H$ | 82 | 78 |
| F-80 | 0.07 | 0.29[d] | 0.016[d] | 35,500 | 27,100 | 15,900 | 10.6 | 25.0 | 21.0 | 96 $R_H$ | 88 | 92 |
| Average | 0.07 | 0.16 | 0.016 | 34,500 | 26,500 | 15,900 | 10.6 | 36.0 | 31.0 | 99 $R_H$ | 85 | 85 |
| F-75 | 0.08 | 0.04[d] | 0.02[d] | 37,300 | 32,000 | 23,000 | 11.5 | 42.0 | 47.0 | 104 $R_H$ | 85 | 100 |
| F-79 | 0.08 | 0.03[d] | 0.02[d] | 35,500 | 26,600 | | 12.9 | 40.0 | 44.0 | 102 $R_H$ | 83 | 91 |
| Average | 0.08 | 0.03 | 0.02 | 36,400 | 29,300 | 19,600 | 12.2 | 41.0 | 45.0 | 103 $R_H$ | 84 | 95 |
| F-76 | 0.09 | 0.04[d] | 0.02[d] | 37,600 | 31,500 | 17,500 | 10.0 | 43.0 | 40.0 | 105 $R_H$ | 97 | 77 |
| F-78 | 0.09 | 0.10[d] | 0.016[d] | 37,800 | 28,100 | 19,800 | 13.4 | 46.0 | 33.0 | 105 $R_H$ | 94 | 98 |
| F-81 | 0.09 | 0.18[d] | 0.02[d] | 36,600 | 26,200 | 16,900 | 10.4 | 39.0 | 50.0 | 99 $R_H$ | 83 | 92 |
| Average | 0.09 | 0.10 | 0.019 | 37,600 | 28,600 | 18,100 | 11.2 | 43.0 | 41.0 | 103 $R_H$ | 95 | 89 |
| F-82 | 0.13 | 0.16[d] | 0.02[d] | 44,900 | 37,700 | 22,600 | 10.6 | 41.0 | 44.0 | 57 $R_H$ | 105 | 112 |
| F-68 | 0.14 | 0.01[d] | 0.02[d] | 48,600 | 43,300 | 25,600 | 10.8 | 35.0 | 33.0 | 64 $R_H$ | 118 | 126 |
| Average | 0.13 | 0.09 | 0.02 | 46,800 | 40,500 | 24,100 | 10.7 | 38.0 | 38.0 | 60 $R_H$ | 111 | 119 |

[a] Value was not obtained with high precision.

[b] 10-kg load, 2/3-in. objective.

[c] 10-kg load, 16-mm objective.

[d] Value being rechecked.

From general observations, however, it may be stated that the addition of equivalent amounts of carbon to Ames thorium results in higher strength and hardness, probably because of the presence in combination of iron, beryllium, silicon, and aluminum. As will be shown later in the program, all these elements, when added singly, tend to harden thorium.

**Effect of Beryllium Additions on the Properties of Pure Thorium.** Additions of 0.02 to 0.7% beryllium were made to the relatively pure thorium. The resulting strength properties of such alloys are listed in Table 5.

Beryllium in amounts of 0.02 to 0.04% does not appear to exert any significant effect on thorium. These small amounts seem to produce some softening, as may be deduced from the hardness values. The small decrease in the hardness of the 0.02, 0.03, and 0.04% beryllium alloys may be associated with deoxidation of the thorium by the beryllium.

Additions of beryllium in amounts of 0.1 to 0.7% have a tendency to increase the strength properties only moderately. Ductility of the alloys appears to be lowered slightly with the beryllium additions in this range. However, there is a definite, but small, increase in hardness.

In summary, the addition of about 0.7% of beryllium to pure thorium seems to strengthen the resulting alloy only mildly. Its hardening power, although small, is definite - probably caused by compound formation in the alloy structure.

**Effect of Chromium Additions on the Properties of Pure Thorium.** Chromium additions were made to the iodide thorium, because in the past two such alloys developed high strength and it may well be that such additions will impart fairly good corrosion-resistance properties to thorium. Five alloys were prepared, and their properties are listed in Table 6.

In general, the addition of chromium to thorium increases its strength and hardness with a corresponding decrease in ductility; however, the two alloys of 1.6 and 2.9% chromium do not support this observation entirely. The two alloys developed lower strength and hardness and a higher ductility than did the 0.76, 4.2, and 5.3% alloys. It will be noted, however, that the 0.76% chromium alloy had a relatively high carbon content; therefore additional alloys will be prepared and studied in order to develop conclusive data. Also, the microstructure of these alloys will be studied so that any further discrepancies of strength properties can be explained.

## MECHANICAL PROPERTIES OF THORIUM AND THORIUM ALLOYS

W. J. Fretague

Tensile specimens of Ames thorium were prepared to determine the effect of extrusion rate on mechanical properties. For this experiment two extrusions of Ames thorium billet A339A were made. Extrusion A339A1 was made at the rate of 600 ft/min, and extrusion A339A2 was made at the rate of 1 ft/min. Three-inch-diameter sections of billet A339A were heated to 850°C for 2 hr prior to extrusion, and both sections (A339A1 and A339A2) were extruded to 1-in.-dia rod (reduction ratio, 9:1). Samples of both extrusions (in the as-extruded condition) were examined for orientation textures. Extrusion A339A1 was reported to have a [114] texture, and extrusion A339A2 was reported to have a major [111] texture and a minor

## TABLE 5

### Effect of Beryllium Additions on the Properties of Pure Thorium

All samples were cold rolled into sheet form, approximately 85% reduction, and annealed at 650 °C for ½ hr

| ALLOY NO. | CHEMICAL COMPOSITION | | | | TENSILE STRENGTH (psi) | YIELD STRENGTH AT 0.2% OFFSET (psi) | PROPORTIONAL LIMIT (psi) | MODULUS OF ELASTICITY (million psi)[b] | ELONGATION IN 2 IN. (%) | REDUCTION OF AREA (%) | HARDNESS | | |
|---|---|---|---|---|---|---|---|---|---|---|---|---|---|
| | Be | C | W[a] | Cu[a] | | | | | | | ROCKWELL | VHN[c] | 136° DPH[d] |
| F-54 | <0.01 | 0.015 | 0.15 | 0.02 | 18,000 | 7,600 | 2,400 | 12.8 | 27.0 | 69.0 | 74 $R_H$ | 40 | 54 |
| F-56 | 0.02 | 0.018 | 0.10 | 0.03 | 19,500 | 6,700 | 4,000 | 8.0 | 38.0 | 71.0 | 60 $R_H$ | 37 | 44 |
| F-55 | 0.03 | 0.008 | 0.20 | 0.02 | 18,600 | 7,000 | 5,000 | 10.0 | 41.0 | 57.0 | 65 $R_H$ | 36 | 47 |
| F-58 | 0.04 | 0.022 | 0.04 | 0.03 | 19,900 | 6,300 | 3,600 | 8.2 | 29.0 | 76.0 | 63 $R_H$ | 37 | 46 |
| F-59 | 0.11 | 0.017 | 0.07 | 0.03 | 21,700 | 7,800 | 4,800 | 7.7 | 38.0 | 67.0 | 71 $R_H$ | 40 | 52 |
| F-86 | 0.32 | 0.02 | <0.001 | 0.03 | 18,500 | 10,700 | 6,100 | | 4.0 | 13.0 | 78 $R_H$ | 53 | 62 |
| F-84 | 0.50 | 0.027 | <0.001 | 0.03 | 24,100 | 12,200 | 8,200 | 13.1 | 29.0 | 36.0 | 75 $R_H$ | 48 | 57 |
| F-85 | 0.69 | 0.01 | <0.001 | 0.03 | 31,600 | 16,900 | 10,300 | 8.2 | 25.0 | 34.0 | 84 $R_H$ | 57 | 72 |

[a] Probably introduced during arc melting.

[b] Value not obtained with precision.

[c] 10-kg load, 2/3-in. objective.

[d] 10-kg load, 16-mm objective.

## TABLE 6

### Effect of Chromium Additions on the Properties of Pure Thorium

All samples were cold rolled into sheet form, approximately 85% reduction, and annealed at 650 °C for ½ hr

| ALLOY NO. | CHEMICAL COMPOSITION | | | | TENSILE STRENGTH (psi) | YIELD STRENGTH AT 0.2% OFFSET (psi) | PROPORTIONAL LIMIT (psi) | MODULUS OF ELASTICITY (million psi)[b] | ELONGATION IN 2 IN. (%) | REDUCTION OF AREA (%) | HARDNESS | | |
|---|---|---|---|---|---|---|---|---|---|---|---|---|---|
| | Cr | C | W[a] | Cu[a] | | | | | | | ROCKWELL | VHN[c] | 136° DPH[d] |
| F-54 | 0 | 0.015 | 0.15 | 0.02 | 18,600 | 7,600 | 2,400 | 12.8 | 27.0[e] | 69.0 | 74 $R_H$ | 40 | 54 |
| F-53 | 0.76 | 0.038 | | | 39,500 | 33,600 | 23,300 | 9.4 | 11.0 | 48.0 | 106 $R_H$ | 85 | 93 |
| F-51 | 1.60 | 0.019 | | | 28,900 | 12,200 | 6,300 | 7.2 | 26.0 | 54.0 | 85 $R_H$ | 52 | 73 |
| F-52 | 2.90 | 0.022 | | | 33,000 | 13,800 | 7,300 | 9.7 | 23.0 | 47.0 | 89 $R_H$ | 62 | 71 |
| F-87 | 4.2 | | <0.001 | 0.03 | 47,900 | 28,500 | 17,800 | | 6.0 | 23.0 | 102 $R_H$ | 85 | 91 |
| F-88 | 5.3 | | <0.001 | 0.02 | 51,300 | 28,200 | 14,000 | | 13.0 | 31.0 | 102 $R_H$ | 86 | 97 |

[a] Probably introduced during melting.

[b] Values not obtained with precision.

[c] 10-kg load, 2/3-in. objective.

[d] 10-kg load, 16-mm objective.

[e] This value obtained on a single test appears to be low.

[110] texture. Duplicate tensile specimens from each extrusion were prepared. One specimen from each extrusion was tested in the as-extruded condition and the other in the annealed condition. The annealing was done in vacuum; the specimens were heated at 750°C for 30 min and furnace-cooled to room temperature. Annealed x-ray specimens from each extrusion are being prepared, and orientation determinations will be made as soon as the specimens are available. Information on the recrystallization textures of the two extrusions will be very helpful in analyzing the results of the tensile tests of the annealed specimens. Table 7 lists the mechanical properties of the as-extruded and annealed specimens of the two extrusions. A decided improvement in tensile strength and yield strength with a corresponding decrease in elongation and reduction in area was noted in the material extruded at the very slow rate (A339A2).

Impact tests were performed on 17 Charpy V-notch impact specimens of Ames thorium to determine the effect of elevated-temperature heat treatment. A 3-in.-dia section of Ames thorium billet A338A was heated at 950°C for 2 hr and extruded to a 5/8-in.-dia rod (reduction ratio, 23:1). This rod was cold drawn to 0.410-in.-square bar, and duplicate specimens 2 1/4 in. long were heated in a purified argon atmosphere at temperatures between 800 and 1600°C in 100°C increments for 30 min and water quenched. Following heat treatments, specimens were machined into Charpy V-notch impact specimens and tested at room temperatures by using the combination of pendulum weight and position that gives maximum capacity (0 to 120 ft-lb) of the impact tester. Table 8 lists the results obtained on impact tests. Specimens quenched from temperatures of 800 through 1100°C give impact values that are fairly consistent. Specimens quenched from 1200°C and above, however, had impact strengths ranging from approximately one half to one seventh of those exhibited by the same material quenched from 800°C and below. Metallographic examination of the fractured impact specimens is in progress to determine whether there is a corresponding change in the microstructure of specimens quenched from 1200°C and higher.

**TABLE 7**

**Mechanical Properties of Ames Thorium**

Billet A339A

| SPECIMEN NO. | CONDITION | TENSILE STRENGTH (psi) | ULTIMATE STRENGTH (psi) | YIELD STRENGTH AT 0.2% OFFSET (psi) | UPPER YIELD POINT (psi) | LOWER YIELD POINT (psi) | REDUCTION IN AREA (%) | ELONGATION IN 2 IN. (%) | PROPORTIONAL LIMIT (psi) | MODULUS OF ELASTICITY |
|---|---|---|---|---|---|---|---|---|---|---|
| A339A1 | As-extruded at fast rate | 30,500 | 66,600 | 26,200 | | | 70.0 | 41.5 | 21,000 | $7.7 \times 10^6$ |
| A339A1A | Annealed* | 26,500 | 58,900 | 18,300 | 18,300 | | 72.7 | 55.6 | 15,100 | $8.0 \times 10^6$ |
| A339A2 | As-extruded at slow rate | 50,600 | 58,200 | 49,600 | | | 37.4 | 21.3 | 40,000 | $13.4 \times 10^6$ |
| A339A2A | Annealed* | 27,400 | 57,600 | 19,700 | 19,700 | 18,800 | 68.4 | 63.0 | 16,200 | $8.1 \times 10^6$ |

*Vacuum annealed at 750°C for 30 min and furnace cooled; test section machined after annealing.

## TABLE 8

### Impact Strength of Heat-Treated Ames Thorium

Charpy V-notch impact specimens

| SPECIMEN NO. | IMPACT ENERGY (ft-lb)* | THERMAL AND MECHANICAL HISTORY |
|---|---|---|
| 1 | 20.5 | Three-inch-diameter billet heated to 950 °C for 2 hr prior to extrusion |
| 2 | 20.5 | Extruded to 5/8-in.-dia rod and cold drawn to 0.410-in.-square bar; duplicate 2 1/4 by 0.410-in.-square specimens heated in a purified argon atmosphere at 800 °C for 30 min and water quenched; machined to final specimen size after heat treatment |
| 3 | 23.5 | Same as Specimens 1 and 2 except heated at 900 °C for 30 min and water quenched prior to machining |
| 4 | 24.0 | |
| 5 | 25.5 | Same as Specimens 1 and 2 except heated at 1000 °C for 30 min and water quenched prior to machining |
| 6 | 25.0 | |
| 7 | 24.0 | Same as Specimens 1 and 2 except heated at 1100 °C for 30 min and water quenched prior to machining |
| 8 | 25.0 | |
| 9 | 10.5 | Same as Specimens 1 and 2 except heated at 1200 °C for 30 min and water quenched prior to machining |
| 10 | 10.5 | |
| 11 | 7.0 | Same as Specimens 1 and 2 except heated at 1300 °C for 30 min and water quenched prior to machining |
| 12 | 8.0 | |
| 13 | 4.5 | Same as Specimens 1 and 2 except heated at 1400 °C for 30 min and water quenched prior to machining |
| 14 | 4.0 | |
| 15 | 4.0 | Same as Specimens 1 and 2 except heated at 1500 °C for 30 min and water quenched prior to machining |
| 16 | 5.0 | |
| 17 | 3.5 | Same as Specimens 1 and 2 except heated at 1600 °C for 30 min and water quenched prior to machining |
| 18 | Specimen broke during machining | |

*The 0-to-120 ft-lb range of the impact tester was used.

## FABRICATION OF THORIUM

W. J. Fretague

**Extrusion.** Ames thorium billets MX325A9, A328A, A338B, A339B, and A343B were extruded to 1 by 2 in. cross-section bars. The bars were cold rolled to 5/8 by 2 in. plates, cut to appropriate lengths, and machined into tensile, Charpy V-notch impact, and torsion specimens.

Ames thorium billet MX322A8 was extruded to 5/8-in.-dia rod by using a Tatmo die insert. After one extrusion the insert was badly scored, and the surface of the extrusion was rough and out-of-round. A Super Cobalt insert was placed in the die holder, and Ames thorium billet MX325A9 was extruded to 5/8-in.-dia rod. The results were better than those obtained with the Tatmo insert on billet MX322A8, but they were still poor by comparison with previous standards. Ames thorium billets A328A, A338B, A339B, and A343B were extruded to 5/8-in.-dia rods by using the Super Cobalt die insert. All billets were heated to 850°C in salt for 2 hr prior to extrusion. This die material appeared to give satisfactory service.

Ames thorium billet MX322B8 was sectioned (transversely) prior to extrusion, and cracks (or voids) were found on both faces of the transverse cut and on both ends of the original billet. The larger piece of the billet was sectioned longitudinally in the Research Shops, and a large shrinkage cavity (or secondary pipe) was discovered near one end (about one third of the way from the end of the original billet). This defect was cut off, and the remainder of the billet was machined into two 1 by 2 in. pieces. An attempt was made to cold roll these pieces, but they cracked badly after only 0.135 in. total reduction (0.015 in. per pass). The cracks developed at right angles to the rolling direction on the surface that was originally near the center of the billet. Further work on this billet was discontinued.

**Billet Defects.** A number of the Ames thorium billets that were sectioned prior to extrusion exhibited seams or voids (typical of solidification shrinkage defects). When such defects are present in a billet they are not self-healing – that is, they are not welded closed by the extrusion process, and if present in test specimens prepared from such a defective extrusion they tend to give erroneous results when tested. Radiography of 3-in.-dia thorium billets to detect flaws prior to extrusion is impossible with the existing equipment of the Division, so other methods of flaw detection were investigated. Three Ames thorium billets and 16 extruded and cold-drawn thorium bars were checked with a Sperry reflectoscope. Of the three billets tested, one was known to be cracked (from visual examination), whereas the other two were thought to be sound. All the extruded and cold-drawn bars seemed to be sound. The reflectoscope worked very well on the cold-drawn material, but the indications obtained on the as-cast billets were rather indefinite. Part of the difficulty with the as-cast billets could be attributed to the rough-machined surface on the ends of the billet. When the crystal intended for use with cast materials was employed, faint indications of defects were obtained in the billet that was known to be defective (MX325B9).

## RECRYSTALLIZATION OF THORIUM

F. H. Eckert

**Ames Thorium.** Specimens 0.071 in. thick were fabricated from Ames thorium

billet A349B (0.040% carbon) by cold rolling thorium plate to 20, 40, 60, and 80% reduction. The thorium plate was heated to 750°C for ½ hr and furnace-cooled before final cold working to precipitate any impurities that might hinder recrystallization studies by simultaneous precipitation. The specimens that were cold worked 80% were then annealed for varying lengths of time at constant temperatures in a lead bath and quenched in cold water.

Figure 1 shows the progress of recrystallization, which was traced by Vickers hardness measurements. The change in microstructure during the isothermal annealing is shown in Figs. 77 and 80 for 550 and 600°C. The effect of temperature on recrystallization is revealed by the microstructures in Fig. 83. (See section on "Metallography Laboratory" for Figs. 77, 80, and 83.)

A rapid drop in the hardness of the Ames thorium specimens isothermally annealed for 1 hr was noted at temperatures varying from 450 to 520°C. Microexamination showed no evidence of recrystallization in the temperature

[redacted]

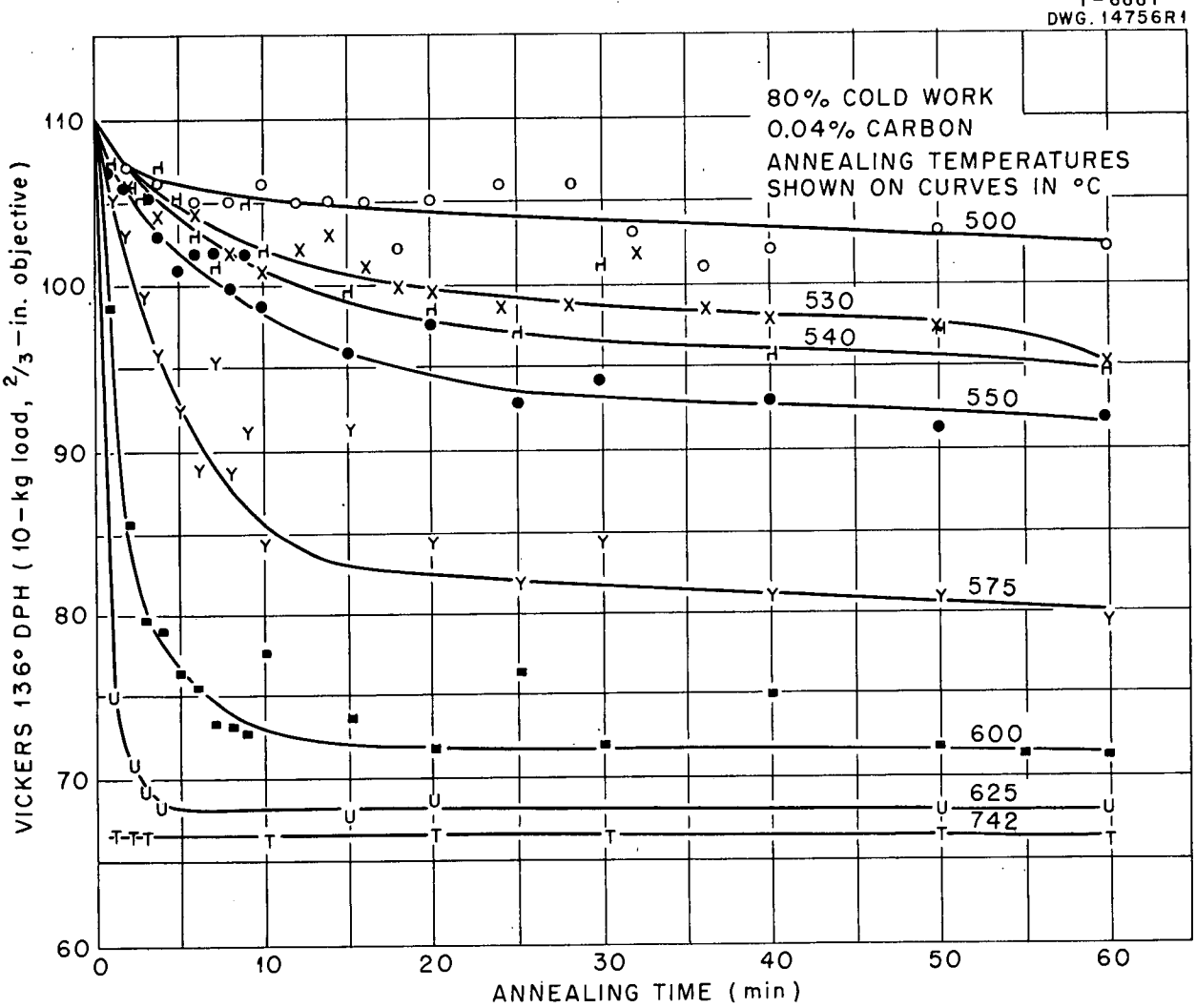


**Fig. 1. Recrystallization Curves for Ames Thorium.**

range, so it is believed that "recovery" and/or possibly some precipitation is responsible for this initial hardness drop. Investigation of the Ames samples rolled to 20, 40, and 60% reduction will be reported at a later date.

**Iodide Thorium.** Iodide crystal-bar thorium was melted in an inert-atmosphere arc furnace by using a nonconsumable tungsten electrode. The resulting thorium buttons were flat rolled and slow-cool annealed at 750°C for ½ hr and then cold rolled with an 80% reduction to 0.061-in.-thick plate specimens. These specimens were then isothermally annealed the same as the Ames specimens, and Vickers hardness measurements were made to trace the recrystallization of the pure thorium. The carbon and qualitative spectrographic analyses of the iodide thorium are given in Table 9.

Isothermal recrystallization curves for iodide thorium are plotted in Fig. 2. Microstructure changes during annealing are shown in Figs. 75, 76, 78, 79, 81, and 82. (See section on "Metallography Laboratory.")

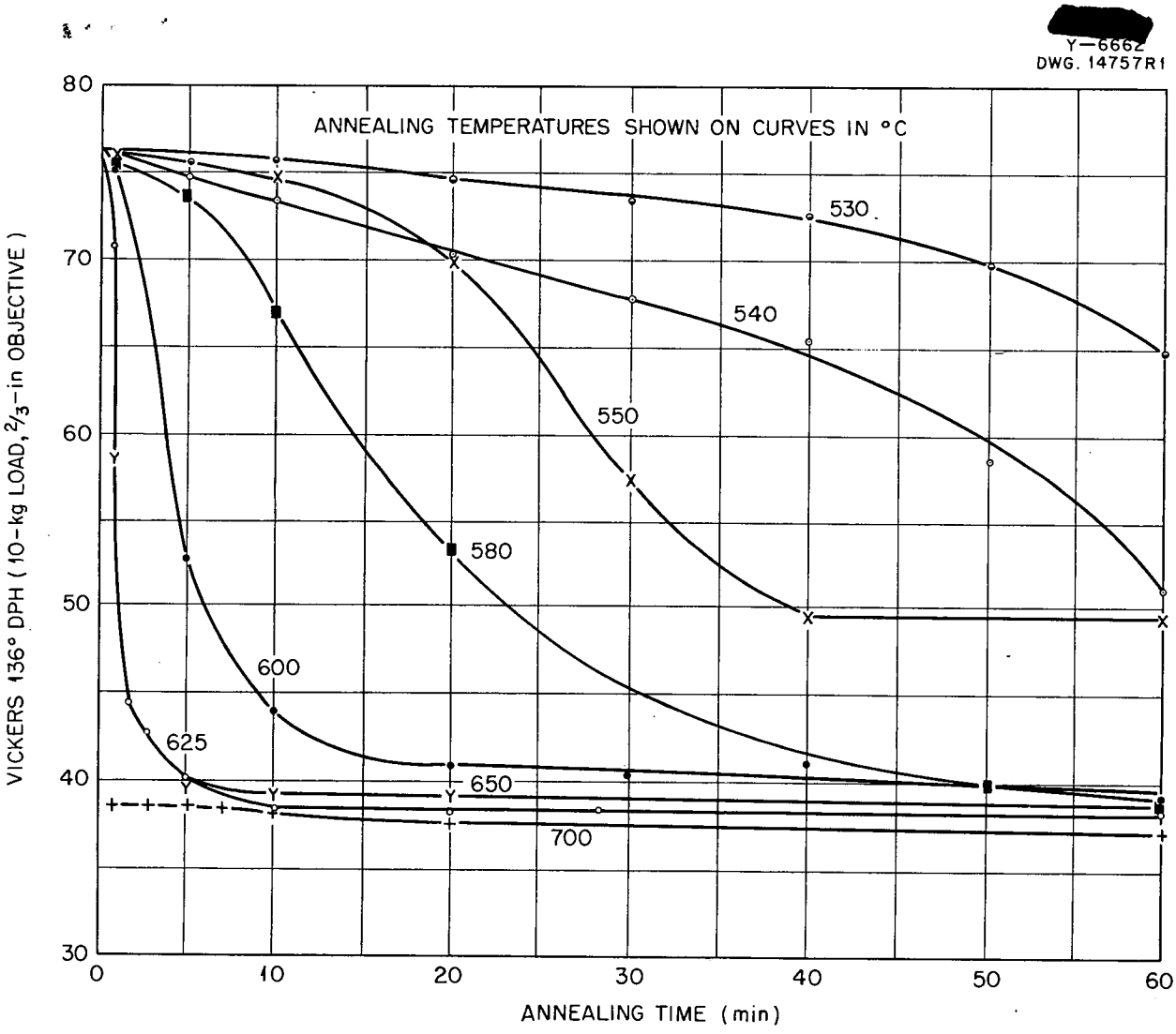


**Fig. 2. Isothermal Recrystallization Curves for Iodide Thorium.**

**TABLE 9**

**Analysis of Iodide Thorium for Recrystallization Studies**

| | |
|---|---|
| Carbon | 0.012% |
| Aluminum | Very weak |
| Chronium | Trace |
| Calcium | Trace |
| Copper | Trace |
| Iron | Trace |
| Silicon | Trace |
| Silver | Faint trace |
| Boron | Faint trace |
| Beryllium | Faint trace |
| Lanthanum | Faint trace |
| Magnesium | Faint trace |
| Nickel | Faint trace |
| Titanium | Faint trace |

The iodide thorium did not exhibit a "recovery" zone as shown in the Ames thorium. Hardness measurements on the iodide thorium remained constant between 400 and 510°C (specimens isothermally annealed for 1 hr), but then the hardness started to drop off rapidly. Microexamination revealed that this hardness drop was the result of recrystallization, which started at 500°C. Investigation of the effect of reduced cold work on the recrystallization of iodide thorium is now in progress.

## RADIATION DAMAGE OF THORIUM

R. E. Adams

A test program has been planned to evaluate the effects of radiation damage on thorium. Because of delays encountered in securing space for irradiation and the time required for cooling before testing, it will be some time before results from the test program are available.

Some preliminary information on radiation damage of thorium has been obtained from tests made on six slugs that had previously been irradiated for another purpose. The slugs were part of a batch of several hundred that were machined from forged and rolled stock sometime during 1948. The slugs were reported to be 4.00 ± 0.010 in. in length, with diameters ranging between 1.355 and 1.360 inches. No other information on the initial size and condition of the individual slugs is available. Thus, data on the effects of radiation damage on these slugs are essentially qualitative.

The slugs were canned in aluminum and irradiated at Hanford early in 1949 at an average neutron flux of $0.7 \times 10^{13}$ neutrons/cm$^2$·sec. They were exposed for 98.5 days and have been stored under water since removal from the pile.

The aluminum cans were removed by dissolution, and dimensions of the slugs were measured by special length and thickness gages. Duplicate measurements could be repeated to within about 0.0003 inch. Length was measured at the center of the slugs, and diameters were measured at several places around and along the slugs. In addition, two or three profile traces were made along the length of each slug. Hardness measurements were also taken by using a conventional hardness tester operated by remote control.

Results of dimensional and hardness measurements on the six slugs are shown in Table 10.

The length measurements indicate that only two of the slugs were not within the given tolerance after irradiation. Since one is longer

**TABLE 10**

**Dimensions and Hardness of Irradiated Thorium Slugs**

| SLUG NO. | LENGTH (in.) | AVERAGE DIAMETER (in.) | AVERAGE HARDNESS (Rockwell B) |
|---|---|---|---|
| 1 | 4.003 | 1.352 | 94 |
| 2 | 3.981 | 1.357 | 81 |
| 3 | 4.006 | 1.359 | 84 |
| 4 | 4.007 | 1.352 | 76 |
| 5 | 4.002 | 1.351 | 87 |
| 6 | 4.013 | 1.352 | 77 |

and the other shorter, it appears that all slugs may not have been made to the specified tolerance. The data do indicate that no serious changes in length occurred during irradiation.

Some variation in diameter of individual slugs was found, but the maximum variation was 0.002 in. in any one slug and consisted only of taper in the slugs. Measured diameters of the slugs average slightly less than the quoted tolerance. Since one slug was almost at the maximum size after irradiation, however, it is again doubtful that the slugs were machined to within the specified tolerance, and it appears that no significant diameter changes occurred.

Profile traces made on the slugs showed no evidence of pits or bumps as great as 0.001 in. in height. Although one trace on a slug showed a slight bow, with the center of the slug being about 0.0015 in. below the two ends, no indication of bowing was found on further traces or traces on other slugs. From these results, it appears that irradiation of thorium under these conditions caused very little, if any, dimensional changes.

Results of the hardness tests show that the irradiated slugs are somewhat harder than normal thorium; however, hardness of thorium is dependent on purity and varies considerably from heat to heat. No hardness data on the slugs in the preirradiated condition is available. As a rough comparison, hardness values quoted for several heats of thorium (produced slightly later than those from which the six slugs were made) ranged between 54 and 80 Rockwell B as-rolled and between 42 and 77 Rockwell B in the annealed condition. Since hardness of the irradiated slugs ranged between 76 and 94 Rockwell B, it appears that some increase in hardness may have occurred as a result of irradiation.

# PREFERRED ORIENTATION OF URANIUM

L. K. Jetter

Examination of the alpha-extruded uranium rods has been completed. Some results of the examination were reported previously,[1,2,3] and textures are summarized and correlated with the fabricating conditions and degree of recrystallization in Table 11.

Rods 1 1/2, 9/10, and 5/8 in. in diameter were extruded through 25-deg conical dies from ingots 3 1/8 in. in diameter at 500°C billet temperature (extrusion ratios, 4.3, 12.1, and 25.0, respectively). The extruded lengths were water-spray quenched as they emerged from the die to retain, insofar as possible, the as-extruded structure. A sample was taken from near the front, middle, and back end of each extruded length and examined in the as-extruded condition. Another sample was taken from near the middle of each extruded length, annealed 1 hr at 550°C, and then examined.

A spherical diffraction specimen 0.500 in. in diameter was machined from each sample so that the center line of the specimen coincided with that of the rod. The spherical surface was lapped to smoothness and electropolished to remove the surface layers deformed by machining and lapping. (The specimen was reduced approximately 0.010 in. in diameter by electropolishing.)

The preferred orientation was determined by the x-ray-diffraction spectrometer technique described in previous reports.[1,4,5] Examination was made on a Norelco Type-12021 Geiger-counter x-ray-diffraction goniometer employing Cu $K\alpha$ radiation. The specimen was rotated at 200 or 360 rpm about its longitudinal axis (the extrusion direction) during exposure.

Plots of the intensity of diffraction vs. the angle $\phi$ between the extrusion direction and the normal to the diffracting plane for various planes for representative specimens are given in Figs. 3 through 20.

The degree of recrystallization was determined from the microstructure and x-ray-diffraction Laue photograms shown in Figs. 21 through 26.

In the as-extruded condition, all samples exhibited a duplex [410]-[010] fiber texture with minor [031], [431], [001], [100] components. Increasing the extrusion ratio resulted in an increase in the strength of the [410] component relative to that of the [010] component with an increase in sharpness of both. (Compare specimens 31, 14, 17.) From the back to the front end of the extruded length of rod given the greatest reduction, there was an increase in the strength of the [410] component relative to that of the [010] component. (Compare specimens 18, 17, 16.)

The degree of recrystallization increased with increase in extrusion ratio and, for the rod given the

(1) *Metallurgy Division Quarterly Progress Report for Period Ending July 31, 1950*, ORNL-827, p. 35-49.

(2) *Metallurgy Division Quarterly Progress Report for Period Ending January 31, 1951*, ORNL-987, p. 17-36.

(3) *Metallurgy Division Quarterly Progress Report for Period Ending July 31, 1951*, ORNL-1108, p. 12-14.

(4) *Metallurgy Division Quarterly Progress Report for Period Ending January 31, 1950*, ORNL-583, p. 37-43.

(5) *Metallurgy Division Quarterly Progress Report for Period Ending January 31, 1952*, ORNL-1267, in press.

TABLE 11

**Fabricating Conditions and Results of Examination of Alpha-Extruded Uranium Rod**

| X-RAY-DIFFRACTION SPECIMEN NO. | EXTRUSION SAMPLE NO. | DIAMETER OF EXTRUDED ROD (in.) | EXTRUSION RATIO | CONDITION | LOCATION OF SAMPLE* | DEGREE OF RECRYSTALLIZATION | TEXTURE | | |
|---|---|---|---|---|---|---|---|---|---|
| | | | | | | | MAJOR | MINOR | TRACE |
| 11 | U9-X1 | 1 1/2 | 4.3 | As-extruded | Front | None | [410]<br>[010] | [031] | [431]<br>[001] |
| 31 | U9-X5 | 1 1/2 | 4.3 | As-extruded | Middle | None | [410]<br>[010] | [031] | [431]<br>[001] |
| 12 | U9-X3 | 1 1/2 | 4.3 | As-extruded | Back | None | [410]<br>[010] | [031] | [431]<br>[001] |
| 13 | U10-X1 | 9/10 | 12.1 | As-extruded | Front | Partial | [410]<br>[010] | | [031]<br>[431]<br>[100] |
| 14 | U10-X2 | 9/10 | 12.1 | As-extruded | Middle | Partial | [410]<br>[010] | | [031]<br>[431]<br>[100] |
| 15 | U10-X3 | 9/10 | 12.1 | As-extruded | Back | Partial | [410]<br>[010] | | [031]<br>[431]<br>[100] |
| 16 | U12-X1 | 5/8 | 25.0 | As-extruded | Front | Complete | [410] | [431]<br>[100] | [010] |
| 17 | U12-X2 | 5/8 | 25.0 | As-extruded | Middle | Nearly complete | [410] | [010] | [431]<br>[100] |
| 18 | U12-X3 | 5/8 | 25.0 | As-extruded | Back | Partial | [410]<br>[010] | | [431]<br>[100] |
| 26 | U9-X4 | 1 1/2 | 4.3 | Annealed | Middle | Complete | [431] | | [410] |
| 52 | U10-X5 | 9/10 | 12.1 | Annealed | Middle | Complete | [431] | [410] | [100] |
| 53 | U12-X6 | 5/8 | 25.0 | Annealed | Middle | Complete | [410] | | [431]<br>[010]<br>[100] |

*Front = 1/4 – Middle = 1/2 – Back = 3/4 of the distance along the extruded length.

greatest reduction, increased from the back to the front end of the extruded length. From this, it would appear that the preferred orientation is related to the grain structure in that the strength of the [410] component increased relative to that of the [010] component with increasing degree of recrystallization.

Upon annealing, the sample initially showing a high degree of recrystallization and a major [410] texture underwent essentially no change, as might be expected. (Compare specimens 17 and 53.) The sample initially exhibiting a deformed structure, and a major [410]-[010] texture developed a single [431] texture upon annealing. (Compare specimens 31 and 26.) It appears then that the recrystallization texture developed in extruded uranium rod is dependent upon the manner in which recrystallization is induced.

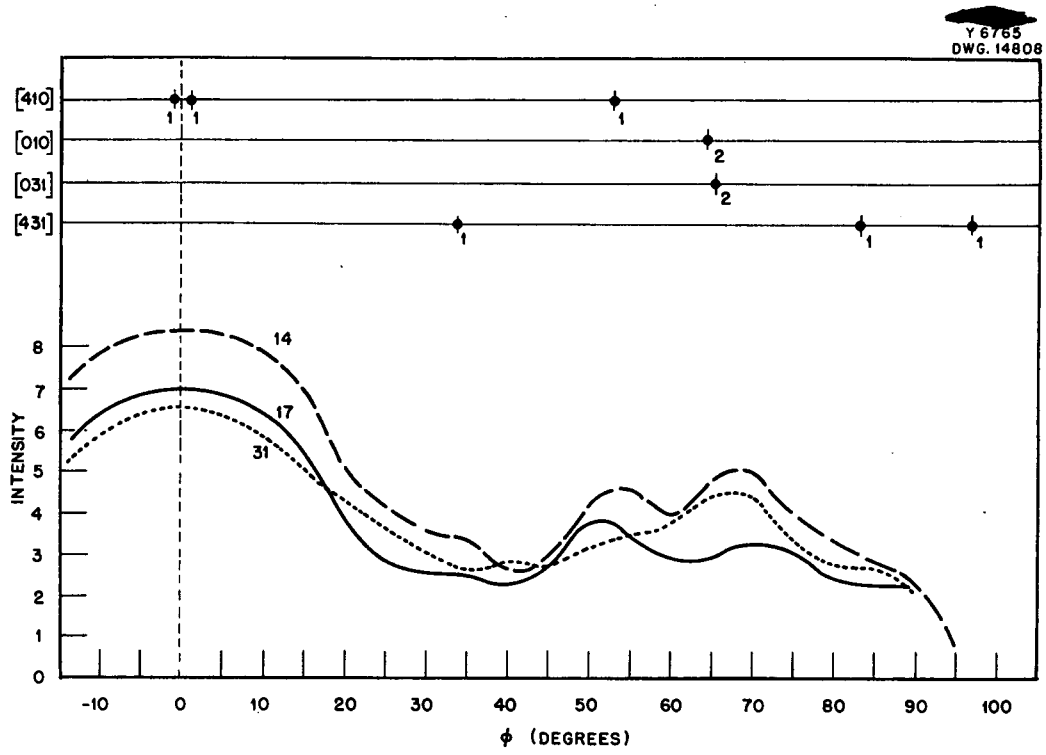


**Fig. 3. Preferred Orientation Plot (110) of Alpha-Extruded Uranium Rod.** Specimen numbers shown on curves.

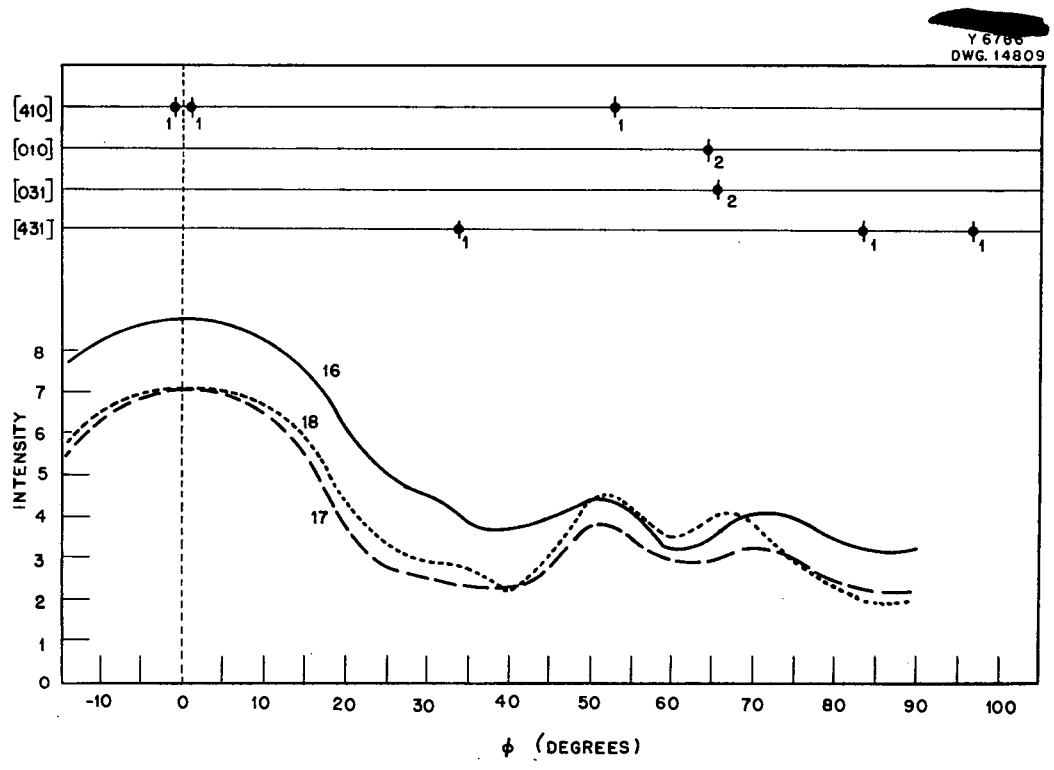


**Fig. 4. Preferred Orientation Plot (110) of Alpha-Extruded Uranium Rod.** Specimen numbers shown on curves.

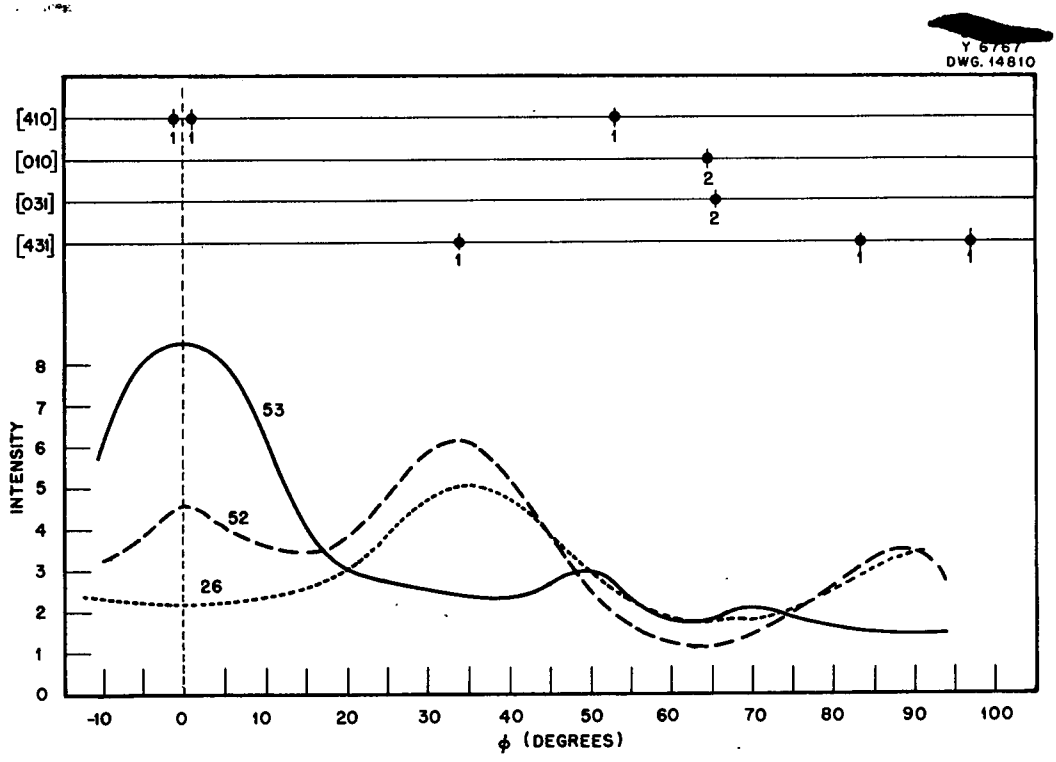


**Fig. 5. Preferred Orientation Plot (110) of Alpha-Extruded Uranium Rod.** Specimen numbers shown on curves.

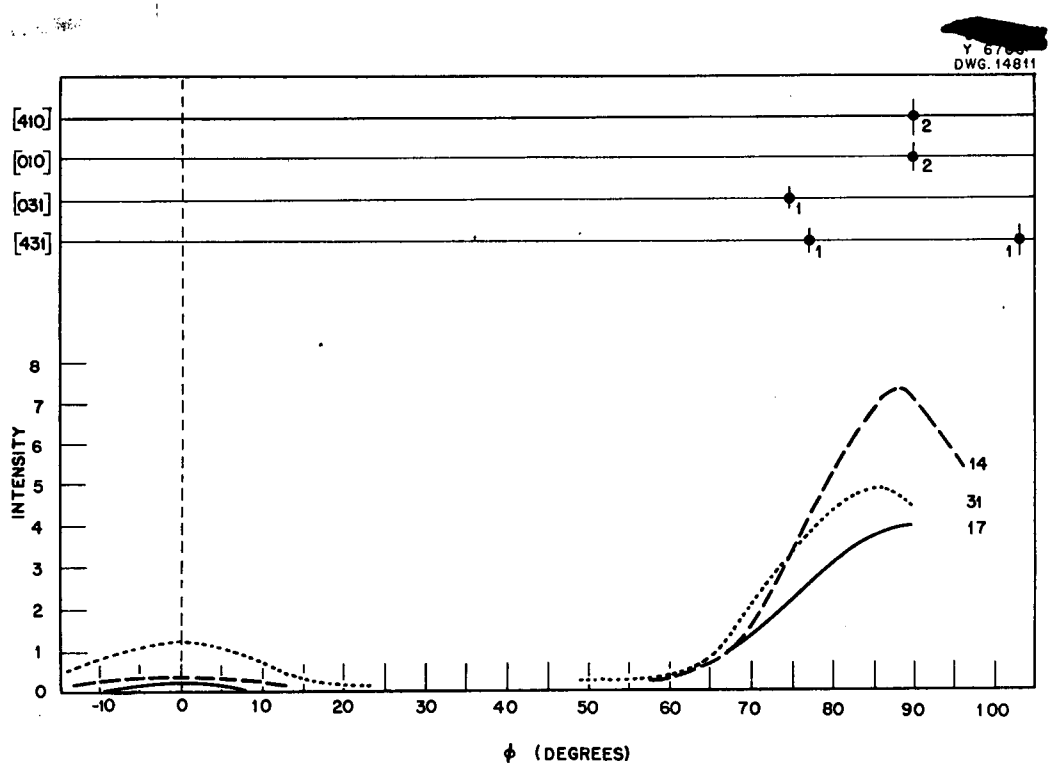


**Fig. 6. Preferred Orientation Plot (002) of Alpha-Extruded Uranium Rod.** Specimen numbers shown on curves.

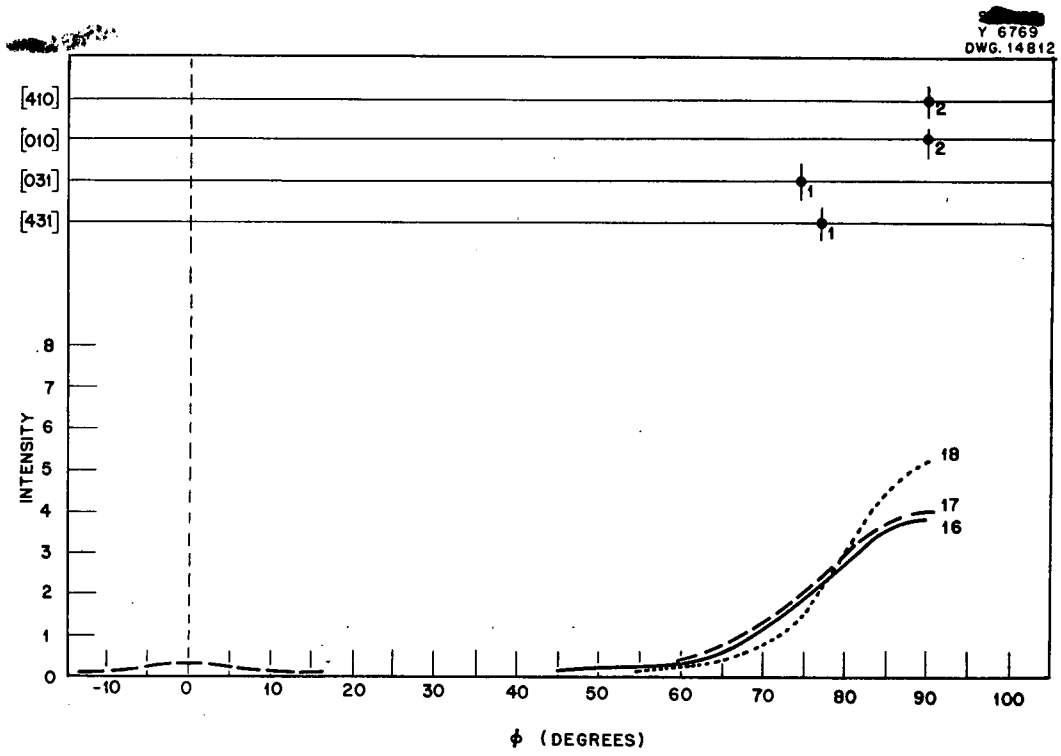


**Fig. 7. Preferred Orientation Plot (002) of Alpha-Extruded Uranium Rod.** Specimen numbers shown on curves.

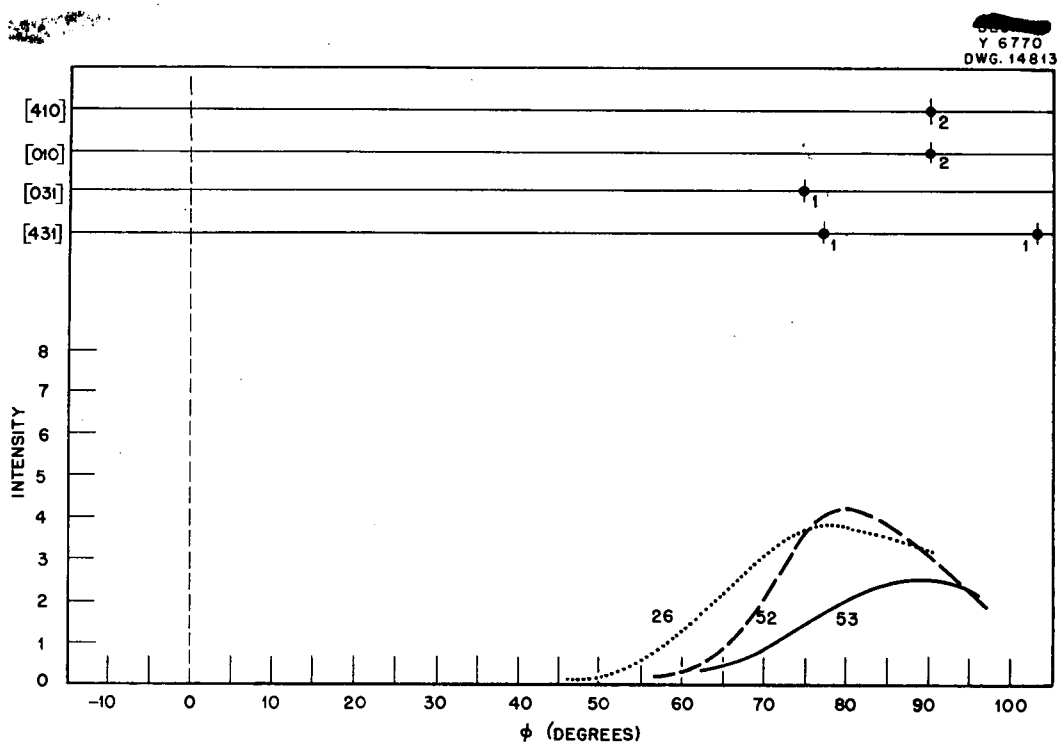


**Fig. 8. Preferred Orientation Plot (002) of Alpha-Extruded Uranium Rod.** Specimen numbers shown on curves.

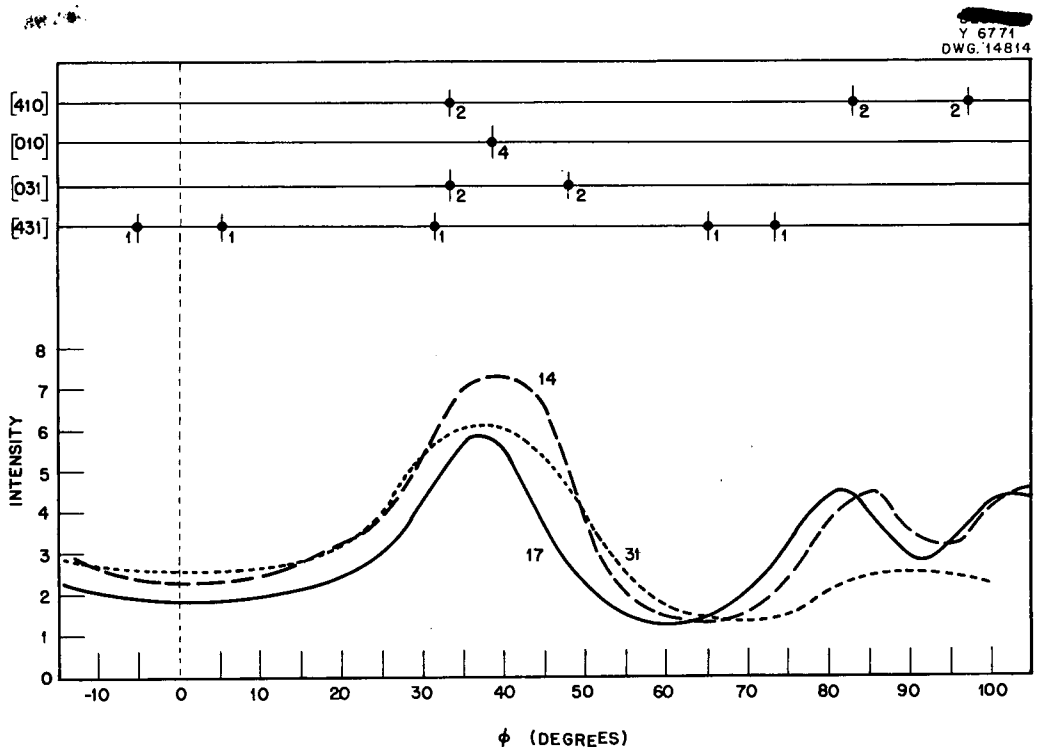


**Fig. 9. Preferred Orientation Plot (131) of Alpha-Extruded Uranium Rod.** Specimen numbers shown on curves.

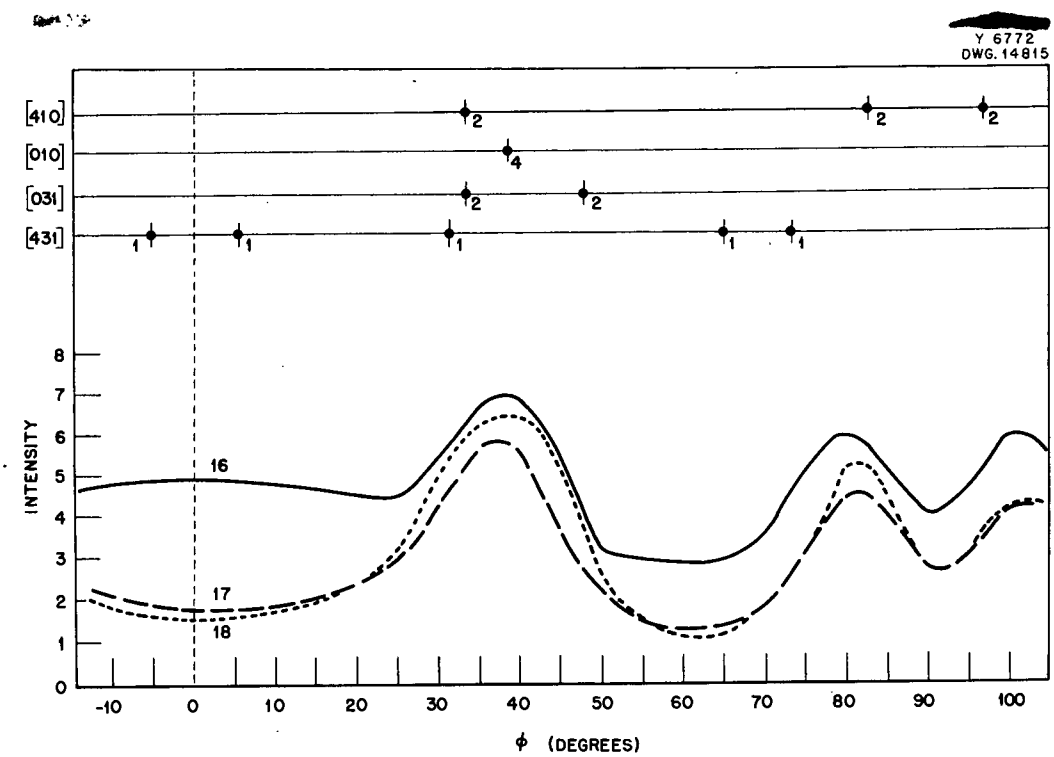


**Fig. 10. Preferred Orientation Plot (131) of Alpha-Extruded Uranium Rod.** Specimen numbers shown on curves.

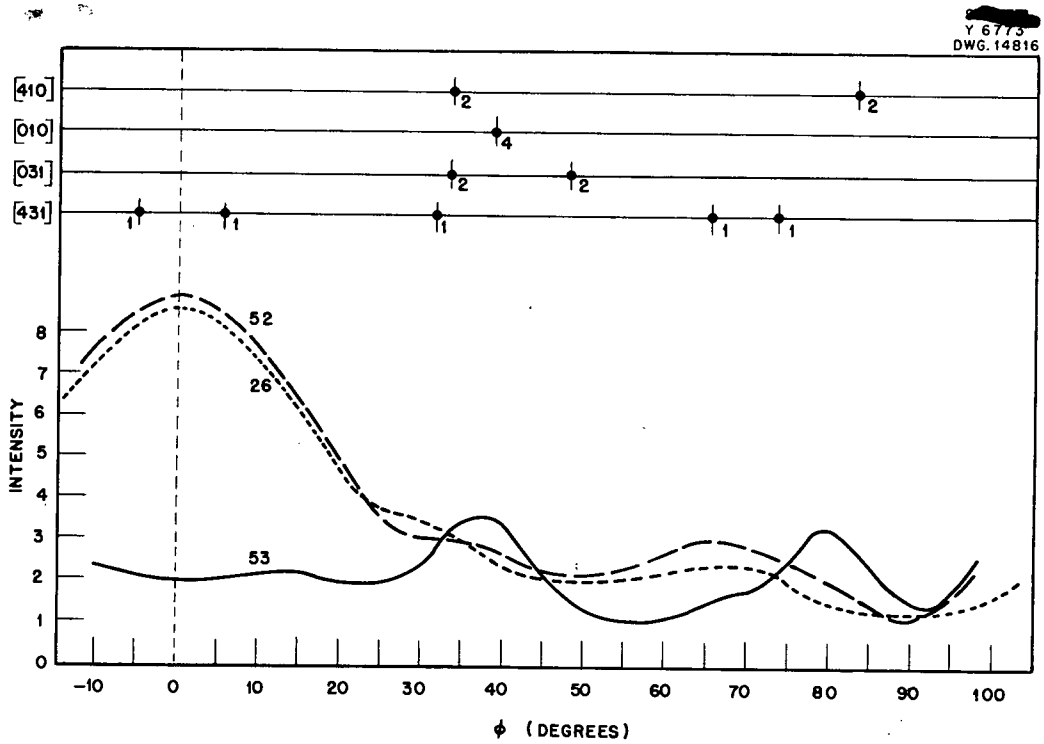


**Fig. 11. Preferred Orientation Plot (131) of Alpha-Extruded Uranium Rod.** Specimen numbers shown on curves.

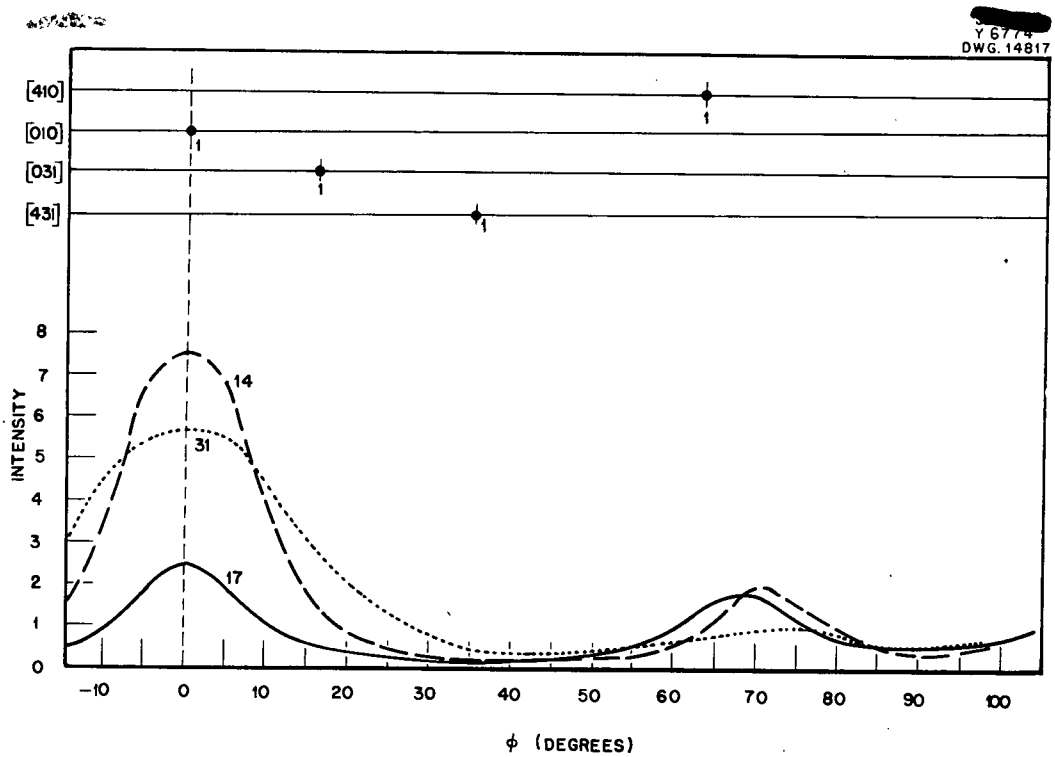


**Fig. 12. Preferred Orientation Plot (040) of Alpha-Extruded Uranium Rod.** Specimen numbers shown on curves.

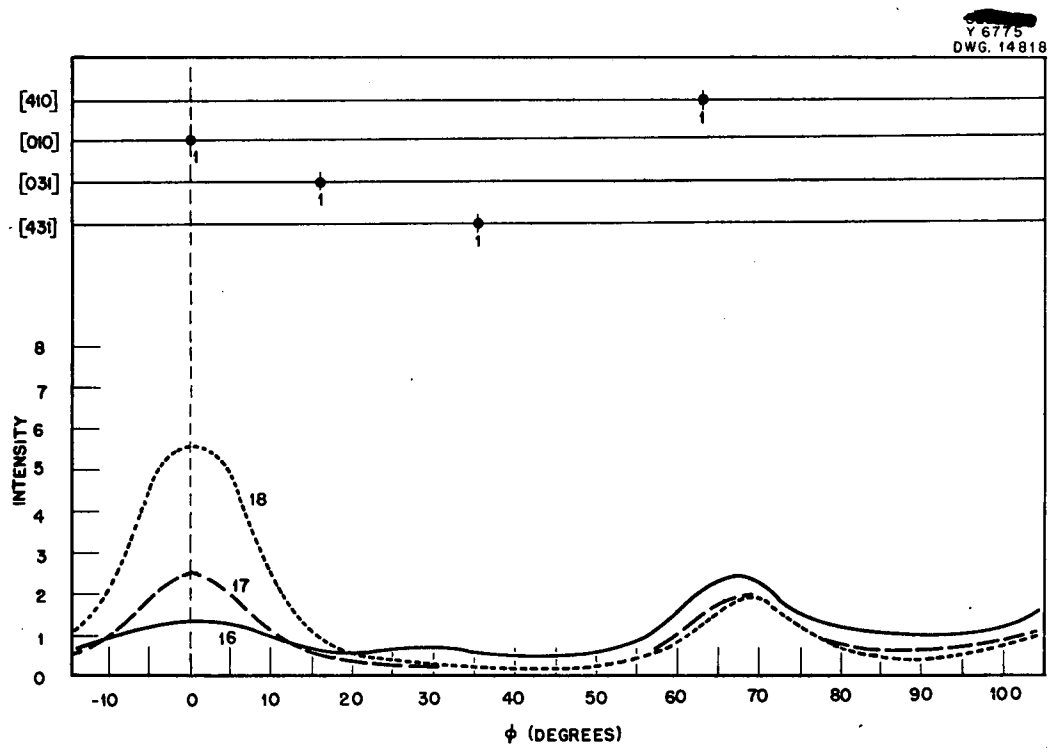


**Fig. 13. Preferred Orientation Plot (040) of Alpha-Extruded Uranium Rod.** Specimen numbers shown on curves.

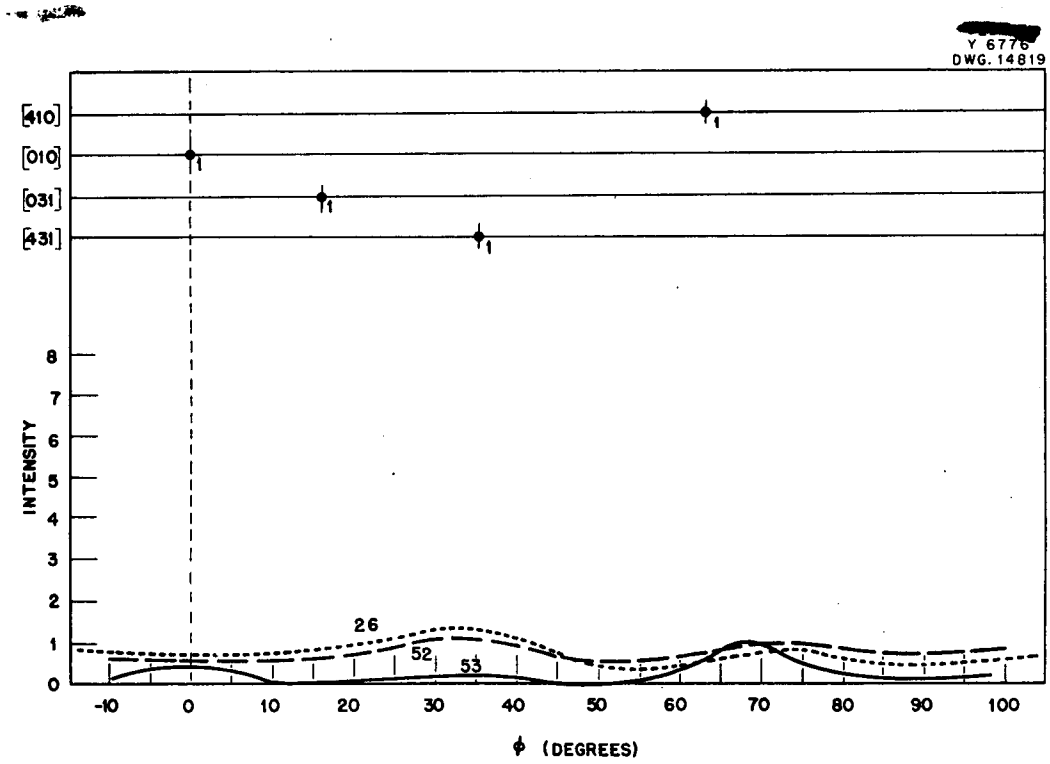


**Fig. 14. Preferred Orientation Plot (040) of Alpha-Extruded Uranium Rod.** Specimen numbers shown on curves.

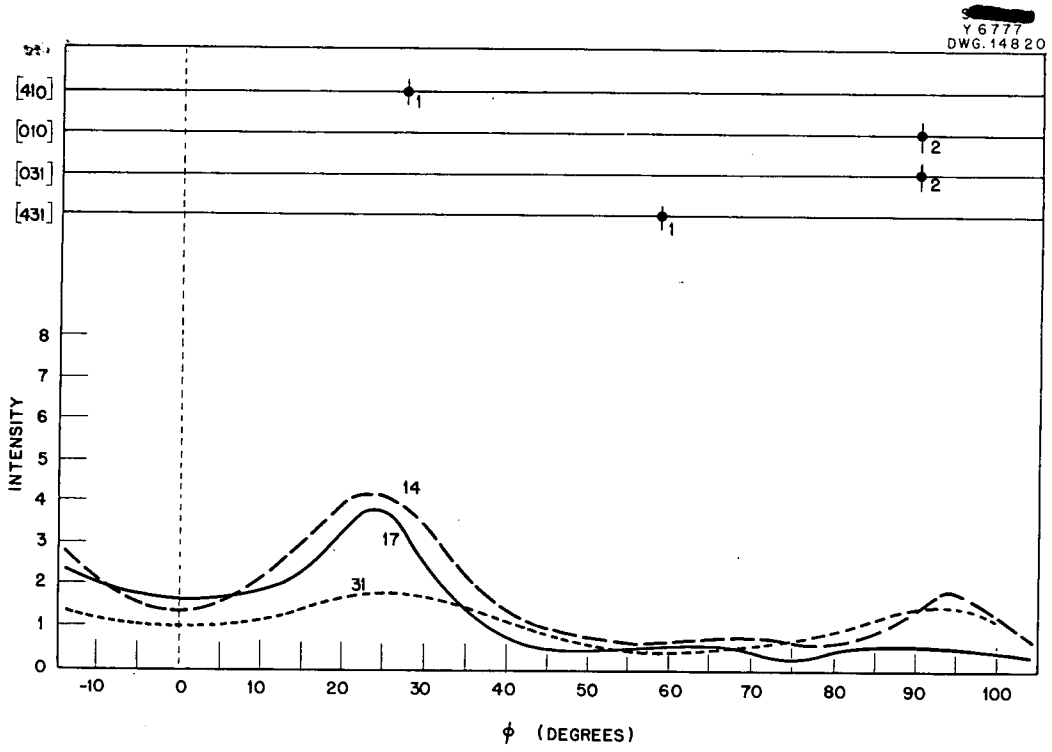


**Fig. 15. Preferred Orientation Plot (200) of Alpha-Extruded Uranium Rod.** Specimen numbers shown on curves.

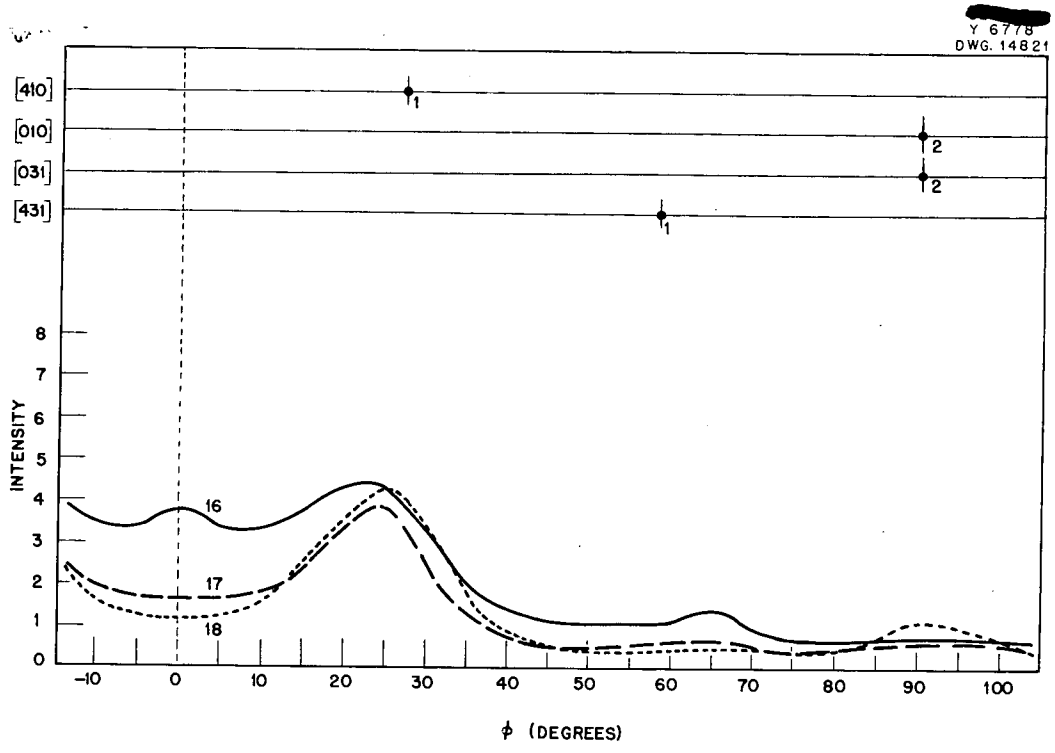


**Fig. 16. Preferred Orientation Plot (200) of Alpha-Extruded Uranium Rod.** Specimen numbers shown on curves.

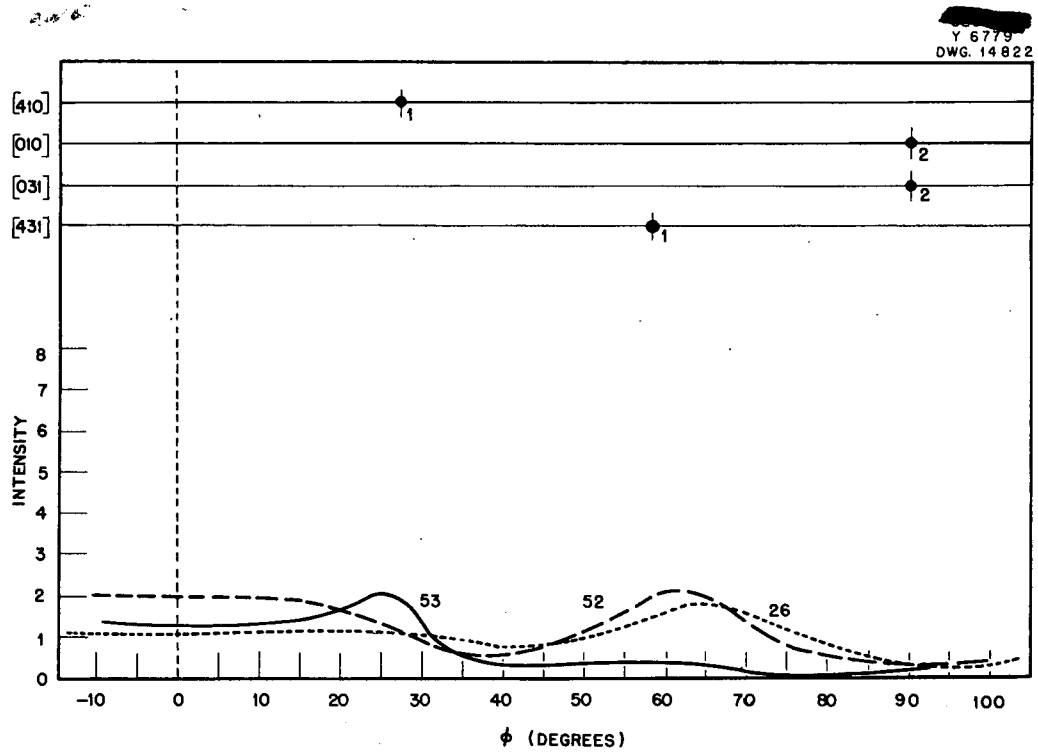


**Fig. 17. Preferred Orientation Plot (200) of Alpha-Extruded Uranium Rod.** Specimen numbers shown on curves.

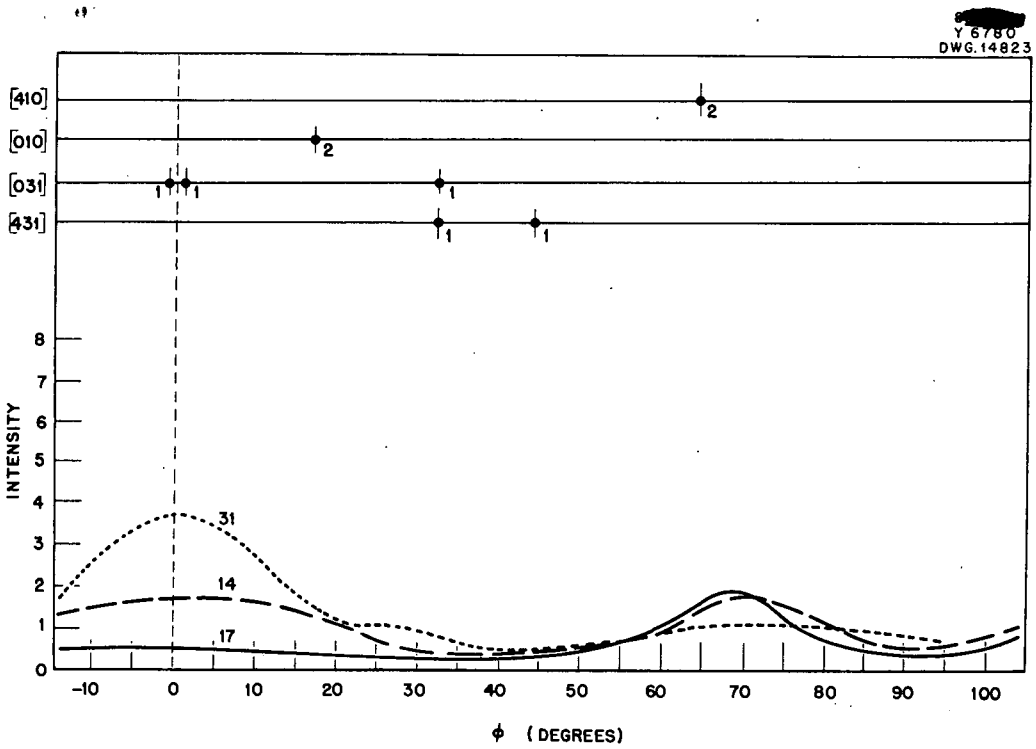


**Fig. 18. Preferred Orientation Plot (041) of Alpha-Extruded Uranium Rod.** Specimen numbers shown on curves.

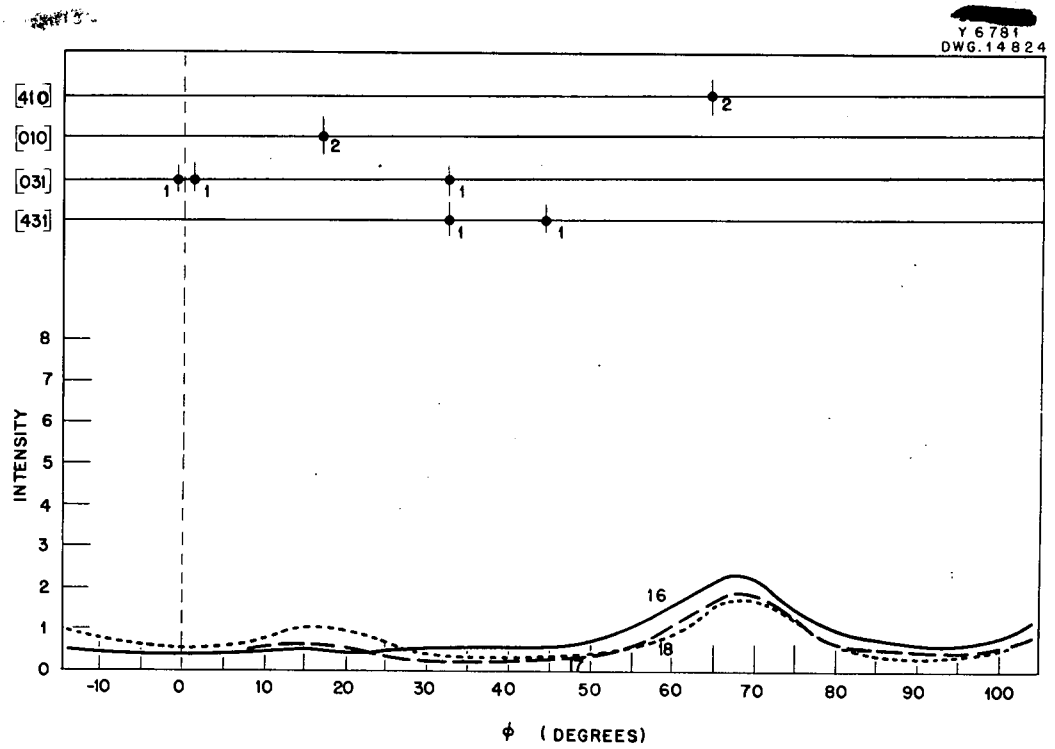


**Fig. 19. Preferred Orientation Plot (041) of Alpha-Extruded Uranium Rod.** Specimen numbers shown on curves.

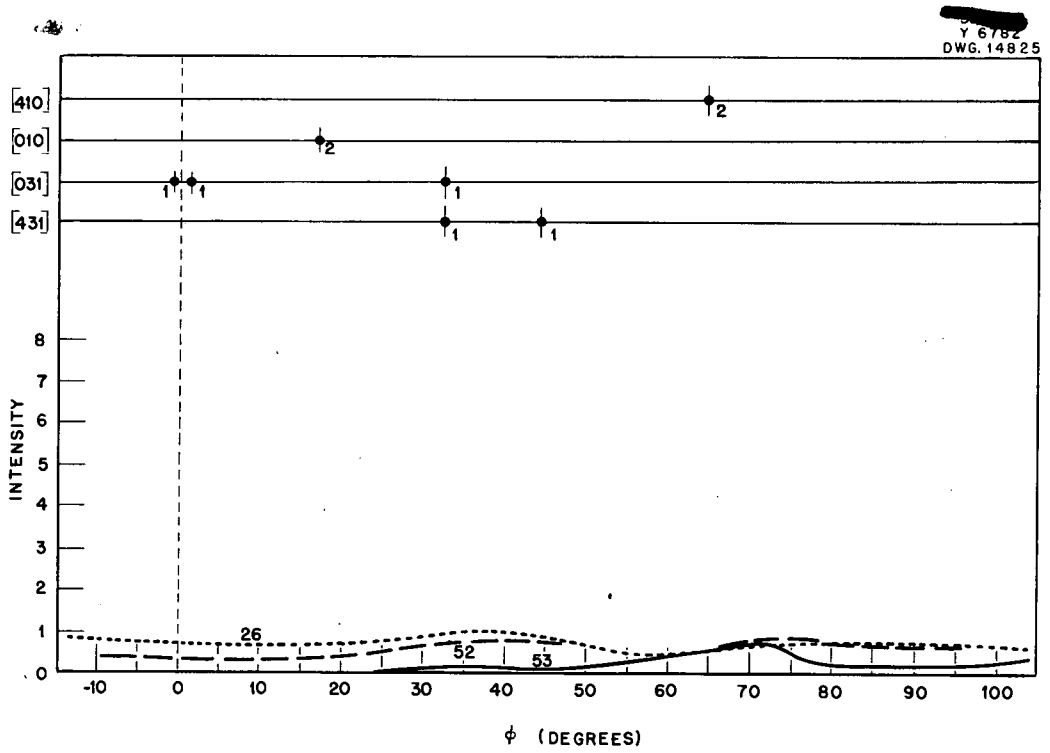


**Fig. 20. Preferred Orientation Plot (041) of Alpha-Extruded Uranium Rod.** Specimen numbers shown on curves.

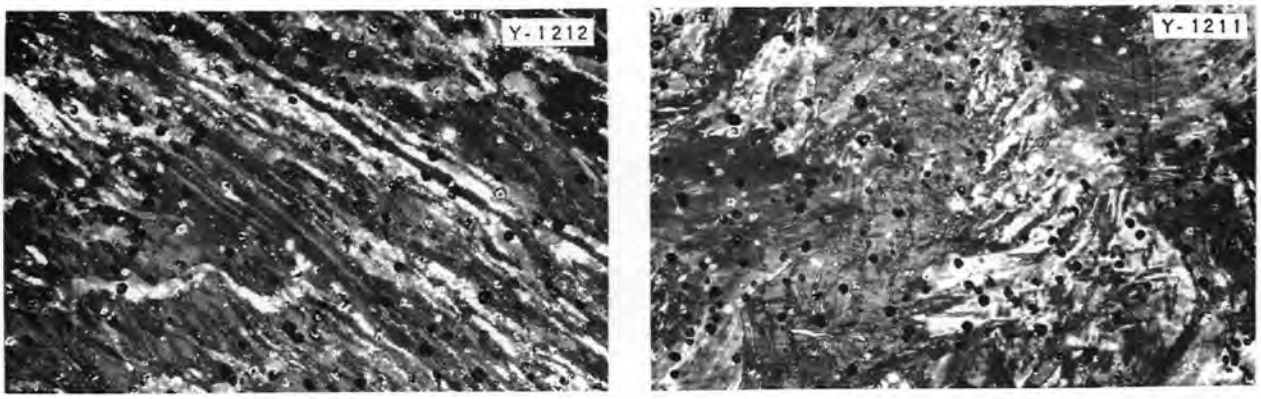


(*a*) 1½-in.-dia extruded rod; middle of extruded length (U9-X5)

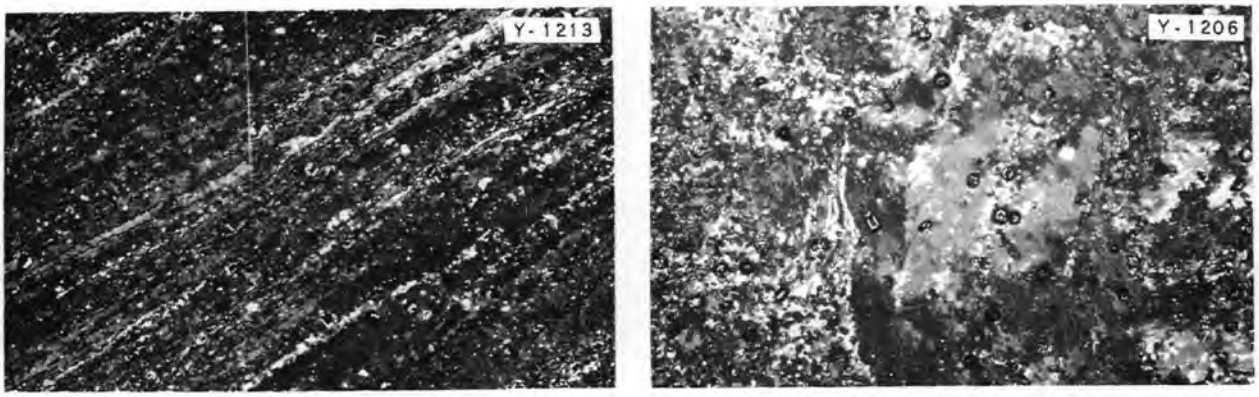


(*b*) 9/10-in.-dia extruded rod; middle of extruded length (U10-X2)

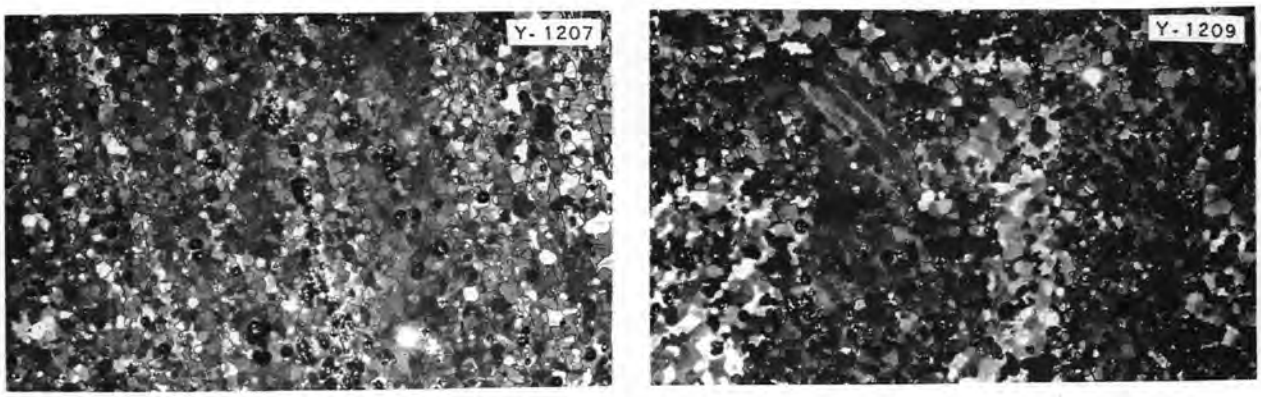


(*c*) 5/8-in.-dia extruded rod; middle of extruded length (U12-X2)

Longitudinal Sections Transverse Sections

**Fig. 21. Photomicrographs Showing the Increase in Degree of Recrystallization with Increasing Extrusion Ratio for Alpha-Extruded Uranium Rod in As-Extruded Condition.**

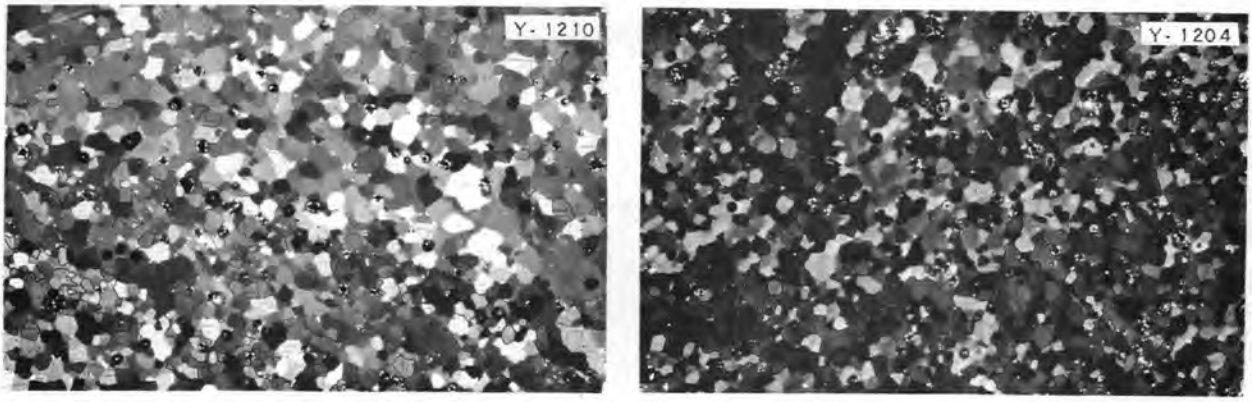


(*a*) 5/8-in.-dia extruded rod; front end of extruded length (U12-X1)

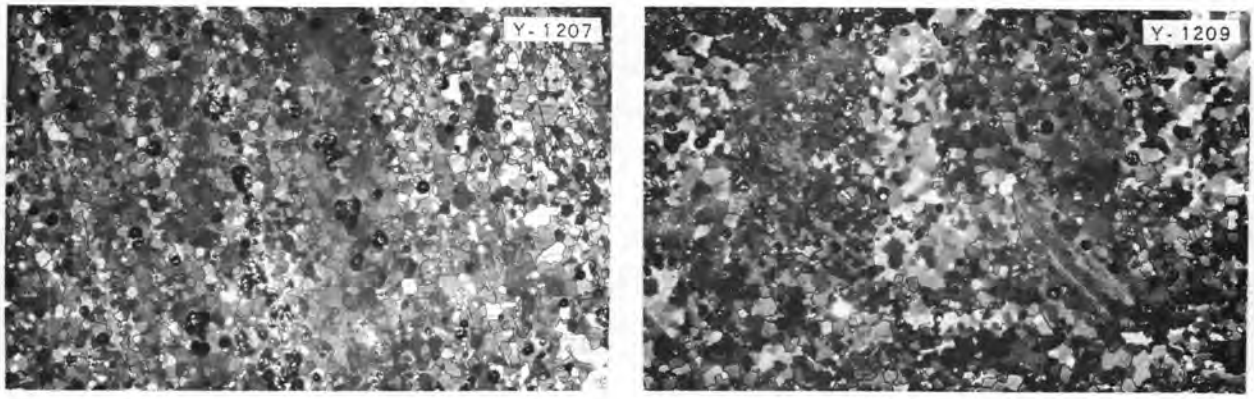


(*b*) 5/8-in.-dia extruded rod; middle of extruded length (U12-X2)

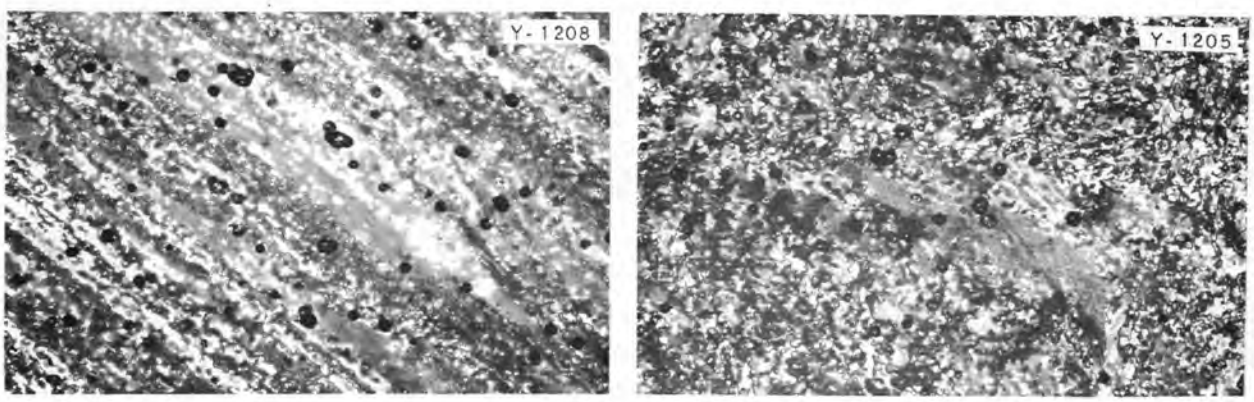


(*c*) 5/8-in.-dia extruded rod; back end of extruded length (U12-X3)

Longitudinal Sections Transverse Sections

**Fig. 22. Photomicrographs Showing the Increase in Degree of Recrystallization from Back to Front End of Alpha-Extruded Uranium Rod in As-Extruded Condition.**

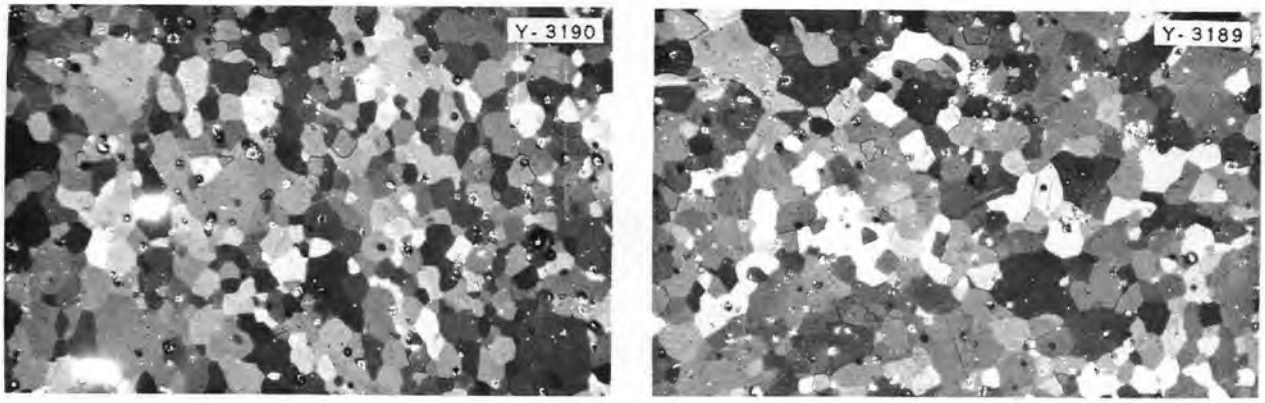


(*a*) 1½-in.-dia extruded rod; middle of extruded length (U9-X4)

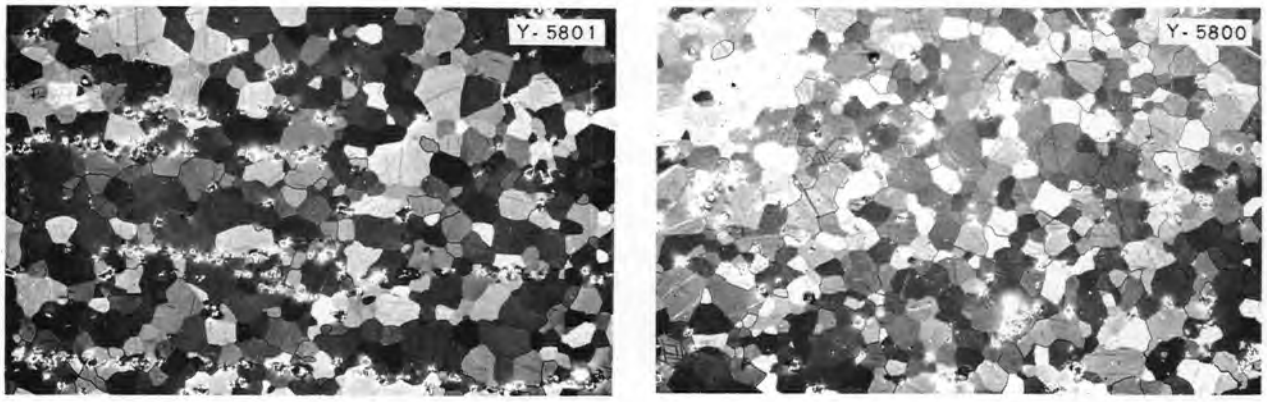


(*b*) 9/10-in.-dia extruded rod; middle of extruded length (U10-X5)

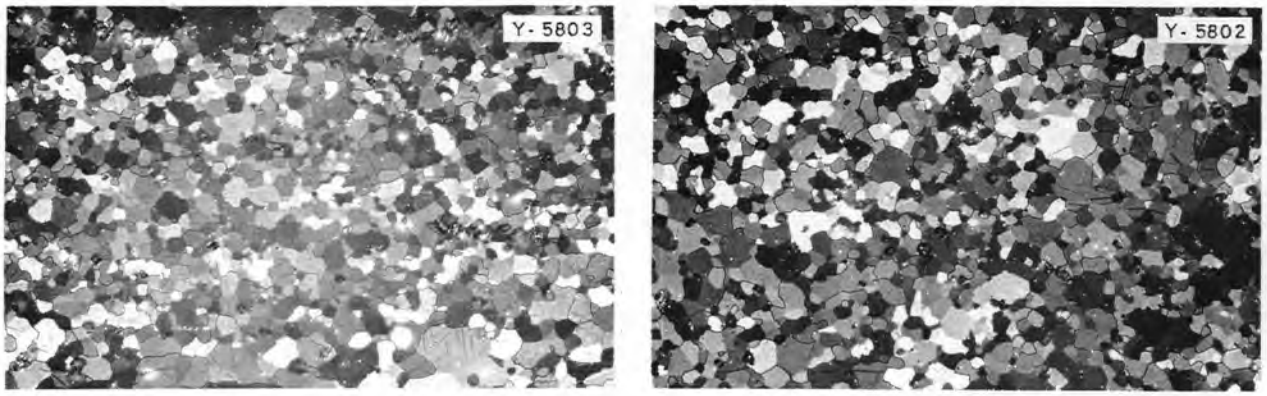


(*c*) 5/8-in.-dia extruded rod; middle of extruded length (U12-X6)

Longitudinal Sections Transverse Sections

**Fig. 23. Photomicrographs Showing the Completely Recrystallized Grain Structure of Alpha-Extruded Uranium Rod in Annealed Condition (1 hr at 550°C).**

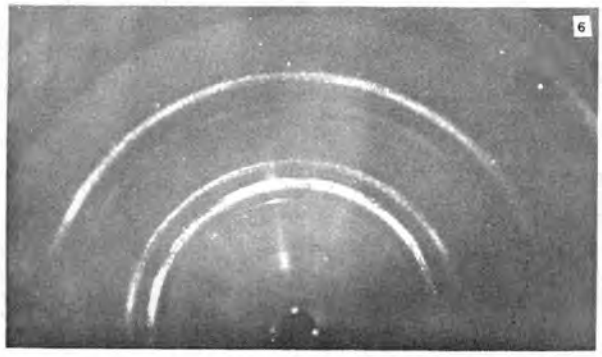


(*a*) 1½-in.-dia extruded rod; middle of extruded length (U9-X5); specimen 6

(*b*) 9/10-in.-dia extruded rod; middle of extruded length (U10-X2); specimen 14

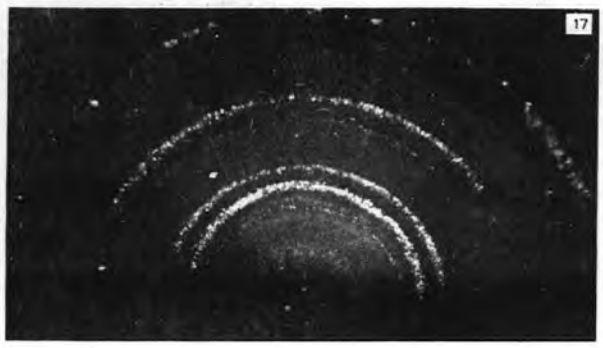


(*c*) 5/8-in.-dia extruded rod; middle of extruded length (U12-X2); specimen 17

**Fig. 24. Laue Photograms Showing the Increase in Degree of Recrystallization with Increasing Extrusion Ratio in Alpha-Extruded Uranium Rod in As-Extruded Condition.**

(*a*) 5/8-in.-dia extruded rod; front end of extruded length (U12-X1); specimen 16

(*b*) 5/8-in.-dia extruded rod; middle of extruded length (U12-X2); specimen 17

(*c*) 5/8-in.-dia extruded rod; back end of extruded length (U12-X3); specimen 18

**Fig. 25. Laue Photograms Showing the Increase in Degree of Recrystallization from Back to Front End of Alpha-Extruded Uranium Rod in As-Extruded Condition.**

(*a*) 1½-in.-dia extruded rod; middle of extruded length (U9-X4); specimen 26

(*b*) 9/10-in.-dia extruded rod; middle of extruded length (U10-X5); specimen 52

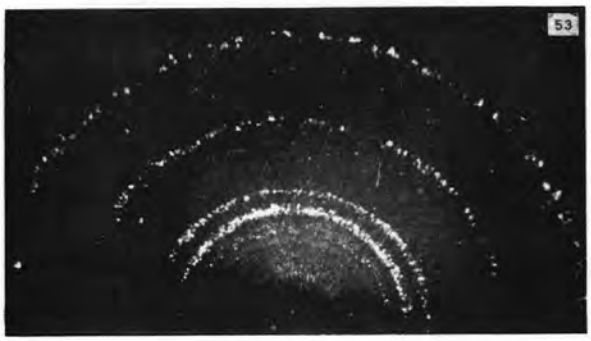


(*c*) 5/8-in.-dia extruded rod; middle of extruded length (U12-X6); specimen 53

**Fig. 26. Laue Photograms Showing the Completely Recrystallized Grain Structure of Alpha-Extruded Uranium Rod in Annealed Condition (1 hr at 550°C).**

# ANP PROGRAM

W. D. Manly

## STATIC CORROSION

D. C. Vreeland L. D. Dyer
R. B. Day E. E. Hoffman

**Corrosion by Fluorides.** A series of screening tests of various materials in molten fluoride No. 14 (composition: 43.5 mole % KF, 44.5 mole % LiF, 10.9 mole % NaF, and 1.1 mole % $UF_4$) have been completed. The tests were run with dehydrated, unpretreated fluoride mixture for 100 hr at 816°C under vacuum. Molybdenum, columbium, Monel, and Stellite No. 25 were apparently unattacked (Fig. 27). All the 300-series stainless steels tested (types-310, -317, -321, -347, and -304 ELC) were attacked to a depth of 1 mil or less, as shown in Fig. 28, except type-304 ELC, which was attacked to a depth of 2 mils. None of the 400-series stainless steels were attacked over 1 mil. *Z* nickel, which was the most severely attacked material of those tested, being affected to a depth of 5 mils, is shown in Fig. 29. The extent of attack on Inconel is shown in Fig. 30. The details of these tests are presented in Table 12.

Static corrosion tests of several materials in fluoride No. 14 with approximately 10% additions of zirconium, sodium, and uranium have been run for 100 hr at 816°C. These additions appeared to have some effect in inhibiting corrosion. Inconel, type-321 stainless steel, and *A* nickel were the materials used. Specimens and tubes from the tests with zirconium and uranium additions had developed surface layers, as shown in Fig. 31. *A* nickel in the sodium-addition test showed some evidence of developing a surface layer. No surface layer was apparent on either Inconel or type-321 stainless steel in the sodium-addition tests, but it is possible that a surface layer may have been inadvertently removed during stripping. Type-321 stainless steel and *A* nickel were not attacked in this series of tests. Inconel was unattacked in the sodium-addition test, and only slightly attacked in the uranium- and zirconium-addition tests. In a previous test with type-309 stainless steel in fluoride No. 14 with a zirconium addition, a surface layer was developed. This layer was examined by x rays and reported to be composed of $UO_2$ and $ZrO_2$. The results of the most recent tests are summarized in Table 13. Tests are now under way using additions of Li, K, Ca, Ti, and Mn.

Temperature-dependence tests in fluoride No. 14 have been completed. Inconel and types-430, -304, and -321 stainless steels have been tested for 100 hr at 538, 704, and 1000°C. Maximum penetrations of both tubes and specimens are listed in Table 14. The results of previous tests of these materials at 816°C are also included for comparison. It would appear that in static corrosion tests with these materials there is little or no effect on the extent of corrosion that can be traced to varying the temperature within the range used. Inconel and type-304 stainless steel appear to be corroded slightly more at the higher temperatures, but corrosion in all tests was so light that the differences may easily have been caused by the inevitable variations in the metal specimens themselves.

Apparently the phenomenon of sensitization occurring in type-304 stainless steel and Inconel has little or no effect on corrosion by the

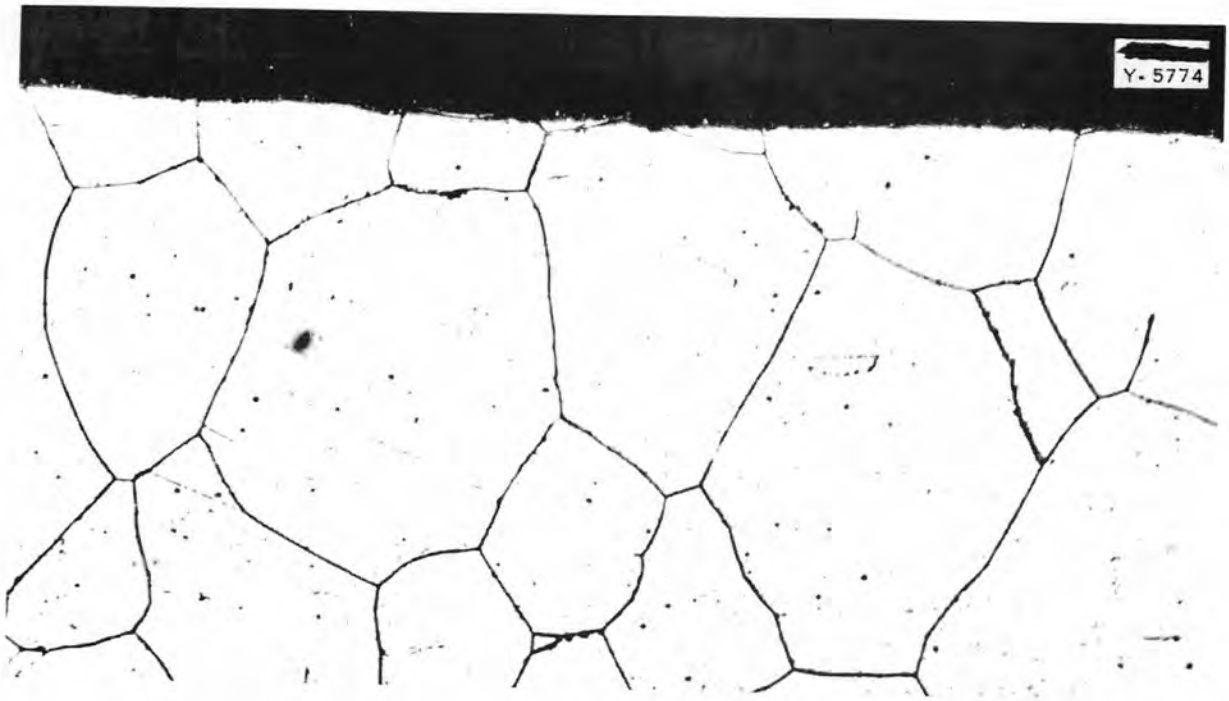


Fig. 27. Stellite No. 25 After Exposure to Fluoride No. 14 for 100 hr at 816°C in Vacuum. 250X.

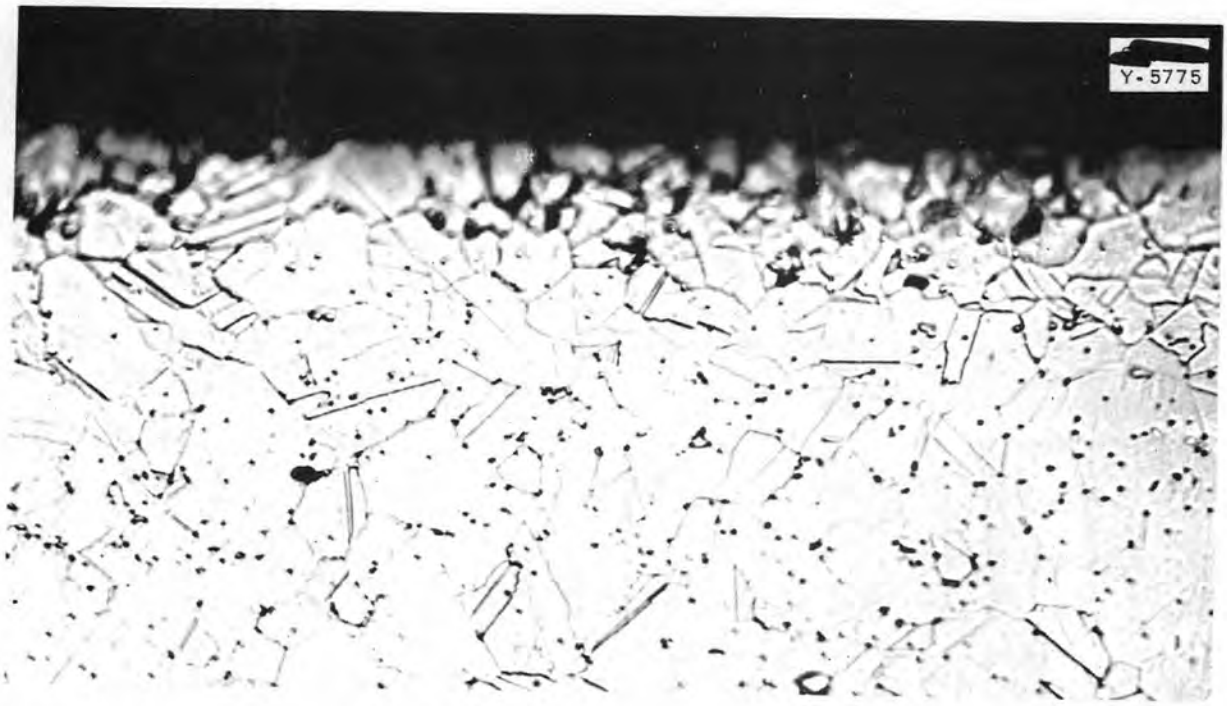


Fig. 28. Type-347 Stainless Steel After Exposure to Fluoride No. 14 for 100 hr at 816°C in Vacuum. 750X.

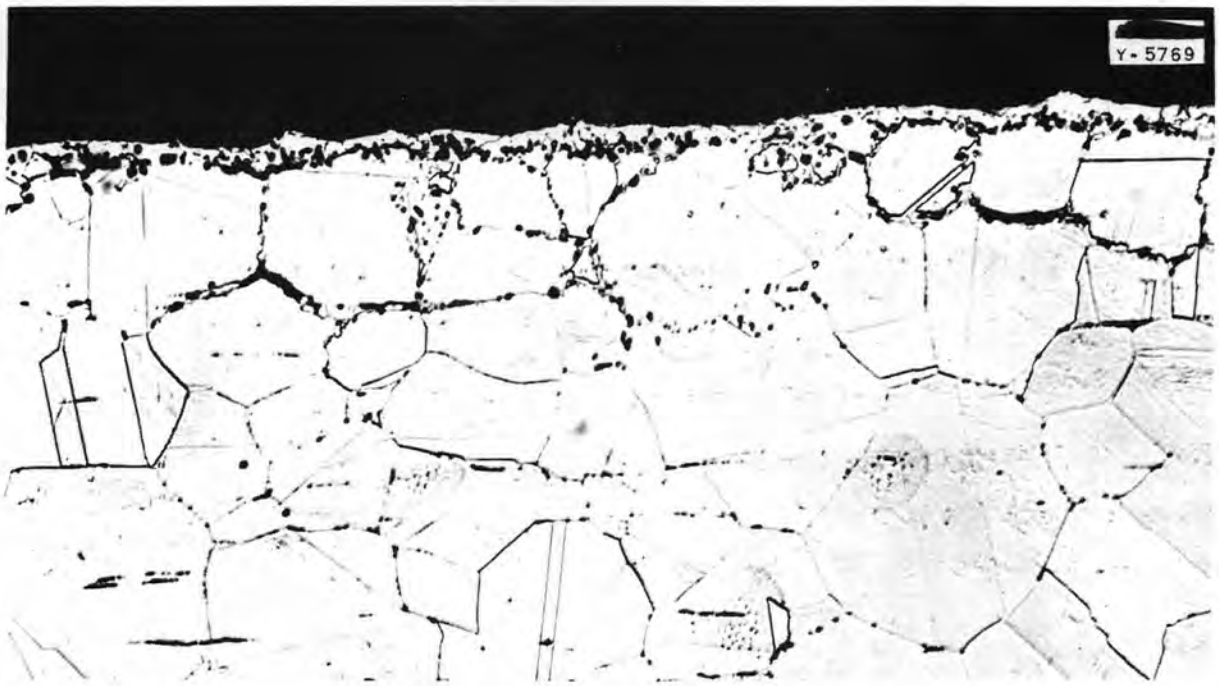


**Fig. 29.** *Z* **Nickel After Exposure to Fluoride No. 14 for 100 hr at 816°C in Vacuum.** 250X.

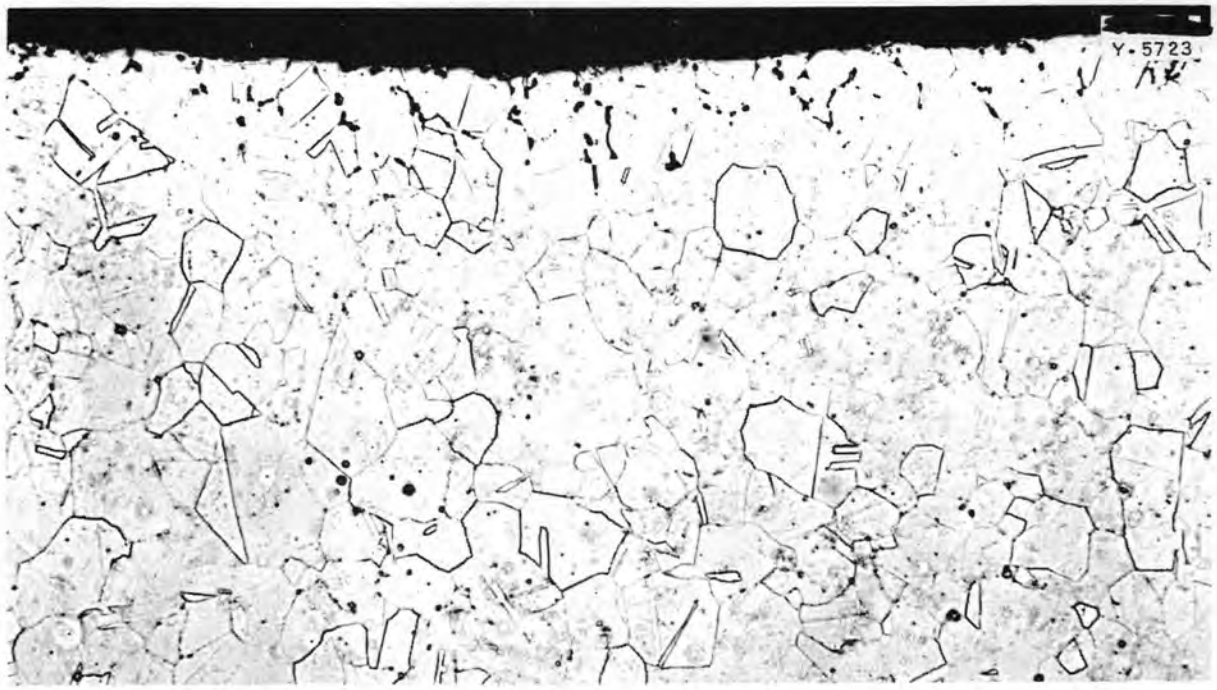


**Fig. 30. Inconel After Exposure to Fluoride No. 14 for 100 hr at 816°C in Vacuum.** 200X.

TABLE 12

Corrosion of Various Materials Tested in Fluoride No. 14 at 816°C for 100 hr in Vacuum

| MATERIAL | DEPTH OF METAL AFFECTED (mils) | METALLOGRAPHIC NOTES |
|---|---|---|
| Globe iron | 2 | Surface of specimen very rough |
| Molybdenum | | Surface of specimen roughened |
| Type-310 stainless steel | 1 | Subsurface voids |
| Type-317 stainless steel | 1 | Intergranular penetration |
| Type-321 stainless steel | 0 to $\frac{1}{2}$ | Intergranular penetration |
| Type-347 stainless steel | 1 | Subsurface voids |
| Type-430 stainless steel | 1 | Slight intergranular penetration and decarburization |
| Type-446 stainless steel | 1 | Subsurface voids |
| Hastelloy B | 0 to $\frac{1}{4}$ | Subsurface voids |
| Hastelloy C | 2 | Subsurface voids |
| Inconel X | 1 | Subsurface voids |
| Stellite 25 (L-605) | | No visible attack |
| Z Nickel | 5 | Voids along grain boundaries |
| Tantalum | 1 | Surface of specimen roughened |
| Columbium | | Surface of specimen roughened |
| Monel | | No apparent attack |
| Nichrome V | 3 | Subsurface voids; some following grain boundaries |
| Inconel | 3 | Subsurface voids; some following grain boundaries |
| Type-304 ELC stainless steel | 2 | Subsurface voids; some following grain boundaries; attack somewhat irregular |
| Nickel plus $\frac{1}{4}$% zirconium | | Specimen unattacked except for a large amount of intergranular voids at one end; test being repeated |

fluoride mixtures under the testing conditions employed. The temperature range for sensitization is usually accepted as 400 to 850°C. The first three test temperatures in Table 14 are within this range. The final test temperature of 1000°C is well over the sensitization range, and yet no significant reduction of corrosion can be noted.

A specimen of type-304 stainless steel that had been electroplated with approximately 8 mils of nickel was lightly cut along one face with a hacksaw to expose the base metal. The specimen was then tested in fluoride No. 14 for 100 hr at 816°C in vacuum. The nickel plating was apparently unattacked, although many voids that may have occurred during plating could

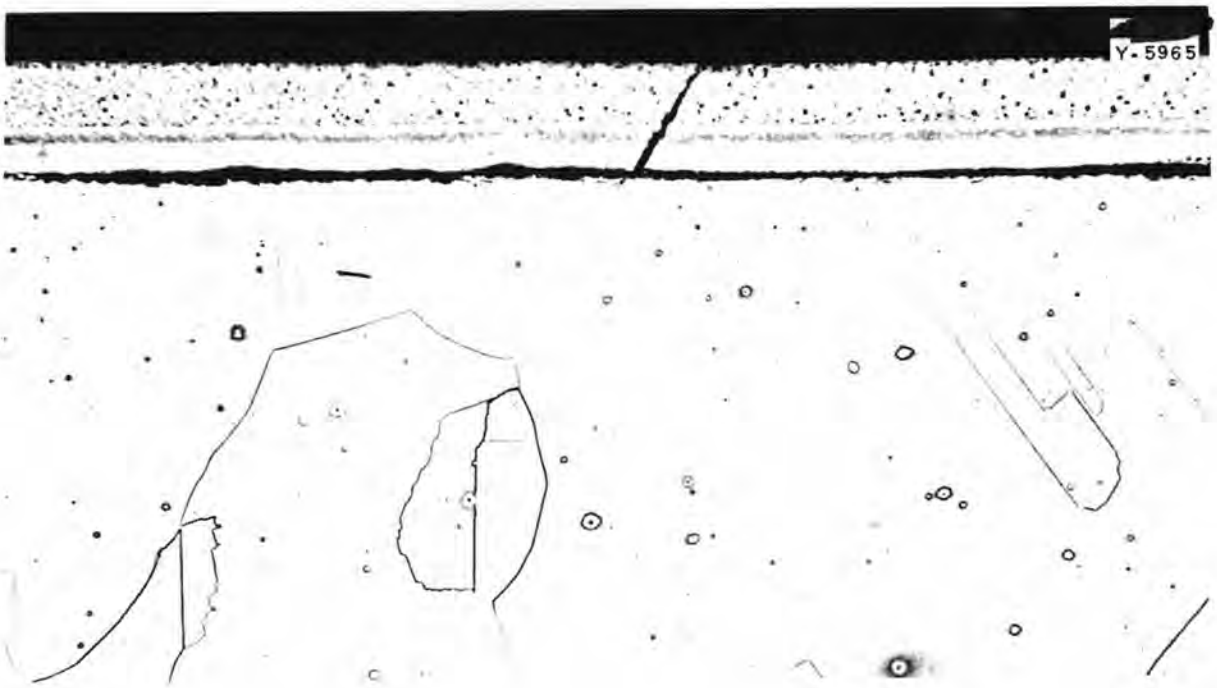


**Fig. 31. *A* Nickel After Exposure to Fluoride No. 14 Plus 10% Zirconium for 100 hr at 816°C in Vacuum.** Note multiphase surface layer. 200X.

**TABLE 13**

**Effect of Approximately 10% Additions of Zirconium, Sodium, and Uranium to Fluoride No. 14 in Static Corrosion Tests at 816°C for 100 hr in Vacuum**

| MATERIAL | ADDITION | METALLOGRAPHIC NOTES |
|---|---|---|
| Type-321 stainless steel | Zr | 1/2-mil surface layer on specimen and tube; no attack |
| Inconel | Zr | 1 1/2-mil surface layer on specimen and tube; subsurface voids to 1 mil under surface layer |
| *A* Nickel | Zr | 2 1/2-mil surface layer; no attack under layer |
| Type-321 stainless steel | Na | No attack |
| Inconel | Na | No attack |
| *A* Nickel | Na | 1/2-mil surface layer on tube only; no attack |
| Type-321 stainless steel | U | 2- to 3-mil surface layer; no attack under layer |
| Inconel | U | 1- to 2-mil surface layer; voids to 1 mil under layer |
| *A* Nickel | U | 2-mil surface layer; no attack under layer |

TABLE 14

**Maximum Penetration of Materials Tested at Various Temperatures in Fluoride No. 14 for 100 Hours**

| MATERIAL | MAXIMUM PENETRATION (mils) | | | | | | | |
|---|---|---|---|---|---|---|---|---|
| | 538°C | | 704°C | | 816°C | | 1000°C | |
| | SPECIMEN | TUBE | SPECIMEN | TUBE | SPECIMEN | TUBE | SPECIMEN | TUBE |
| Inconel | Slight roughening | Slight roughening | 4 | 1½ | 1½ | 3 | 3 | 3 |
| Type-430 stainless steel | <1 | <1 | ½ | ½ | ¼ | ¼ | Specimen lost | No attack |
| Type-304 stainless steel | <1 | <1 | 2 | 1½ | 2 | 2 | 1½ | 1 |
| Type-321 stainless steel | <1 | <1 | <1 | <1 | ½ | ½ | 1½ | 1½ |

be noted. At the sawcuts, the type-304 stainless steel appeared to be more severely attacked than any other corrosion specimen yet tested in fluoride. There was approximately 12 mils of what could be either corrosion product or unremoved fluoride. Beneath this was 15 mils of severe intergranular attack. A photomicrograph of the specimen is shown in Fig. 32. The results of this test might be interpreted as indicating that an electrochemical type of attack had taken place. Where it has been established that electrochemical attack takes place in aqueous corrosion, it is well known that if a metal is coated with a more noble metal and then the coating is broken to expose a relatively small area of the anodic material beneath the cathodic coating, the small exposed area will suffer from accelerated corrosive attack. It would appear that a similar process had taken place in the test with molten fluoride.

**Corrosion by Hydroxides.** A series of tests in sodium hydroxide of some specimens of Inconel and Inconel X that were plated with different thicknesses of nickel by the International Nickel Company has been completed. All the specimens with platings under 4 mils were severely attacked, as shown in Fig. 33. Several of the specimens with thicker platings were unattacked, even though the nickel plating appeared to have many voids, as shown in Fig. 34. Nickel plating as a means of protecting materials against attack by hydroxides does not appear to be entirely dependable. When protection is afforded, it is complete and excellent; but when this protection is not complete, attack is very severe. The plated specimens used were vacuum-diffusion heat treated before test. Tests were for 100 hr at 816°C in vacuum. A summary of metallographic observations is listed in Table 15.

There was some indication in several tests that when Inconel is tested in sodium hydroxide, additions of manganese may be beneficial in inhibiting attack. This effect was first noticed when Inconel tube and header assemblies brazed with a 60% Mn-40% Ni brazing

alloy were tested for the Welding and Brazing Section. When tested in regular static corrosion tests with sodium hydroxide, Inconel is severely attacked, and the entire thickness of a 35-mil specimen is often affected. In order to check the possible inhibiting characteristics of manganese, static corrosion tests were run with approximately 4 and 1 1/2% additions of manganese powder and a 1 1/2% addition of electrolytic manganese. Two tests were also run in which the sodium hydroxide was pretreated by heating in the presence of electrolytic manganese for 24 hr at 816°C before test. After pretreatment the sodium hydroxide analyzed 1% manganese. The manganese additions did seem to have some inhibiting effect on corrosive attack, and the manganese powder additions were the most effective; however, corrosion was still quite severe even with these additions. A specimen from one of the tests (100 hr, 816°C, vacuum) in which manganese powder was added to the sodium hydroxide is shown in Fig. 35. Table 16 summarizes the results of these tests.

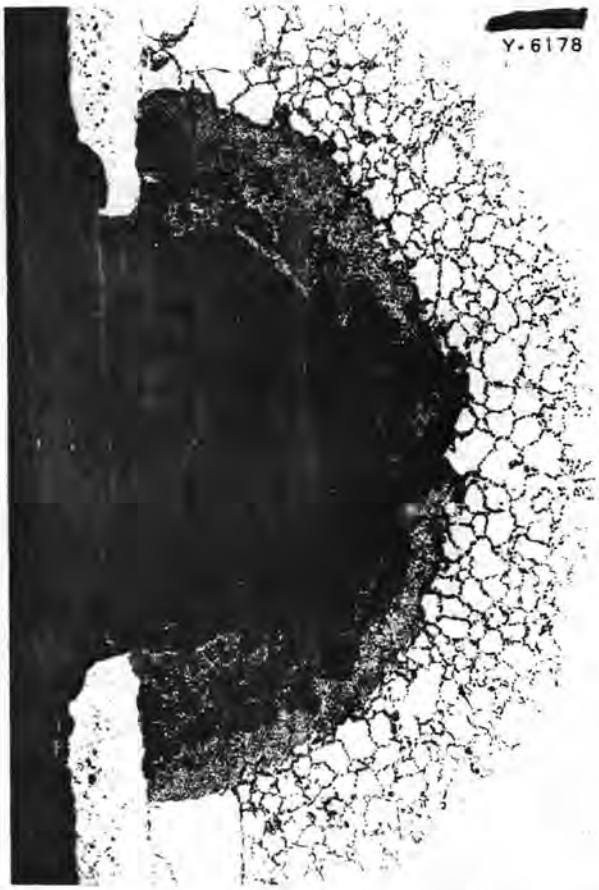


**Fig. 32. Nickel-Plated Type-304 Stainless Steel Exposed to Fluoride No. 14 for 100 hr at 816°C in Vacuum.** Photograph taken after nickel plating had been cut away to expose the base metal. 50X.

A nickel-zirconium alloy (1/4% zirconium) was tested in sodium hydroxide. This alloy has attracted attention because of its better physical properties at high temperature as compared with pure nickel. The results of the static corrosion test (100 hr, 816°C, vacuum) were encouraging. The only attack that could be noted was 1/2 mil of light intergranular penetration.

**Uranium Solubility in Sodium Cyanide.** Several tests have been run in an effort to determine the solubility of uranium in sodium cyanide. It was considered necessary to filter the molten sodium cyanide after a soaking period at high temperature to eliminate any particles of uranium that might be present, so the tests were conducted in the following manner. A piece of 1/2-in.-OD type-1035 steel tubing with an iron filter welded at the center was used as the test container. At the start of each test sodium cyanide containing uranium turnings was sealed into the lower end of the tube. After holding for 100 hr at 816°C, the tube was inverted and held for 24 hr at 816°C in order to allow the molten sodium cyanide to filter into the other end of the test tube. When the filtering was completed, the tube was allowed to cool. The sodium cyanide was then removed and analyzed for uranium. The analyses of the three tests are listed in Table 17. Since the tests were run in a type-1035 steel tube, iron analyses

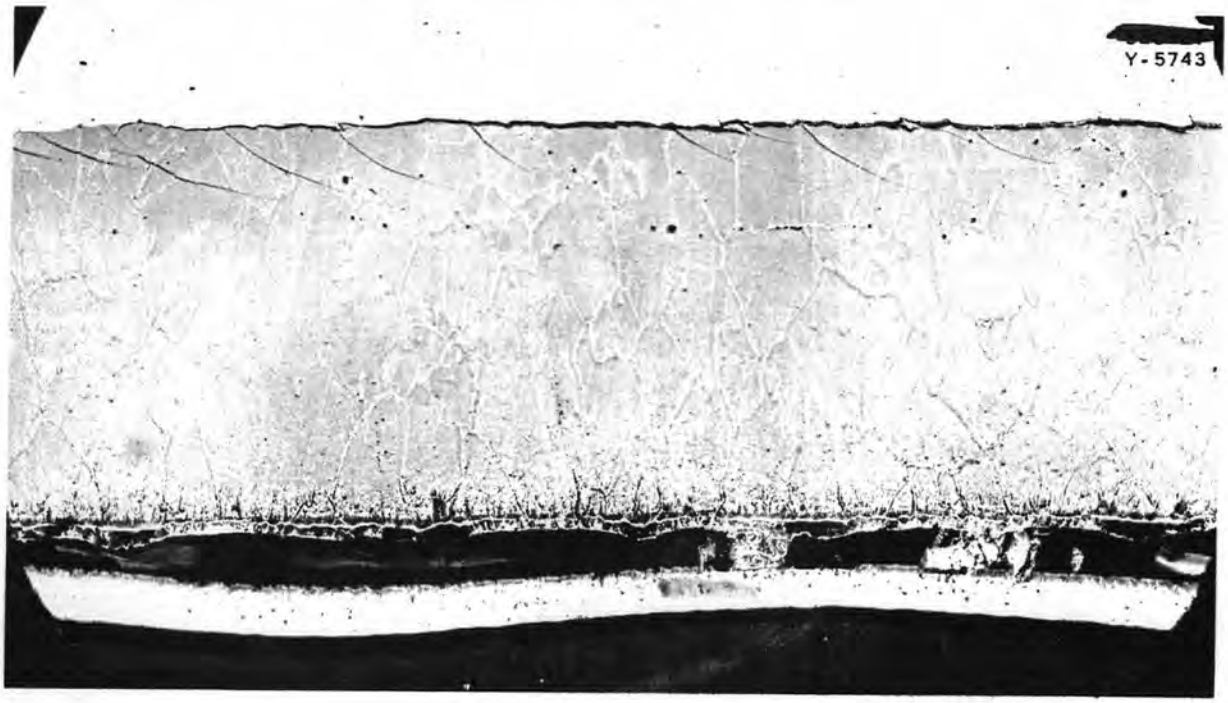


Fig. 33. Nickel Plating (2 mils) on Inconel *X* After Exposure to Sodium Hydroxide for 100 hr at 816°C in Vacuum. 75X.

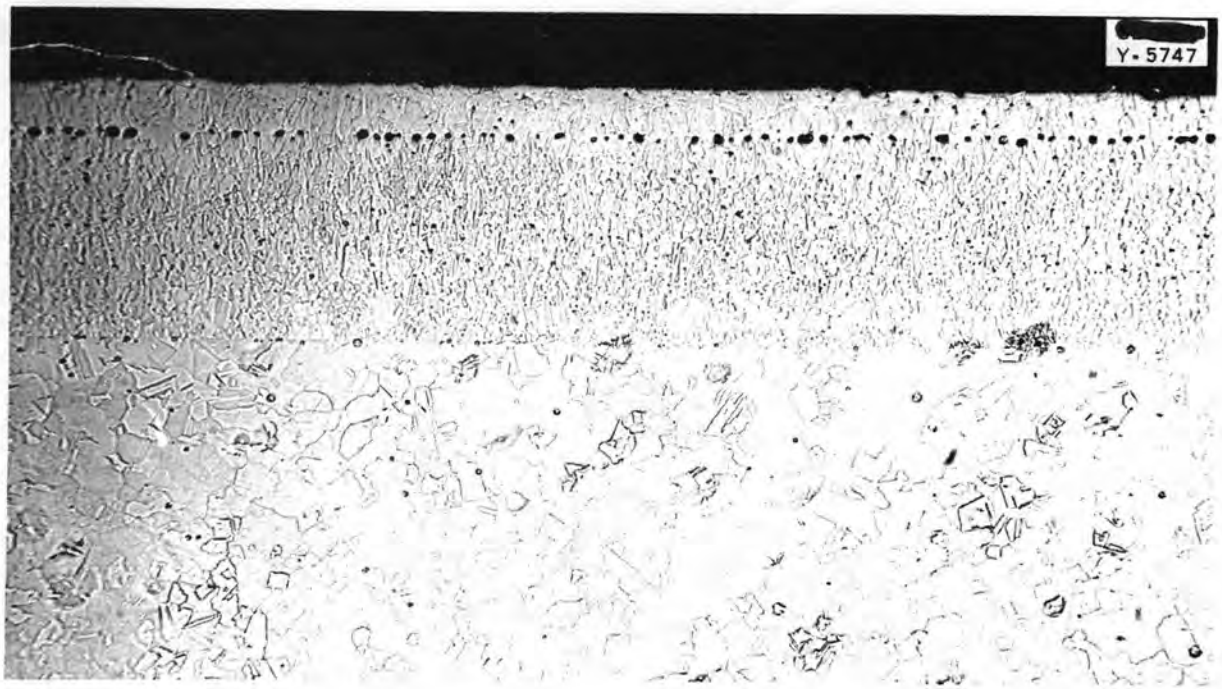


Fig. 34. Nickel Plating (12 mils) on Inconel After Exposure to Sodium Hydroxide for 100 hr at 816°C in Vacuum. 100X.

TABLE 15

Corrosion of Nickel-Plated Materials in Sodium Hydroxide at 816°C for 100 hr in Vacuum

| MATERIAL | METALLOGRAPHIC NOTES |
|---|---|
| 1-mil nickel plate on Inconel X | 45 mils of oxide on specimen between plating and specimen; unattacked material decreased from 241 to 180 mils |
| 2-mil nickel plate on Inconel X | Most of specimen covered with 10 to 35 mils of oxide on base material; no attack on plating or base material along part of specimen |
| 3-mil nickel plate on Inconel X | Corrosion product up to 50 mils between plating and specimen |
| 4-mil nickel plate on Inconel X | Base material unattacked; no thickness change; some voids apparent in nickel plating |
| 8-mil nickel plate on Inconel | No apparent attack on plating or base material; no thickness change |
| 12-mil nickel plate on Inconel | No apparent attack; some voids apparent in nickel plating |
| 26-mil nickel plate on Inconel X | 51 mils of oxide on base material; unattacked base material decreased from 241 to 182 mils; many voids in plating |

were also made. The relatively high percentage of uranium in test 1 may have been the result of a leak between the filter and the tube wall. A small amount of free sodium was found in the upper part of the tubes at the conclusion of the tests. Since sodium cyanide is hygroscopic, it is possible that much of the uranium united with the water that was present instead of dissolving in the sodium cyanide. Therefore, it is planned to run similar tests with dehydrated sodium cyanide to determine whether the solubility of uranium can be increased.

In cooperation with the Physical Chemistry Section, studies are being made of reactions that can occur in fused hydroxide media. In making these studies, compounds have been prepared that are believed to be $NaNiO_2$ and $NaFeO_2$. This is the first time that $NaNiO_2$ has been shown to exist. In preparing the $NaNiO_2$, chemically pure sodium hydroxide was heated in a nickel tube at 700°C and oxygen was bubbled through the melt for 48 hours. The tube of hydroxide was then quenched in oil, and the top portions of the melt were immediately placed in absolute ethanol. When the hydroxide had dissolved, black crystals were obtained. The crystals were washed with absolute ethanol until the washings failed to turn a phenolphthalein solution red. The product was vacuum dried over Drierite.

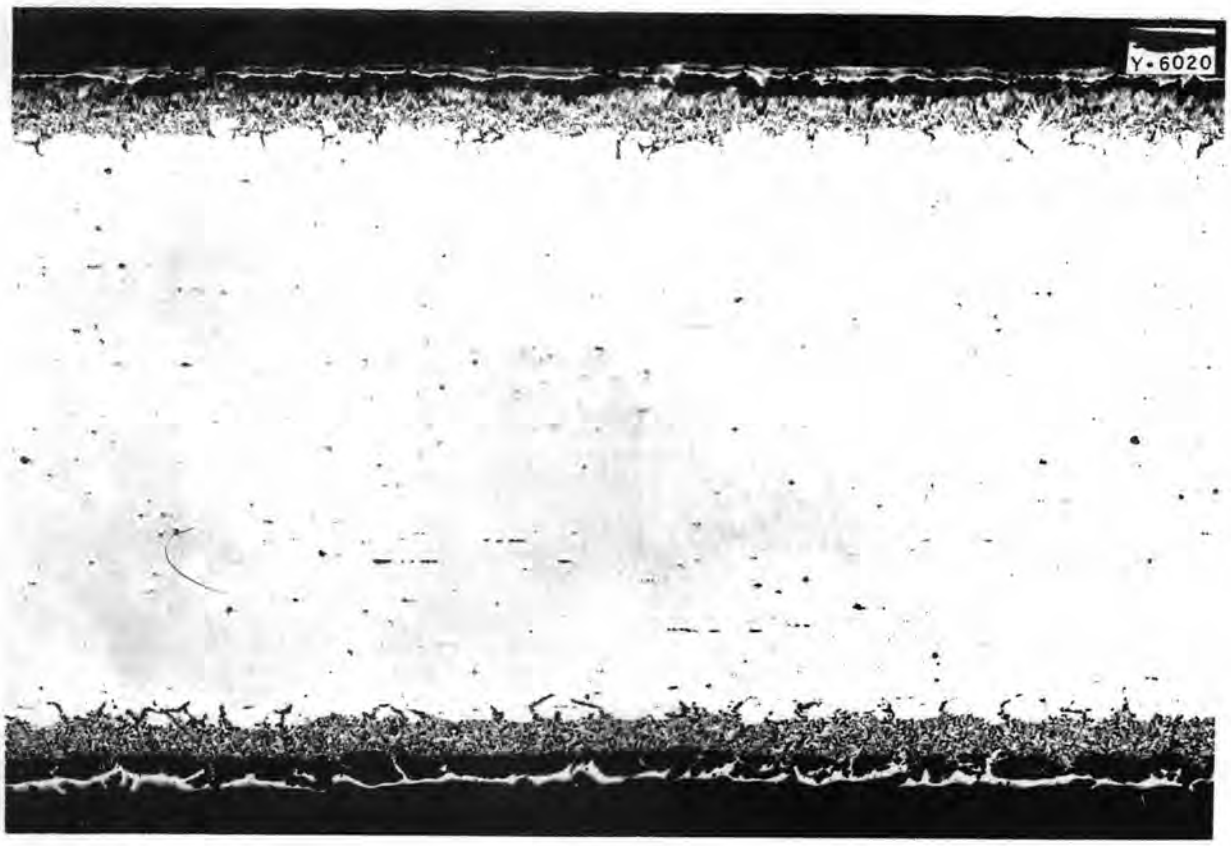


**Fig. 35. Inconel After Exposure to Sodium Hydroxide with 1 1/2% Manganese Powder for 100 hr at 816°C in Vacuum.** 100X.

A similar procedure in which water was substituted for the alcohol produced a compound that was identified by x-ray diffraction as $Ni_2O_3 \cdot H_2O$ – a known compound. The compound obtained by washing with alcohol gave an x-ray-diffraction pattern that could not be identified; however, this compound reacted with water to form $Ni_2O_3 \cdot H_2O$.

The product obtained by washing with absolute alcohol was analyzed for nickel, sodium, and carbon, and the results are given in Table 18.

In a similar experiment in which a Globe iron tube was used as the container for the molten hydroxide, crystals formed that were identified by x-ray diffraction as $NaFeO_2$.

**Effect of Pickling Treatments on Oxide Coatings.** Types-321, -304, and -446 stainless steel and Inconel were tested in some experiments with various pickling procedures to determine the efficiency of the pickling procedures on these alloys. Three-inch lengths of 1/2-in. tubing were welded at one end to subject them to the oxidizing conditions that occur in tube preparation prior to static corrosion testing. After welding, the tubes were cut in half, longitudinally, to facilitate observation of the interior surface of the tube during and after pickling. Some tests were conducted by using 1 by 1 by 1/4 in. specimens that had been oxidized in an air-atmosphere furnace at various temperatures to test the action of these

**TABLE 16**

**Effect of Manganese Additions on Inconel Tested in Sodium Hydroxide at 816°C for 100 hr in Vacuum**

| BATH | METALLOGRAPHIC NOTES |
|---|---|
| NaOH | Specimen attacked throughout along most of its length; near the center 23 mils of an original 34 mils remained unattacked |
| NaOH plus 1 1/2% electrolytic manganese | Ends of specimen attacked through entire thickness; one half of specimen length suffered complete attack; other half of specimen (center section) had 29 mils unattacked material and 3 mils intergranular penetration |
| NaOH plus 1 1/2% manganese powder | Uniform corrosion around edge of specimen; 3 mils of metal plus oxide layer and a 1-mil layer of metal plus voids; unattacked material decreased from 34.5 to 29 mils |
| NaOH plus 4% manganese powder | 4 mils of oxide plus metal and 2 mils of metal plus voids; unattacked material decreased from 33 to 26 mils |
| NaOH pretreated with electrolytic manganese | Attack very irregular; unattacked material averaged 17 mils in thickness; corrosion product varied from 10 to 12 mils |
| NaOH pretreated with electrolytic manganese | 6 mils of corrosion product plus metal; unattacked material decreased from 34.5 to 28 mils |

**TABLE 17**

**Analyses of Uranium and Iron in Test of Uranium Solubility in Sodium Cyanide**

| TEST | URANIUM (%) | IRON (%) |
|---|---|---|
| 1 | 0.026 | 0.01 |
| 2 | 0.001 | 0.026 |
| 3 | 0.001 | 0.038 |

pickling solutions on oxide coatings that were heavier than could be obtained on the welded tubing. Before pickling, the test specimens were degreased by immersion in a 10% solution of sodium phosphate at 93°C (200°F) for 15 min and then rinsed with warm water.

**TABLE 18**

**Analysis of Product Washed with Absolute Alcohol**

| ELEMENT | PERCENTAGE FOUND | THEORETICAL PERCENTAGE FOR $NaNiO_2$ |
|---|---|---|
| Nickel | 51.02 | 51.6 |
| Sodium | 21.2 | 20.2 |
| Oxygen | | 28.2 |
| Carbon | 0.1 | 0.0 |

The following pickling treatments were tried:

1. (*a*) Immerse in Virgo for 15 min at 615°C and rinse in cold water. Immerse in 10% $H_2SO_4$, using thiourea as inhibitor, for 30

min at 65°C and rinse in hot water, cold water, and again in hot water. Immerse in 10% $HNO_3$ plus 1 1/2% hydrofluoric acid for 10 min at 60°C and rinse in cold and hot water. Immerse in 20% $HNO_3$ for 1/2 hr at 60°C and rinse in cold water, hot water, and dry.

(*b*) Substitute Hibitite for thiourea in 1 (*a*).

2. (*a*) Immerse in Virgo for 15 min at 615°C and rinse in cold water. Immerse in 10% $H_2SO_4$, using thiourea as inhibitor, for 30 min at 65°C and rinse in hot water, cold water, and again in hot water.

(*b*) Substitute Hibitite for thiourea in 2 (*a*).

3. (*a*) Immerse in 10% $H_2SO_4$, using thiourea as inhibitor, for 30 min at 65°C and rinse in hot water, cold water, and again in hot water. Immerse in 10% $HNO_3$ plus 1 1/2% HF for 10 min at 60°C and rinse in cold and hot water. Immerse in 20% $HNO_3$ for 1/2 hr at 60°C and rinse in cold and hot water.

(*b*) Substitute Hibitite for thiourea in 3 (*a*).

4. Immerse in a solution of 10% $HNO_3$ and 4 to 5% HF for 30 min at 30°C and rinse in cold water.

Treatments that were most successful in these tests were 3 (*b*) for types-321 and -304 stainless steel and 4 for type-446 stainless steel and Inconel. Treatment 4 for type-446 stainless steel and Inconel was effective only for the light-temper-color type of oxide films. Treatment 3 (*b*) for types-304 and -321 stainless steel appeared to be helpful on all types of oxides tested, but it was most effective on thin coatings. Detailed results of these tests are listed in Table 19.

**Service Work.** Approximately 35 static corrosion tests have been run for the Welding and Brazing Section on various brazing alloys and brazed tube-to-header assemblies.

## DYNAMIC CORROSION

G. M. Adamson K. W. Reber

The program of dynamic corrosion testing continued during this quarter. It now appears that Fulinak 14 ( a mixture of $UF_4$, LiF, NaF, and KF) will not be used as the fuel-coolant, but since it is the only fuel-coolant that is readily available, tests with it have continued. Considerable corrosion has been measured with all the container materials tested with Fulinak 14. Flinak 12 (a nonuranium-bearing mixture of LiF, NaF, and KF) is less corrosive than Fulinak, and the addition of a small amount of NaK decreases its corrosive action even more. The attack in Inconel is probably a leaching out of the chromium.

The dynamic corrosion work this quarter has been carried out with the use of thermal convection loops identical to those described in previous reports. The results of the tests are summarized in Tables 20, 21, and 22. Table 20 summarizes results from the loops constructed of Inconel, Table 21 summarizes those from the 300- and 400-series stainless steels, and Table 22 those from the remaining materials. A study of the data presented in these tables leads to the following conclusions:

1. If Fulinak 14 is used as the circulating media, all stainless steel loops will plug in a relatively short time. Loops constructed of 400-series

## TABLE 19

### Results of Pickling Tests

| MATERIAL | PICKLING TREATMENT | PERCENTAGE WEIGHT LOSS AFTER PICKLING | APPEARANCE BEFORE PICKLING | APPEARANCE AFTER PICKLING |
|---|---|---|---|---|
| Type-321 stainless steel | 1 (*a*) | 0.29 | Light oxide film near weld | Clean but dull surface |
| Type-446 stainless steel | 1 (*a*) | 3.62 | Light oxide film near weld | Clean but dull surface; material pitted |
| Inconel | 1 (*a*) | 0.37 | Light oxide film near weld | Clean but dull surface; some pitting |
| Type-321 stainless steel | 1 (*b*) | 0.38 | Light oxide film near weld | Clean but dull surface |
| Type-446 stainless steel | 1 (*b*) | 1.97 | Light oxide film near weld | Clean but dull surface; material pitted |
| Inconel | 1 (*b*) | 0.38 | Light oxide film near weld | Clean but dull surface; some pitting |
| Type-321 stainless steel | 2 (*a*) | 0.24 | Light oxide film near weld | Clean but very dull surface |
| Type-446 stainless steel | 2 (*a*) | 3.08 | Light oxide film near weld | Very dull surface; material pitted |
| Inconel | 2 (*a*) | 0.11 | Light oxide film near weld | Surface very dark |
| Type-321 stainless steel | 2 (*b*) | 0.23 | Light oxide film near weld | Surface very dark |
| Type-446 stainless steel | 2 (*b*) | 3.64 | Light oxide film near weld | Surface dark; rough and pitted |
| Inconel | 2 (*b*) | 0.01 | Light oxide film near weld | Surface dark |
| Type-321 stainless steel | 3 (*a*) | 0.05 | Light oxide film near weld | Very clean surface |
| Type-446 stainless steel | 3 (*a*) | 2.18 | Light oxide film near weld | Clean but dull surface; material pitted |
| Inconel | 3 (*a*) | 0.19 | Light oxide film near weld | Clean but dull surface; some pitting |
| Type-321 stainless steel | 3 (*b*) | 0.03 | Light oxide film near weld | Surface very bright and smooth |
| Type-446 stainless steel | 3 (*b*) | 1.20 | Light oxide film near weld | Dull surface |
| Inconel | 3 (*b*) | 0.12 | Light oxide film near weld | Surface fairly clean but dull |
| Type-304 stainless steel | 3 (*b*) | 0.024 | Light-temper-color oxide coating | Oxide removed; surface bright |
| Type-304 stainless steel | 3 (*b*) | 0.14 | Uniform black color | Oxide removed; dull surface |
| Type-304 stainless steel | 3 (*b*) | 1.4 | Heavy black oxide | Oxide removed; many pits in metal |
| Type-304 stainless steel | 3 (*b*) | 2.5 | Heavy black oxide | Oxide removed; many pits in metal |
| Type-446 stainless steel | 4 | 0.0047 | Light-temper-color oxide coating | Oxide removed |
| Type-446 stainless steel | 4 | 0.0095 | Uniform black color | Oxide removed from only a few spots |
| Type-446 stainless steel | 4 | 0.085 | Heavy black oxide | Oxide not removed |
| Type-446 stainless steel | 4 | 0.11 | Heavy black oxide | Oxide not removed |
| Inconel* | 4 | 0.043 | Light-temper-color oxide coating | Oxide removed |
| Inconel* | 4 | 0.044 | Uniform black color | Oxide not removed |
| Inconel* | 4 | 0.21 | Heavy black oxide | Oxide not removed |
| Inconel* | 4 | 0.23 | Heavy black oxide | Oxide not removed |

*1 by 1 by ¼ in. specimen.

TABLE 20

Inconel Loops

| LOOP NO. | COOLANT | TIME OF CIRCULATION (hr) | REASON FOR TERMINATION | HOT LEG TEMPERATURE (°F) | METALLOGRAPHIC NOTES | | CHEMICAL NOTES |
|---|---|---|---|---|---|---|---|
| | | | | | HOT LEG | COLD LEG | |
| 78 | Flinak 12 | 1000 | Scheduled | 1500 | Layer of pits, 0.005 in.; intergranular attack, 0.010 in.; considerable grain growth | No attack; possibly a very thin deposit | Cr increased, Fe decreased; Cr slightly higher in cold leg |
| 214 | Flinak 12 + NaK | 500 | Scheduled | 1500 | Slight intergranular attack, 0.001 to 0.003 in. | Penetration, 0.001 in.; no metal deposition | All impurities low; Ni slightly higher than normal |
| 210 | Fulinak 14 | 500 | Scheduled | 1500 | Layer of pits, 0.010. in., with maximum of 0.015 in.; possible surface layer, 0.002 in. | Slight roughening | Large increase in Cr, Fe decreased, Ni variable; Cr higher in cold leg |
| 211 | Fulinak 14 | 524 | Scheduled | 1500 | Intergranular pitting attack, 0.004 to 0.008 in.; some pitting in grains | Metallic deposit, 0.0005 in.; no attack | Cr increased, Fe decreased; even distribution |
| 212 | Fulinak 14 | 37 | Leak | 1500 | Intermittent layer of intergranular pits, 0.005 in. | No attack | Cr, Fe, and Ni all showed large increases in both hot and cold leg |
| 213* | Fulinak 14 | 500 | Scheduled | 1500 | Intergranular pitting, 0.002 to 0.011 in.; some pitting in grains | Thin continuous metallic layer with an intermittent nonmetallic layer on it | Large increase in Cr, Fe decreased; no systematic distribution |
| 218 | Fulinak 14 | 500 | Scheduled | 1300 | Intergranular pitting, 0.006 to 0.010 in. | Metallic deposit, 0.0001 to 0.001 in.; there appeared to be two layers; the second layer was not continuous and contained inclusions | Cr increased, Fe decreased, % F decreased; no systematic distribution |
| 219 | Fulinak 14 | 480 | Heater failure | 1500 | Heavy pitting, 0.005 to 0.013 in. | Wall rough, with thin layer; bottom layer metallic with discontinuous nonmetallic layer (particles) on top | Large increase in Cr, Fe decreased; cold leg high in Fe and Cr |
| 216 | Fubena 17 | 574 | Scheduled | 1500 | | | |
| 217 | Fubena 17 | 500 | Scheduled | 1500 | | | |

*The Inconel in this loop was hydrogen fired and the loop operated under hydrogen atmosphere.

# TABLE 21

## Stainless Steel Loops

| LOOP NO. | TYPE OF STAINLESS STEEL | COOLANT | TIME OF CIRCULATION (hr) | REASON FOR TERMINATION | HOT LEG TEMPERATURE (°F) | METALLOGRAPHIC NOTES | | CHEMICAL NOTES |
|---|---|---|---|---|---|---|---|---|
| | | | | | | HOT LEG | COLD LEG | |
| 111 | 316 | Flinak 12 | 174 | Leak[a] | 1500 | Intergranular attack, 0.010 in.; some wall reduction; tremendous grain growth | No attack; continuous layer, 0.001 in.; some grain growth | Large increase in Cr, Fe variable |
| 116 | 316 | Flinak 12 | 500 | Scheduled | 1500 | Some intergranular pitting, 0.002 to 0.004 in.; surface layer shows grain growth | Thin continuous metallic deposit with inclusions | No impurities increased; no systematic variation |
| 119 | 316 | Flinak 12 + NaK | 500 | Scheduled | 1500 | Surface rough with some depressions, 0.002 in.; no pitting or intergranular attack | No attack or deposit | All impurities very low - much lower than at start |
| 112 | 316 | Fulinak 14 | 82 | Plug | 1500 | Intergranular attack, 0.008 in.; grain growth | Intermittent thin layer; grain growth | Large increase in Cr, Fe decreased |
| 113 | 316 | Fulinak 14 | 123 | Plug | 1500[b] | Intergranular attack, 0.008 in.; some pitting | Thin deposited layer | Large increase in Cr, irregular decrease in Fe; higher in cold leg |
| 118[c] | 316 | Fulinak 14 | 147 | Plug | 1500 | Intergranular attack, 0.005 to 0.012 in.; some grains removed | Rough surface with 0.001-in. layer | Cr increased, Fe decreased; highest in cold horizontal leg |
| 121 | 316 | Fulinak 14 | 153 | Plug | 1300 | Heavy intergranular attack, 0.008 to 0.010 in.; some grains removed | Deposited layer, 0.0005 to 0.0015 in., irregular in thickness | Increase in Cr, decrease in Fe; no systematic distribution |
| 275 | 347 | Fulinak 14 | 39 | Leak | 1500 | Intergranular attack 0.008 to 0.013 in.; tremendous grain growth | Metallic deposit, 0.0005 to 0.001 in.; contains inclusions | Cr increased with no large variation; Fe decreased irregularly |
| 276 | 347 | Fulinak 14 | 125 | Plug | 1500 | Intergranular attack, 0.002 to 0.004 in. | Rough surface with a thin deposited layer | Cr increased, Fe decreased; both slightly higher in cold leg |
| 251 | 310 | Fulinak 14 | 75 | Plug | 1500 | Very heavy intergranular pitting, 0.008 to 0.015 in.; surface rough; tremendous grain growth | General nonmetallic deposit with thin metallic layer; some crystals attached to surface | Cr increased, Fe decreased; cold leg slightly higher |
| 252 | 310 | Fulinak 14 | 368 | Plug[d] and instrument failure | 1500 | | | |
| 40 | 410 | Fulinak 14 | 9 | Plug | 1500 | No pitting or intergranular attack up to 0.010 in. removed; considerable martensitic structure | Metallic deposit with inclusions; slight attack; grain growth | Cr increased, Fe decreased; both higher in cold leg |
| 43 | 410 | Fulinak 14 | 12 | Plug | 1500 | No pitting or usual intergranular attack; however, many grains are loose; considerable martensitic structure | Metallic deposit with inclusions; grain growth | Cr increased in cold leg but only slightly in hot leg; Fe decreased but varied |
| 48 | 430 | Fulinak 14 | 8 | Plug | 1500 | Heavily pitted, 0.002 in.; generally removed ~0.002 in. | Metallic deposit with inclusions; surface rough under the deposit | Cr increased, Fe decreased; both higher in hot leg |
| 49 | 430 | Fulinak 14 | 9 | Plug and leak | 1500 | | | |

[a] Gas leak around spark plug.

[b] Operated for 72 hr at 1500°C and at 1600°C for remaining time.

[c] This loop was hydrogen fired and the loop operated under hydrogen atmosphere.

[d] Metallic plug found in lower cold leg.

TABLE 22

Miscellaneous Loops

Hot leg temperature: 1500°F

Coolant: Fulinak 14

| LOOP NO. | MATERIAL | TIME OF CIRCULATION (hr) | REASON FOR TERMINATION | METALLOGRAPHIC NOTES | | CHEMICAL NOTES |
|---|---|---|---|---|---|---|
| | | | | HOT LEG | COLD LEG | |
| 104 | Nickel | 500 | Scheduled* | Surface polished; no pitting or intergranular attack; up to 0.009 in. removed; some grain growth | No attack; layer or crystals 0.001 to 0.003 in. | Fe and Cr unchanged; Ni higher in cold leg |
| 107 | Nickel | 1000 | Scheduled | | | |
| 340 | Monel | 117 | Leak | No pitting or intergranular attack | No attack; no deposit | No appreciable change in impurities |
| 365 | Nimonic | 500 | Scheduled | Intergranular pitting 0.008 to 0.013 in.; few spots, 0.015 in. | No attack; thin deposited layer | Cr increased, Fe decreased; slight increase in nickel |

*Some evidence of plugging, crystals found in all sections.

stainless steel would plug in a shorter time than those constructed of 300-series stainless steel.

2. Inconel loops do not plug when fluorides are circulated in them; however, considerable corrosion is evidenced.

3. By comparing either Inconel or stainless steel loops in which Flinak 12 has been circulated with those in which Fulinak 14 has been circulated, it is evident that the presently available uranium tetrafluoride accelerates both plugging and corrosion.

4. When Fulinak 14 is circulated in a loop in which chromium is one of the alloying elements, the chromium concentration of the Fulinak increases and the iron concentration decreases. Little, if any, change takes place in the nickel and uranium concentrations.

5. When Flinak 12 is circulated, no large changes are found in the concentration of the impurities.

6. A thin metallic layer is deposited on the walls of the cold leg. This deposit is usually thickest in the top, or hotter, part of the cold leg.

7. The addition of NaK to Flinak 12 reduces corrosion in both Inconel and in type-316 stainless steel and suppresses formation of the metallic-layer deposit.

8. The mechanism of plugging in the loops has not been determined. Definite crystal masses were found only in loops 43, 252, and 104. In the other loops either no metallic crystals or only a few scattered ones were found. The Chemistry group has checked melting points and viscosities of both hot and cold leg material without finding changes from the original values.

9. The attack is about the same at 1300°F as it is at 1500°F.

Progressive layers were drilled from the inside of the hot leg of Inconel loop 210. This loop had

circulated Fulinak 14 for 500 hr with a hot leg temperature of 1500°F. Table 23 shows the composition of the various layers. It is obvious from Table 23 that chromium was being leached out of the alloy and that iron and nickel were essentially unchanged. Still unexplained is the fact that the total percentage composition gradually decreases toward the inside surface of the pipe.

Some magnetic tests, made by the Metallographic Section, show that in Inconel chromium leaching follows a straight-line interface, whereas in type-316 stainless steel it is more nearly confined to the grain boundaries. These tests are illustrated in Figs. 71 and 72. Figure 71 shows an Inconel specimen before and after the iron colloid was added and Fig. 72 shows similar treatment of the type-316 stainless steel specimen. (See section on "Metallographic Laboratory" for Figs. 71 and 72.)

In the second phase of this work two types of tests are being used to obtain preliminary data: (1) a tube-burst test to furnish hoop stress data in a fluoride medium and (2) a stress-rupture test using a fluoride bath. In the stress-rupture test, dead-weight loading is transmitted to a small sample by means of bellows. Elongation is measured by movement of the end of the load lever arm. The sample is held in a bath of fluorides at 1500°F. One section of the tube wall is reduced to a known wall thickness to serve as the gage length. This test yields only time-to-rupture and total elongation data.

Table 24 is a summary of the stress-rupture data obtained with Inconel specimens in Fulinak 14 at 1500°F – the Inconel was used in the as-received condition. The data are compared with data obtained in argon atmospheres by the Physical Testing Section of the Metallurgy Division. Their data were also obtained with fine-grain as-received material.

In addition to the tests listed in Table 24, one Inconel sample has now been under a stress of 4000 psi for 350 hr and another under a stress of 5000 psi for 525 hours. Neither specimen has yet shown a large amount of elongation.

**TABLE 23**

**Composition of Layers Cut from Hot Leg of Inconel Loop 210**

| DEPTH OF CUT (in.) | COMPOSITION (%) | | | | | | | | | |
|---|---|---|---|---|---|---|---|---|---|---|
| | Fe | Ni | Cr | Fe/Ni | KF* | LiF* | NaF* | UF* | Fe + Cr + Ni | TOTAL |
| 0.001 | 7.22 | 81.4 | 5.2 | 0.088 | 1.2 | 2.2 | 0.4 | | 93.8 | 97.6 |
| 0.004 | 7.60 | 81.4 | 5.9 | 0.093 | 0.3 | | 0.1 | | 94.9 | 95.3 |
| 0.009 | 7.18 | 81.1 | 7.0 | 0.089 | 0.4 | 1.1 | 0.15 | None detected | 95.3 | 96.9 |
| 0.014 | 6.98 | 79.6 | 9.15 | 0.088 | 0.4 | 0.7 | 0.3 | None detected | 95.7 | 97.1 |
| 0.019 | 6.88 | 79.4 | 11.3 | 0.087 | 0.15 | 0.4 | 0.15 | None detected | 97.6 | 98.3 |
| Normal Inconel | 7 | 77 | 15 | 0.091 | | | | | 99.0 | 99.0 |

*These figures were calculated from the amount of metal found spectrographically.

**TABLE 24**

**Stress-Rupture Data**

| STRESS (psi) | TIME TO RUPTURE (hr) | |
|---|---|---|
| | IN FULINAK 14 | IN ARGON |
| 12,500 | 7 | 6 |
| 10,000 | 20 | 19 |
| 7,500 | 22.5 | 80 |
| | 31 | |
| | 14.5 | |
| 5,000 | In test | 270 |

One Inconel sample was run in the tube-burst test and failed in 688 hr under a stress of 2100 psi. The sample blistered in an irregular manner, so the elongation could not be determined.

## PHYSICAL METALLURGY OF CORROSION

A. D. Brasunas L. S. Richardson

The study of mass transfer and corrosion in molten caustic and molten fluoride continues, with the maximum effort being focused on fluoride systems. Seesaw tests are in progress in an attempt to develop an inhibitor to mass transfer in both caustic and fluoride No. 14. A small portion of the work is concerned with an attempt to understand the fundamental aspects of fluoride corrosion (hole formation) and metal transport.

**Mass Transfer in Molten Hydroxide.** Since excess oxygen in the form of nickel oxide additions to sodium hydroxide has resulted in greatly increased mass transfer of nickel in nickel tubes, a series of tests were made in which oxygen-getters, including Na, NaH, Zr, Be, Mg, and Al, were added. None have had substantially beneficial effects; in fact, several additions resulted in increased mass transfer. A photomicrograph through a crystal attached to a tube wall is shown in Fig. 36. Various atmospheres were also sealed into the specimen tubes; these variables, too, had no visible beneficial effect. Additional tests are in progress.

A summary of the seesaw tests and results to date appear in Table 25. The temperatures reported are the values obtained from readings of spot-welded thermocouples attached to the ends of the specimen tube, and they do not represent temperatures inside the tube. Measurements of the bath temperature have shown that the bath at the cold end is 30°C hotter than indicated by the cold zone thermocouple, and the bath at the hot end is 60°C cooler than indicated by the hot zone thermocouple. Thus the gradients indicated in Table 25 are 90°C greater than actually experienced by the molten caustic during the test.

The following general observations may be made from a study of the data in Table 25:

1. Excess oxygen strongly promotes crystal formation.

2. Removal of excess oxygen with getters does not eliminate mass transfer.

3. Atmosphere variations ($H_2$, A, $O_2$, vacuum) had no beneficial effect under the conditions of test.

4. There is a temperature limit (see tests SSH-3a and SSH-46) below which mass transfer can be minimized for a certain length of time.

5. Additions of Na, Mn, NaH, NiO, and $O_2$ greatly accelerate mass transfer.

A standpipe test using *A* nickel and sodium hydroxide has demonstrated that both deposition and solution can occur

**Fig. 36. Nickel Crystals at Inner Surface of Nickel Tube Containing Sodium Hydroxide Plus 5% Sodium.** Seesaw test SSH-15. Note that the crystals are attached at a very small area. 100X.

**Fig. 37. Nickel Layer Deposited on Nickel Tube at 700°C in Sodium Hydroxide.** Note oxide layer separating deposited metal from base metal. Copper plating was used to maintain layer intact. 1000X.

TABLE 25

**Results of Various Test Conditions on Mass Transfer of Nickel in Nickel Tubes Containing Sodium Hydroxide**

| TEST NO. | TEST CONDITIONS | | | | | |
|---|---|---|---|---|---|---|
| | TIME (hr) | NO. OF CYCLES | ENVIRONMENT | HOT ZONE TEMPERATURE (°C) | COLD ZONE TEMPERATURE (°C) | AMOUNT OF NICKEL CRYSTALS DEPOSITED AT COLD ZONE |
| SSH-3a | 117 | 14,000 | Vacuum | 797 | 505 | Light to moderate |
| SSH-3b | 100 | 12,000 | Vacuum | 600 | 377 | Practically none |
| SSH-4a | 125 | 45,000 | Vacuum | 645 | 475 | Light |
| SSH-6 | 72 | 19,600 | Oxygen | 750 | 540 | Very heavy |
| SSH-8 | 147 | 39,500 | Hydrogen | 740 | 520 | Moderate |
| SSH-9 | 147 | 39,500 | Hydrogen | 765 | 515 | Moderate |
| SSH-10 | 250 | 69,000 | Argon | 775 | 560 | Light to moderate |
| SSH-15 | 8 | 2,000 | Vacuum + 5% Na | 715 | 500 | Heavy |
| SSH-16 | 8 | 2,000 | Vacuum + 10% NaH | 750 | 500 | Heavy |
| SSH-17 | 0.2 | 50 | Vacuum + 30% NaH | 750 | 300 | (Failed at start) |
| SSH-31 | 104 | 28,000 | Vacuum + 1/4% Al | 750 | 660 | Light to moderate |
| SSH-32 | 104 | 28,000 | Vacuum + 1/4% B | 750 | 665 | Light |
| SSH-33 | 104 | 28,000 | Vacuum + 1/4% C | 770 | 660 | Moderate |
| SSH-34 | 104 | 28,000 | Vacuum + 1/4% Mn | 770 | 650 | Very heavy |

at 700°C, provided suitable thermal gradients are present to support this action. A region at 700°C showed deposition when adjacent areas were at a higher temperature. Another region, also at 700°C, showed solution when adjacent areas were at a lower temperature. A transverse section of a deposition zone is shown in Fig. 37. The grey particles between the base metal and deposited metal are believed to be oxide particles.

**Mass Transfer in Molten Fluoride.** Seesaw tests with fluoride-containing Inconel tubes are being made to determine (1) the extent of corrosion as a function of time, (2) the extent of corrosion as a function of temperature, and (3) whether additives can inhibit corrosion and/or mass transfer. Several tests were begun to determine the extent of corrosion and mass transfer in simple systems – that is, iron or nickel with fluoride No. 14 or sodium fluoride. Work is also continuing with the standpipe test apparatus in which temperature gradients and atmospheres are more easily controlled than in the seesaw apparatus.

Inconel tubes containing fluoride No. 14 are being evaluated for corrosion resistance as a function of time at 1500°F in the seesaw test. Tests have been run at 50, 100, 200, 500, and 750 hours. The specimen in the long-time test that has been in continual operation for well over two months is still being cycled. Although this series of tests is not fully evaluated, it indicates, at least, that long-time operation of a fluoride-containing Inconel system is feasible.

The cold zone of an Inconel test specimen (SSF-26) containing fluoride No. 14, which was tested for 450 hr (163,000 cycles) at a hot zone temperature of 790°C and a cold zone temperature of 607°C, showed an unexpected nonmetallic deposit. In addition to an abundance of $UO_2$ crystals and some metal crystals, a light-green phase formed at the coldest portion. This phase was separated from the bulk fluoride mixture in that region, and the two mixtures were analyzed spectrographically. The results are given in Table 26.

**TABLE 26**

**Spectrographic Analysis of Phases in Cold Portion of Seesaw Test SSF-26**

| ELEMENT | SPECTROGRAPHIC INDICATION | |
|---|---|---|
| | BULK FLUORIDE MIXTURE | LIGHT-GREEN MIXTURE |
| Na | Very strong | Very strong |
| Li | Very strong | Not found |
| K | Very strong | Not found |
| U | Very strong | Strong |
| Fe | Weak | Moderate |
| Ni | Trace | Moderate |
| Cr | Moderate | Strong |

The most significant difference between the two mixtures is the absence of Li and K in the light-green phase, which would indicate that the phase was essentially NaF with dissolved compounds of U, Fe, Ni, and Cr, and that it probably had a very high melting point. A separation of this phase at some cool, localized zone would obviously be extremely detrimental.

An iron seesaw test specimen containing fluoride No. 14 was operated for 120 hr (31,400 cycles) with a hot zone temperature of 675°C and a cold zone temperature of 495°C. Preliminary examination has indicated that a very large amount of iron crystals formed in the cold zone (Fig. 38). Since the crystal formation is very much more than has been encountered in similar tests with Inconel, more detailed study of this and similar tests is in progress.

Inconel that was cycled for 170 hr (16,000 cycles) at a hot zone temperature of 750°C and a cold zone temperature of 530°C showed only a trace of metal crystal formation; when examined metallographically, void formation to a maximum depth of 0.004 in. was observed. As may be seen in Fig. 39, some areas of the surface were not attacked at all. No satisfactory explanation for this behavior has been proposed.

## PHYSICAL CHEMISTRY OF CORROSION

G. P. Smith, Jr. J. V. Cathcart
W. H. Bridges

**Hydroxide Corrosion Studies.** A new type of thermal convection apparatus, designated as the "cold finger apparatus," has been developed for use in the corrosion testing of hydroxides. This new apparatus has several advantages over the thermal convection loops previously used in this work.[1] Since fewer welds were required in its construction, there is a smaller chance of leaks or cracks developing than in the loops. Furthermore, because the cold finger apparatus can be put into operation in a relatively short time as compared with a loop, much less time is lost when a breakdown occurs. Since the main purpose of the hydroxide corrosion study is the determination of the influence of blanketing atmospheres on mass transfer in hydroxide-metal systems, the cold finger apparatus is also superior to the loops in that it

[1] *Metallurgy Division Quarterly Progress Report for Period Ending January 31, 1952*, ORNL-1267, in press.

**Fig. 38. Iron Crystals Embedded in Fluoride No. 14.** Seesaw test SSF-11. Test conditions: hot zone temperature 675°C; cold zone temperature 495°C; 31,400 cycles; 120 hours. 5X.

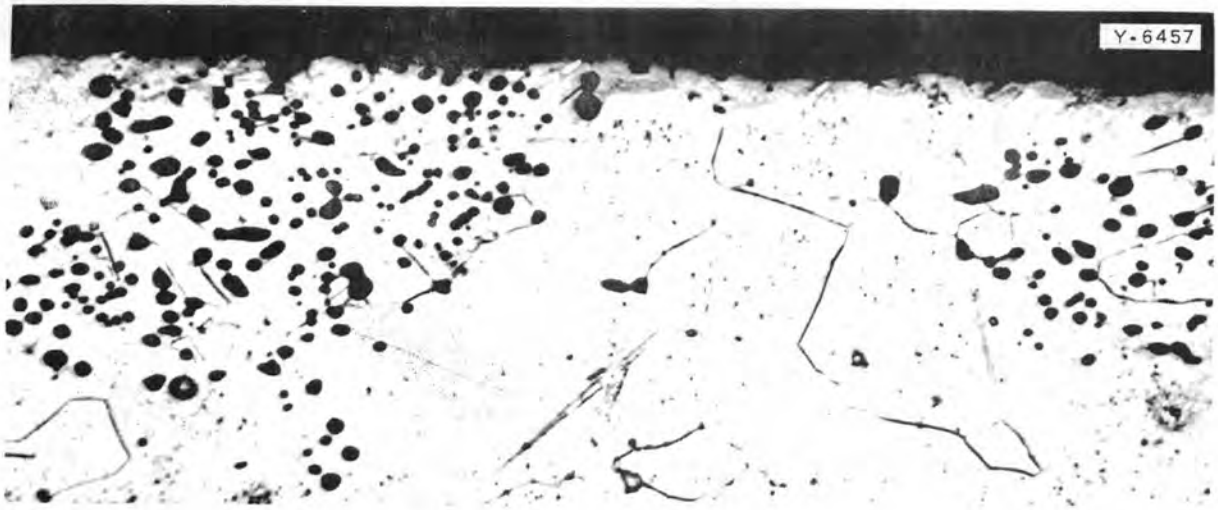


**Fig. 39. Surface of Inconel Specimen as Seen During Metallographic Examination.** Specimen from hot zone of seesaw test SSF-1 after 170 hr at 750°C. 500X.

allows a greater area of contact between the hydroxide and the atmosphere above it. Furthermore, in the cold finger apparatus a given volume element of the hydroxide is always closer to the hydroxide-atmosphere interface than the corresponding volume element in a loop. It is probable that the effective rate of flow in a loop is greater than that in the new apparatus; but the rate of flow in the cold finger apparatus is sufficiently large to cause copious mass transfer under conditions that are known to produce mass transfer in a loop.

The cold finger apparatus consists of a small-diameter tube that is sealed off at one end and then inserted into a larger pot containing molten hydroxide. The inside of the small tube is cooled by a jet of air to create a temperature differential between the inner tube, or "cold finger," and the walls of the hydroxide pot. This temperature difference sets up convection currents in the hydroxide.

The apparatus (shown in Fig. 40) consists of a cold finger made of 1/2-in. nickel tubing with a wall thickness of 0.035 inch. A nickel plug is welded into the bottom of the cold finger. The air jet, which extends down the inside of the cold finger, consists of a small-diameter pyrex tube connected to an air supply. The hydroxide pot is constructed from 1 1/2-in. nickel pipe with a 1/8-in. plate welded on the bottom. The pot is hung on nickel wires from a nickel strap fastened near the top of the cold finger. This assembly is sealed through a Kovar seal to a glass tube extending down from the outer joint of a pyrex ground-glass joint. This joint is fitted over a quartz inner joint to which a quartz jacket is sealed.

Heating is accomplished by an electric tube furnace, and the temperature of the cold finger is measured by a thermocouple embedded in the nickel plug at the bottom. A second thermocouple attached to the outside of the hydroxide pot serves to measure the temperature of the walls of that vessel. A third thermocouple, fastened on the outside of the quartz jacket, is connected to an appropriate temperature control instrument.

With the apparatus completely assembled except for the quartz jacket, the hydroxide pot is filled with commercial c.p.-grade sodium hydroxide pellets. The quartz jacket is then put in place and the hydroxide dehydrated at 500°C under a vacuum of approximately 0.04-mm Hg for 48 hours. The temperature is then increased until the outside of the hydroxide pot reaches the desired

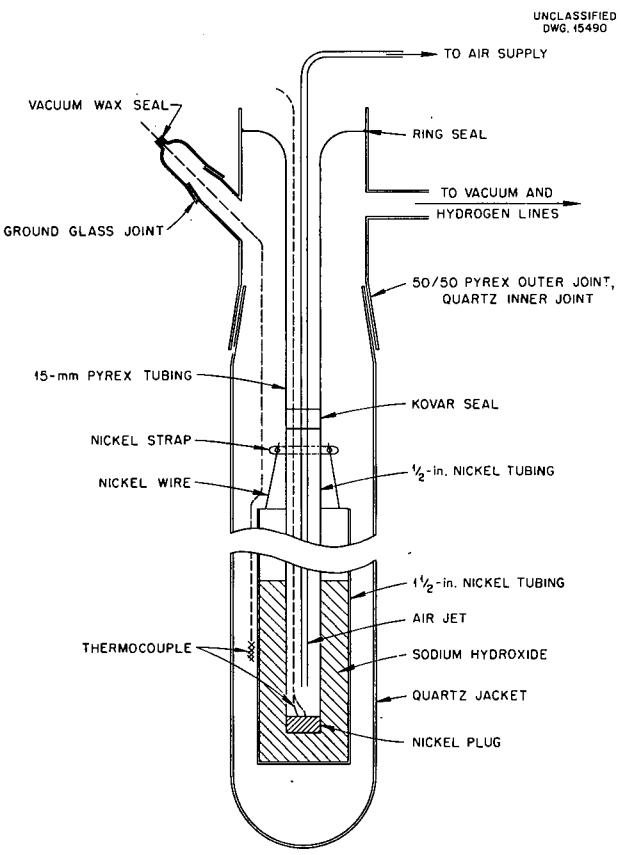


**Fig. 40. Cold-Finger Thermal Convection Apparatus.**

temperature. At the same time the air jet is turned on and regulated so that the cold finger remains at a temperature of approximately 500°C.

Thus far two runs have been made in this apparatus. In the first the hydroxide was blanketed with a hydrogen atmosphere. The pot walls and the cold finger were maintained at temperatures of 625 and 525°C, respectively, for a period of 117 hours. Neither loose dendritic crystals nor mass transfer of any sort was noted during this run.

The second run was carried out under vacuum. After dehydration the system was sealed off under a vacuum of about 0.04-mm Hg, and the temperature was adjusted so that the pot walls and the cold finger were at 725 and 500°C, respectively. Shortly after the temperature was raised to 725°C, the pressure inside the apparatus began to rise slowly, presumably because of gases given off from the hydroxide. A steady state was reached at a pressure of approximately 200-mm Hg. This run lasted for 48 hours. Heavy mass transfer occurred between the walls of the dehydration pot and the cold finger, and large quantities of dendritic crystals were observed on the surface of the cold finger.

The cold finger apparatus appears to be a satisfactory substitute for the conventional thermal convection loop, and it has the advantages of simpler design and construction and greater ease of operation.

It has been shown, at least under the conditions specified for the first run, that a blanketing atmosphere of hydrogen effectively stops mass transfer in a nickel-sodium hydroxide system. This conclusion is in agreement with the results obtained in semistatic tests[2] in which sodium hydroxide was heated in a nickel crucible in air. In these experiments, in which the temperature of the crucible walls was approximately 600°C, considerable mass transfer was observed. These experiments and the cold finger tests were roughly comparable except for differences in the blanketing atmospheres and the increased circulation in the cold finger; therefore, it has been concluded that the presence of hydrogen probably tends to reduce mass transfer in a nickel-sodium hydroxide system.

Construction of the apparatus for three new cold fingers has been completed, and tests of the type described will be continued. Higher temperatures will be studied, and an effort will be made to determine whether an inert atmosphere such as helium or argon reduces mass transfer to the same extent as hydrogen. A design for a forced-circulation cold finger is also being considered.

A second, modified thermal convection apparatus, representing a simplification of both the thermal convection loop and the cold finger apparatus, has been constructed and given preliminary testing. Because of its simplicity it was easy to erect, required a small amount of laboratory space, and could be put into operation in a short period of time.

The apparatus, designated as the TCA or thermal convection apparatus, is shown in Fig. 41. It consists of a 1-ft length of 1-in.-dia nickel tubing with a 1/8-in. plate welded on the bottom. A Kovar seal is attached to the top end. A nickel vane about 3 in. long is positioned inside the tube near the bottom, and there is sufficient space below the vane to permit circulation.

[2] *Metallurgy Division Quarterly Progress Report for Period Ending October 31, 1951*, ORNL-1161, p. 25 and 38.

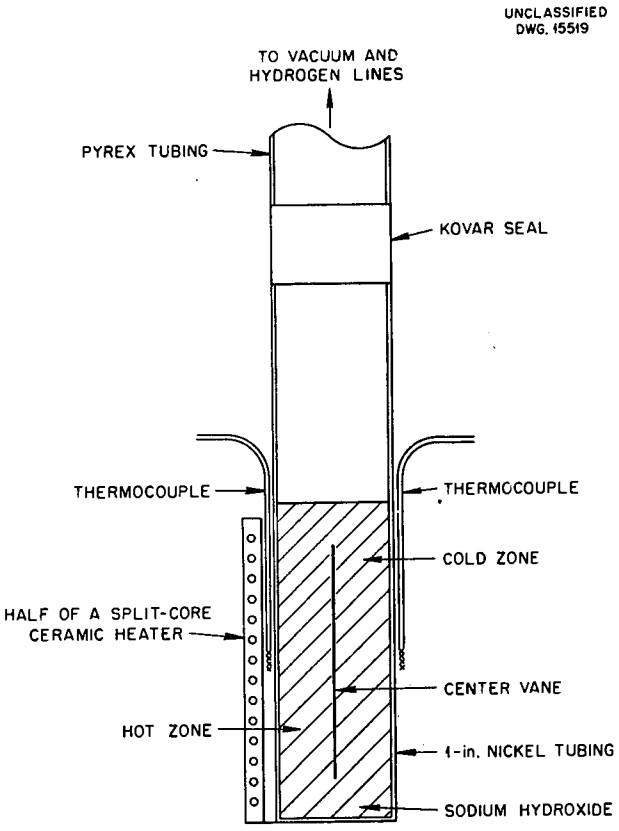


**Fig. 41. Thermal Convection Apparatus, TCA.**

The operating procedure is as follows: c.p.-grade sodium hydroxide pellets are loaded into the tube until the level of the hydroxide is slightly above the top of the central vane. The tube is then placed between 4-in., split-core, semicircular heaters and the system connected to hydrogen and vacuum lines. The heaters are turned on and the hydroxide dehydrated at a temperature of 500°C under a pressure of about 50 $\mu$ for 24 hours. The desired blanketing atmosphere is then introduced, and one of the semicircular heaters removed; thus one side of the apparatus is exposed to the atmosphere. The power in the other heater is increased until the wall temperature on the hot side of the apparatus reaches 800°C. This procedure results in the formation of a temperature differential between opposite sides of the tube; hence, convection currents are set up in the hydroxide in the tube.

In order to determine whether the circulation in this new apparatus was great enough to allow an appreciable amount of mass transfer to occur, two runs were made under a static vacuum. The first run lasted 160 hr with hot and cold side temperatures of 800 and 525°C, respectively. When the apparatus was cut open, it was found that because too much hydroxide had been put in, a very large cold zone was formed and made the interpretation of the results difficult. The walls in the hot zone in the vicinity of the heater were highly polished, whereas those in the cold zone had a roughened appearance. Massive deposits of crystals were found only at the hydroxide-vacuum interface, where a considerable quantity of crystals was observed.

A second run was made with hot and cold zone temperatures of 800 and 650°C, respectively, and an air jet was directed at a point just below the top of the center vane in the cold zone. The run was terminated after 100 hr of operation because a leak developed in the wall of the hot zone. The presence of this leak resulted in heavy oxidation in the interior of the tube, but a considerable quantity of black crystals adhered to the walls of the cold zone in the vicinity of the area cooled by the air jet and led to the assumption that a very appreciable amount of mass transfer had occurred. A very heavy deposit of black crystals, amounting almost to a plug, was again observed at the hydroxide-vacuum interface.

On the basis of these results it was felt that the TCA represented an apparatus which, because of its simplicity and ease of operation, might be well suited to preliminary corrosion

testing of new systems. It is planned to continue the development of the apparatus.

**Liquid Metal-Solid Metal Interactions.** A constant temperature salt bath capable of operating in the temperature range of 300 to 450°C was constructed to provide the isothermal environment required for solid metal-liquid metal equilibrium experiments. With the present temperature control equipment, it is possible to control thermal cycling and temperature gradients in the bath to within about 1°C when the bath is at 400°C.

The bath consists of a stainless steel pot, 10 in. in diameter and 17 in. deep, surrounded by suitable insulating material. The thermostating liquid is a 50:50 mixture (by weight) of sodium nitrate and sodium nitrite. Both thermal cycling and thermal gradients are reduced by stirring the bath vigorously. The bath is mounted on an elevating mechanism so that the apparatus used in the equilibrium studies can be attached to appropriate hydrogen and vacuum lines before immersion in the salt bath.

The temperature of the thermostat is controlled by a Chromel-Alumel thermocouple attached to a Leeds & Northrup Speedomax-D.A.T. unit. Inherent inaccuracies in base-metal thermocouples, such as those caused by strains or inhomogeneities, make it impossible to determine the exact degree of control furnished by this arrangement, but the measurements that have been made indicate that thermal cycling and temperature gradients in the bath do not exceed 1°C.

In the future it is planned to use a resistance thermometer and an electronic Meuller Bridge as temperature control instruments. Such an arrangement should greatly increase the accuracy of temperature control.

It was considered desirable to determine the shape that a copper crystal assumes when it is in equilibrium with a copper-bismuth solution, since it is believed that a clear-cut answer to this question will enable a decision to be reached as to the relative importance of surface forces in determining the equilibrium form of a metallic single crystal. In an effort to approach a state of equilibrium in the system, a copper single crystal was brought into contact with an exactly saturated solution of copper in bismuth. The apparatus used is shown in Fig. 42. It consists of three pyrex glass bulbs connected by fritted-glass disks. As may be seen in the figure, a small, single-crystal sphere of copper was held in position in the side arm of the central compartment of the apparatus. Deoxidized bismuth and a small slug of polycrystalline copper were sealed into the top compartment. The entire apparatus was then immersed

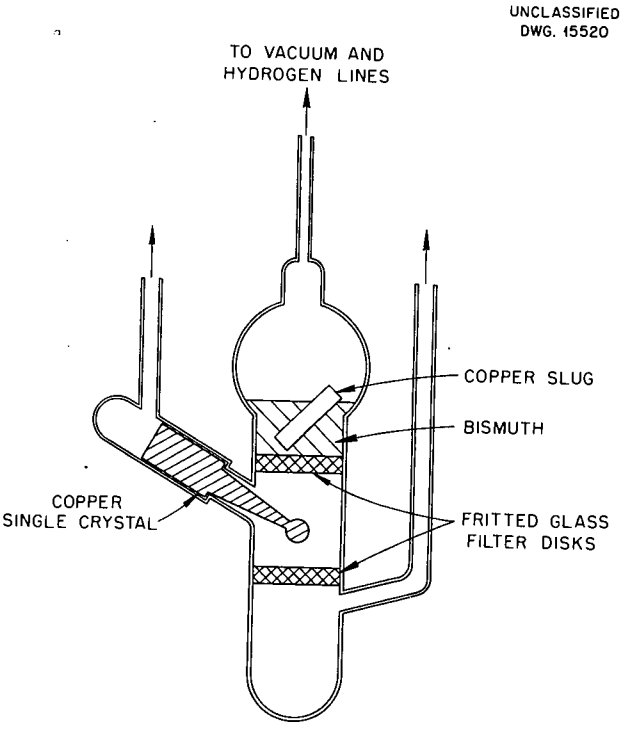


**Fig. 42. Liquid Metal-Solid Metal Interaction Apparatus.**

in the constant temperature bath, and both the copper crystal and the bismuth were deoxidized in hydrogen for 24 hr at 400°C.

After the bismuth in the top compartment had been saturated with copper, the resulting solution was filtered into the second compartment where it came in contact with the copper crystal. The system was allowed to remain in this position for 100 to 150 hr at 400°C, after which time the bismuth solution was filtered into the third compartment and the entire apparatus removed from the salt bath.

It is believed that this procedure allowed the immersion of a clean copper single crystal in a saturated solution of copper in bismuth in which the oxide content had been greatly reduced. At no time was air allowed to enter the system, and all transfer of material was carried out so that the temperature equilibrium was not disturbed.

It was found that a copper sphere treated in the manner described maintained its generally spherical shape but that its surface was covered by a large number of small crystal facets. Macroscopically these facets were shown by the occurrence of specular reflections from the surface of the sphere. Under the microscope the facets themselves were clearly visible. Facets in the vicinity of a (111) pole are shown in Fig. 43. It was also noted that the facets tended to follow strain lines on the crystals, particularly on the stem of the crystal (Fig. 44) where the facets appeared to follow lines resembling lathe tool markings. The crystals used were originally shaped on a lathe, but prior to contact with the copper-bismuth solution they were polished mechanically with metallographic emery paper and carefully electropolished. In addition, the crystals were annealed in hydrogen at 400°C for about 24 hr

**Fig. 43. Copper Sphere Slowing Facets in the Vicinity of a (111) Pole.**

**Fig. 44. Stem of Copper Single Crystal in Which Facets Follow Strain Lines.**

before the interaction occurred, which indicates that surface rearrangements on a copper crystal may be sensitive to very small strains in the crystal.

By the use of x-ray-diffraction techniques it was established that the facets consisted of (111), (110), and (210) crystallographic planes. The (111) surfaces were more pronounced than the other two. It was also found that these facet surfaces were perpendicular to the corresponding crystallographic directions of the sphere. Thus (111) facet planes were detected only in the vicinity of (111) poles and similarly for the (110) and (210) surfaces.

These results were regarded as an indication that (111), (210), and (110) planes appear on the equilibrium form of a copper crystal in contact with a saturated bismuth solution at 400°C. This conclusion must be regarded as tentative because of the small temperature variations in the salt bath. It is possible that these small temperature changes might have allowed growth to occur by one of the mechanisms previously discussed.[3] Also, the formation of facets may have been partly caused by the presence of very small residual strains such as those mentioned. The energy represented by these strains may have been sufficient to cause the observed surface rearrangements.

From a practical standpoint, the sensitivity of surface rearrangement to small residual strains in the metal is of relatively minor importance when compared with the over-all problem of mass transfer in liquid metal-solid metal systems. However, should the problem of mass transfer be successfully solved, serious consideration might have to be given to the effect on valve facings and bearing surfaces of surface rearrangements resulting from strains. The roughening of such surfaces might be expected to lead to leaky valves or ruined bearings.

Several experiments have been planned that, it is hoped, will clarify the uncertainty regarding the origin of the surface rearrangements observed. First, it is felt that the temperature control of the salt bath can be improved. It is also believed that variations in the initial surface preparation given to the copper crystals will help to confirm these results. Finally, an experiment is planned in which the copper crystal is a sphere with (111), (210), and (110) planes cut on it. If these planes are true equilibrium planes, facets should not form on them when they are in contact with a saturated bismuth solution.

**Hydroxide Chemistry.** Studies are being made to determine what chemical reactions can occur in fused hydroxide media. The particular reactions being investigated are those which may be relevant to understanding and controlling mass transfer and corrosion by fused hydroxides. This research is at present a cooperative effort between Borie of the X-Ray group, Dyer of the Corrosion group, Richardson of the Physical Metallurgy Corrosion group, and Smith of the Physical Chemistry group. Each worker is able at the present to contribute only a small amount of time, except Dyer who is contributing about half of his time.

Most of the present studies have been confined to an examination of the solid reaction products produced in a system originally consisting of solid nickel, liquid sodium hydroxide, and gaseous oxygen. One experiment has been conducted in which iron was

(3) *Metallurgy Division Quarterly Progress Report for Period Ending October 31, 1951*, ORNL-1161, p. 36.

substituted for nickel. Some of the results of these experiments are presented in the reports of other sections. No conclusions can be drawn at this time, because all the experimental information is tentative, except the identification of the new compound sodium nickelate (III).

## MECHANICAL TESTING

R. B. Oliver D. A. Douglas
J. W. Woods

**Uranium.** Alpha-rolled uranium bars and bars that were alpha rolled and beta treated are being tested in vacuum at 500°C and at stresses from 1700 to 4500 psi. Design curves will be constructed from these and earlier data showing the times to several elongations, times to rupture, and the creep rates as a function of stress.

The effects of several atmospheres on the creep properties of uranium have received some attention. Two beta-treated bars were loaded to 2220 psi at 500°C in vacuum. One of the tests was conducted in vacuum only, whereas the other test was conducted alternately in vacuum and in a hydrogen atmosphere (3000 $\mu$). Figure 45 shows the results of the two tests; the hydrogen caused a marked increase in the creep rate, but upon re-evacuation the creep rate returned to the same rate as for the specimen tested in vacuum only. A similar pair of tests was conducted at stresses of 1720 psi but in a nitrogen (3000 $\mu$) instead of a hydrogen atmosphere. The data are presented in Fig. 46; the nitrogen did not appear to increase the creep rate, but upon re-evacuation the creep rate was reduced to considerably less than that observed for the specimen tested in vacuum only. When the test in nitrogen was discontinued, a large amount of scale was observed on the surface of the specimen; x-ray-diffraction analysis indicated that the scale was principally $UO_2$. It is felt that there was oxygen in the untreated gas and the resultant oxidation accounts for the observed behavior. The experiment will be repeated with purified nitrogen gas.

**Thorium.** All thorium testing during the past quarter was on an Ames billet having a nominal carbon content of 0.040%. Specimens are being tested at 16,000, 17,000, and 18,000 psi in vacuum at 300°C. One silver-plated bar is being tested in an argon atmosphere at 300°C. All extensions reported were measured optically. Previous reports have shown that for stresses up to 16,000 psi the rupture life is far in excess of 3500 hr and that a very low creep rate is exhibited, but at 19,000 psi very fast flow rates are observed and the rupture life is less than 50 hours. The specimen now in test at 18,000 psi has run for 450 hr with a total elongation of 12% and has maintained a creep rate of 0.006%/hr for the past 200 hours. When this test fails, another one will be conducted at 18,500 psi.

Experiments with thorium in hydrogen and nitrogen atmospheres, similar to those reported for uranium, have been conducted. Nitrogen had no detectable effect on the creep properties. Hydrogen caused a marked increase when first admitted to the chamber; however, this effect diminished with time and no marked change was noted when the chamber was re-evacuated. The over-all effect of the hydrogen treatment was to reduce the creep rate to a value much lower than that observed for a test in vacuum only. Figure 47 presents the results for several thorium tests. It is interesting to note that the silver-plated thorium bar, which was not evacuated and out-gassed, exhibited a greater creep rate than the thorium bar from the same extrusion that was tested in vacuum.

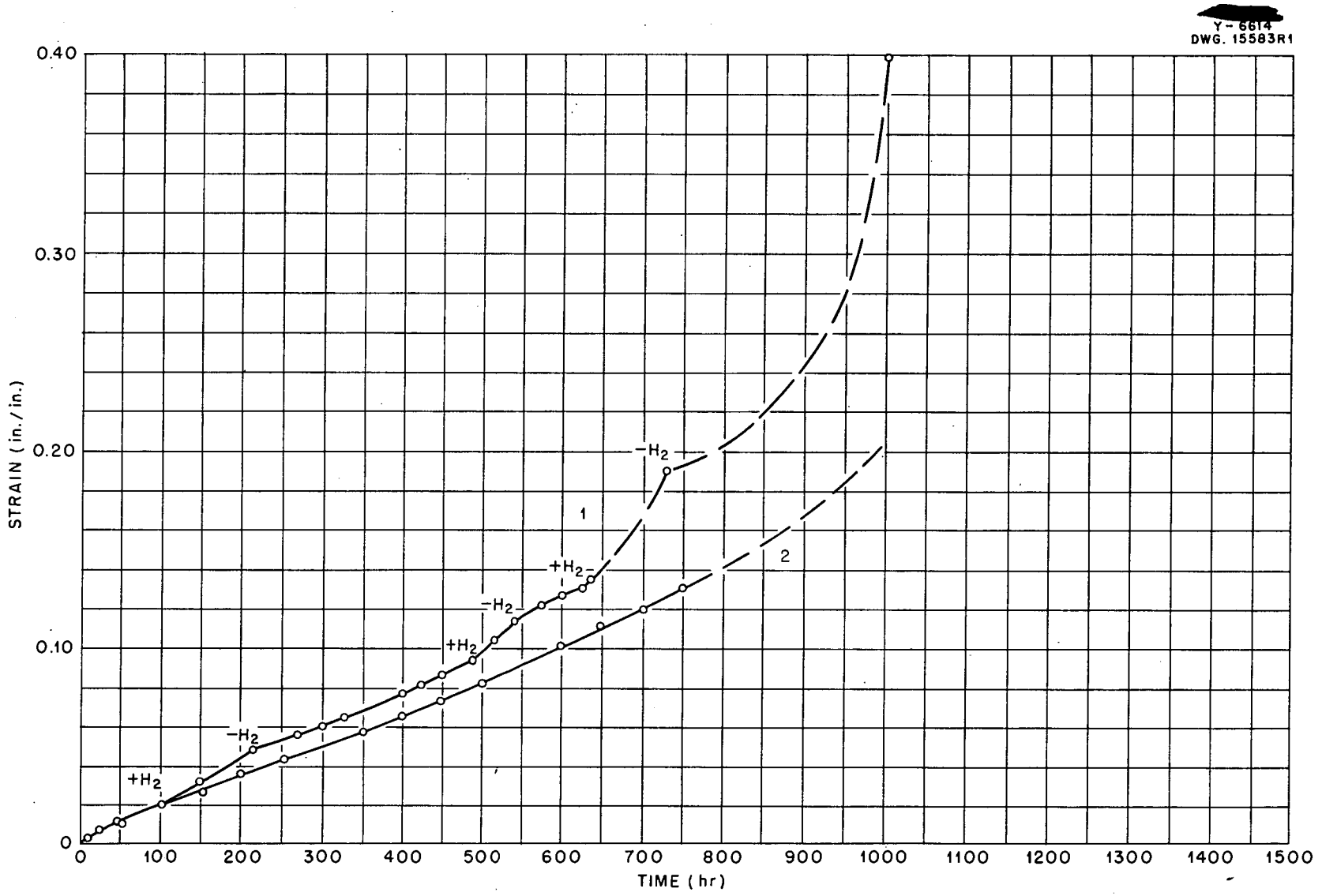


**Fig. 45. Creep Rate of Beta-Treated Normal Uranium Tested at 500°C and 2220 psi.** Curve 1: alternate vacuum (0.05 micron) and hydrogen (3000 microns). Curve 2: vacuum (0.05 micron) only. Dashed section estimated from dial gage data.

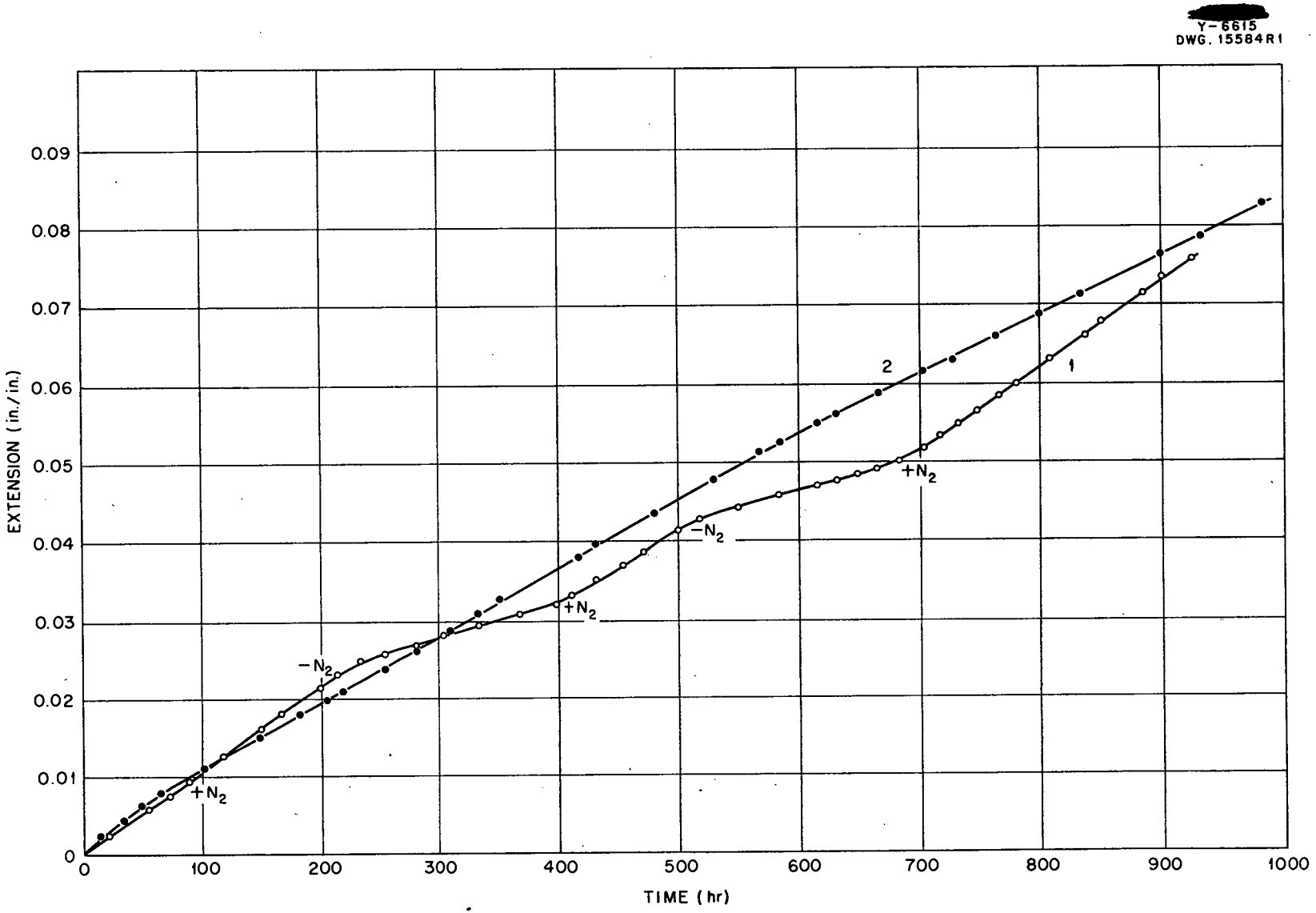


**Fig. 46. Creep Rate of Beta-Treated Normal Uranium Tested at 500°C and 1720 psi.** Curve 1: alternate vacuum (0.05 micron) and nitrogen (3000 microns). Curve 2: vacuum (0.05 micron) only.

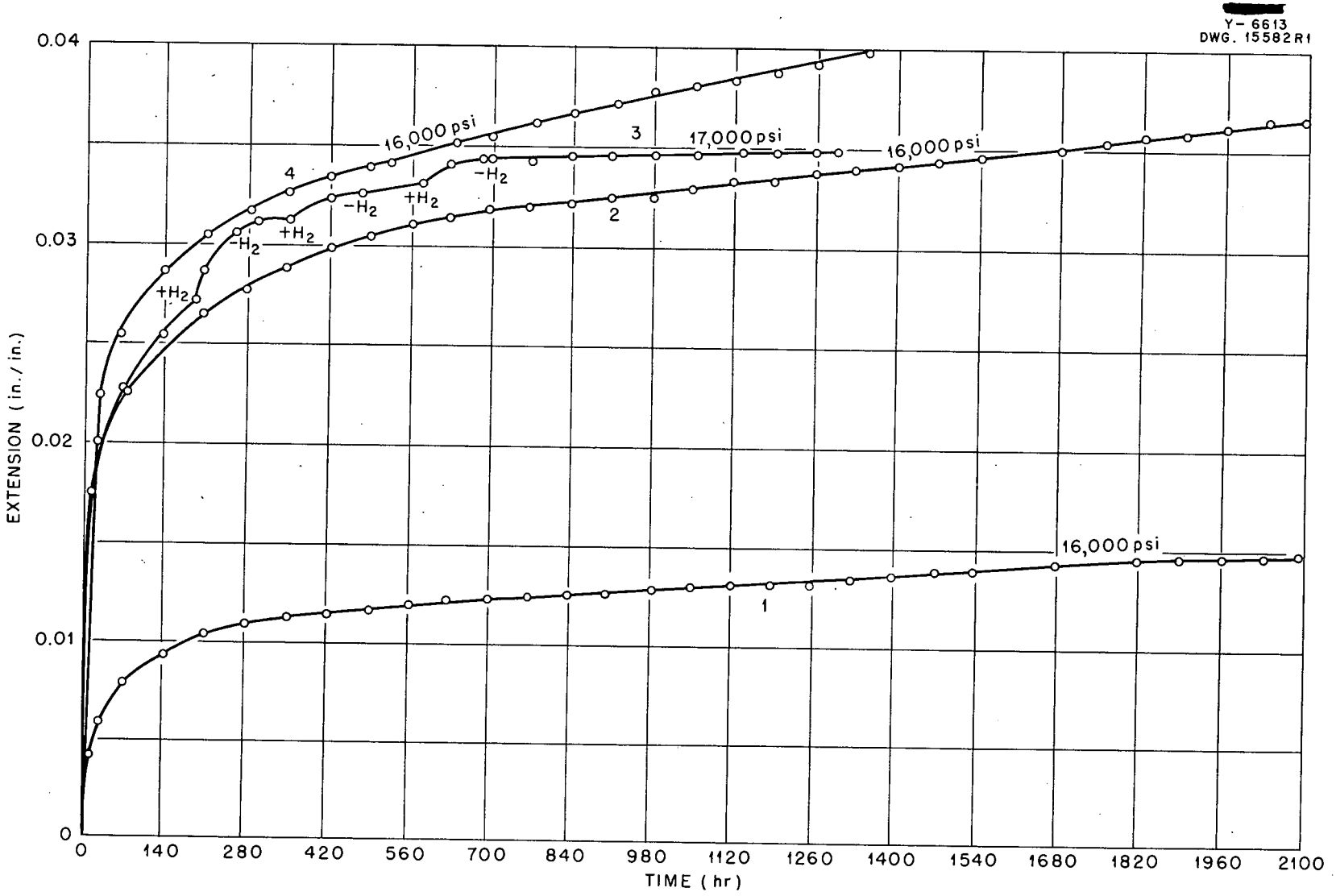


**Fig. 47. Creep Rate of Extruded Thorium Tested at 300°C.** Curve 1: as-extruded, deformed 5% in tension prior to testing in vacuum (0.05 micron) at 16,000 psi. Curve 2: as-extruded, tested in vacuum (0.05 micron) at 16,000 psi. Curve 3: as-extruded, tested in alternate vacuum (0.05 micron) and hydrogen (3000 microns) at 17,000 psi. Curve 4: as-extruded, silver plated, and tested in argon (atmospheric pressure) at 16,000 psi.

**Facilities for Stress-Rupture Testing in Liquid Metals and Fused Salts.** The installation of facilities for stress-rupture testing in liquid metals and fused salts is complete and the testing machines were calibrated with a standard sheet test specimen on which SR-4 strain gages were mounted; the specimen was calibrated against a standard proving ring.

The testing chambers were originally designed to contain sodium or other low-melting-point materials. A few minor design changes are being made because of the change in program and the need for data from tests with the higher melting fused fluorides. When the chambers were constructed the material under consideration for the reactor was type-316 stainless steel; however, the present emphasis is on Inconel, so several new chambers incorporating the above modifications are being constructed of Inconel. Containers to charge and empty the testing chambers have been designed and are being constructed; these containers, although designed to fit the original apparatus, will also fit the apparatus to be used with the fluoride mixtures. Testing with molten fluorides will be started soon after the first lot of fluoride mixture is received.

The primary purpose of these tests will be to study the effe t of stress-corrosion on the creep rate and stress-rupture life of these materials. Both Inconel and type-316 stainless steel are to be tested in the modified apparatus in an argon atmosphere in the same stress ranges as they were previously tested in the old apparatus. A comparison of the two sets of data will establish the effects of the inherent variables of the new testing systems, and thus the results of the corrosive action can be studied.

**Inconel.** Both fine- and coarse-grained specimens of Inconel are being tested at stresses from 1500 to 4500 psi in argon at 815°C. The expected test duration in this stress range is from 800 to 3000 hr; upon completion of the tests revised design curves will be compiled. A short series of tests at 815°C in air are being initiated to obtain data for a comparison of the effects of oxidation and fluoride attack on the creep rate and rupture life.

**Type-316 Stainless Steel.** Specimens are being tested in argon in both the old and the modified chambers at 5300, 5800, 6300, 6800, and 7300 psi. These duplicate sets of data will serve to correlate the work in the two types of testing chambers and will furnish data for a design curve for type-316 stainless steel tested in argon.

## FABRICATION

E. S. Bomar, Jr., J. H. Coobs, H. Inouye

**Loose Powder Bonding.** In the development of fuel elements utilizing solid fuel, a variety of possible configurations have been suggested for incorporating the fuel with a structural material. One method of fabrication would be to bond a fuel-bearing powder to an appropriate backing material by sintering of the powder either with or without application of pressure.

Preliminary experiments to prepare flat sheets covered on one side with a sintered fuel-bearing powder were carried out in a furnace at the Micro-Metallic Corporation in New York and reported previously.[4,5]

(4) *Metallurgy Division Quarterly Progress Report for Period Ending April 30, 1951*, ORNL-1033.

(5) *Metallurgy Division Quarterly Progress Report for Period Ending July 31, 1951*, ORNL-1108.

Since then, a furnace with a suitable reducing atmosphere has been made available at ORNL and used for further work on this problem.

The several variables that have been investigated are sintering temperature, sintering time, fuel component particle size, cold working and resintering, surface preparation, and sintering under load. Samples processed to include these variables were examined metallographically for evaluation of results.

The trend apparent from the examinations was toward improved strength of bond between the backing sheet and powder with increasing sintering temperatures. After sintering at 1300°C and lower temperatures, bonding of the 30% (by volume) $UO_2$-70% type-302 stainless steel mixture was very poor, but the samples sintered at 1360°C or higher showed considerable tenacity, even on bending. However, heating to these high temperatures caused transformation of some of the austenite to delta ferrite, which appeared as needle-like crystals in the type-302 stainless steel matrix and as a band about individual grains of the type-316 stainless steel. The latter distribution of the ferrite might possibly lead to preferential grain-boundary attack if the backing were subsequently exposed to one of the coolants of current interest.

The presence of the magnetic phase in the type-316 stainless steel was shown by placing a drop of an aqueous suspension of a colloidal iron compound on the surface of the metallographic specimens and then exposing the samples to a magnetic field. A more complete description of the use of this technique is outlined in the "Metallographic Laboratory" section of this report.

In contrast to the results obtained with samples sintered at the Micro-Metallic Corporation, the surface preparation of the type-316 stainless steel sheet had little effect on the degree of bonding to the powder layer. Some small benefit may have been obtained by roughening by sand blasting or by using annealed, as-received stock instead of electropolished sheet.

The sintering-time study indicated that there was no appreciable increase in the quality of the bond obtained when the samples were heated for periods up to 2 hr compared with the quality obtained when a sample was held at temperature for 30 minutes.

An increase in $UO_2$ particle size from −325 mesh toward 100 mesh was accompanied by better bonding between powder and backing sheet.

Gravity loading during sintering in the range of from ½ to 5 psi resulted in a slight improvement in the density of the powder layer.

*Material and Procedure.* The metal used in these bonding experiments was type-302 stainless steel (−325 mesh) and the fuel component was $UO_2$ fired to 2100°C in a hydrogen atmosphere. U. S. standard screens were used for sizing particles.

A Globar-heated ceramic-tube furnace was used for all the experiments, except the runs requiring loading of the samples. The latter were carried out in a larger molybdenum-wound furnace equipped with an Inconel tube. The furnace atmosphere in each instance was hydrogen that had been passed over a platinum catalyst and through an activated-alumina drying column. The type-316 stainless steel stock was annealed in the hydrogen atmosphere prior to coating with the powder mixture.

*Sintering Temperature.* The first samples prepared to evaluate the possibilities of bonding a fuel-bearing loose powder to a backing plate were run at temperatures of 1250 to 1280°C. These samples showed only a moderate degree of bonding, so higher sintering temperatures were selected for the series reported here.

The four samples shown in Fig. 48 were sintered at 1300, 1325, 1360, and 1385°C, respectively. The powder layer is composed of 30% by volume (-200, +325 mesh) $UO_2$-70% (-325 mesh) type-302 stainless steel. The powder mixture was placed on the backing and leveled to approximately 0.030 in. thickness.

Metallographic examination of the samples after sintering disclosed a relatively high degree of consolidation and bonding in the 1385°C sample, but there was successively poorer bonding as the sintering temperature was dropped to 1300°C. The retention of $UO_2$ during polishing increased in the same order. The powder layer could quite easily be scraped off the low-temperature samples.

There was a tendency toward dusting of the powder layer even when the very high sintering temperature was used. In an effort to consolidate the powder layer, the composites were rolled to a 40% reduction in area and reheated to 1250°C for 30 minutes. These samples are also pictured in Fig. 48. Similar reduction treatment was given to the samples for each of the following experiments.

*Surface Preparation.* Backing plates prepared by electropolishing and by sand blasting were tested along with the sintering temperature samples to evaluate surface preparation effects. The results showed slightly better bonding for as-received or sand-blasted sheet than for electropolished sheet.

*Sintering Time.* Examination of the time-at-temperature variable was made by testing samples for 1/4, 1/2, 1, and 2 hours. These results are shown in Fig. 49. Inspection of the bonds indicated only a mild improvement, if any, for samples sintered more than 30 minutes.

Duplicate samples from this group were also given a 40% cold reduction and reheated to 1250°C for 30 minutes. In every case the results were essentially the same. The rolled and sintered samples showed well-consolidated structures with relatively small porosity. The $UO_2$ retention in several instances was poor - the $UO_2$ pulled out when the samples were polished. The poor retention of $UO_2$ is thought to be the result of partial crushing of the oxide particles during rolling.

*Oxide Particle Size.* The quality of the bond between the metallic particles in the powder layer and the backing sheet showed general improvement as the particle size of the $UO_2$ was increased. Particle sizes ranging from -100 +140 mesh to -325 mesh were used. The better continuity with the larger particle sizes is shown in Fig. 50; both the as-sintered samples (1300°C for 45 min) and the rolled and resintered counterparts are illustrated in this figure. Cold rolling followed by reheating at 1250°C resulted in considerable compacting (also illustrated in Fig. 50).

*Sintering Under Load.* Samples were loaded during sintering by using steel weights to obtain unit pressures of 1/2 to 5 psi. Cross sections of these samples, shown in Fig. 51, indicate that no gross improvements were achieved by the maximum loading used.

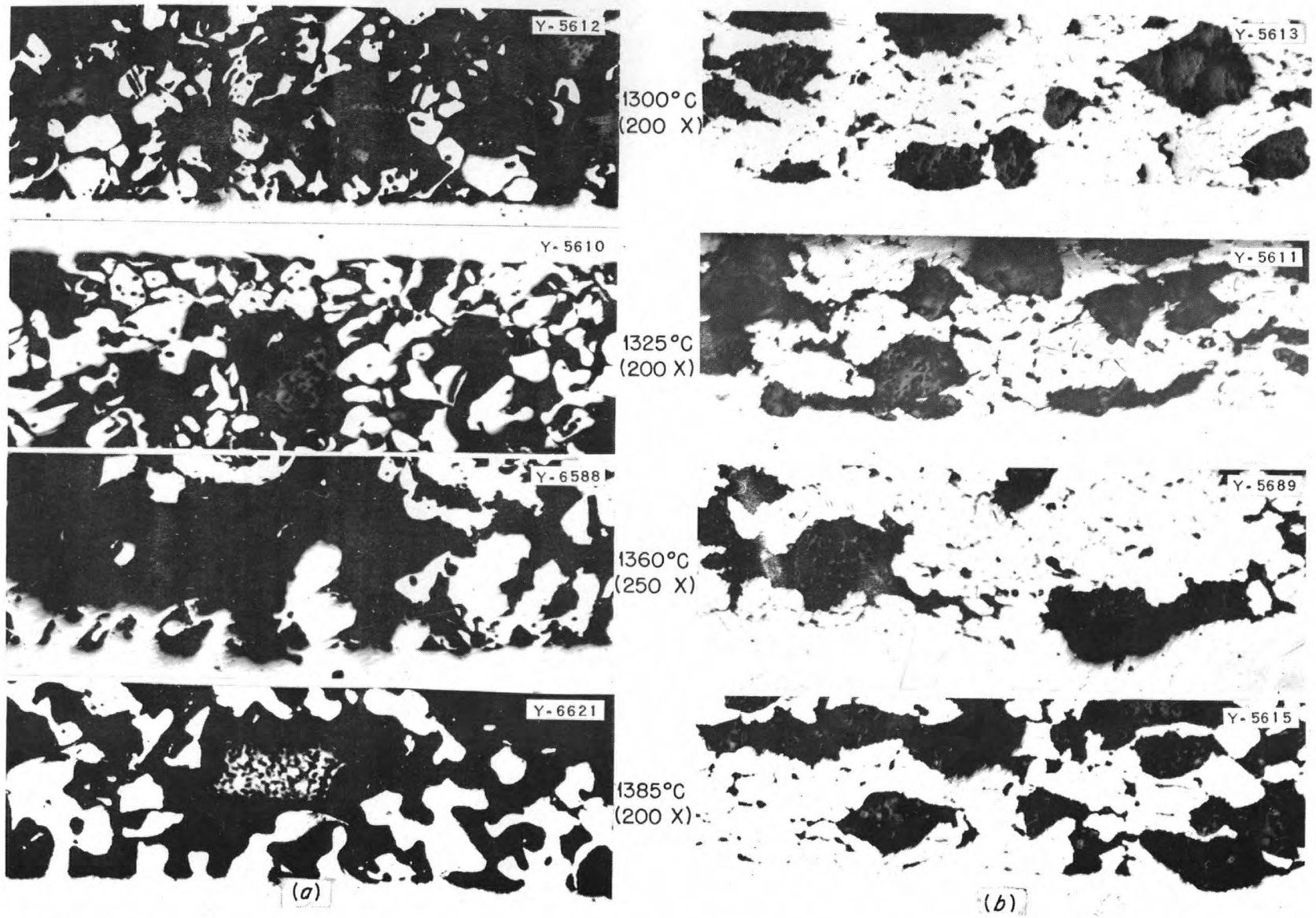


**Fig. 48. Bonding of Fuel-Bearing Powder to Type-316 Stainless Steel Sheet at Various Sintering Temperatures.** (*a*) As-sintered for 45 minutes. (*b*) Cold rolled to 40% reduction in area and resintered 30 min at 1250°C.

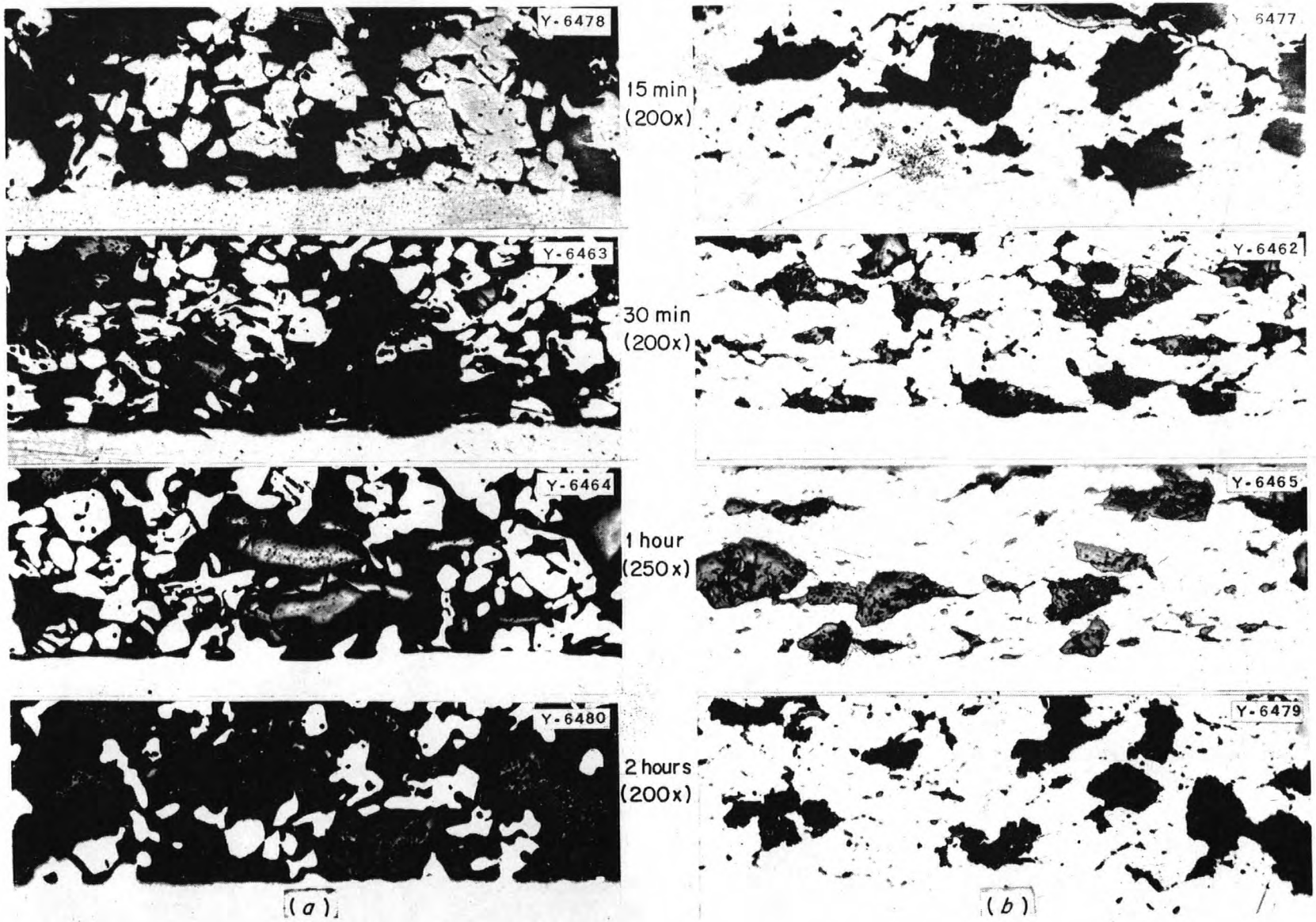


**Fig. 49. Bonding of Fuel-Bearing Powder to Type-316 Stainless Steel Sheet at Various Sintering Times.** (*a*) As-sintered at 1300°C. (*b*) Cold rolled to 40% reduction in area and resintered 30 min at 1250°C.

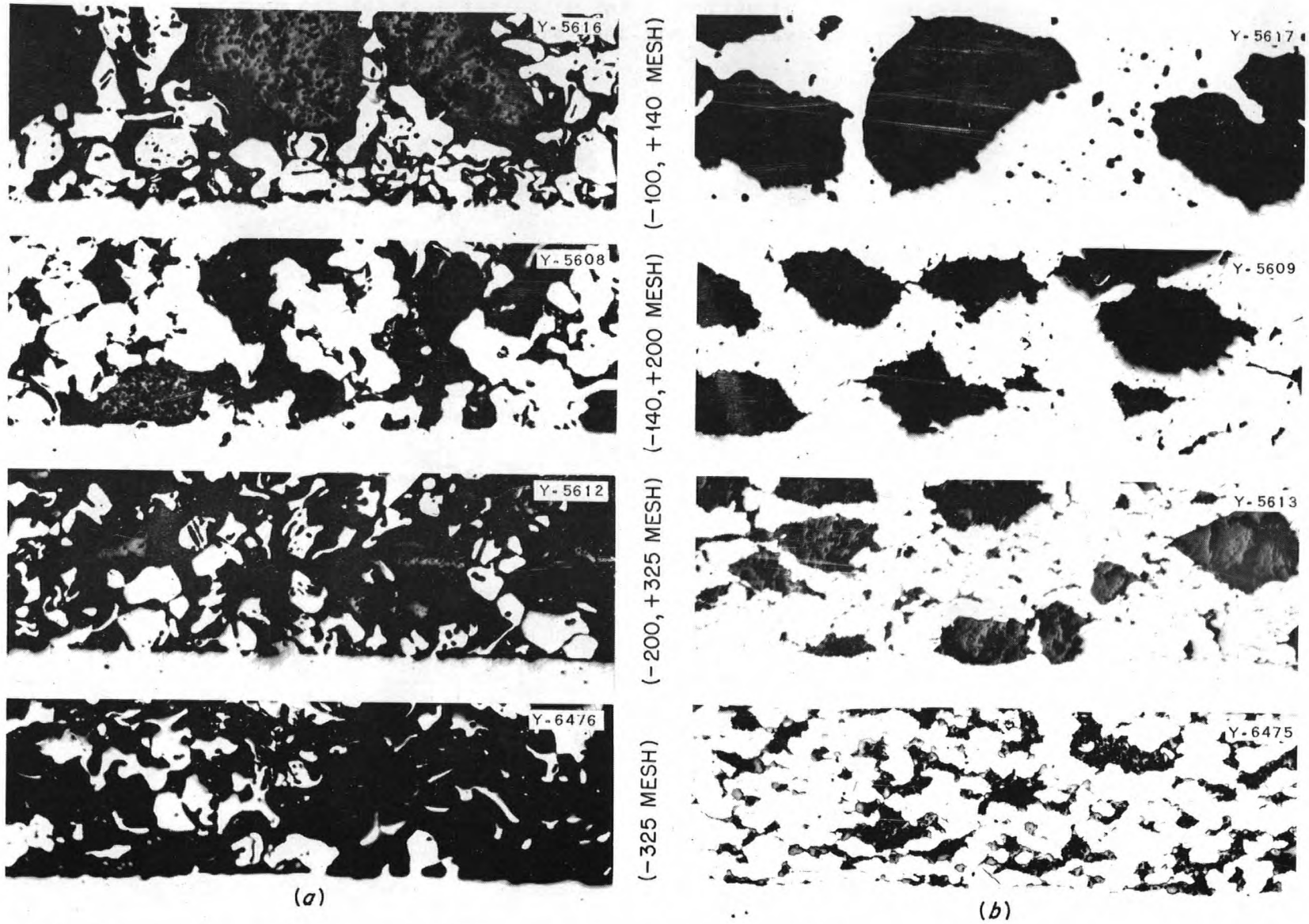


**Fig. 50. Bonding of Fuel-Bearing Powder of Various Particle Sizes to Type-316 Stainless Steel Sheet.** (*a*) As-sintered for 45 min at 1300°C. (*b*) Cold rolled to 40% reduction in area and resintered 30 min at 1250°C. 200X.

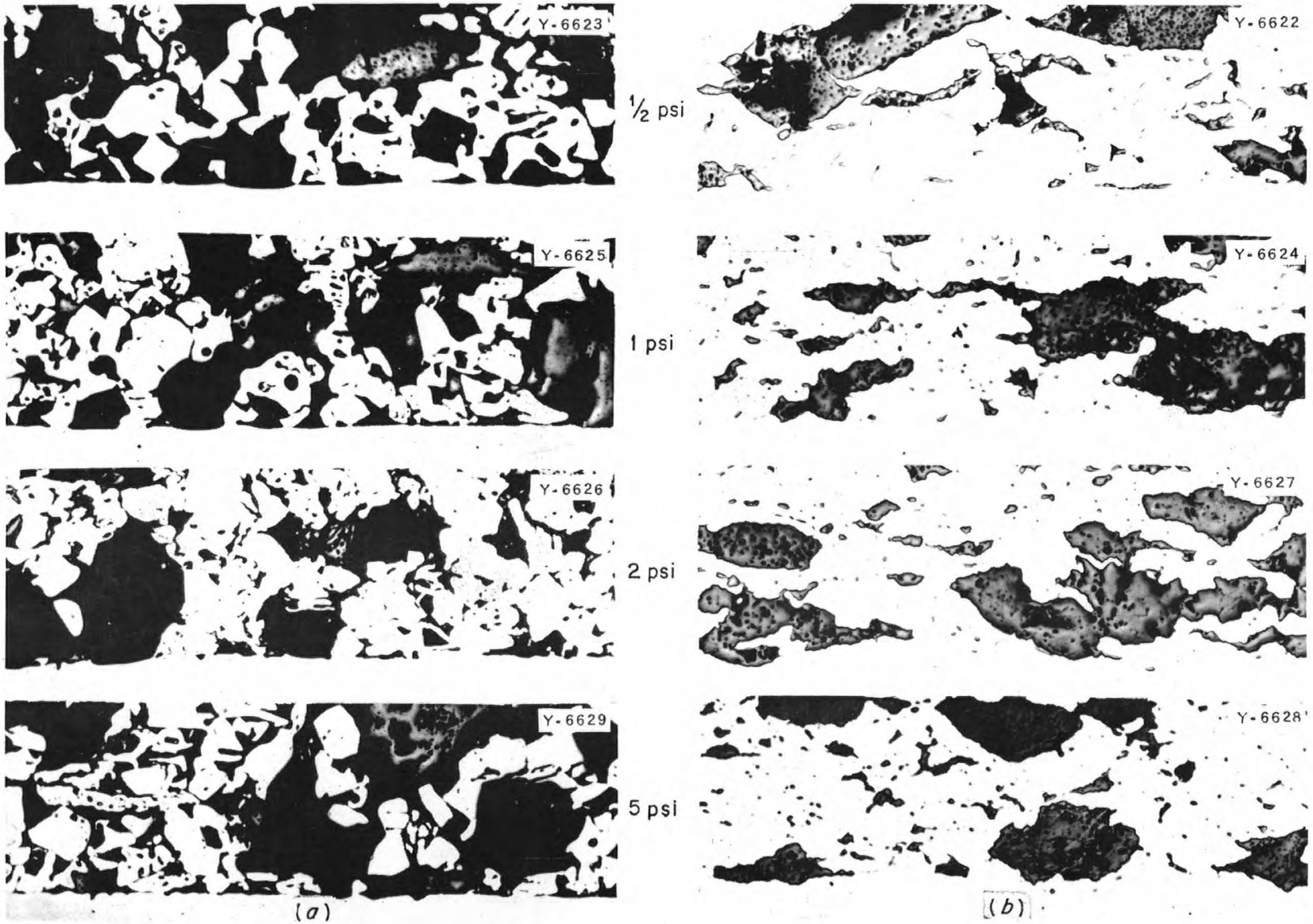


**Fig. 51. Bonding of Fuel-Bearing Powder to Type-316 Stainless Steel Sheet at Various Static Loadings.** (*a*) As-sintered for 30 min at 1250°C. (*b*) Cold rolled to 40% reduction in area and resintered 30 min at 1250°C. 200X.

**ARE Control and Safety Rods.** The design of the ARE control and safety rods has been completed, and fabrication of the components has begun. After considering the availability of stock for the cans and the time schedule to be met, it was decided to make the cans of the types-316 and -304 stainless steel tubes on hand. These are admittedly not the best materials for compatibility with boron carbide and perhaps not the best from the standpoint of self-welding; however, the delay necessary to obtain the more desirable type-430 stainless steel tubing is prohibitive. The cans are being fabricated by the Y-12 Machine Shops and will be loaded with boron-containing slugs and brazed with Wall-Colmonoy Nicrobraze by the welding group.

Fabrication work has begun on the safety rod slugs, which will be hot pressed from an iron-boron carbide mixture containing 56% by weight (80% by volume) boron carbide. The iron-boron carbide mixture was selected because of the special fabrication problems associated with pure boron carbide. The mixture will be prepared by milling boron carbide for 16 hr in a steel mill with steel balls and blending it for 8 hr with the requisite amount of -325 mesh iron powder. This mixture will be fabricated by hot pressing at 1520°C and 2500 psi in graphite dies. Several slugs of intermediate size have been fabricated successfully with densities of 2.80 g/cc or better (about 80% of theoretical) and with acceptable dimensional tolerances. The hot-pressing furnace for the full-size slugs is being constructed.

Two of the iron-boron carbide slugs have been canned and brazed. One was cut open to check for reaction between the boron carbide and the container, and no reaction was found. The second is being held at 815°C for 100 hours.

The requirements for the regulating rod (shim rod) are somewhat different. For this rod a small amount of boron (3 to 12.5 g) must be uniformly dispersed in a material relatively transparent to neutrons, such as $Al_2O_3$. A preliminary slug was made by hot-pressing a mixture composed of 90% $Al_2O_3$ (grade 38-500) plus 10% $B_4C$ at 1750°C in a graphite die under a pressure of 2500 psi. Metallographic examination revealed that the two materials are compatible and that these conditions will probably be satisfactory for fabrication of full-size slugs. A second slug containing 0.74% by weight (-325 mesh) $B_4C$, prepared by the same technique, had a density of 3.45 g/cc (86% of theoretical) and possessed satisfactory physical properties and dimensional tolerances.

## BRAZING

G. M. Slaugther

The primary objective of the high-temperature brazing alloy investigation during the past few months has been to screen out brazing alloys for use in ANP type of applications. Flowability and static corrosion tests in sodium hydroxide and fluoride No. 14 baths are being used. After these preliminary investigations have been completed, promising alloys can be further studied in physical property tests such as butt-tensile tests (at both room and elevated temperatures), elevated-temperature creep tests, dynamic corrosion tests, and room- and elevated-temperature ductility tests. Such screening procedures seem appropriate because of the large number of alloys now under consideration.

The results of preliminary investigations of eight high-temperature brazing alloys are recorded in Table 27. The melting points given for the

TABLE 27

Properties of High-Temperature Brazing Alloys

| BRAZING ALLOY | APPROXIMATE MELTING POINT (°F) | BRAZING TEMPERATURE (°F) | FLOWABILITY OBSERVATIONS | STATIC CORROSION RESULTS ON BRAZED INCONEL | | STATIC CORROSION RESULTS ON BRAZED TYPE-316 STAINLESS STEEL | |
|---|---|---|---|---|---|---|---|
| | | | | IN FLUORIDE NO. 14 | IN NaOH | IN FLUORIDE NO. 14 | IN NaOH |
| Nicrobraz (70.17% Ni-13.95% Cr-5.86% Fe-4.59% Si-4.92% B) | 1850 | 2050 | Excellent | Slight attack with leaching of boron | Extremely severe | Slight | Severe |
| 60% Mn-40% Ni | 1850 | 1960 | Poor flow and cracking is prevalent | Severe | Severe | | |
| 60% Pd-40% Ni | 2260 | 2320 | Excellent | No apparent attack | Severe | | |
| 60% Pd-37% Ni-3% Si | 2150 | 2200 | Excellent | Moderate | Severe | Moderate | Severe |
| 16.5% Cr-10.0% Si-73.5% Ni | 2100 | 2200 | Moderate | | | | |
| 16.5% Cr-10.0% Si-2.5% Mn-71.0% Ni | 2100 | 2200 | Moderate | Severe | Severe | Moderate | Severe |
| 64% Ag-33% Pd-3% Mn | 2130 | 2200 | Excellent | Slight | Severe | Very slight | Severe |
| 75% Ag-20% Pd-5% Mn | 2100 | 2200 | Excellent | Severe | Severe | | |

various alloys are only approximate and will vary some since chemical analyses of various heats of the same alloy differ slightly.

Static corrosion tests on joints brazed with some of these alloys are being made. The tests of Nicrobrazed joints on Inconel and type-316 stainless steel in both sodium hydroxide and fluoride No. 14 have been completed. Fluoride No. 14 has a relatively minor corrosive effect on both types of joints, as can be seen in Figs. 52 and 53; sodium hydroxide was much more severely corrosive, as can be seen in Figs. 54 and 55.

The 60% Mn-40% Ni alloy is extremely brittle and many brazed joints made with this alloy cracked severely, as illustrated by Fig. 56. Since this brazing alloy has low resistance to corrosion in fluoride No. 14 and sodium hydroxide and relatively poor flow properties, it appears to be unsuitable for the ANP type of applications. Photomicrographs of Inconel joints brazed with this alloy and tested in fluoride No. 14 and sodium hydroxide are shown in Figs. 57 and 58. It can be seen that the brazing alloy is attacked rather severely in both cases.

The 60% Pd-40% Ni brazing alloy has excellent flowability properties, and from the rather limited experimental data obtained to date, it seems to have better-than-average resistance to corrosion by the fluorides. The insignificant attack of the fluoride No. 14 bath on an Inconel joint brazed with this alloy is shown in Fig. 59. It can be seen that intimate bonding with the base metal is obtained during brazing, since the grain boundaries of the Inconel proceed directly across the interface.

The 37% Ni-60% Pd system with 3% silicon added for its effect upon melting-point lowering was also investigated. The silicon addition caused phenomenal flow, which is illustrated by the Inconel flowability test specimen shown in Fig. 60. It can be seen that the brazing alloy flowed all the way along the 6-in. joint and even flowed up the scratches. However, the room-temperature tensile strength of type-316 stainless steel joints butt-brazed with the alloy was low, and the brazed joint was very brittle. Standard 0.505-in.-dia butt-brazed tensile bars were tested to obtain an indicative value of the quality of the joints, and the results showed a tensile strength of 48,500 psi with a brittle fracture. The fracture occurred along the centerline of the brazed joint - its appearance is illustrated in Fig. 61. The resistance to corrosion of Inconel brazed joints in fluorides seems to have been lowered somewhat by the addition of the silicon to the 37% Ni-60% Pd system.

Two brazing alloys of the Ni-Cr-Si-Mn type have been investigated in preliminary experiments. The 16.5% Cr-10.0% Si-73.5% Ni alloy and the 16.5% Cr-10.0% Si-2.5% Mn-71.0% Ni alloy have desirable flowability characteristics but are apparently attacked to some extent by the fluorides and rather severely by sodium hydroxide. A complete set of photomicrographs showing the extent of corrosion will be presented when available.

Two silver-base brazing alloys of the compositions 64% Ag-33% Pd-3% Mn and 75% Ag-20% Pd-5% Mn, which melt at approximately 2100°F, have been investigated, and it has been shown that the flowability of these alloys is very good. The results of static corrosion tests are incomplete at the present time. When in contact with fluoride No. 14 bath, the brazed joint of 64% Ag-33% Pd-3% Mn on type-316

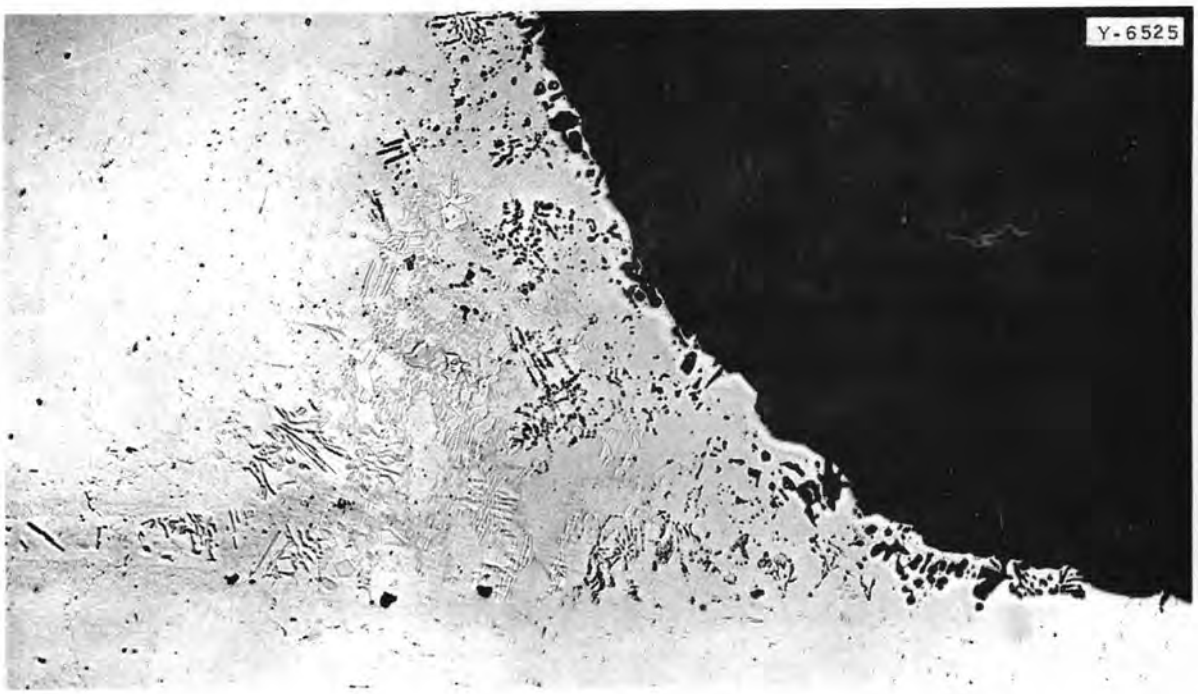


**Fig. 52. Nicrobrazed Inconel Joint Tested in Fluoride No. 14 Bath for 100 hr at 1500°F.** Slight attack can be seen. Unetched. 150X.

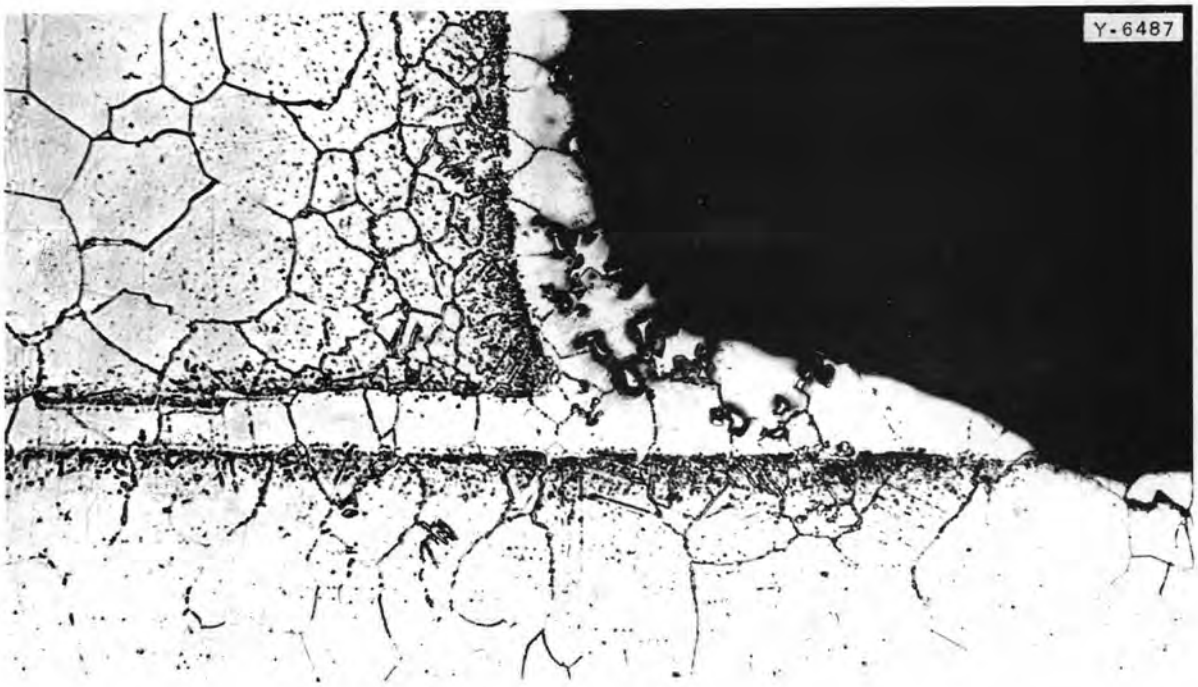


**Fig. 53. Nicrobrazed Type-316 Stainless Steel Joint Tested in Fluoride No. 14 Bath for 100 hr at 1500°F.** The brazing alloy was severely pitted. Etched with aqua regia. 200X.

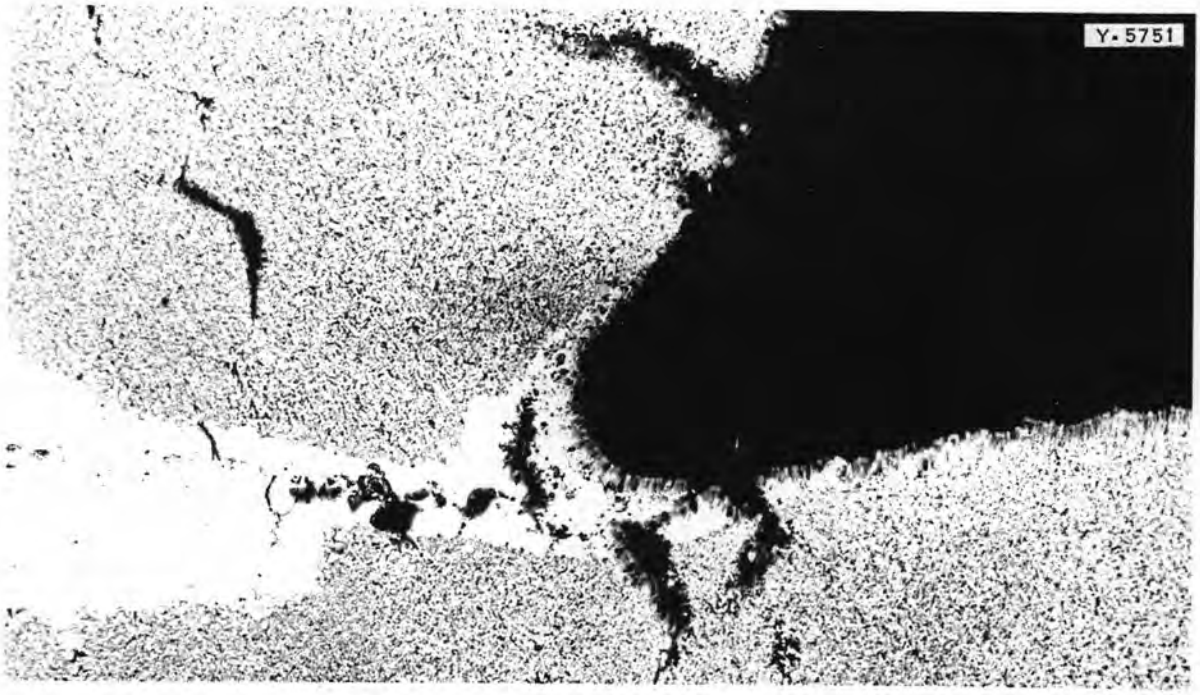


**Fig. 54. Nicrobrazed Inconel Corrosion Specimen Tested in Sodium Hydroxide for 100 hr at 1500°F.** Extremely heavy attack present. Unetched. 250X.

**Fig. 55. Nicrobrazed Type-316 Stainless Steel Joint Tested in Sodium Hydroxide for 100 hr at 1500°F.** The brazing alloy was severely attacked. Etched with aqua regia. 200X.

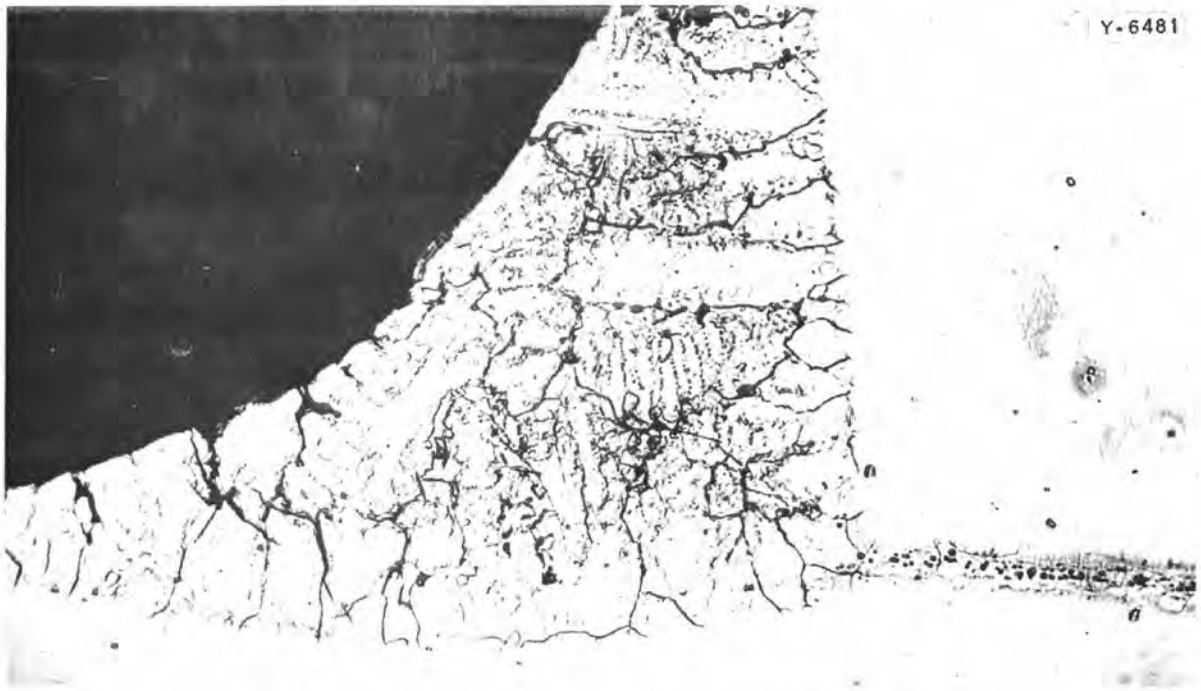


**Fig. 56. Inconel Joint Brazed with a 60% Mn-40% Ni Alloy Showing the Extreme Propensity of the Alloy for Cracking.** Etched with mixed acids. 50X.

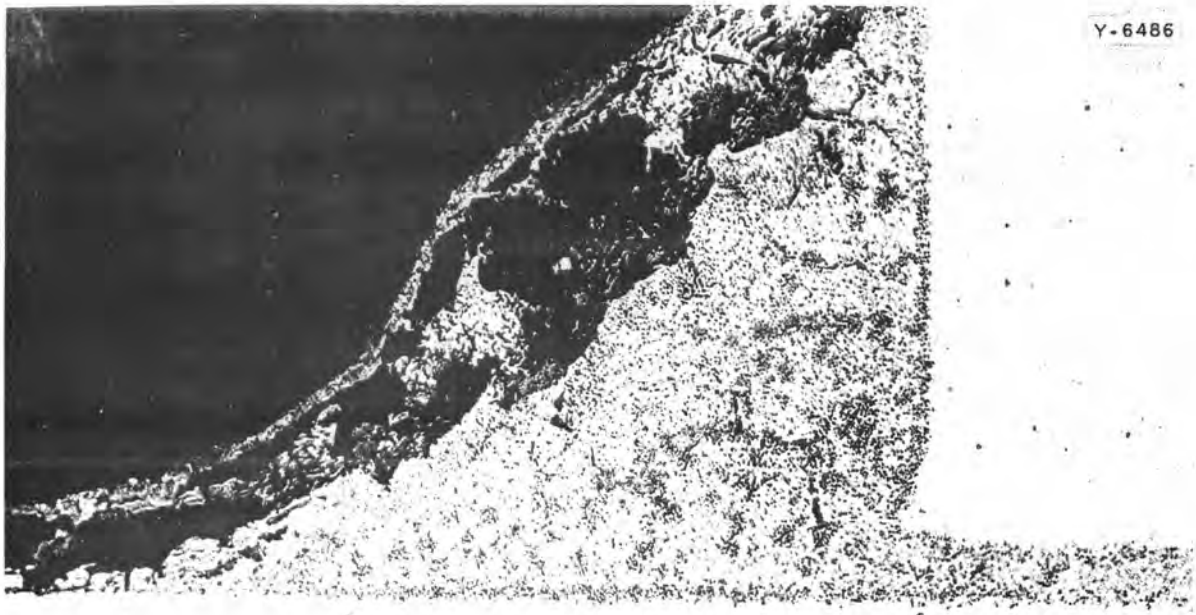


**Fig. 57. Inconel Joint Brazed with a 60% Mn-40% Ni Alloy and Tested in Fluoride No. 14 Bath for 100 hr at 1500°F.** The brazing alloy was severely attacked. Unetched. 150X.

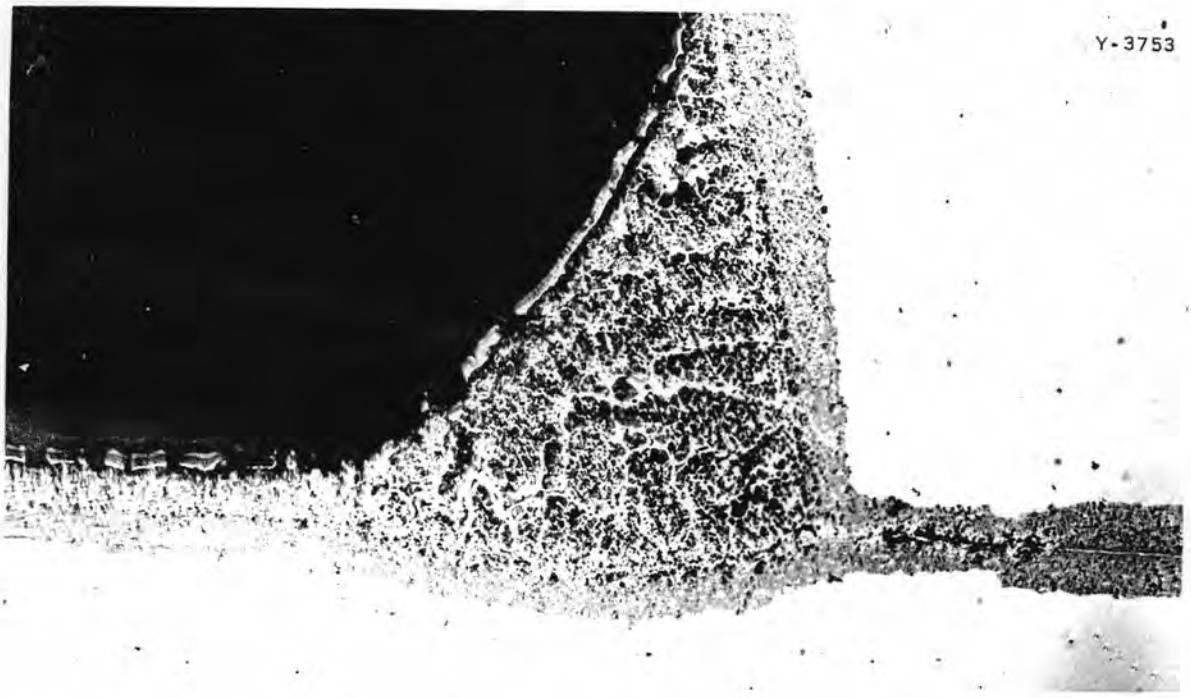


**Fig. 58. Inconel Tube-to-Header Corrosion Specimen Brazed with a 60% Mn-40% Ni Alloy and Tested in Sodium Hydroxide for 100 hr at 1500°F.** Heavy general attack on the alloy can be seen. Unetched. 100X.

**Fig. 59. Inconel Joint Brazed with a 60% Pd-40% Ni Alloy and Tested in Fluoride No. 14 Bath for 100 hr at 1500°F.** Excellent surface bonding is evidenced - the grain boundaries extend across the brazed interface in many places. No corrosive attack can be seen. Etched with aqua regia. 100X.

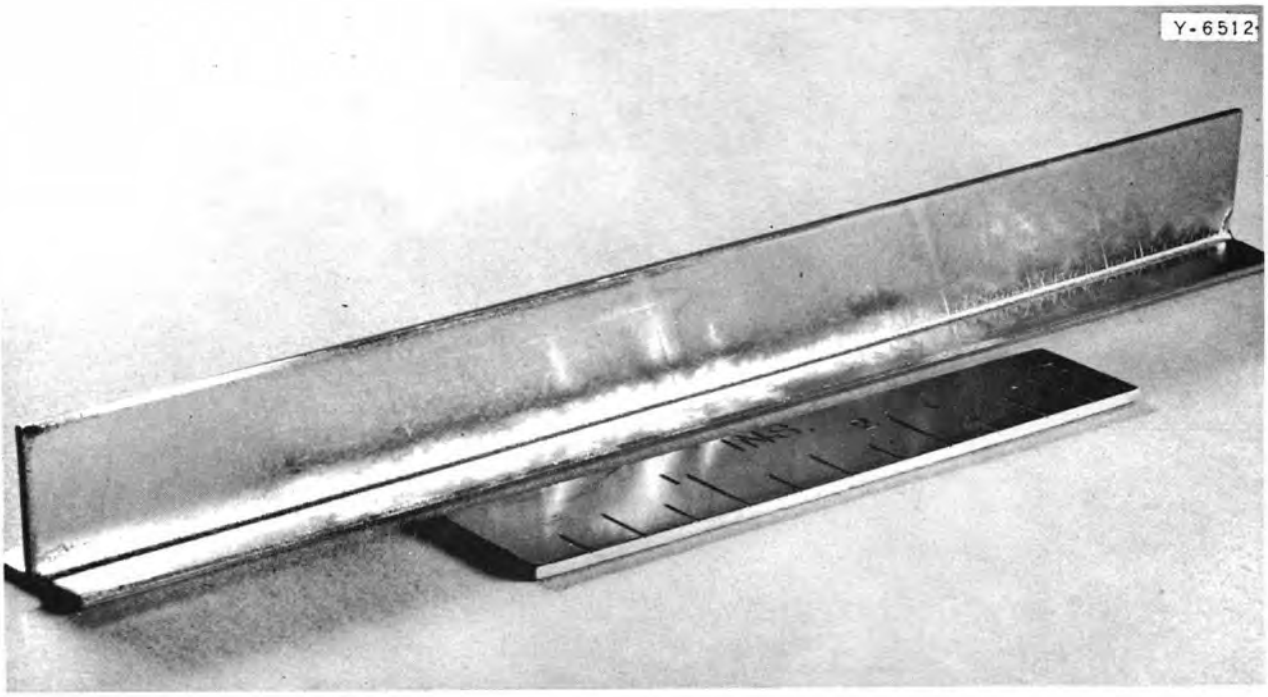


**Fig. 60. Typical Inconel Flowability Test Specimen Brazed with 60% Pd-37% Ni-3% Si.** The excellent flowability characteristics of this alloy are shown - it actually flows along the scatches.

**Fig. 61. Section of an As-Tested Type-316 Stainless Steel 0.505-in. Tensile Test Bar Brazed with a 60% Pd-37% Ni-3% Si Alloy.** The bar fractured in a brittle manner at 48,500 psi, and the elongation in a 2-in.-gage length was 7%. Fracture occurred along the center of the brazed joint. Etched with aqua regia. 200X.

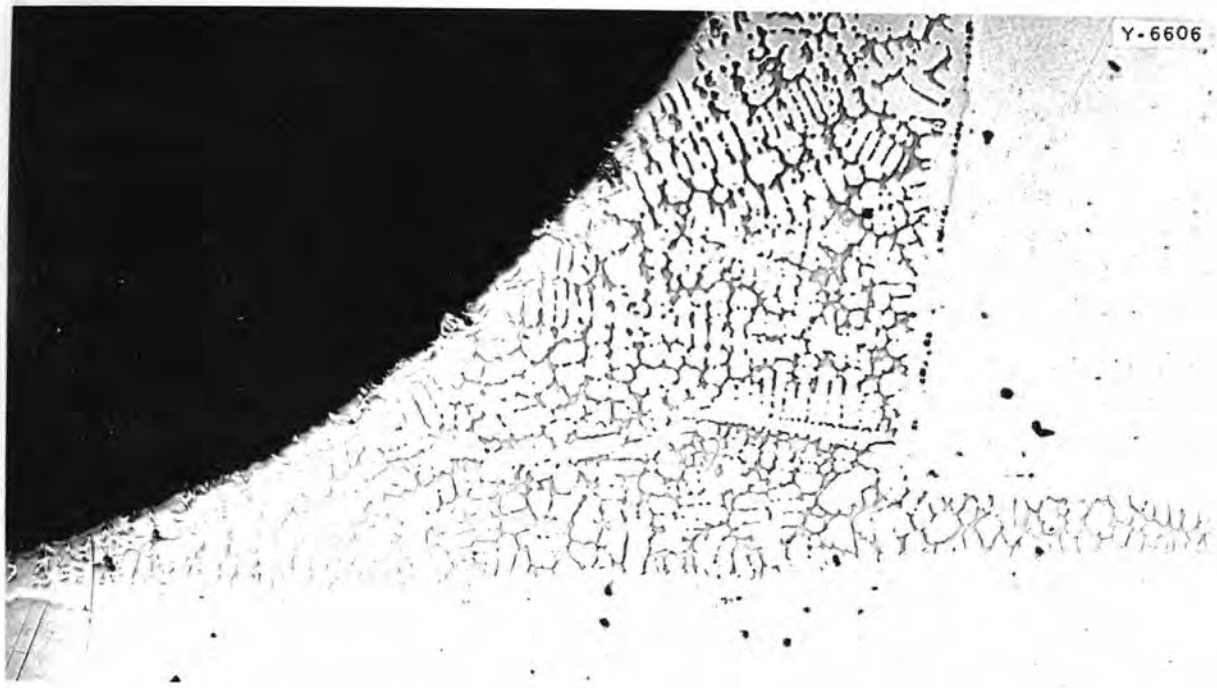


**Fig. 62. Type-316 Stainless Steel Joint Brazed with a 64% Ag-33% Pd-3% Mn Alloy and Tested in Fluoride No. 14 Bath for 100 hr at 1500°F.** The brazed joint was apparently unattacked. Unetched. 100X.

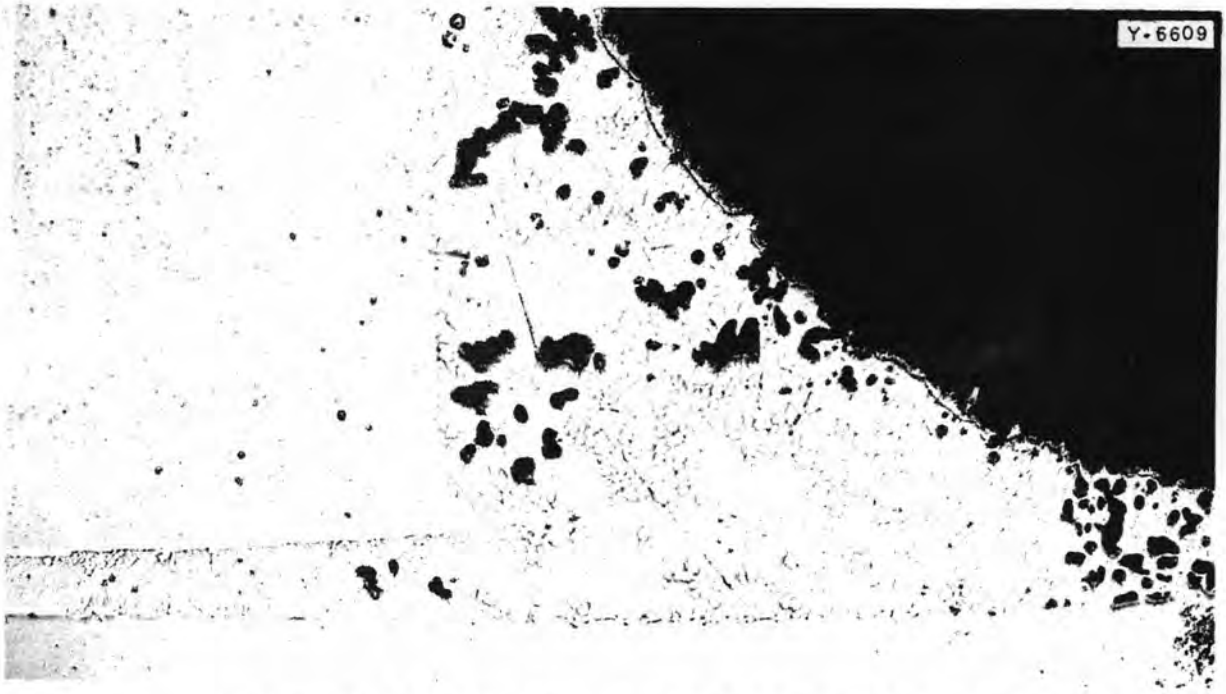


**Fig. 63. Inconel Joint Brazed with a 75% Ag-20% Pd-5% Mn Alloy and Tested in a Fluoride No. 14 Bath for 100 hr at 1500°F.** The brazing alloy was attacked to a considerable extent as is shown by the large voids in the fillet. Unetched. 100X.

**Fig. 64. Type-316 Stainless Steel Joint Brazed with a 64% Ag-33% Pd-3% Mn Alloy and Tested in Sodium Hydroxide for 100 hr at 1500°F.** The fillet of brazing alloy contained many large voids, and the base metal was severely attacked. Unetched. 100X.

stainless steel was only slightly attacked, whereas the Inconel joint brazed with 75% Ag-20% Pd-5% Mn was severely attacked. These brazed joints are illustrated in Figs. 62 and 63. The extreme attack of sodium hydroxide on a brazed joint of 64% Ag-33% Pd-3% Mn on type-316 stainless steel is shown in Fig. 64.

Further attempts are being made to lower the melting point of the 40% Ni-60% Pd alloy by the addition of a third component. A 1% beryllium addition and a 10% manganese addition are being studied, but more work has to be done before the desirability of such additions can be determined.

## WELDING

P. Patriarca

**Cone-Arc Welding.** It was considered desirable as a result of previous preliminary experiments to determine some practical aspects of cone-arc welding techniques as applied to tube-to-header heat exchanger fabrication. This study was given precedence over the long-range approach of determining the individual and combined effects of the various cone-arc welding process variables such as arc time, arc current, material and material size, and physical geometry of header design.

The equipment used for cone-arc welding experiments has been described previously.[6] A series of headers were fabricated to conform to a closely packed tube-hole arrangement in a circular header. The header material was type-304 stainless steel sheet, 1/8 in. in thickness. Nineteen tube

(6) *Metallurgy Division Quarterly Progress Report for Period Ending January 31, 1952*, ORNL-1267.

holes were drilled to receive 0.100-in.-OD type-316 stainless steel tubing with a wall thickness of 0.010 inch. The basic pattern was an equilateral triangle with a tube hole at each apex; each tube hole was 0.100 in., or one diameter, from its nearest neighbor. Tube hole-to-header edge distances were initially chosen as 0.050 in., but they were increased in subsequent experiments to 0.100 inch. Welding conditions were chosen by experiment before being applied to a 19-hole header assembly for a consistency evaluation.

Figure 65 illustrates a series of typical tube-to-header consistency determinations. Each header was fabricated by using a different welding condition to illustrate the flexibility of the cone-arc process. The welding conditions are listed in Table 28 and are in reference to Fig. 65.

Cone-arc welds within the limits of the material and joint design of this investigation may be made over a range of welding conditions. Although the welds illustrated in Fig. 65 are not representative of a systematic study, their examination reveals trends that will be verified by future work.

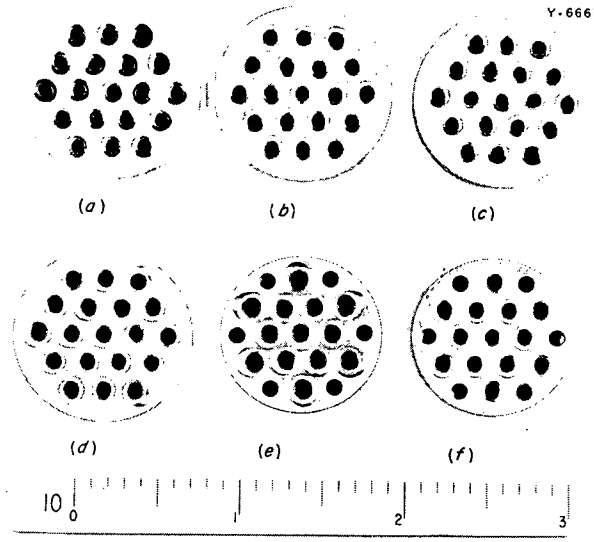


**Fig. 65. Typical Cone-Arc Welds of 1/8-in. Type-304 Stainless Steel Header Sheets and Type-316 Stainless Steel Tubes, 0.10 in. OD, 0.010-in. Wall Thickness.**

**TABLE 28**

**Welding Conditions for Tube-to-Header Joints**

| HEADER DESIGNATION | DISTANCE FROM ELECTRODE TIP TO PLANE OF WORK (in.) | ARC CURRENT* (amp) | ARC TIME (sec) |
|---|---|---|---|
| *a* | 0.020 | 64 | 1.5 |
| *b* | 0.050 | 60 | 1.8 |
| *c* | 0.040 | 70 | 1.2 |
| *d* | 0.100 | 70 | 2.0 |
| *e* | 0.100 | 84 | 1.4 |
| *f* | 0.050 | 60 | 1.8 |

*Direct current.

It appears from a comparison of welds *a*, *b*, *c*, and *f* with welds *d* and *e* (Fig. 65) that the primary effect of shortening the arc distance is to recess the cone-arc weld. Welds *a*, *b*, and *c* illustrate the comparable net effect of increasing current with a corresponding decrease in arc time (within limits). It is believed, however, that a thorough metallographic examination is required to determine the effects on variables such as weld penetration.

Welds *d* and *e* illustrate the combined effect of further increasing arc length, arc current, and arc time. A condition is reached that indicates superfluous welding, which is apparent by observing the relatively large welds and the tendency to form a rosette pattern on the header edges. The heat flow pattern, the uniformity of which seems to be an important variable in cone-arc welding, appears to have been distorted on prolonged heating as a result of increasing arc time or higher currents unless accompanied by a marked decrease in arc time. It may be noted that the outer holes of header *e* do not contain welded tubing. The distance from the tube periphery to header edge in this case was 0.050 inch. This distance upset the uniformity of the heat flow pattern, and no welding conditions were found that would give satisfactory welds. The application of welding condition *b* to weld *f*, which is identical in geometry with weld *e*, was also unsatisfactory when applied to the outer holes. Melting concentrated toward the header edge and gave erratic results, and in many instances the tube peripheries were only partly welded.

The superfluous nature of welds made under welding condition *e* is illustrated in Fig. 66. This photomicrograph is typical of cone-arc welds with good fit-up. The effect of

**Fig. 66. Transverse Section of a Typical Tube-to-Header Cone-Arc Weld of 1/8-in. Type-304 Stainless Steel Header Sheets and Type-316 Stainless Steel Tubes, 0.10 in. OD, 0.010-in. Wall Thickness.** 10X.

an associated problem appeared upon examination of the weld. Arcs that are terminated instantaneously without a current taper tend to leave a crater. Examination of the periphery of cone-arc welds revealed a small spot characterized by a small amount of scale. A cross section of such a spot with the middle of the weld surface exposed appears in Fig. 66. The extent of the crater indicates that the resulting porosity is not a serious problem. The presence of a single pronounced crater on the cone-arc weld periphery tends to confirm the belief that the cone arc may be a single, rotating-arc beam.

The fabrication of test assemblies by cone-arc welding will continue, and studies to evaluate the fundamental effects of the cone-arc welding variables will receive attention concurrently.

# CERAMICS LABORATORY

J. M. Warde
C. E. Curtis
L. M. Doney
S. D. Fulkerson
J. R. Johnson
A. J. Taylor
G. D. White

## ORGANIZATION

The staff for present operations of the ceramic laboratory is complete, and the group has been organized into two sections – a research and developmental section and a section that renders assistance to other divisions.

## RESEARCH PROGRAM

A research program has been adopted that is to include an extensive study of Cermets, ceramic coatings, hafnia, and changes in ceramic materials due to radiation. The program also provides for developing laboratory facilities for measuring physical properties of ceramic materials.

## DESIGN AND BUILDING OF EQUIPMENT

The following equipment was completed or was in the process of construction during the past quarter:

1. thermal expansion equipment, consisting of a vacuum dilatometer (platinum-wound furnace) intended for the determination of thermal expansion of solids in the range 200 to 1300°C under vacuum or controlled atmosphere conditions, and a high-temperature dilatometer (molybdenum-wound furnace) for thermal expansion determinations up to 1600°C under controlled atmosphere conditions;

2. resistor furnaces, both molybdenum wound, primarily for firing Cermets up to 1750°C, and vacuum-strip, for melting-point determinations up to 3000°C;

3. a vacuum induction furnace, which will be used for sintering ceramic materials in vacuum or controlled atmospheres up to 2500°C and will be installed upon the purchase and delivery of a motor-generator set;

4. gas-fired furnaces, both a high temperature, zirconia lined, firing chamber, 10 by 10 by 12 in., for temperatures up to 1900°C, and a high temperature, MgO or $ZrO_2$ lined, tangentially fired, firing chamber, 4 in. in dia by 4 in. deep, for temperatures up to 2000°C;

5. high-temperature x-ray equipment designed to obtain x-ray patterns of material in the range from room temperature to 2000°C;

6. thermal diffusivity apparatus to be used for measuring thermal diffusivity of ceramic materials at temperatures up to 2000°C;

7. ice calorimeter equipment to be used for precise measurements of heat capacity of materials at temperatures up to 1500°C;

8. stress-rupture apparatus for measuring stress-rupture of ceramic materials at temperatures up to 1300°C;

9. pyrometer and thermocouple calibration equipment.

## HAFNIA RESEARCH

Hafnia received from the Chemistry Division contained the following principal impurities, according to spectroscopic analysis: Zr, 0.35%; Ti, 1.00%; Fe, 0.10%; Na, 0.04%. It

has been demonstrated that this material can be changed from the monoclinic to the cubic crystal form by the addition of 8 mole % of calcium oxide and firing for 1 hr at 1600°C in air. This behavior, not previously noted in the literature, is similar to that of zirconium oxide, which is commercially stabilized in the same manner to increase heat-shock resistance.

The thermal expansion behavior of hafnia from room temperature to 1300°C was determined; no inversions were found in this range.

Equimolecular mixtures of $HfO_2$ and $SiO_2$ were fired for 1 hr at 1500°C; x-ray examination indicated that hafnium silicate was synthesized by this procedure.

## CERAMIC COATINGS

**Fluoride-Resistant Coatings.** Work was started on the development of a phosphate-glass composition for coating mild steel (10-10) to provide resistance to uranium fluoride; specimens are being tested at K-25.

**Zirconium Enameling.** A ceramic coating applied to zirconium showed promising behavior in retarding oxidation of the metal during hot rolling.

**Copper Enameling.** A ceramic coating was successfully applied to the inside of a copper tube to provide insulation between mercury and the tube wall in a convection measurement apparatus. This work was done for the ANP program.

**Stainless Steel Enameling.** A ceramic coating applied to three steels (types 347, 316, and 302) successfully retarded oxidation of the metals during a 100-hr test at 900°C. A new, boron-free coating for stainless steel is being developed.

## RADIATION DAMAGE STUDIES

An investigation of the effect of radiation on various ceramic materials has been started. Test specimens of 30 different ceramic materials are being prepared in the form of thin disks, 3/4 in. in dia by 20 mils thick, that will be sent to Hanford for irradiation for periods of 3 and 6 months.

## LITHIUM-GLASS DIFFUSION BARRIER

Lithium glass has been proposed as a diffusion barrier to aid in separating lithium isotopes. A trial method, utilizing a fused lithium salt bath behind a glass barrier of suitable composition and an electrical force to drive lithium ions through the barrier is now being tested.

## REPORTS

The following reports have been completed or are being prepared: (1) "Bibliography of Hafnium Oxide, Hafnium Carbide, and Hafnium Silicate," (2) "Crucible Handbook," (3) "Ceramic Materials as Related to Reactor Program," (4) "Vapor Pressures of Ceramic Materials."

## SERVICE WORK

**Petrographic Examinations.** Investigations of ARE fuels are being carried out for the ANP program. Petrographic analyses of $UO_3$ grains are being made periodically for the HRE program.

**Fabrication of a Ceramic Mold for Making Single Crystals of Aluminum.** An alumina mold was prepared for making single crystals of aluminum; however, the mold did not perform satisfactorily owing to solution between the crucible and metal. Other molds will be prepared from zircon

brick and magnesium oxide. This work was requested by the Solid State Division.

**Firing Lava Insulators.** Routine heat treatment was given to parts for the calutron (requested by Stable Isotopes Division).

**Fabrication of Thoria Crucible.** This work for the Stable Isotopes Division was completed.

**Fabrication of Insulators.** It was found that hot-pressed beryllia insulators gave excellent service in the calutron.

# HOMOGENEOUS REACTOR PROGRAM

E. C. Miller

The Metallurgy Division's participation in the Homogeneous Reactor Project continues to be limited largely to miscellaneous consultation and service work because of the unavailability of manpower, although a beginning has been made on the titanium phases of the program.

## CORROSION

Participation in the corrosion test program has involved assistance to the dynamic corrosion group of the Reactor Experimental Engineering Division in the procurement and preparation of test specimens and the metallographic examination of corroded components removed from the system.

## WELDING OF STAINLESS STEEL

An effort has been made to follow the extensive programs being carried on by various technical societies and committees, industrial groups, and commission contractors toward solution of the problems of welding austenitic stainless steels in thick sections.

## NONDESTRUCTIVE TESTING

The nondestructive testing program being carried out in cooperation with the Y-12 Research Engineering section has involved, in addition to the routine inspection of welds and components by x rays and dye penetrants, the procurement and use on an experimental basis of an ultrasonic reflectoscope and an Audigage instrument. The Audigage instruments are of particular interest as possible means for following the progress of corrosion attack.

## RADIATION DAMAGE STUDIES

Some earlier work by Argonne National Laboratory, in cooperation with the Solid State Division of ORNL, on the impact strength of carbon steels indicated a reduction of the impact strength in the range above the transition temperature, as well as a pronounced increase in the transition temperature after irradiation. Further study of this effect has been initiated by the Solid State Division in connection with metallurgical problems of the HRP. Impact specimens of AISI 1040 steel have been prepared for irradiation in the X-10 graphite pile for periods of one to two months. Control of irradiation temperatures and metallurgical history will be maintained to determine possible effects on the HRE pressure vessel. Similar tests are planned to evaluate austenitic stainless steels and titanium.

## HRE CONTROL PLATES

E. S. Bomar J. H. Coobs
H. Inouye

The attempt to fabricate stainless-steel-clad Boral laminates of intermediate size met with some difficulty. Several laminates made by using aluminum-clad Boral cores and copper-coated stainless steel cladding were rolled at 600°C to ensure good bonding. At this temperature the Boral was reduced preferentially and built up sufficient pressure ahead of the rolls to burst the laminates after four or five passes. Moderation of the rolling schedule seemed ineffective when the total reduction exceeded 30%.

A successful rolling schedule was then devised in which two laminates of intermediate size (2 by 8 in.) were prepared by using three passes at 600°C to obtain 20% reduction and two additional passes at 500°C to obtain a total reduction of 30%. Apparently full-size plates may be fabricated by this means. However, such laminates have a definite disadvantage – the plates are rolled at temperatures in the cold-working range for stainless steels and the cladding thus becomes progressively harder, more difficult to reduce uniformly by rolling, and more difficult to bend to its final configuration.

The original request for the stainless-steel-clad boron carbide laminates included the suggestion that adaptation of the technique currently in use for fuel-plate fabrication to the preparation of laminates with iron or stainless steel as the core matrix be investigated. In order to evaluate this technique, a series of compacts containing 37% by volume (-200 mesh) boron carbide in iron, nickel, type-302 stainless steel, type-410 stainless steel, and chromium powders were pressed and sintered at 1150°C for 30 minutes.

Analyses of the compacts (Table 29) show that in all cases the boron carbide reacted with the matrix metal to form either a brittle, intermetallic or low-melting-eutectic phase. The reaction was accompanied by growth of the pressed compact, and there were detrimental effects on physical properties.

Laminates prepared by hot rolling gave uniformly poor results. The cladding of several laminates containing iron and type-302 stainless steel matrix cores, rolled at 1225°C, was attacked by the core material, and most of the center portion of the laminate seemed to melt away. Several other laminates containing iron, type-410 stainless steel, and chromium matrix cores, rolled at 1050 to 1125°C, blistered badly because of ruptures within the core.

**TABLE 29**

**Analysis of Various Compacts Containing Boron Carbide**

| COMPOSITION | DENSITY (%) | | PROPERTIES |
|---|---|---|---|
| | GREEN | SINTERED | |
| Ni-$B_4C$ | | | Ni-B eutectoid formed and flowed out of compact |
| Fe-$B_4C$ | 76.5 | 70.0 | Brittle, fairly strong; liquid phase formed |
| Type-302 stainless steel-$B_4C$ | 74.0 | 59.5 | Very brittle; liquid phase formed |
| Type-410 stainless steel-$B_4C$ | | | Very brittle, weak |
| Cr-$B_4C$ | | | Brittle, poorly sintered |

The use of copper was suggested as the metallic in the core, and investigation revealed that it does not react with or dissolve appreciable amounts of boron or carbon at temperatures far above its melting point. A laminate with a copper-boron carbide core prepared by sintering a mixture of copper powder and coarse boron carbide, cold pressing, resintering, and cold rolling, was hot rolled successfully at 1000°C with 50% reduction in seven passes. Examination revealed a fair bond between core and cladding, as shown in Fig. 67, and the finished laminate was easily bent to a 1-in. radius without failure. When bent to a shorter radius, the laminate failed by shear through the core and revealed the strength of the bond.

This method of preparing laminates had to be immediately adopted for preparation of the full-size plates because of a revised time schedule for completion of the project. The core material was prepared as a mixture of 16.3% by weight boron carbide, containing 71% boron, and U. S. Metals Refining Company, type "C" electrolytic-copper powder, which was mixed with 2% stearic acid as a binder and pressed at 25 tons per square inch. The binder was then removed by heating in air at 400°C and sintering in a hydrogen atmosphere at 950°C for 2 hours. The compacts were then repressed at 50 tons per square inch, resintered for 15 min to promote densification, and repressed, if necessary, to further reduce the thickness. Preparation was completed by rolling to the desired thickness, loading into the frame of the laminates, evacuating, sealing, and finally hot rolling as described. It was discovered that the large plates had to be evacuated during preheating and sealed to prevent swelling and blistering, which were probably caused by volatile components remaining from the binder.

**Fig. 67. Interface of Type-347 Stainless Steel Cladding and Copper-Boron Carbide Core.** 200X. Reduced 18%.

The rolled laminates were then sheared 1/8 in. from the edge of the core and sealed with the automatic heliarc welder. In this operation the copper-boron carbide mixture shows an additional advantage over Boral in that its higher melting point and thermal conductivity reduce the chances of melting the edge of the core during welding, which would produce a faulty weld.

All finished plates, except No. 8, were x rayed and measured before delivery. The data on these plates, as delivered, are given in Table 30.

The boron carbide content of the plates runs slightly below that necessary to supply the minimum of 100 mg of boron per square centimeter requested. Fortunately, the two large plates, Nos. 12 and 14, contained a large fraction of the total boron carbide and thus quite close to the required minimum of boron. The deficiencies may, in general, be charged to lack of familiarity with the properties of the mixture of powders used. If additional plates are requested, more accurate control of the components will be maintained. As a demonstration, plate No. 16 is being prepared with about 107 mg of boron per square centimeter.

## TITANIUM WELDING

A. R. Olsen

Preliminary work on the variables involved in welding titanium has been started. To date, two grades of commercially pure material have been welded in a dry box in a purified helium atmosphere by using a heliarc torch. The samples were welded by the welding group and the tensile and bend tests were made by the physical testing group. Original plans for use of a constant-moment bend-to-failure test evolved into a free bend test because of the high ductility of the sample welds.

The scouting test gave preliminary indications that with proper precautions against contamination the welding of commercially pure titanium requires no more care than that exercised in the production of high-quality stainless steel welds. There is no significant difference between

**TABLE 30**

**Data on HRE Control Plates**

| PLATE NO. | TOTAL CORE WEIGHT (g) | BORON (g) | CORE AREA (in.$^2$) | BORON (mg/cm$^2$) |
|---|---|---|---|---|
| 6 | 56.3 | 6.53 | 10.8 | 93.0 |
| 10 | 55.7 | 6.46 | 10.3 | 97.3 |
| 5 | 82.8 | 9.62 | 15.6 | 95.5 |
| 9 | 82.9 | 9.62 | 15.6 | 95.5 |
| 1 | 108.3 | 12.56 | 20.0 | 97.5 |
| 8 | 108.2 | 12.56 | | |
| 12 | 599.3 | 69.5 | 107.9 | 100.0 |
| 14 | 596.3 | 69.2 | 111.0 | 97.0 |

butt welds in which only the base plate is fused and wide-angle V joints in which filler metal is added with each part. Also, current and voltage changes in the range 30 amp at 15 v to 64 amp at 20 v seem to have little effect on the physical properties of the welds, provided the welding speeds are slow enough to guarantee complete fusion. Some difficulty in this regard was found at the lower current and voltage settings. Test samples were found to fail outside of the weld area under tension and in the center of the fusion zone in bending when Ti-75A was the base plate and in the heat-affected zone under tension and the fusion zone in bending when RC-70 was the base plate.

A few sample joints of titanium-to-zirconium were also attempted. They all failed because of a brittle fracture in the fusion zone adjacent to the titanium.

Further work on this project will include some corrosion tests of welds.

## PROPERTIES OF TITANIUM AND ZIRCONIUM

W. J. Fretague

Experimental work to determine the effects of various impurity elements on the impact properties of titanium and zirconium was started in late March. Iodide titanium is being used as a starting material. Three samples (one from each end of the rod and one from the center) were cut from the as-deposited bar, and Tukon hardness (Vickers 136° DPH) measurements (10-kg load, 16-mm objective) were made. Table 31 lists the hardness values obtained. Samples of the as-deposited bar were submitted for oxygen, nitrogen, and hydrogen analysis by the vacuum-fusion method.

**TABLE 31**

**Vickers Hardness of As-Deposited Titanium**

| LOCATION IN BAR | VICKERS 136° DPH HARDNESS (10-kg load, 16-mm objective) | |
|---|---|---|
| | READINGS TAKEN AT RANDOM | CENTER WIRE READINGS |
| Large end | 69.4 | 89.2 |
| | 71.0 | |
| | 77.2 | |
| | 74.5 | |
| | Average 73.0 | |
| Center | 58.1 | 81.2 |
| | 62.7 | |
| | 67.5 | |
| | 58.1 | |
| | Average 61.6 | |
| Small end | 55.9 | Wire not visible, readings taken in center of transverse section averaged 76.62 |
| | 69.1 | |
| | 69.4 | |
| | Average 64.8 | |
| | Over-all Average 66.6 | |

An unalloyed iodide-titanium melt was prepared from the iodide-titanium bar by arc melting in the small, water-cooled copper-hearth, water-cooled tungsten-electrode, d-c arc furnace. A slight weight gain (0.5027 g in 42.0312 g) was observed on melting, and since the cause of this weight increase was unknown, samples of the as-melted material for oxygen, nitrogen and hydrogen vacuum-fusion analysis were obtained. In addition, a metallographic sample was submitted for microstructure and Vickers hardness determination. An increase of 12 points in Vickers hardness was obtained on melting (from 66.6 average for as-deposited to 78.6 average for as-melted).

The as-melted iodide titanium was swaged from approximately 0.5 in. in diameter by 4 in. long to 0.243-in.-dia. rod, and a length of approximately 10 in. was obtained. Swaging was stopped at this point because the surface started to roughen slightly. All swaging was done without intermittent annealing. A piece was cut from one end of the swaged rod and submitted to the Research Shop for preparation of a spherical x-ray specimen of the type used by the x-ray laboratory for orientation determinations. Enough additional material was provided for a metallographic specimen, and the turnings from the machining operation will be collected and submitted to the Chemistry Division for a determination of the tungsten content of the titanium melt by activation analysis. (A similar determination will be made on the first zirconium melt prepared).

The remainder of the swaged rod was vacuum annealed at 950°C for 4 hr and furnace cooled. A second piece for x-ray and metallographic samples was cut from the annealed rod (adjacent to the first x-ray sample) and the balance of the rod (approximately 6 1/4 in. long) was submitted to the Research Shop for preparation of a modified, Izod-type, impact test specimen of the type used by the Solid State Division in work on radiation damage.

The actual machining operations were closely supervised; the Solid State Division contributed techniques developed through the preparation of a number of specimens of this type but not of the same material. Inspection of the finished specimen by shadowgraph and stereoscopic microscope showed that the iodide-titanium impact specimen produced by the Research Shop compared favorably with the specimens produced in the Solid State Division Shop.

The small, impact testing machine located in the Solid State Division Building is now being altered to permit transition temperature studies of irradiated materials within the hot cell. The various component parts that required alteration are being prepared in the Research Shops, and the estimated completion date for the job is June 16, 1952. As a result, no impact tests are planned before this date.

# X-RAY LABORATORY

B. S. Borie, Jr. R. M. Steele

## CRYSTAL STRUCTURE OF NiOOH

**Identification and Chemical Composition.** The specimen used in the determination of the crystal structure of NiOOH, prepared and submitted by L. D. Dyer, consisted of rather dull, black platelets from which flakes were easily removed with a needle. Chemical analysis showed the specimen to contain 61% nickel and 3% sodium, and the remainder was presumably oxygen and water. If the formula of the compound were NiOOH (or $Ni_2O_3 \cdot H_2O$), chemical analysis should show 64% nickel. The small quantity of sodium found in the specimen might possibly be due to the presence of NaOH, although there is no diffraction evidence for this. An x-ray-spectrometer pattern of the material is consistent with the diffraction data given by Cairns and Ott[1] for $Ni_2O_3 \cdot H_2O$.

**Cell Size and Number of Formula Weights per Unit Cell.** A series of precession photographs of a small, single crystal of the sample mounted with grease on a glass fiber were taken. Both copper and molybdenum radiation were used. From these data the unit cell was found to be rhombohedral, $a$ = 7.17 Å and $\alpha$ = 22.84 degrees. For convenience the structure will be referred to hexagonal axes in the following discussion. In this system the cell dimensions are $a'$ = 2.84 Å and $c'$ = 20.95 Å.

Five reflections, not part of the diffraction pattern of NiOOH, were observed and identified as $Ni(OH)_2$ (hexagonal, $a$ = 3.114 Å and $c$ = 4.617 Å). Although the crystals of this component are apparently badly distorted, they are essentially monocrystalline and coherent with the NiOOH lattice. The $c$ and $a$ axes of the two phases are parallel.

The density of the sample, measured picnometrically, is 3.8 g/cc. From this and the cell size given above, the number of formula weights per unit cell is 3.6. Since the presence of either $Ni(OH)_2$ or NaOH would tend to make the measured density large and since the hexagonal cell is triply primative, it may be assumed that there are three formula weights per unit cell.

It should be noted that the presence of a little $Ni(OH)_2$ does not affect the usefulness of the chemical analysis. The weight per cent of the nickel in this compound is essentially the same as that of NiOOH.

**Determination of the Space Group and Atomic Parameters.** Of the rhombohedral-centered space groups only $C_{3i}^2$, $D_3^7$, and $D_{3d}^5$ will accommodate atoms in sets of three or sets of three and six. For all three of these space groups the available positions are:

(000, 1/3 2/3 1/3, 2/3 1/3 2/3) +

$3a$: 000

$3b$: 001/2

$6c$: $00Z$, $00\bar{Z}$ .

The oxygen atoms must lie in positions $6c$ since one of the two available sets of threefold positions must be occupied by nickel. The origin was chosen so that the nickel atoms are in positions $3a$.

(1) R. W. Cairns and E. Ott, "X-Ray Studies of the System Nickel-Oxygen-Water. II. Compounds Containing Trivalent Nickel," *J. Am. Chem. Soc.* **55**, 534 (1933).

Fair agreement between observed and calculated intensities, as shown in Table 32, was accomplished by the use of an oxygen parameter of $Z = 0.38$. Only reflections of the type $h01$, as observed from a zero level precession photograph, are included in the table. The artificially high temperature factor of exp $[-5 \sin^2 \theta/\lambda^2]$ used for the calculated values is justified by the fact that the crystal was quite imperfect, which caused all reflections to be broad and those of large $\sin \theta/\lambda$ to appear weakened.

Table 33 is a comparison of observed and calculated $\sin^2 \theta$ values for the Debye-Scherrer pattern. The experimental data of this table are those of Cairns and Ott.[1] Since line positions were measured with a millimeter rule and not a comparator, the agreement seems satisfactory. One line (at $2\theta$ = 34 deg, intensity "very weak") of the pattern given by Cairns and Ott does not agree with any of the calculated reflections and remains unexplained.

**TABLE 32**

**Observed and Calculated Intensities for NiOOH**

| hkl | INTENSITY | |
|---|---|---|
| | CALCULATED | OBSERVED |
| 003 | 9840 | S++ |
| 006 | 1670 | S+ |
| 009 | 263 | W- |
| 00,12 | 138 | W |
| 102 | 847 | S |
| 105 | 1253 | S |
| 108 | 922 | M+ |
| 1011 | 314 | M |
| $10\bar{1}$ | 312 | M |
| $10\bar{4}$ | 162 | W+ |
| $10\bar{7}$ | 268 | W |
| $10,\overline{10}$ | 392 | M |
| $10,\overline{13}$ | 339 | W- |

**Discussion of the Structure.** A drawing illustrating the packing of atoms in the structure is shown in Fig. 68. It is clear from the illustration that the structure consists of oxygen-nickel-oxygen "sandwiches," with the normal to the layers being the $c$ axis. The two oxygen layers within a sandwich are essentially close-packed, with the small nickel ions lying in interstices. Each nickel has six oxygen nearest neighbors, and the Ni-O separation is about 1.95 Å. Thus the

**TABLE 33**

**Observed and Calculated $\sin^2 \theta$ for NiOOH**

| hkl | $\sin^2 \theta$ | |
|---|---|---|
| | CALCULATED | OBSERVED |
| 003 | 0.012 | 0.012 |
| 006 | 0.049 | 0.050 |
| $\bar{1}11$ | 0.100 | 0.099 |
| 102 | 0.104 | 0.106 |
| $\bar{1}14$ | 0.120 | |
| 009 | 0.122 | |
| 105 | 0.132 | 0.131 |
| $\bar{1}17$ | 0.165 | |
| 108 | 0.185 | |
| 00,12 | 0.195 | |
| $\bar{1}1,10$ | 0.233 | |
| 10,11 | 0.262 | 0.258 |
| 110 | 0.295 | 0.293 |
| 00,15 | 0.305 | |
| 113 | 0.307 | 0.309 |
| $\bar{1}1,13$ | 0.327 | |
| 116 | 0.343 | 0.345 |
| 10,14 | 0.365 | |
| 201 | 0.394 } | 0.396 |
| 022 | 0.398 } | |

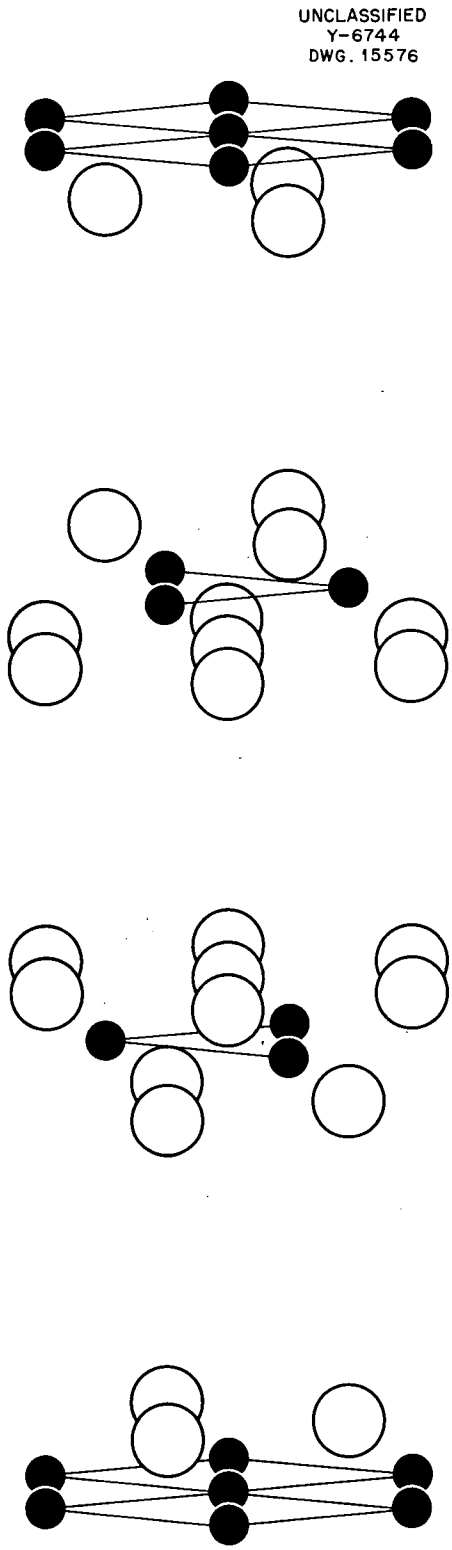


**Fig. 68. Packing of Atoms in NiOOH.**

radius of the nickel ion is about 0.6 Å, which is approximately what would be expected. The radius of trivalent cobalt is 0.65 Å and that of iron is 0.67 Å.

Each oxygen has six oxygen neighbors at 2.84 Å within its layer and three oxygen neighbors at about 2.5 Å in the adjacent plane of oxygens. There are three nickel ions coordinated to each oxygen within a sandwich.

The abnormally large oxygen-oxygen separation between sandwiches is about 5 Å. The extremely weak interlayer forces resulting from this unusual structure should account for the graphite-like appearance of the crystals.

The structure is not isomorphous with the oxyhydroxides of iron and aluminum, both of which are orthorhombic with anions in almost perfect hexagonal close packing.[2] Strangely, the structure is similar to $NaFeO_2$ (rhombohedral, with hexagonal axes $a'$ = 3.019 Å, $c'$ = 15.934 Å). Iron atoms occupy positions analogous to nickel in NiOOH, and the oxygen parameter is reported to be 0.378.[2] Whether the hydrogen of NiOOH is structurally similar to sodium in $NaFeO_2$ is not known, and at this point personnel working on the problem are not willing to hazard a guess.

Future work on the structure should include an effort to prepare samples that are free of nickel hydroxide and sodium. A more accurate density measurement should be made, and carefully measured intensity data should be obtained to establish the oxygen parameter. A determination of the structure of $NaNiO_2$, a preliminary account of which is included in this report, will probably contribute to

[2] R. W. G. Wyckoff, *Crystal Structures*, Interscience, New York, 1948.

an understanding of the compound, since the structures appear to be related. Because of the unusual anion configuration existing in the structure, the data should, to a greater degree than usual, be gathered with care and interpreted with caution.

### CRYSTAL STRUCTURE OF $NaNiO_2$

Work has started on the structure of a compound identified as $NaNiO_2$, which was submitted by L. D. Dyer. By chemical analysis the sample contains 51.0% nickel, 21.2% sodium, and 27.8% oxygen. The formula $NaNiO_2$ would predict 51.6% nickel, 20.2% sodium, and 28.1% oxygen.

The dimensions of its *c*-centered monoclinic unit cell, as determined by Weissenberg photographs and a rotation photograph, are $a$ = 5.336 Å, $b$ = 2.855 Å, $c$ = 5.596 Å, and $\beta$ = 110.44 degrees. The density of the sample was measured to be 4.6 g/cc; if there are two formula weights per unit cell, the theoretical density is 4.74 g/cc.

Atomic positions in the bimolecular unit cell have not yet been found. The compound is unstable enough to react with carbon dioxide and water from the air to form sodium carbonate monohydrate on the surface of the crystals. A powder pattern of the carbonate was found superimposed on the rotation pattern of a crystal exposed to air for several days.

Accurate intensity measurements from which the structure will be deduced must await the development of a technique that will prevent the formation of the carbonate. It seems likely that this may be accomplished by housing a single crystal in a glass capillary during x-ray exposure.

Initial indications are that the compound is similar to $NaFeO_2$. Although the iron compound is rhombohedral, it may be referred to monoclinic axes. It is then *c*-centered and its cell dimensions are: $a$ = 5.23 Å, $b$ = 3.02 Å, $c$ = 5.59 Å, and $\beta$ = 108.1 degrees. The similarity between this cell size and that given for $NaNiO_2$ is striking. Approximate intensity measurements from photographs of $NaNiO_2$ are also consistent with the hypothesis that the structures are closely related.

An investigation of the structure of a crystal of $NaNiO_2$ after sodium depletion by reaction with air is also planned. The data available indicate that hydrogen goes into the structure and replaces sodium and that the valence state of nickel remains unchanged. It is hoped that observation of the manner in which $NaNiO_2$ (or NiOONa) transforms to NiOOH will lead to a better understanding of the crystal chemistry of both compounds.

## METALLOGRAPHIC LABORATORY

R. J. Gray R. S. Crouse
T. K. Roche

There has been considerable interest in the examination of metallographic specimens to determine the location of ferromagnetic areas in nonferromagnetic alloys after test.

A procedure developed previously[1] was adapted for examination of the specimens. Colloidal iron is suspended in a soap-water solution. A drop of the solution is placed on a metallographic specimen that has been polished and etched in the conventional manner. After placing a cover glass on the mounted specimen, the specimen is placed on the metallograph and an electromagnet is positioned on the specimen. The electromagnet is controlled by a double-throw double-pole switch to reverse the polarity or to obtain a neutral position (Fig. 69).

The introduction of a magnetic field to the specimen results in the interruption of the Brownian movement of the iron colloid and an attraction of the colloid to any ferromagnetic area present. This so-called "magnetic etch" has been very useful in the examination of $UO_2$ fuel plates for homogeneity and stainless steel and Inconel specimens for corrosion effects after exposure to fluoride fuels.

A $UO_2$ fuel plate made of type-310 stainless steel plates and a core of type-310 stainless steel components (not type-310 stainless steel powder) and $UO_2$ was examined by the method described. Photomicrographs were made of the same fields before and after using the magnetic etch (Fig. 70). The ferromagnetic patches are evident by the attraction of the iron colloid. A high concentration of the colloid is shown at the boundary of the ferromagnetic patches.

An Inconel specimen taken from a thermal convection loop was also examined, and as before photomicrographs were made before and after using the magnetic etch (Fig. 71). The surface exposed to the fluoride fuel revealed a ferromagnetic layer approximately three-fourths that of

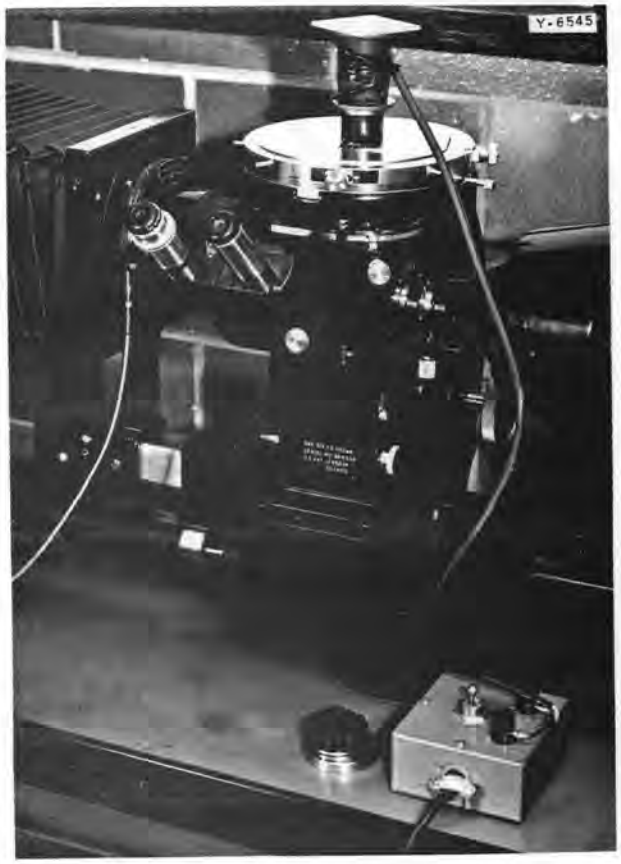


**Fig. 69. Electromagnet Positioned on Mounted Specimen for Magnetic-Etch Examination.**

[1] H. S. Avery, V. O. Homerberg, and E. Cook, *"Metallographic Identification of Ferromagnetic Phases," Metals & Alloys* **10**, 353 (1939).

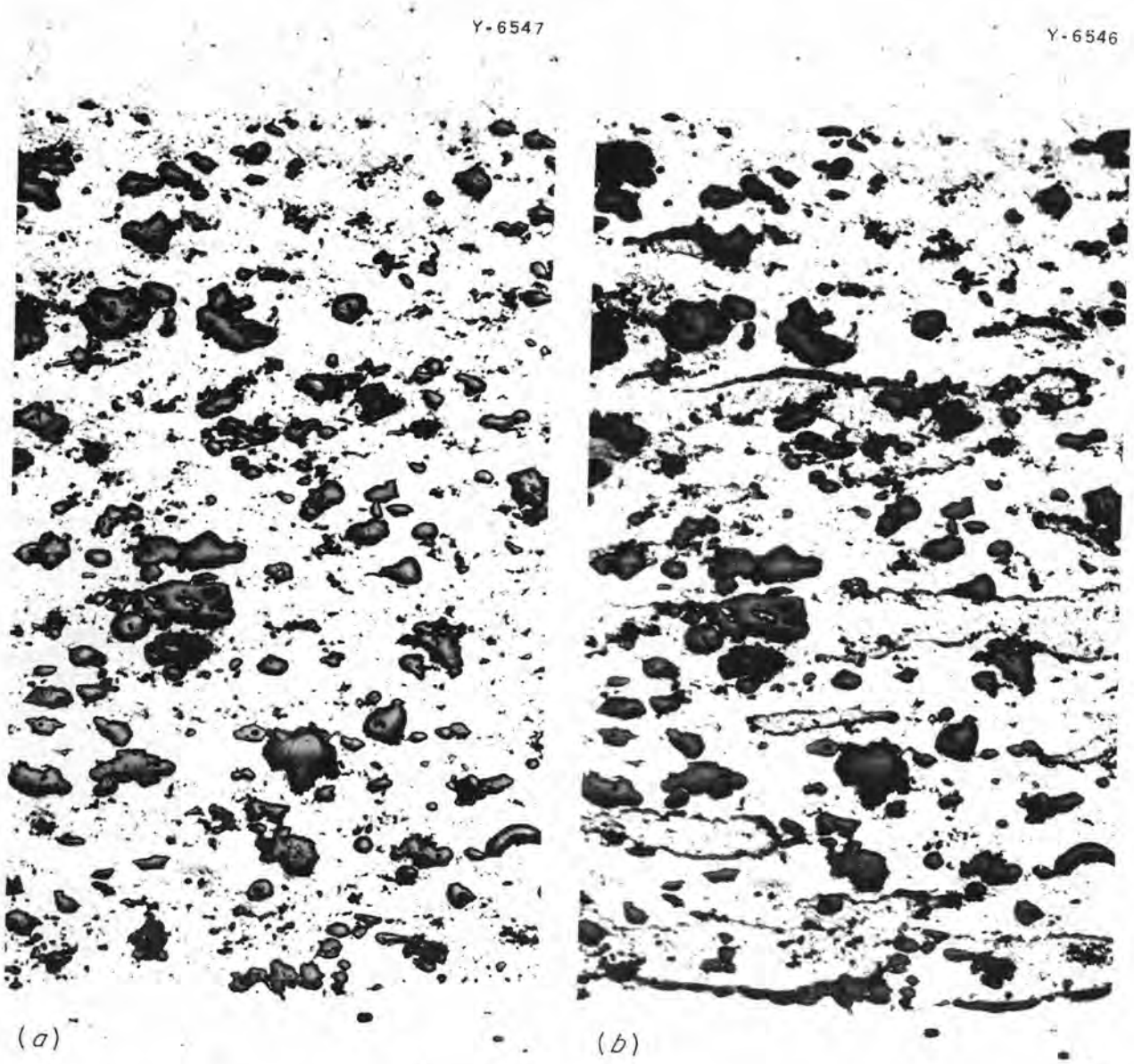


**Fig. 70. Fuel Plates Composed of Type-316 Stainless Steel Plates and a Core of $UO_2$ and the Components of Type-316 Stainless Steel.** (*a*) Without magnetic etch. (*b*) With magnetic etch. As-polished. 250X.

the apparent corrosion depth. A qualitative microspectrographic examination of this surface area showed the chromium-to-nickel ratio to be lower in this general area by a factor of 2 to 3 as compared with the interior area unaffected by the fluoride. The curie point for Inconel is reported to be approximately 8% chromium.

A type-316 stainless steel specimen exposed to a fluoride fuel was sectioned at an angle to increase the corrosion-affected area. The area adjacent to the grain boundaries showed a transformation with the chemical etch (Fig. 72*a*). The magnetic etch showed this transformation, which is probably alpha iron, to be ferromagnetic (Fig. 72*b*).

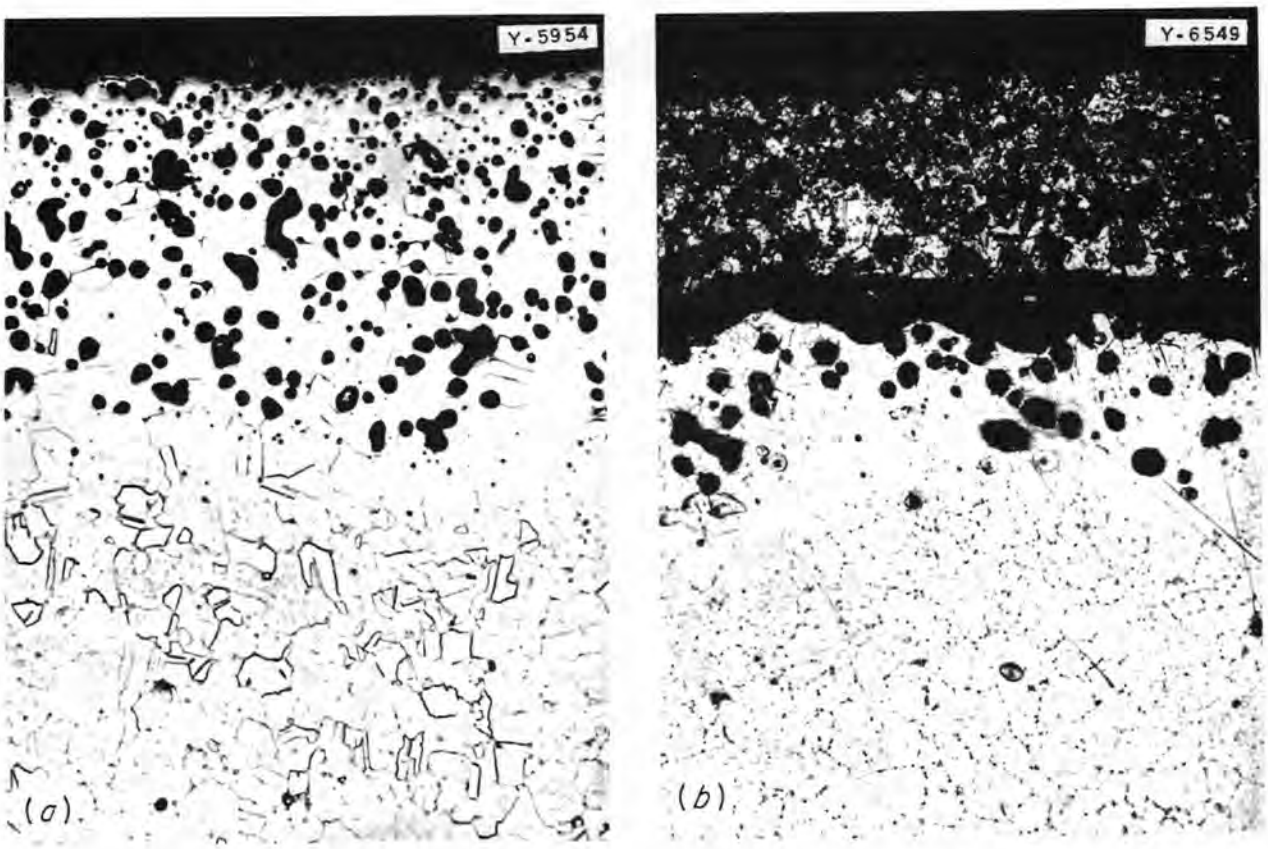


**Fig. 71. Inconel Thermal Convection Loop Exposed to Fluoride Fuels.** (*a*) Without magnetic etch. (*b*) With magnetic etch. Depth of ferromagnetic layer shown by collection of iron colloid. Etched with aqua regia. 250X.

## METALLOGRAPHIC EXAMINATION OF THORIUM AND THORIUM ALLOYS

R. J. Gray

The problem of preparing thorium and thorium alloys for metallographic examination has been quite difficult. Mechanical polishing resulted in preservation of the inclusions that were present; but unless grain boundaries were outlined by some precipitate, grain-boundary delineation was almost impossible without the use of severe etchants and then only for macroscopic examination.

Effort has been concentrated on the preparation of specimens by electrolytic methods because of the short time usually involved and the resulting undisturbed metal surface. One popular electrolyte, the 10:1 glacial acetic acid-perchloric acid mixture, was used for some time. A suitable surface was obtained except for the poorly revealed grain boundaries for recrystallization and grain-growth studies. The best results have been achieved with an electrolyte of 15 parts of absolute ethyl alcohol and 1 part of perchloric acid.

Specimens are ground to about a 400-grit paper and then polished with a 4- to 8-$\mu$ diamond paste on hard-finished broadcloth. They are then electrolytically polished at 35 v, with the electrolyte being maintained at room temperature and turbulently

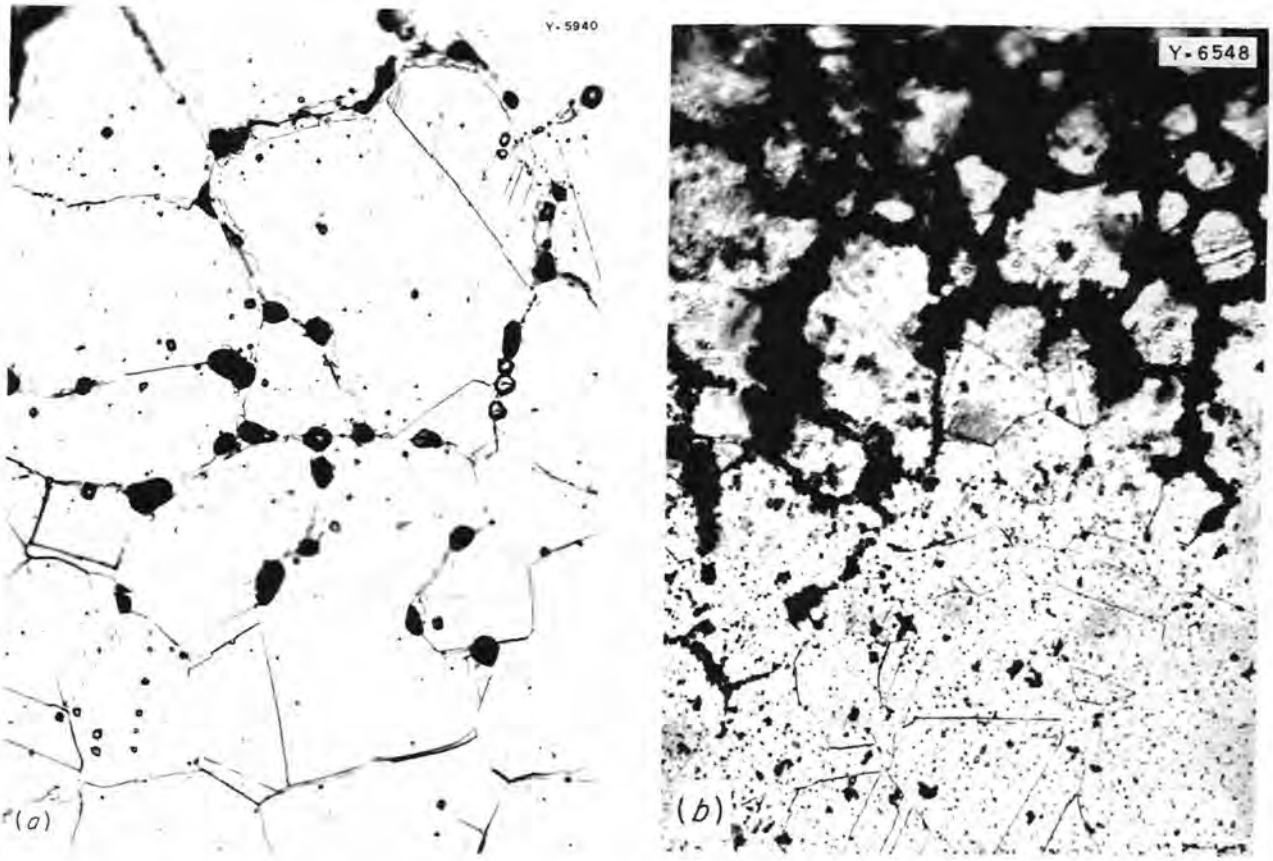


**Fig. 72. Type-316 Stainless Steel Exposed to Fluoride Fuel.** (*a*) Without magnetic etch. 1200X. (*b*) With magnetic etch. 500X. Grain boundary transformation to a ferromagnetic phase is shown by the collection of the iron colloid. Etched with aqua regia.

agitated. A Bakelite mounted specimen can be used to make contact with the specimen through the back of the mount. The time required for electrolytic polishing is about 10 to 15 seconds. After the specimen is removed from the electrolytic cell it is rinsed with alcohol, and it is then ready for examination. A chemical etch is sometimes used with alloys to show the structure to better advantage.

A transverse view of the Battelle iodide crystal-bar thorium is shown in Fig. 73. The base wire is on the left, and the deposited thorium appears as radially shaped grains.

The structure of arc-melted crystal bar is shown in Fig. 74. Here one problem that has been encountered in the electrolytic polishing of thorium and also in mechanical polishing to some degree is the "peppered finish" of the specimen. This pseudo-precipitate is also present in other metals, such as tantalum, prepared by electrolytic polishing. The possibility of this being only a polishing texture is not positive, but indications are favorable for this explanation. The presence of such a finish is not too objectionable except in dilute alloy additions in which a small amount of precipitate is difficult to isolate and identify.

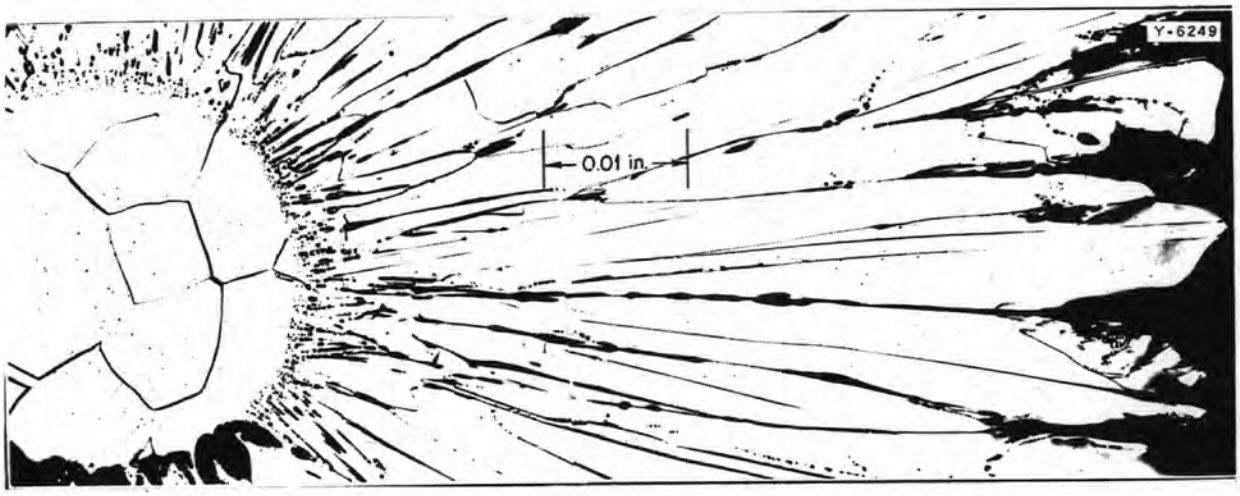


Fig. 73. Transverse Section of Battelle Iodide Crystal-Bar Thorium.

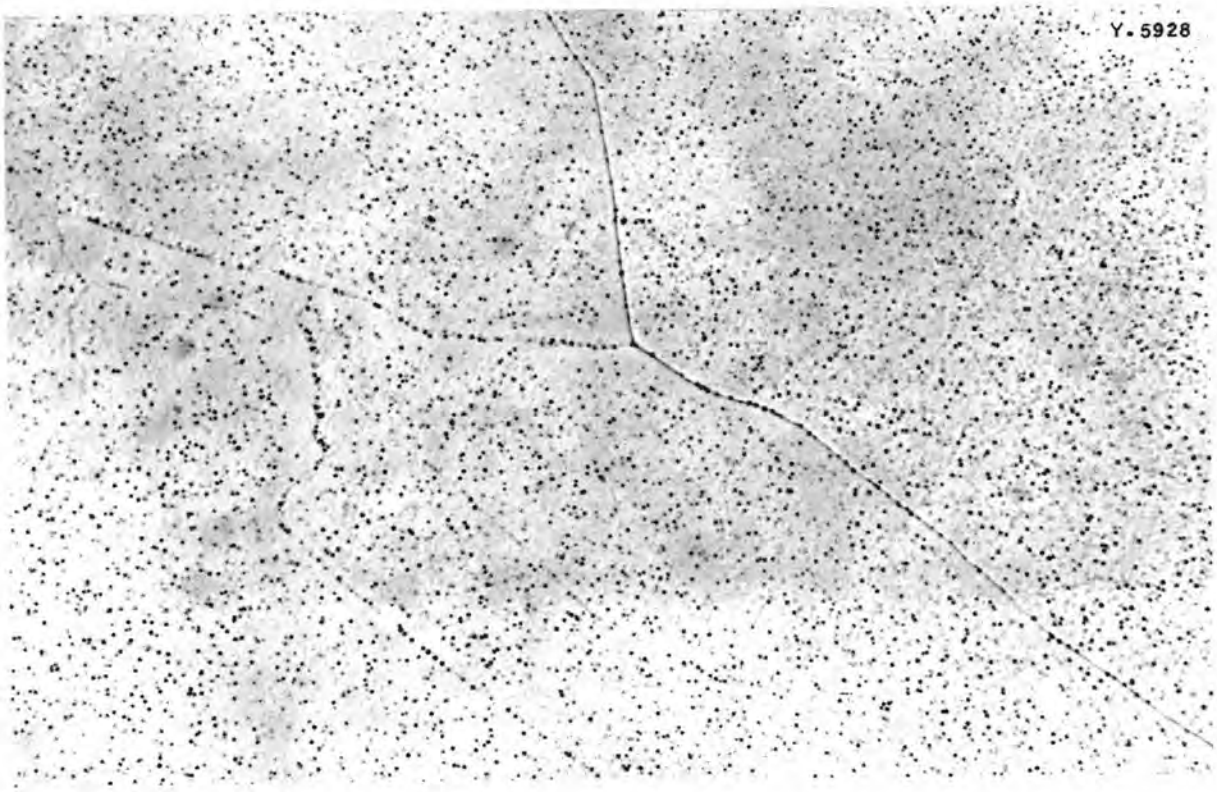


Fig. 74. Arc-Melted Crystal-Bar Thorium. 250X.

Recrystallization in its early stages is divulged by this method of polishing. For a series of recrystallization studies, the crystal bar was arc melted by a nonconsumable electrode method in which a positive pressure of purified argon was used. The as-cast button was 80% cold worked and recrystallized for various times and temperatures. Examinations were made on longitudinal sections.

Recrystallization at 530°C for 5, 10, 20, 40, and 60 min is shown in Fig. 75. The 80% cold-worked structure with a DPH of 76 (10-kg load) is shown at the top left of Fig. 75 for comparison. One hour at 530°C resulted in a DPH of 51. Recrystallization was just visible at 10 minutes. Some thorium dioxide was present, as shown by the scattered dark patches. Recrystallization at 550°C for 1, 5, 10, 20, and 60 min is shown in Fig. 76 for comparison with recrystalization at 530°C (Fig. 75). Recrystallization was apparent after 5 min, and 60 min at 550°C gave a DPH of 50.

For comparison, the Ames thorium was recrystallized at 550°C after the same percentage of cold work and for the same periods (Fig. 77) as for the crystal-bar thorium (Fig. 76). The cold-worked structure had a DPH of 110, and the specimen annealed for 60 min had a DPH of 91. Recrystallization was apparent at 5 min, and small grains were present after 60 minutes. Some grains were visible in the cold-worked crystal bar after 1 min at 580°C, as shown in Fig. 78. Complete recrystallization with a hardness of DPH 38 was present after 60 minutes.

The crystal bar annealed at 600°C for the same periods as shown in Fig. 79, had grains visible after 1 min and a nonuniform grain size after 60 min with a DPH of 39.

A comparison was again made between Ames thorium (Fig. 80) and crystal-bar thorium (Fig. 79). Small grains were visible in the Ames thorium annealed at 600°C after 1 min; however, as would be expected, the grain size was much smaller after 60 min. The DPH value after 60 min was 71.

An anneal of the crystal-bar thorium at 650°C, as shown in Fig. 81, had only a slight difference in uniformity of grain size after 5 min or 60 minutes. The hardness was DPH 38 after 60 minutes. The difference in grain size is shown in Fig. 82 after annealing the 80% cold-worked crystal-bar thorium for 60 min at various temperatures from 500 to 742°C.

A comparison was again made with Ames thorium (Fig. 83). The differences in grain size between the crystal-bar and the Ames thorium are shown in Figs. 82 and 83.

(*a*) Cold worked

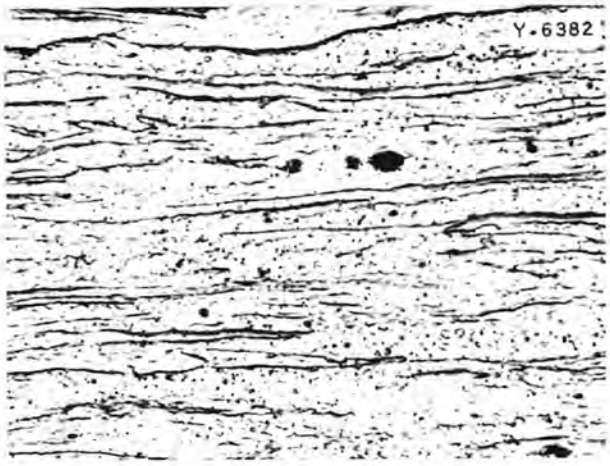


(*b*) Annealed 5 min

(*c*) Annealed 10 min

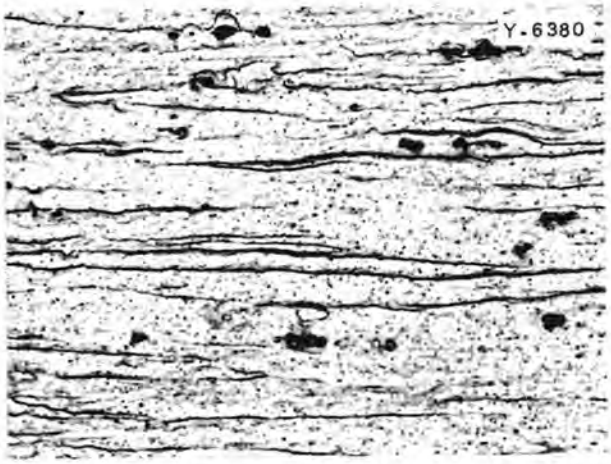


(*d*) Annealed 20 min

(*e*) Annealed 40 min

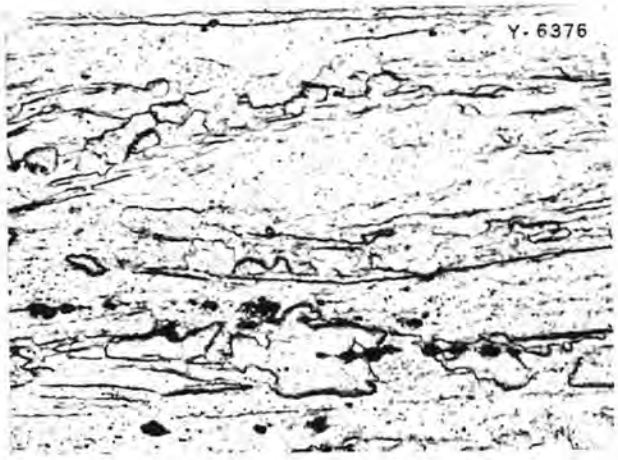


(*f*) Annealed 60 min

**Fig. 75. Recrystallization of Crystal-Bar Thorium 80% Cold Worked and Annealed at 530°C.** 250X.

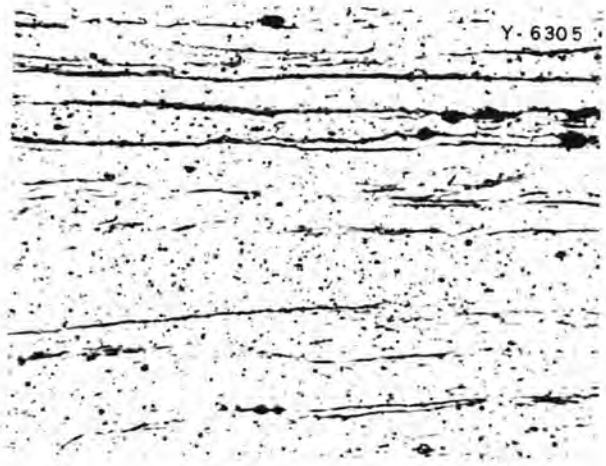


(*a*) Cold worked

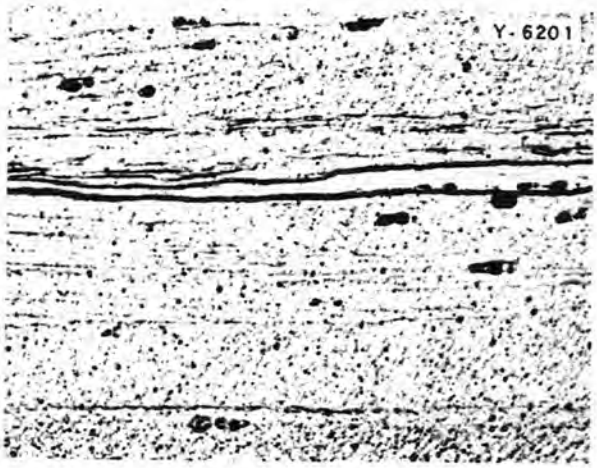


(*b*) Annealed 1 min

(*c*) Annealed 5 min

(*d*) Annealed 10 min

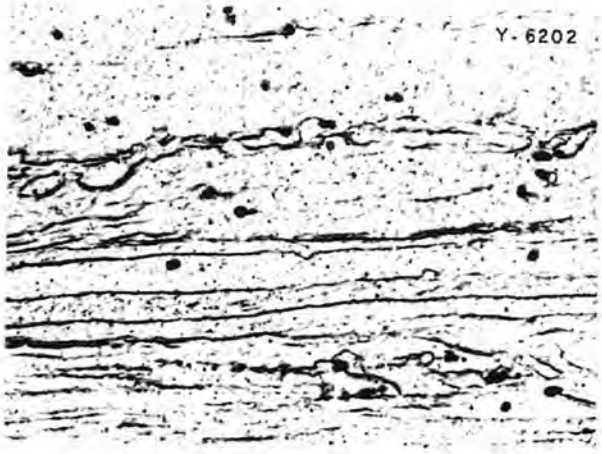


(*e*) Annealed 20 min

(*f*) Annealed 60 min

**Fig. 76. Recrystallization of Crystal-Bar Thorium 80% Cold Worked and Annealed at 550°C. 250X.**

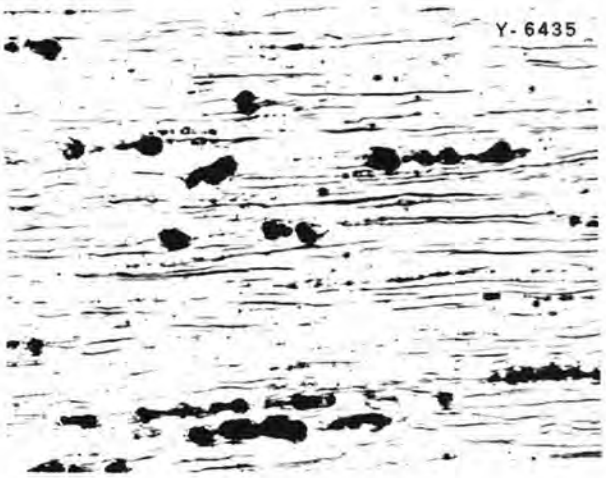


(*a*) Cold worked

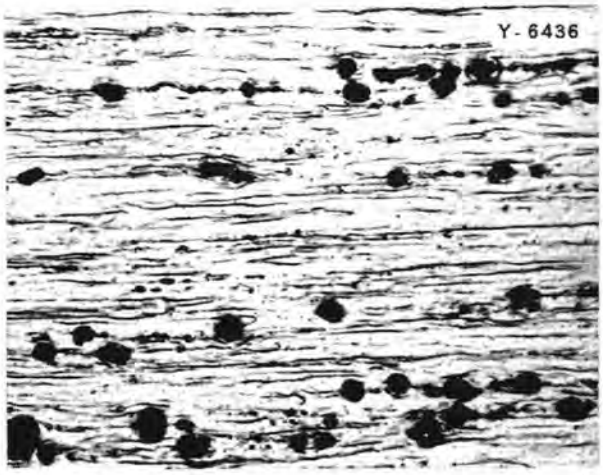


(*b*) Annealed 1 min

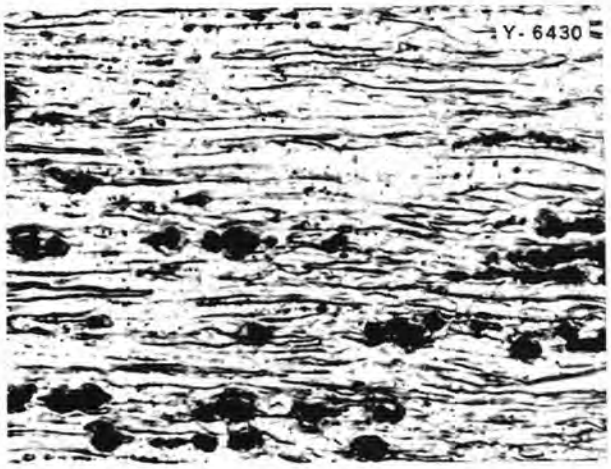


(*c*) Annealed 5 min

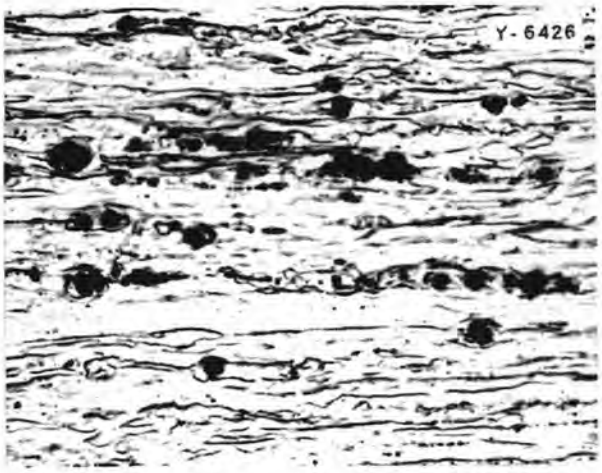


(*d*) Annealed 10 min

(*e*) Annealed 20 min

(*f*) Annealed 60 min

**Fig. 77. Recrystallization of Ames Thorium 80% Cold Worked and Annealed at 550°C.** 250X.

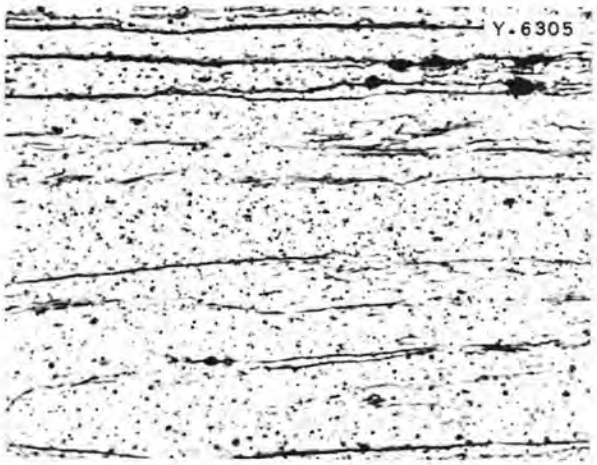


(*a*) Cold worked

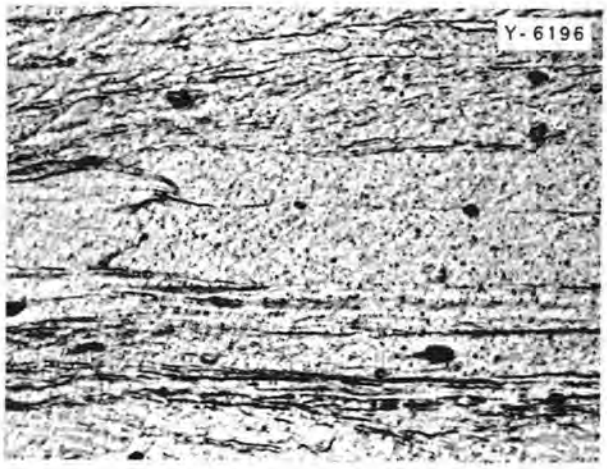


(*b*) Annealed 1 min

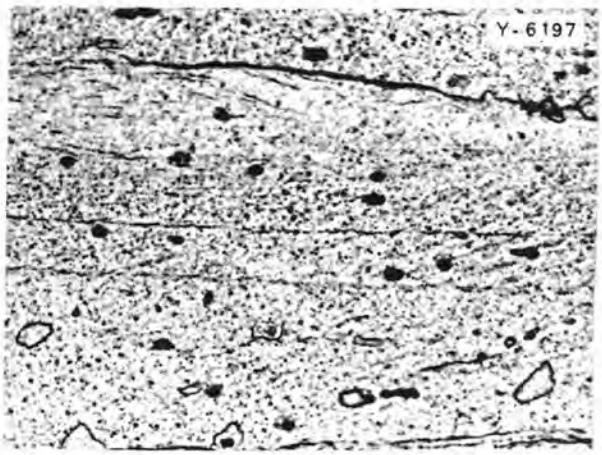


(*c*) Annealed 5 min

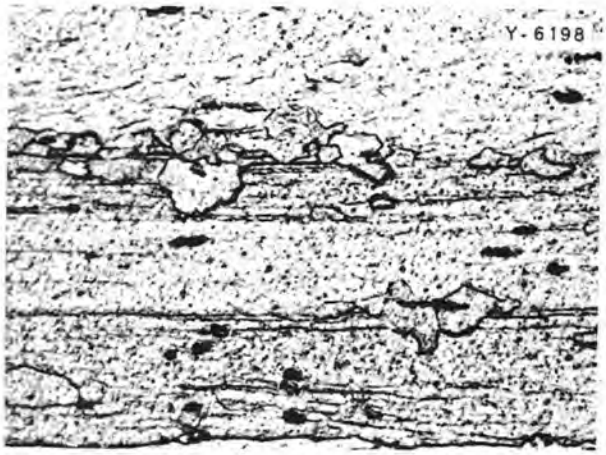


(*d*) Annealed 10 min

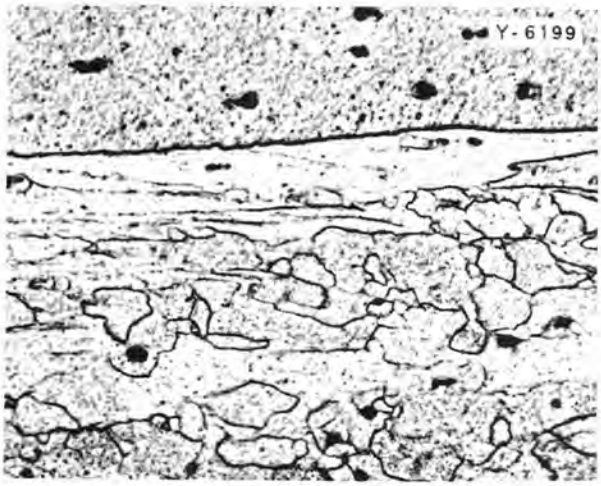


(*e*) Annealed 20 min

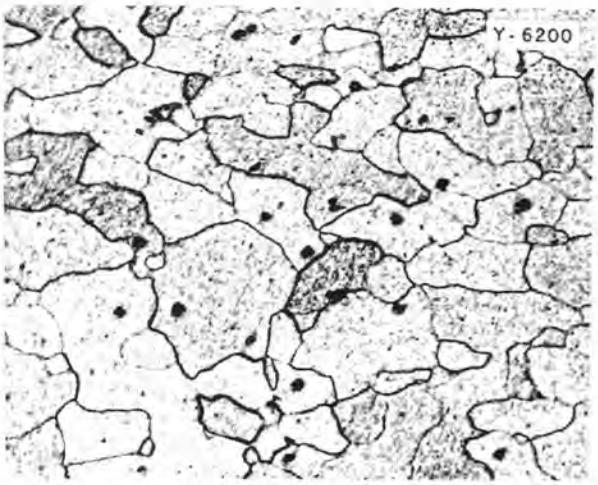


(*f*) Annealed 60 min

**Fig. 78. Recrystallization of Crystal-Bar Thorium 80% Cold Worked and Annealed at 580°C.** 250X.

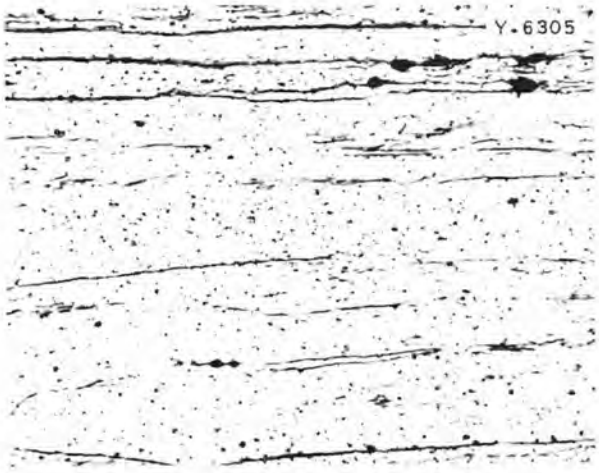


(*a*) Cold worked

(*b*) Annealed 1 min

(*c*) Annealed 5 min

(*d*) Annealed 10 min

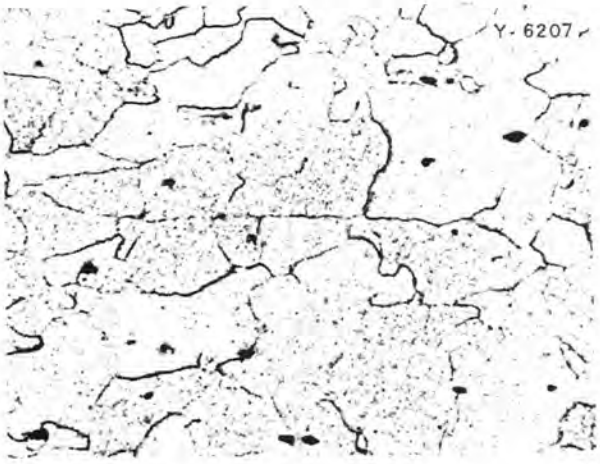


(*e*) Annealed 20 min

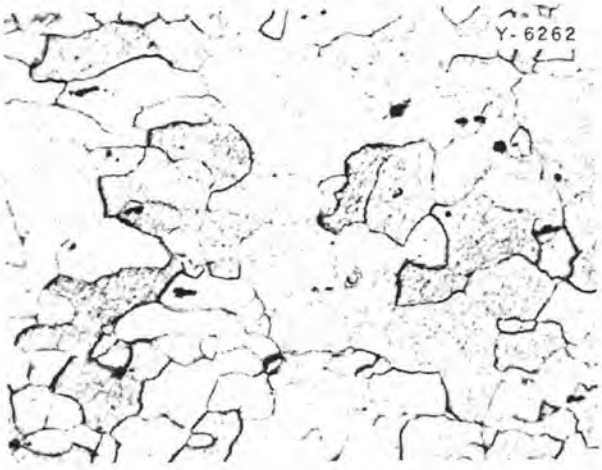


(*f*) Annealed 60 min

**Fig. 79. Recrystallization of Crystal-Bar Thorium 80% Cold Worked and Annealed at 600°C.** 250X.

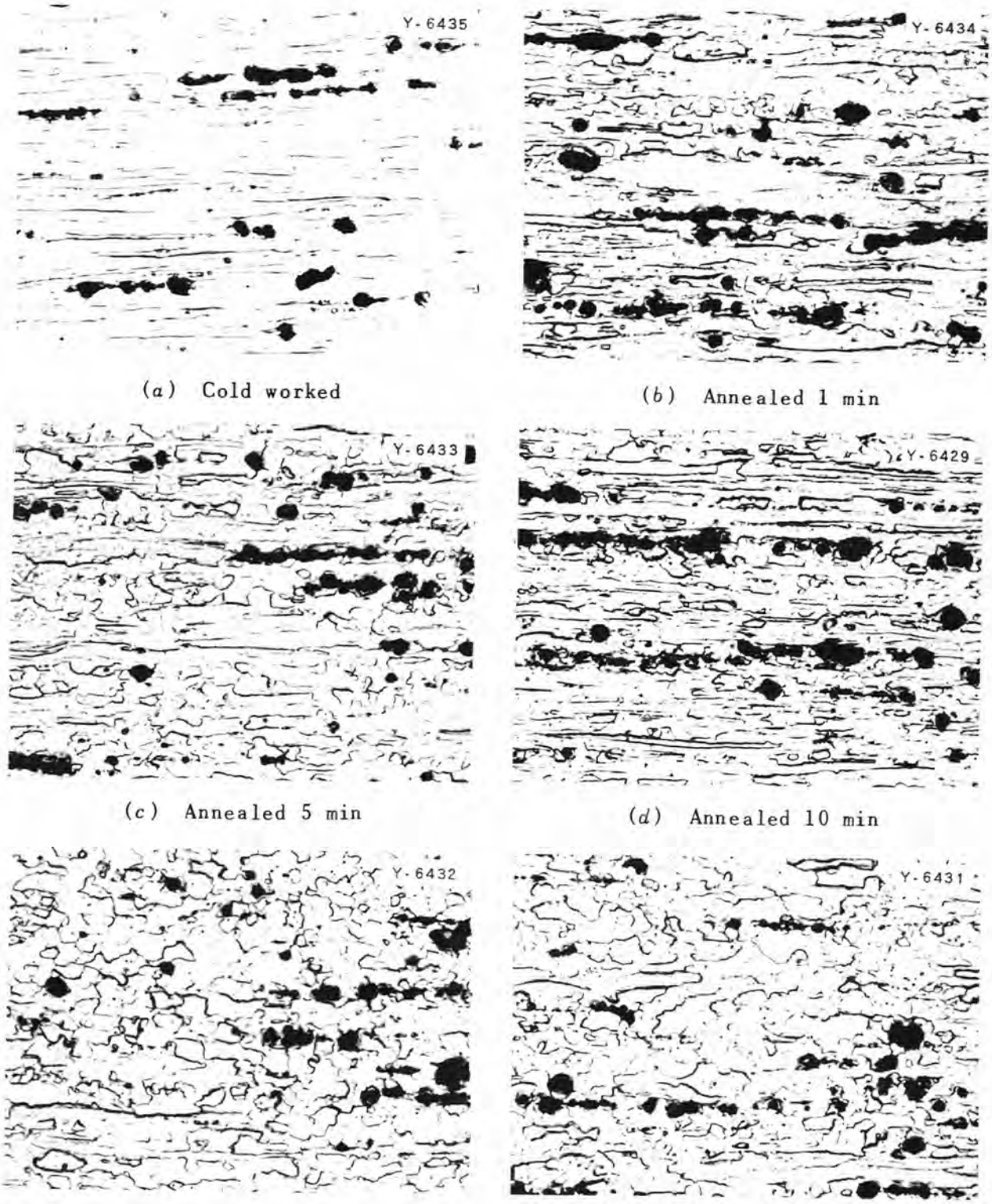


(*a*) Cold worked

(*b*) Annealed 1 min

(*c*) Annealed 5 min

(*d*) Annealed 10 min

(*e*) Annealed 20 min

(*f*) Annealed 60 min

**Fig. 80. Recrystallization of Ames Thorium 80% Cold Worked and Annealed at 600°C.** 250X.

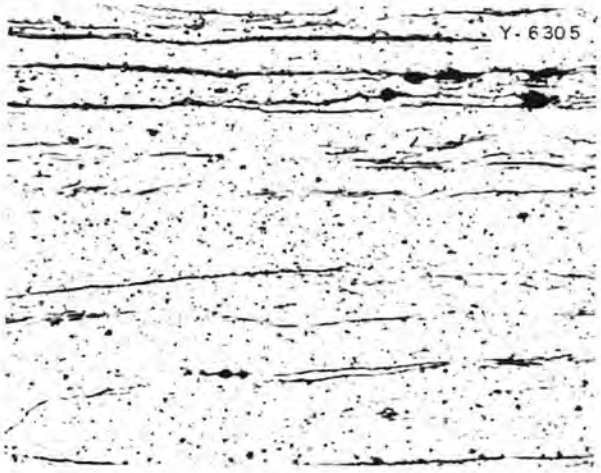


(*a*) Cold worked

(*b*) Annealed 1 min

(*c*) Annealed 5 min

(*d*) Annealed 10 min

(*e*) Annealed 20 min

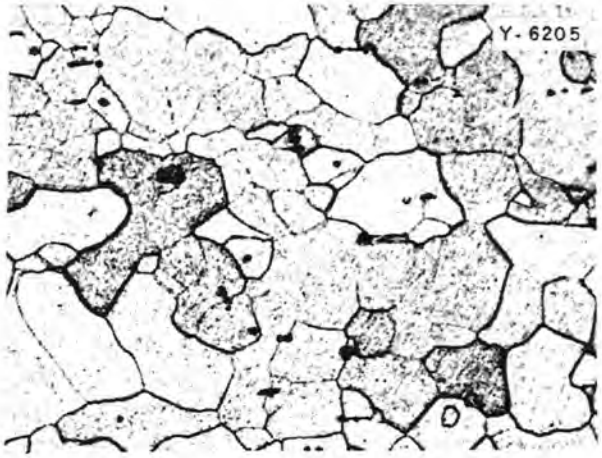


(*f*) Annealed 60 min

**Fig. 81. Recrystallization of Crystal-Bar Thorium 80% Cold Worked and Annealed at 650°C.** 250X.

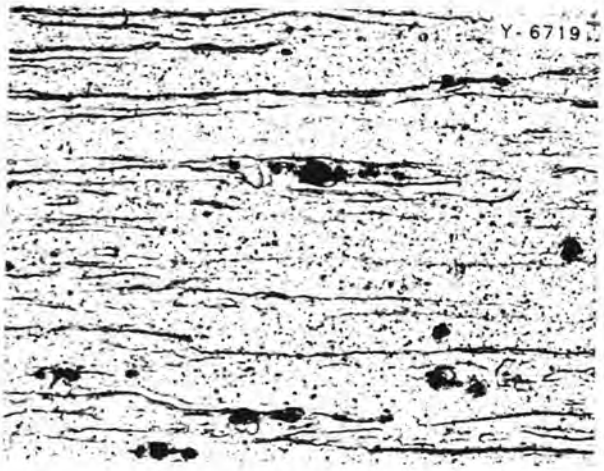


(*a*) Annealed at 500°C

(*b*) Annealed at 530°C

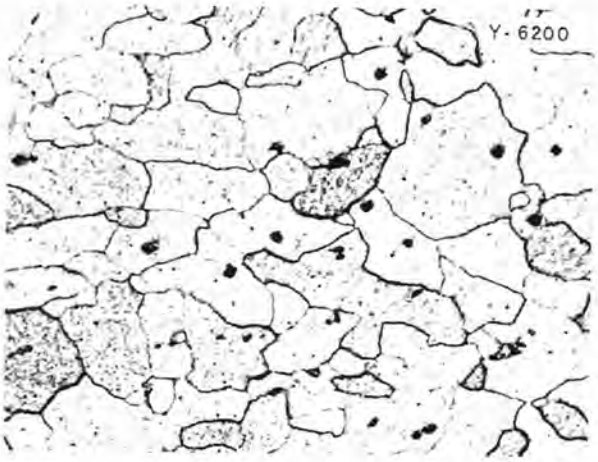


(*c*) Annealed at 580°C

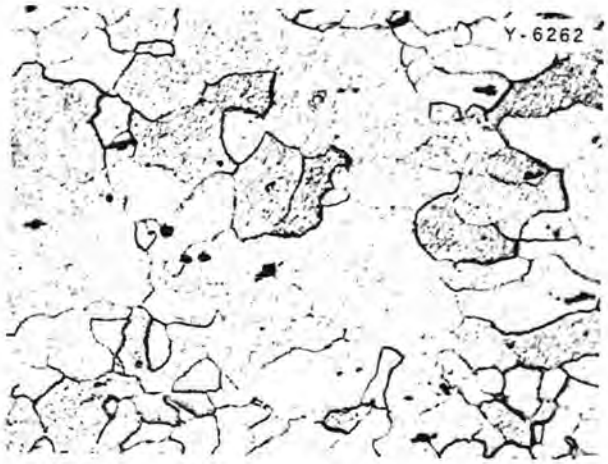


(*d*) Annealed at 600°C

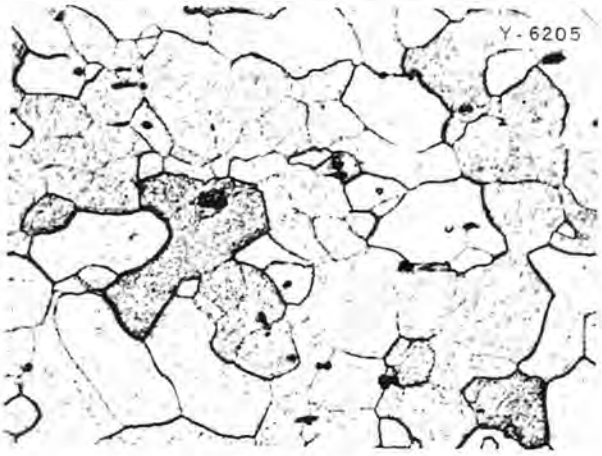


(*e*) Annealed at 650°C

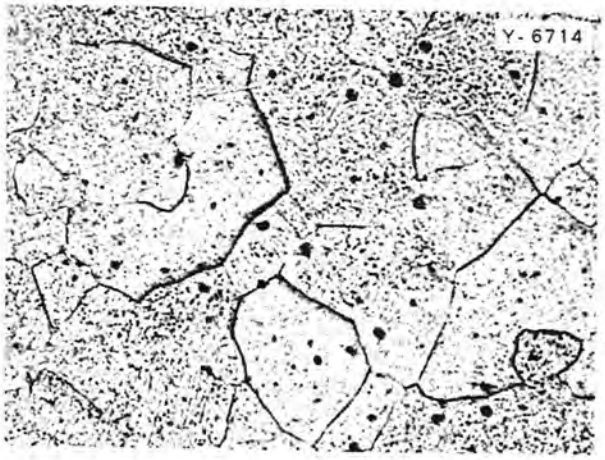


(*f*) Annealed at 742°C

**Fig. 82. Recrystallization of Crystal-Bar Thorium 80% Cold Worked and Annealed 60 Minutes.** 250X.

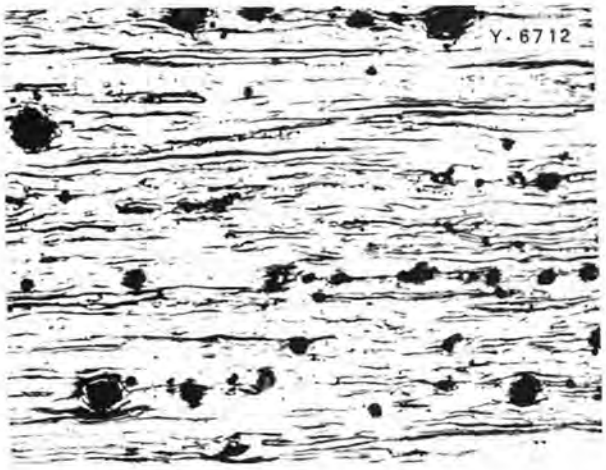


(*a*) Annealed at 500°C

(*b*) Annealed at 530°C

(*c*) Annealed at 580°C

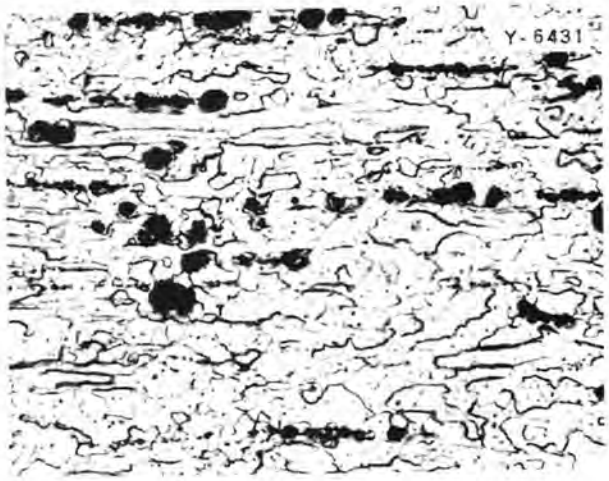


(*d*) Annealed at 600°C

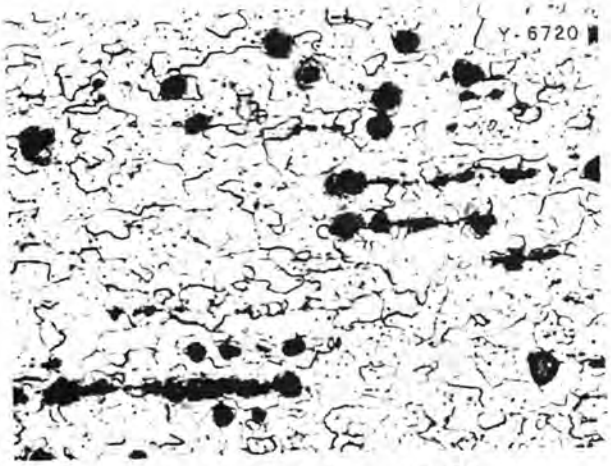


(*e*) Annealed at 650°C

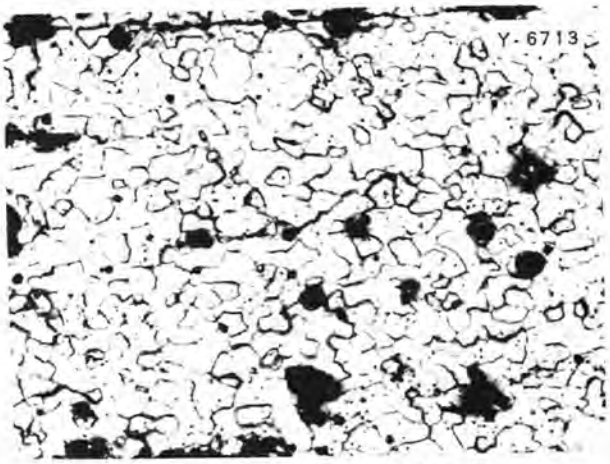


(*f*) Annealed at 742°C

**Fig. 83. Recrystallization of Ames Thorium 80% Cold Worked and Annealed 60 Minutes.** 250X.

# EXPERIMENTAL PLATE-CLADDING PROGRAM

J. E. Cunningham R. B. Small

## CLADDING OF URANIUM WITH ZIRCONIUM

R. J. Beaver T. A. Olson

In reviewing the properties of protective materials for reactor fuels operating at elevated temperatures, it becomes apparent that low-hafnium zirconium has many advantages to offer. Foremost among the advantages are the following: it combines strength, ductility, and corrosion resistance with a low neutron-absorption cross section. In addition, there is no evidence of an intermetallic compound present that could embrittle a uranium-zirconium bond. Because of the benefits to be gained and the fact that success appeared likely, an investigation was initiated to produce uranium plates bonded with zirconium by roll cladding.

Inasmuch as no design figures were stipulated, a number of billet designs were available. The technique of picture-framing the uranium in zirconium was considered but eliminated in favor of the design shown in Fig. 84. The reason for initially using circular cylinders was that they resulted in considerable saving in machining costs as well as a 250% saving in zirconium. Also, the probability of obtaining edge bonding was improved. The billets were subsequently rolled to flat plates in the manner depicted in Fig. 85. Alpha-extruded uranium bar was used as the core element and Bureau of Mines arc-melted sponge zirconium was used as the cladding material.

Methods of preparing and sealing these billets were investigated. Of the 21 circular billets rolled, 15 had cores that had just been freshly machined. The remaining six cores were electropolished prior to assembling. There seemed to be no apparent difference in bonding characteristics. Prior to assembling, all components were degreased in Triclene "D" vapor, and later an acetone rinse was added to the cleaning procedure.

The first procedure used in assembling and sealing was to press-fit the uranium and zirconium cap core into the zirconium frame and seal by heliarc welding the cap to the frame in a dry box. Unfortunately, the helium was of questionable purity and the dry box leaky. The first ten billets were sealed in this manner. The initial billet was rolled at 1150°F with no sheath. The results revealed that the zirconium must be protected from the atmosphere. The following two billets were sheathed in steel and rolled at 1150°F. Difficulty was immediately encountered because the steel sheath cracked while being rolled. After the second rolling, the temperature was increased to 1175°F. Copper was then substituted as the sheathing material, and the billets rolled nicely in such sheathing, except that when the reductions per pass were less than 15% serious edge cracking of the underlying zirconium occurred. This effect is shown in Fig. 86. Ten billets were sealed in the dry box and rolled at 1175°F with surface-increase ratios ranging from 4:1 to 15:1. Surface-increase ratios were used as reduction criteria instead of cross-section reduction ratios because of the billet geometry.

Chisel, bend, and shear tests indicated that a fair bond had been obtained across the flat portions of plates from billets prepared in this manner, but bonding never occurred at

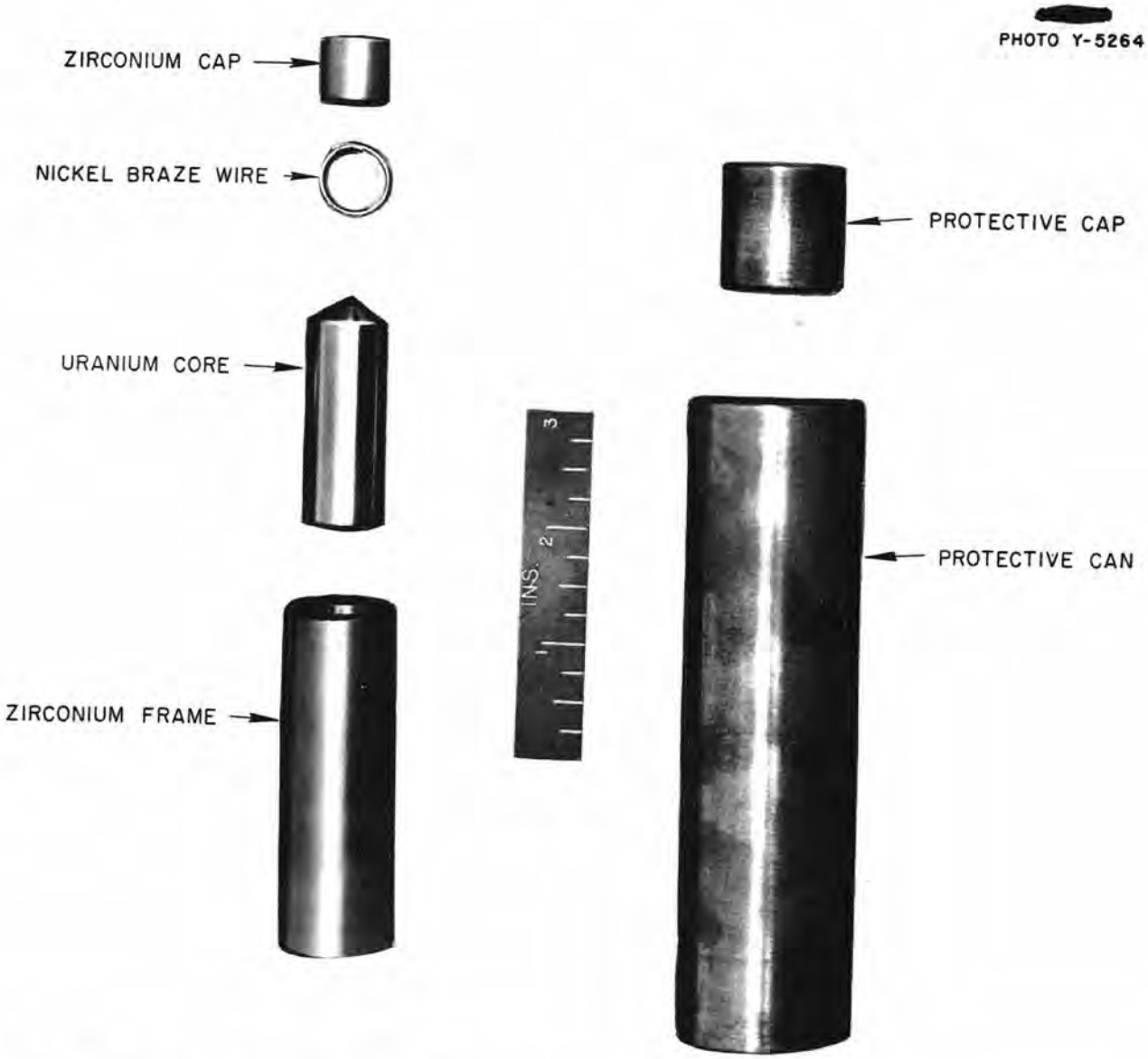


**Fig. 84. Unit Parts of Billet Assembly Used in Roll-Cladding Zirconium to Uranium.**

the edges. Figure 87 is a photomicrograph showing the bond between the uranium and zirconium of a plate rolled at 1150°F with a surface increase ratio of 7:1. Although a shear test revealed that the plate had a strength of 35,000 psi, a number of unbonded regions existed at the interface.

Results obtained with sealing under a helium atmosphere indicated that a more efficient means of sealing would be that of brazing the cap to the frame under vacuum. The apparatus developed for this method is shown in Fig. 88. The vacuum system consists of a Welch Duo Seal vacuum pump capable of evacuating to 0.1 $\mu$, a DPI Type

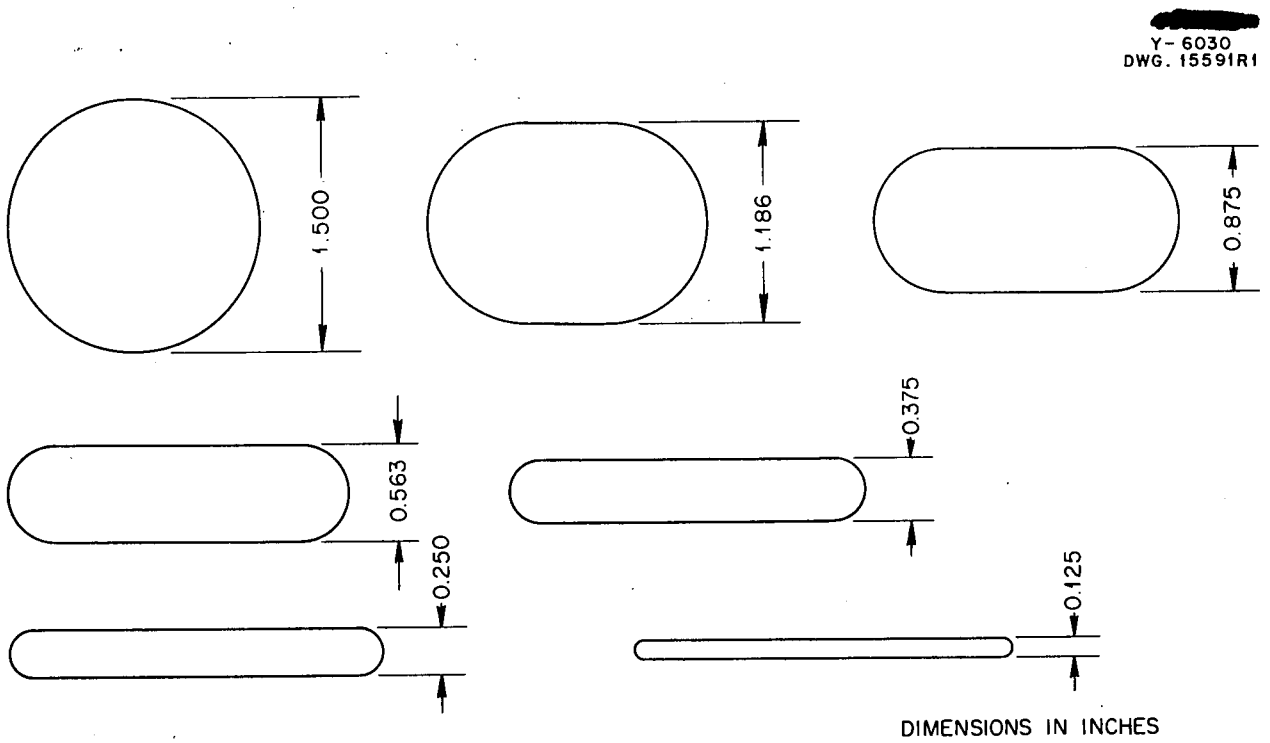


**Fig. 85. Cross-Sectional Views Showing Deformation of Zirconium-Uranium Circular Billet During Rolling Sequence.**

VMB 7 roughing diffusion pump that can be operated at a forepressure of 500 $\mu$, and a DPI Type VM220A diffusion pump that operates at a forepressure of 100 microns. A cold trap between the VM220A diffusion pump and the 2 1/2-in.-dia header prevents vapors from diffusing back into the system. A Hastings thermocouple gage capable of accurately measuring vacuums in the range above 10 $\mu$ is located between the cold trap and the main valve. A DPI ion gage for measuring vacuums lower than 1 $\mu$ is located behind the main valve and between the 1/2- and 2 1/2-in.-dia vacuum ports. The attachment to the vacuum consists of a 2-in.-dia pyrex glass jar, the bottom 5 1/2-in. length of which was reduced to 1 5/8 in. in dia to provide closer linkage between the induction coil and the cylinder. A Kovar metal tube sealed to the top of the jar provides a means for brazing the unit to a copper dome. A 10-in. long, 1/2-in.-dia copper tube connects the copper dome to the vacuum port. All joints are made leak tight by soldering with 60 wt % tin-lead alloy solder.

The technique followed for evacuating and brazing the billet in the apparatus is to assemble the billet by slipping the uranium core into the zirconium cylinder and placing the zirconium cap into the frame above the core. The top end of the cap is spun to a slightly larger diameter than the body of the cap so that the abutment can rest on the ring of braze metal that is placed on the shoulder of the zirconium frame. The cap fits loosely into the frame and provides an interstice through which the inside of the billet can be evacuated. A 1 1/8-in.-dia quartz tube is placed around the cylinder to protect the pyrex during the brazing operation and the unit is placed in the

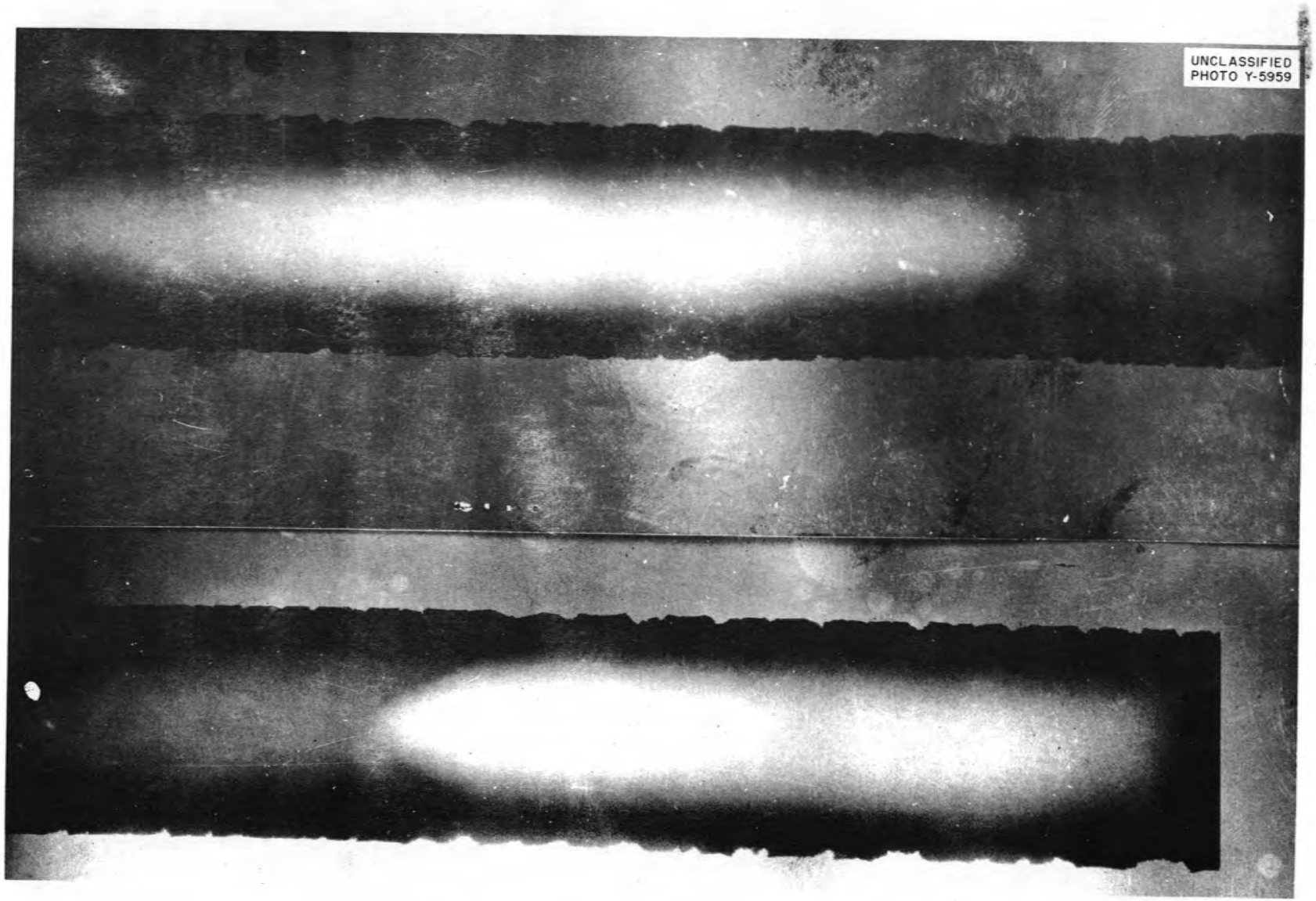


Fig. 86. Radiograph of Plate No. 8 Showing Cracking Along Edges.

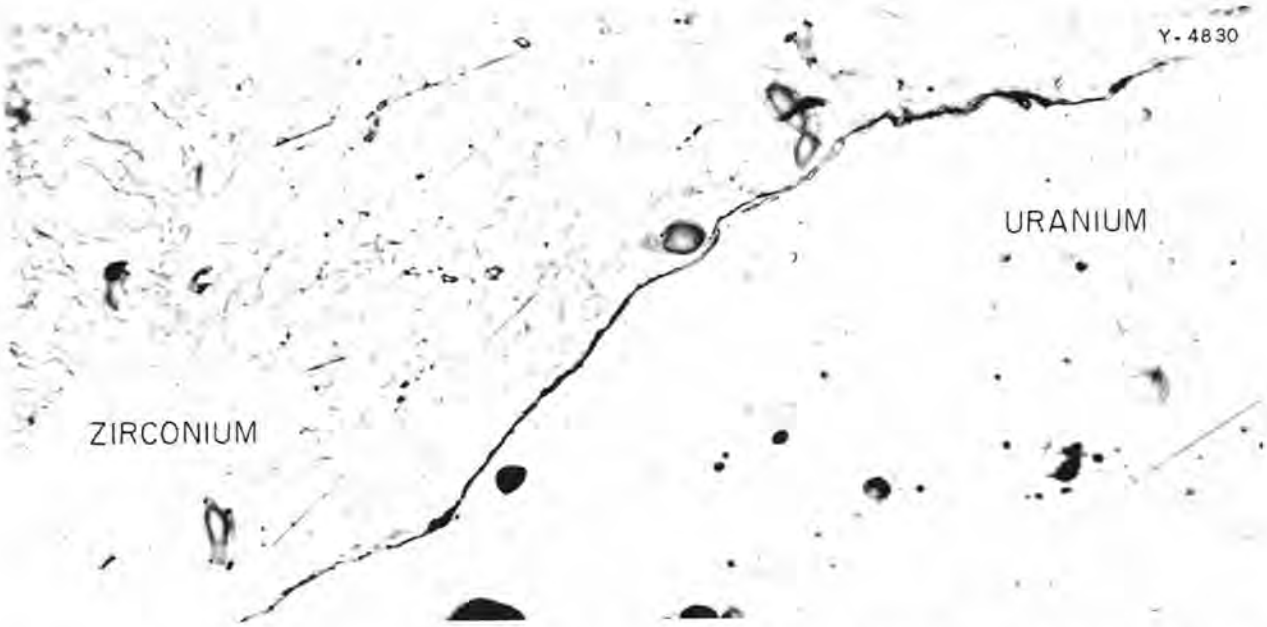


**Fig. 87. Bond Between Uranium and Zirconium Rolled at 1150°F.** Etched with acetic and perchloric acids. 1000X.

pyrex glass jar. The jar containing the billet is then connected to the vacuum system and evacuated for about 16 hours. The vacuum is maintained at approximately 0.1 micron.

Means for heating the billet for degassing and brazing is provided by the Lepel spark-gap oscillator. A 5-turn coil of 3/8-in.-dia copper tubing is placed around the glass jar near the bottom portion of the billet and connected to the leads of the oscillator. The oscillator is then switched on and the billet is heated by induction from room temperature to approximately 600°F and degassed for 1 hour. After allowing the billet to cool for a period of 15 min while still under vacuum, the coil is moved to the top of the billet and the oscillator is tuned to its peak output. When the braze metal is melted the cap is sealed to the frame. Silver, nickel, and titanium have been used successfully as the brazing metal; however, silver and titanium cannot be used in cladding uranium because of their high neutron-absorption cross sections.

Four billets, prepared in the manner described above, were sheathed in copper and rolled at 1175°F. The surface-increase ratios varied from 8:1 to 14:1. Chisel tests, shear tests, and metallographic examination revealed an improvement in the zirconium-uranium bond. Figure 89 shows the bond interface between uranium and zirconium on the flat portion of the clad plate. Figure 90 is a photomicrograph of the same bond taken at twice the magnification, and it can be seen that a slight amount of diffusion occurred, but it is quite apparent that this method of sealing resulted in improvement. Figure 91 shows bonding at one edge of the plate; here again there is evidence of good bonding. Figure 92 shows bonding at the other edge. An unbonded region at the tip end leads to some uncertainty as to whether edge bonding can be accomplished by using this preparation and rolling technique.

A section from the middle portion of a plate was quenched from 720°C into room temperature water with no apparent

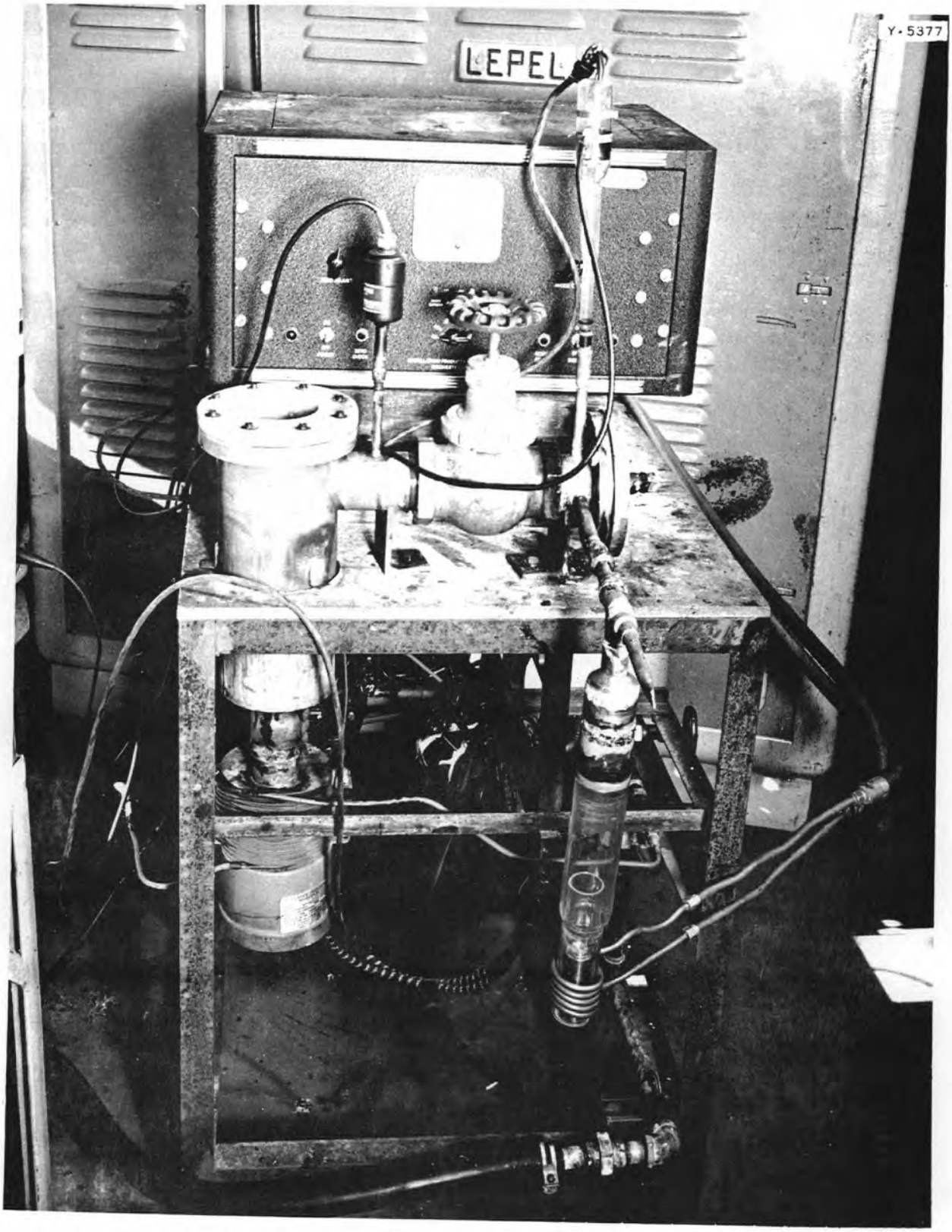


Fig. 88. Vacuum Apparatus used in Evacuating and Sealing Uranium-Zirconium Billets.

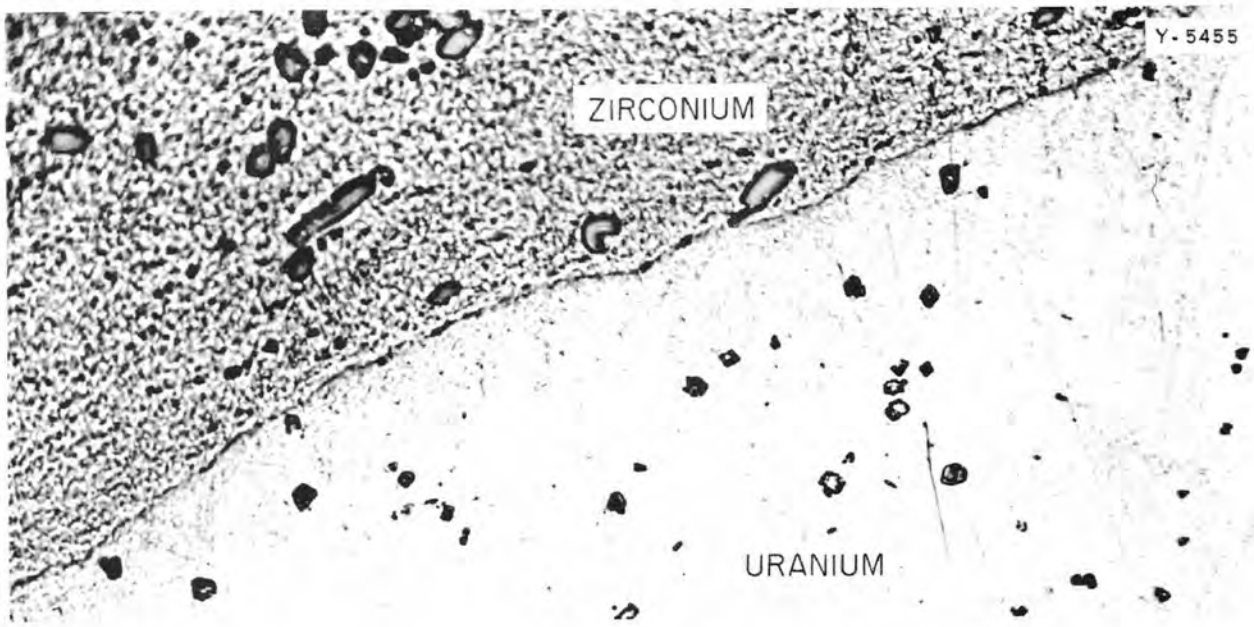


**Fig. 89. Bond Between Uranium and Zirconium on the Flat Portion of the Clad Plate.** Etched with acetic and perchloric acids. 500X.

**Fig. 90. Same as Fig. 89 Shown at Twice the Magnification.** Etched with acetic and perchloric acids. 1000X.

**Fig. 91. Bonding at Edge of Uranium-Zirconium Plate.** Etched with acetic and perchloric acids. 500X.

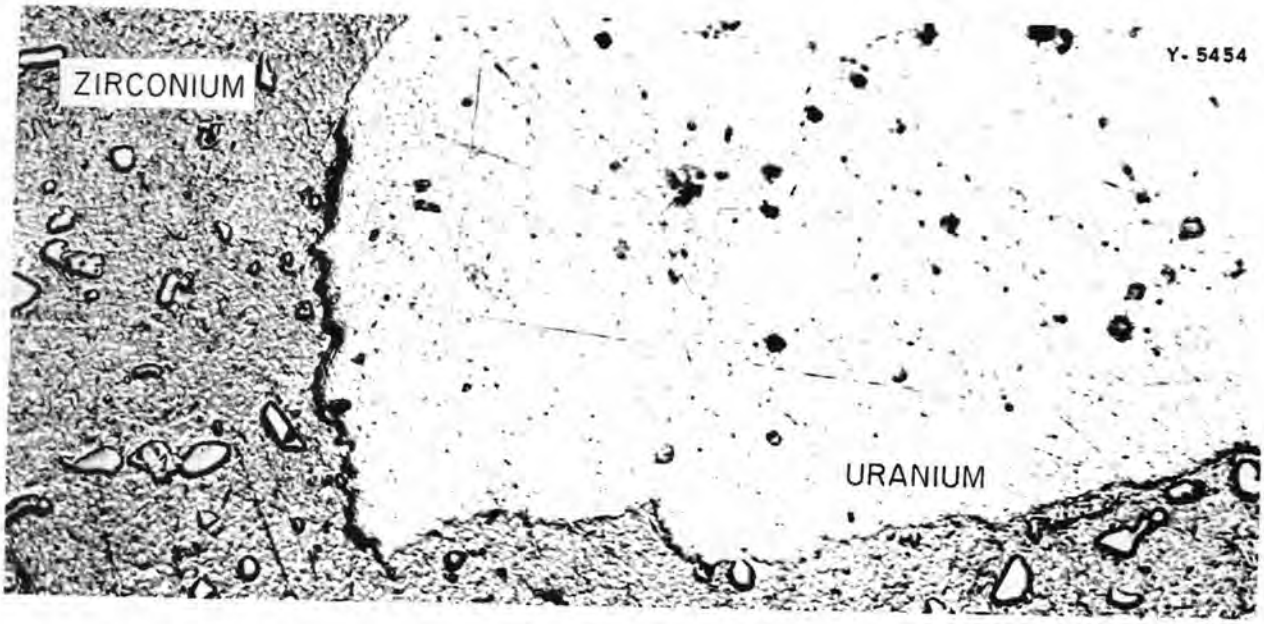


**Fig. 92. Bonding at Edge of Uranium-Zirconium Plate.** Etched with acetic and perchloric acids. 500X.

failure. Another section was bombarded by protons in the Y-12 calutron for 24 hr at 1 kw/in.$^2$ with no ill effects.

Figure 93 illustrates the shear test design that was used to support chisel test and metallographic specimens. As can be seen, the design calls for a slit to be made through the zirconium and uranium on one side and a slit to be made through the zirconium only on the other side, leaving a shear area of approximately 0.045 in.$^2$. Table 34 correlates billet preparation and amounts of total reduction with shear values. It can be noted that plates produced from evacuated billets are considerably better than those sealed in an inert atmosphere. Also an increase in reduction improves the bond strength of the plates prepared from evacuated billets. However, plates produced from billets prepared in the dry box under a helium atmosphere show no improvement by increasing the total amount of reduction. It seems possible that this may be due to helium entrapment at the interface, which causes unwelded regions that remain unaffected by increasing total reduction.

Because of the uncertainty of the bonding at the edges of plates produced by the procedures described above, it was felt that rolling at 1750°F would induce sufficient diffusion to secure

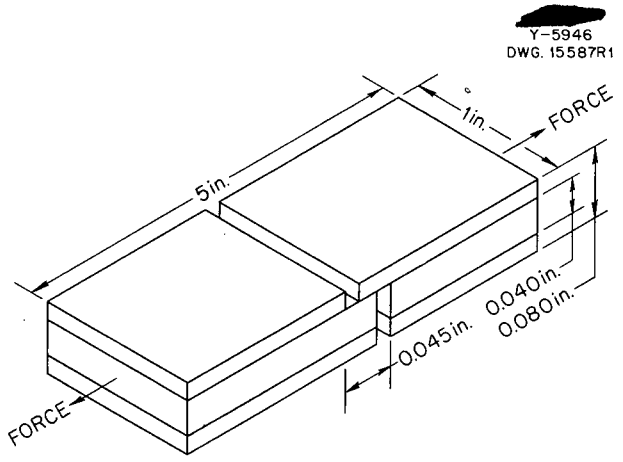


**Fig. 93. Schematic Drawing of Shear Test Sample Used to Determine Mechanical Strength of Bond Between Uranium and Zirconium.**

**TABLE 34**

**Effect of Preparation and Sealing Technique on Bond Strength of Zirconium-Clad Uranium Plates**

| PLATE NO. | SHEARING FORCE (lb) | SHEAR AREA (in.$^2$) | BOND STRENGTH (psi) | SURFACE INCREASE RATIO* |
|---|---|---|---|---|
| 2** | 1595 | 0.0455 | 35,000 | 7:1 |
| 10** | 1725 | 0.0495 | 35,000 | 11:1 |
| 14*** | 2540 | 0.0527 | 48,300 | 8:1 |
| 16*** | 2600 | 0.0430 | 60,500 | 14:1 |

*Ratio of final surface area to original surface area.

**Sealed in dry box under questionable inert atmosphere.

***Sealed by brazing in vacuum.

bonding at the edges. A previous experiment showed that rolling completely in the gamma-uranium temperature range (above 1420°F) was not feasible. A procedure was initiated in which a billet, sealed under vacuum, was rolled through approximately half of the rolling sequence at 1175°F, reduced approximately another 22% at 1750°F, and then finished at 1175°F. The billets were necessarily sheathed in steel, and the inside of the steel can was oxidized to prevent formation of the eutectic that occurs between steel and zirconium at approximately 1650°F. Four billets were rolled in this manner.

Serious difficulty was encountered as a result of the high-temperature treatment. Because of the extreme plasticity of uranium in comparison with zirconium during the rolling at 1750°F, uranium tended to build up at the plate edges. Figure 94 shows the cross section of a plate rolled completely at 1175°F. It can be seen that the core has a uniform thickness in the middle portion but gradually tapers toward the edge. The bottom view of Fig. 95 shows the cross section of a plate in which the 1175°F rolling was interrupted by a 22% reduction at 1750°F. The dumbbell effect, caused by rolling in the gamma-uranium temperature range, is quite apparent. However, this effect is considerably relieved when the plate is subjected to 20% cold working, as shown in the upper view. Figure 96 shows the bulging effect along the plate length caused by the high-temperature treatment. This problem was never solved because the billet design was changed at the same time the effect became apparent. However, it is believed that further investigation would reveal a solution to the problem.

The high-temperature rolling resulted in enough diffusion to obtain bonding at the edges. Figure 97 shows the bond at the edges, and Fig. 98 shows the bond at the flat portions of such a plate. Figure 99 is a similar photomicrograph taken at twice the magnification. The laminar structure existing in the zirconium adjacent to the bond interface can be seen. It is possible that this structure represents the eutectoid of the uranium-zirconium phase diagram. Plates have been produced in this manner with zirconium-cladding thicknesses as low as 0.004 inch. Figure 100 shows sections of these plates after various physical deformations. It is apparent from such tests that the plates are able to withstand considerable stress.

Although the circular billet design served adequately for the initial studies, it became quite apparent that the complete framing type of jacket design had several limitations. First, the method does not lend itself readily to production of extra long plates because of the problem in maintaining alignment during rolling. Second, the resulting plate width is necessarily fixed. Furthermore, obtaining edge bonding is difficult, even under the most favorable conditions. For these reasons, the modified rectangular billet design, shown in Fig. 101, was adopted to permit production of large-scale, double-clad plate from which plates of any desired length or width could be sheared. However, this method would not be suitable for production cladding of enriched-uranium metal or alloys.

No provision has been made for obtaining edge bonding in the rectangular design. Currently attempts are being made to close these exposed edges by welding with an automatic, straight-line welding machine. The new design is economical in that it minimizes the consumption of zirconium and results in the minimum of machining.

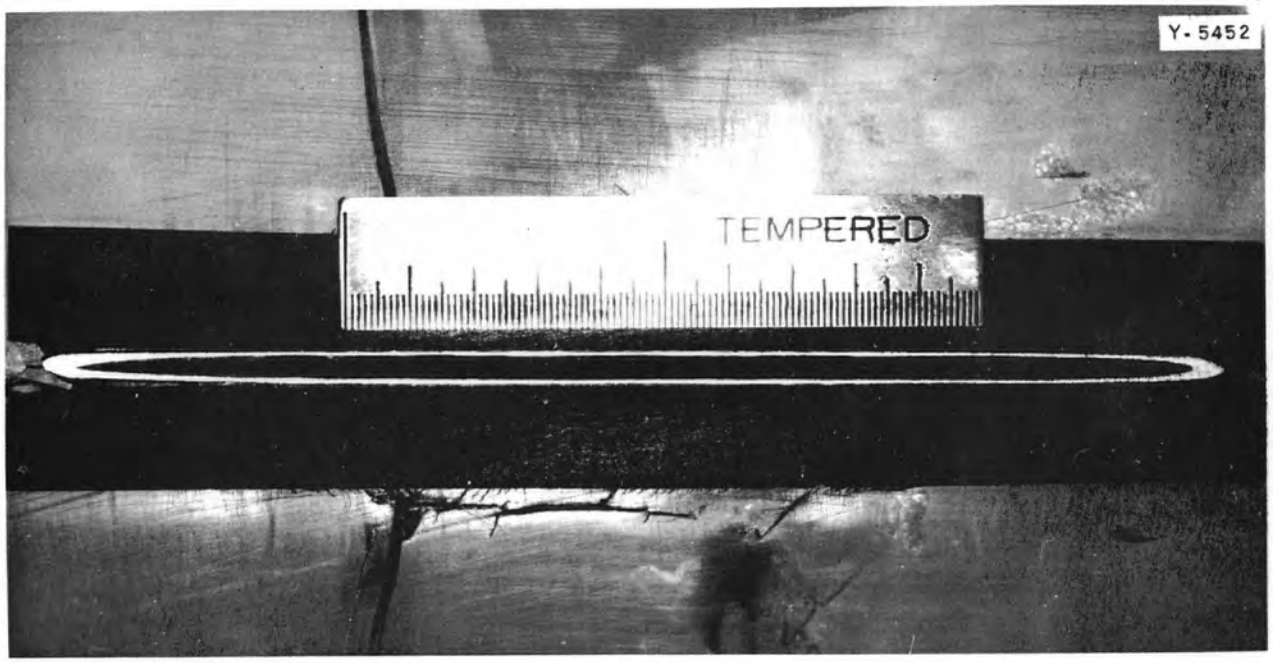


Fig. 94. Cross Section of Plate Rolled Completely at 1175°F.

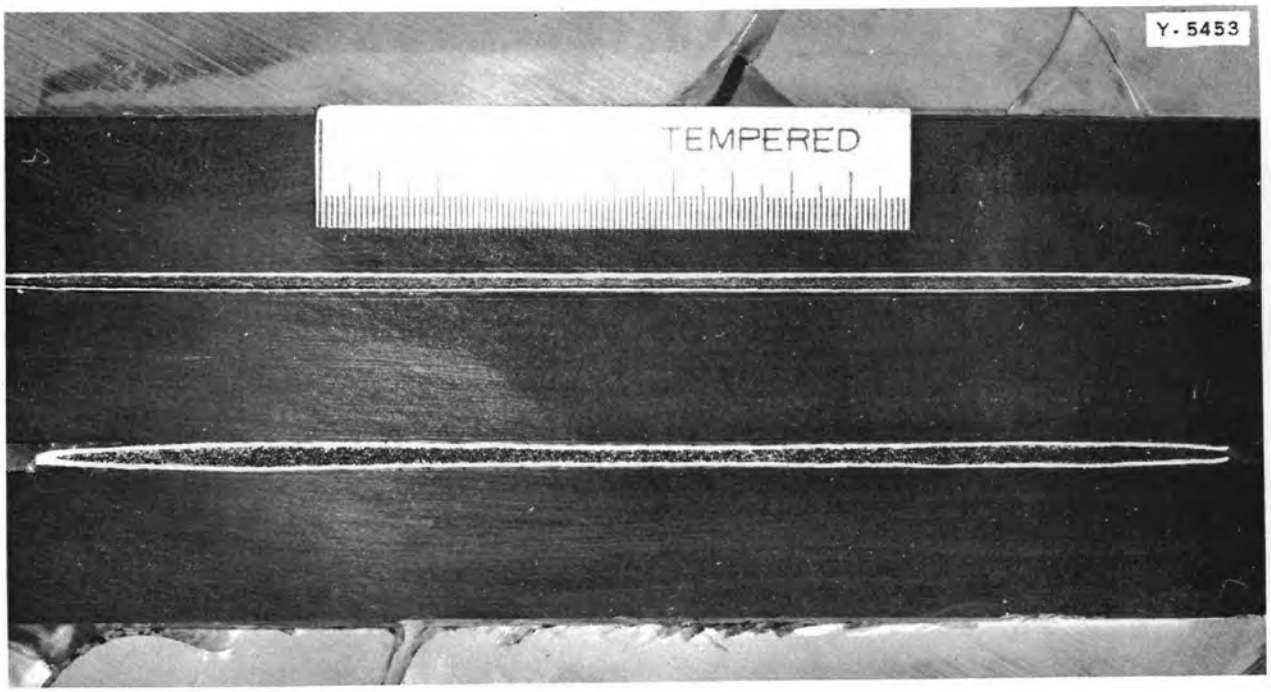


Fig. 95. Cross Sections of Plate Rolled at 1175°F, Reduced 22% at 1750°F, and Subsequently Cold Reduced 20%.

The method of preparing and sealing billets generally follows the pattern described below:

1. Weld bottom steel cover plate to steel frame.

2. Place core elements in well of steel frame.

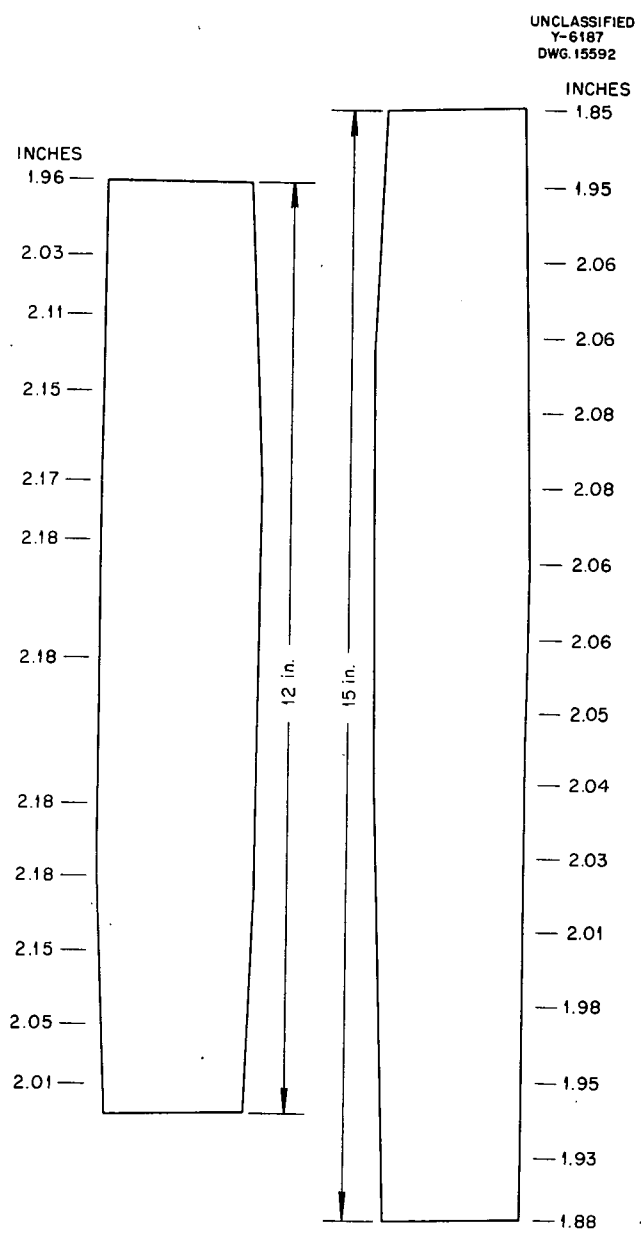


**Fig. 96. Bulging Along the Length of Plate Caused by Rolling at 1750°F.**

3. Weld top cover plate to frame while passing helium through evacuating tube. (The helium blanket protects the uranium from oxidation.)

4. Quench in water.

5. Leak test on Westinghouse leak detector.

6. Evacuate to less than 1 $\mu$ for 16 hours.

7. Purge twice with helium.

8. Evacuate for 1 hour.

9. Seal billet by forging evacuating tube.

The uranium cores are obtained from cast stock and are electropolished prior to assembling. The zirconium cover plates are obtained from Bureau of Mines arc-melted sponge that has been sheathed in steel and hot rolled to finished size.

Six billets were sheathed in 0.25% carbon firebox-grade steel and rolled at 1175°F. Every billet cracked during some stage of the rolling sequence, and as a result the plates had either little or no bonding. It became apparent that a more detailed investigation would be necessary before further billets could be rolled in this steel at this temperature. Rather than delay the output of the plates, a 0.04% carbon, titanium-killed steel (Tinamel) was obtained as a substitute steel. Nine billets have been rolled successfully in this type of steel sheath. Inspection of the bonding has been limited to metallographic observations. The interface between the uranium and zirconium does not appear to have the optimum bonding characteristics established in previous work. Figure 102 is a photomicrograph of the poorest bond, and Fig. 103 is a photomicrograph of the average bond in such

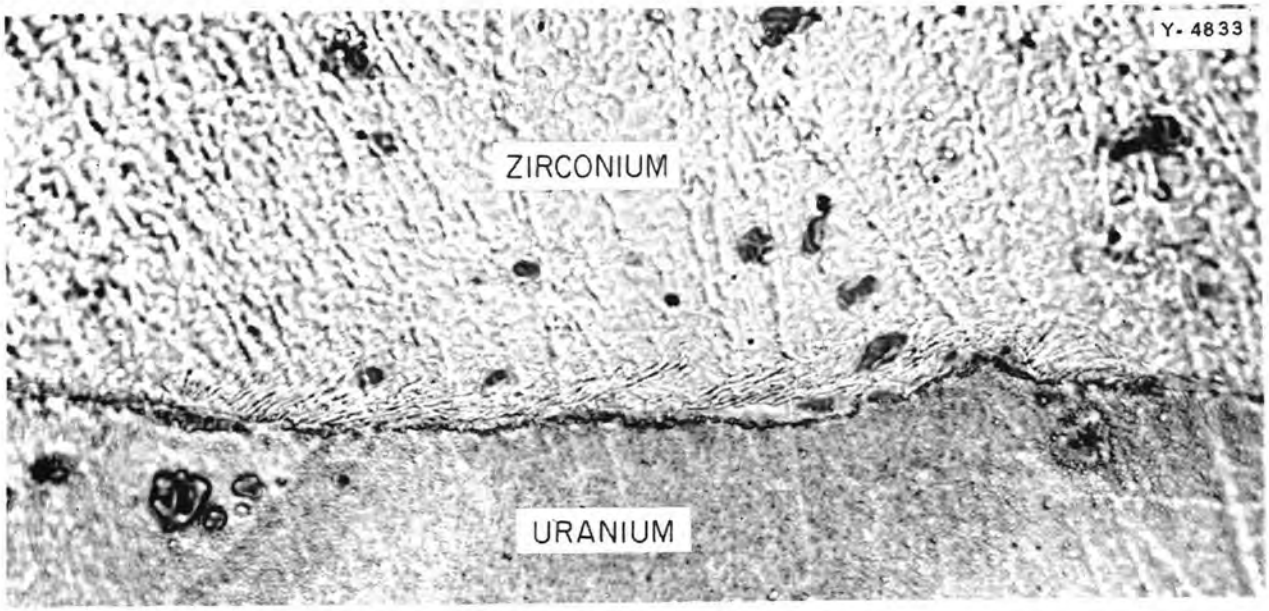


**Fig. 97. Bonding at the Edge of Uranium-Zirconium Plate.** Etched with acetic and perchloric acids. 1000X.

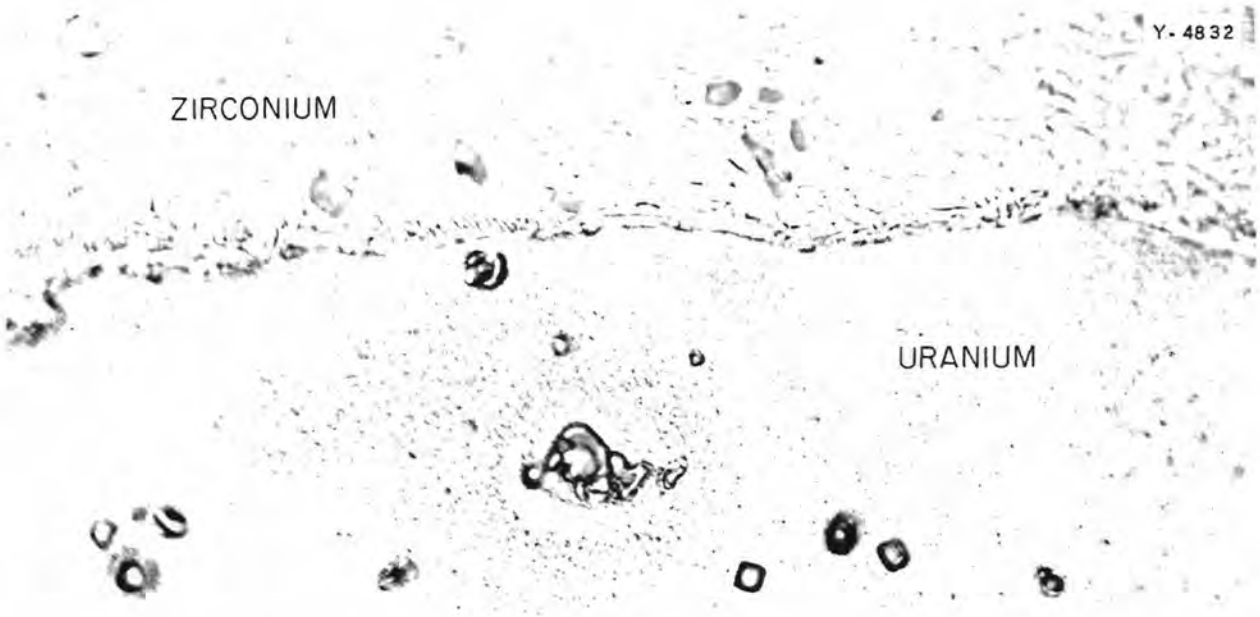


**Fig. 98. Bonding at the Flat Portions of Uranium-Zirconium Plate.** Etched with acetic and perchloric acids. 1000X

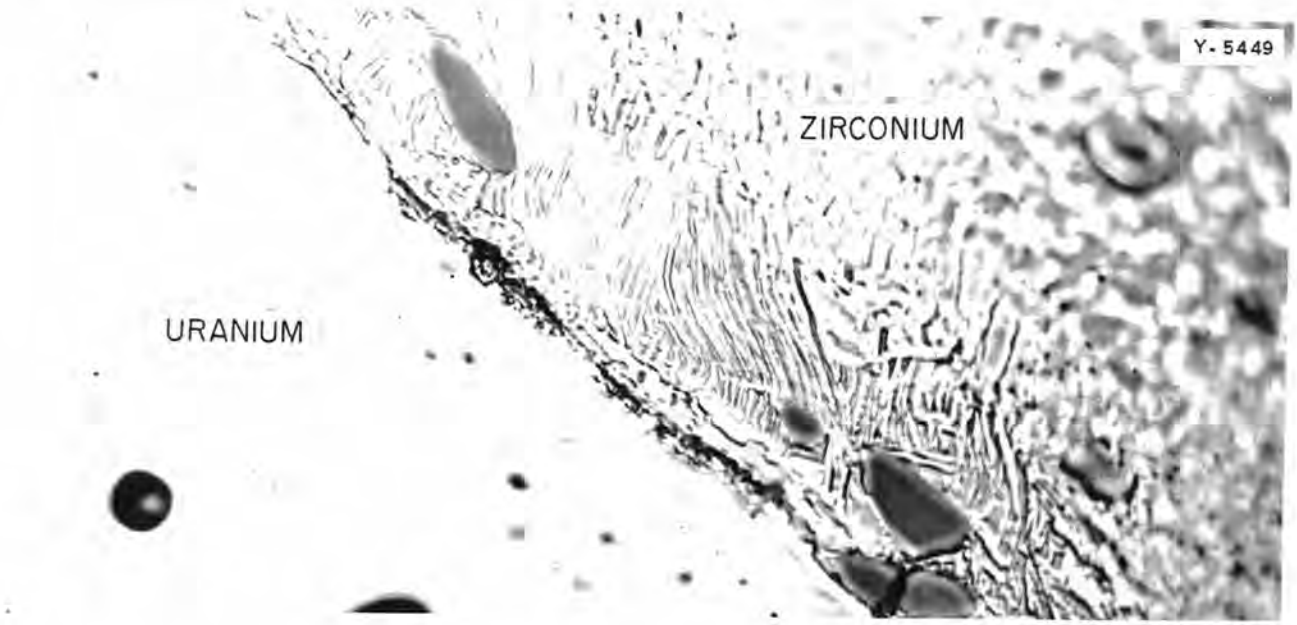


**Fig. 99. Similar specimen as in Fig. 98 Shown at Twice the Magnification.** Etched with acetic and perchloric acids. 2000X.

a plate. Since the assumption that the vacuum in these billets was below 1 $\mu$ has been found to be erroneous, a method of accurately measuring vacuums below 1 $\mu$ has been provided. It appears that a vacuum in the range of $1 \times 10^{-5}$ to $5 \times 10^{-5}$ mm Hg can be attained, and the effect of such a vacuum should result in an improvement in bonding characteristics.

### CLADDING OF THORIUM WITH ZIRCONIUM

J. J. Lawless R. J. Beaver

A preliminary investigation has been in progress to develop suitable techniques for bonding thorium to zirconium by roll cladding. The circular billet design shown in Fig. 104 was used initially. After 17 billets were rolled with little success, the billet design shown in Fig. 105 was resorted to and some pertinent information was obtained. This type of billet required that the steel can be vacuum tight because any leak or failure would automatically oxidize the core elements during the heating and rolling operations. Canning material is an important factor in this problem and is worthy of considerable study.

The type of billet shown in Fig. 105 was prepared by first welding the tubes and bottom cover plate to the steel frame. After cooling the steel to room temperature, the thorium core and zirconium cover plates were inserted. In order to minimize heating of the core elements and prevent their oxidation during the welding of the top steel cover plate, the assembly was placed in a tray of water 1/2 in. deep and a gentle flow of helium was passed through the billet.

Particular emphasis was placed on studying the effects of reduction, rolling temperature, surface preparation, and internal billet atmosphere. In studying metal surface preparation, it was found that several techniques

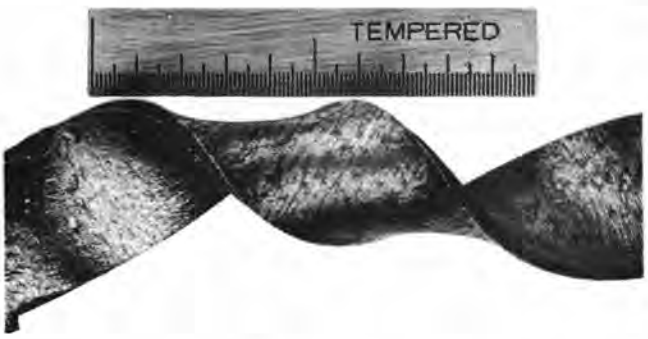


(*a*) Torsion. 2.25X.

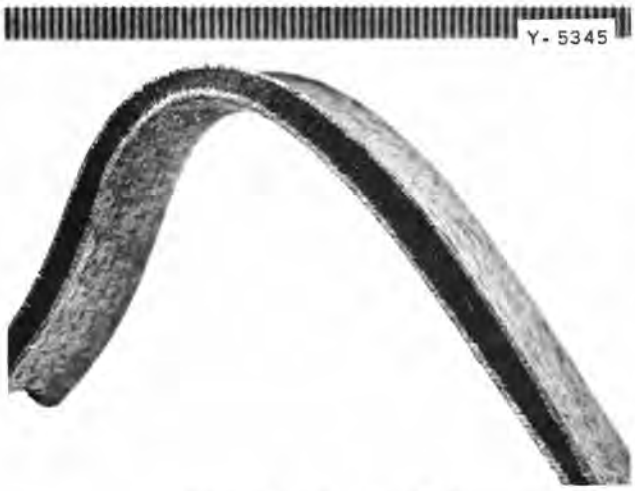


(*b*) Bend. 4.5 X.

(*c*) Fracture. 9.5X.

**Fig. 100. Sections of Plate Shown in Figs. 97, 98, and 99 After Undergoing Torsion, Bend, and Fracture.**

might be acceptable. However, the importance of this variable, although minor in comparison with temperature, reduction, and atmosphere, may become more critical at some later date when better control of the other variables has been attained.

Machining, wire brushing, electropolishing, and shot blasting (zirconium only) were all found to be practical and effective procedures for cleaning mating surfaces to be bonded. Electropolished thorium seems to have a degree of passivity and somewhat resists reoxidation at lower temperatures.

The degree of vacuum within the billet was found to affect bonding. Some preliminary tests were made by heating thorium and zirconium at different vacuums. The tests indicated that the atmosphere within the billet should be in the range of 1 ppm of total active gases if contamination at the bond interface was to be avoided.

The bond shown in Fig. 106 was obtained by rolling a billet that had been evacuated only. Figure 107 shows the bond in another plate that had been rolled from a billet subjected to alternate evacuation and flushing with helium and outgassing at 1000°F before sealing at a pressure below 5 microns. The results represented in Figs. 106 and 107 were confirmed in several tests. In each case the reductions and rolling temperatures were effectively the same.

Attempts to produce bonds by rolling plates in which the billet had been sealed in either air or helium atmospheres were failures.

Temperatures between 400 and 1500°F result in release of adsorbed gases to a degree sufficient to promote reoxidation of the thorium if the gases are not removed immediately. Above a critical temperature, in the range of 1800°F, the oxides of thorium apparently

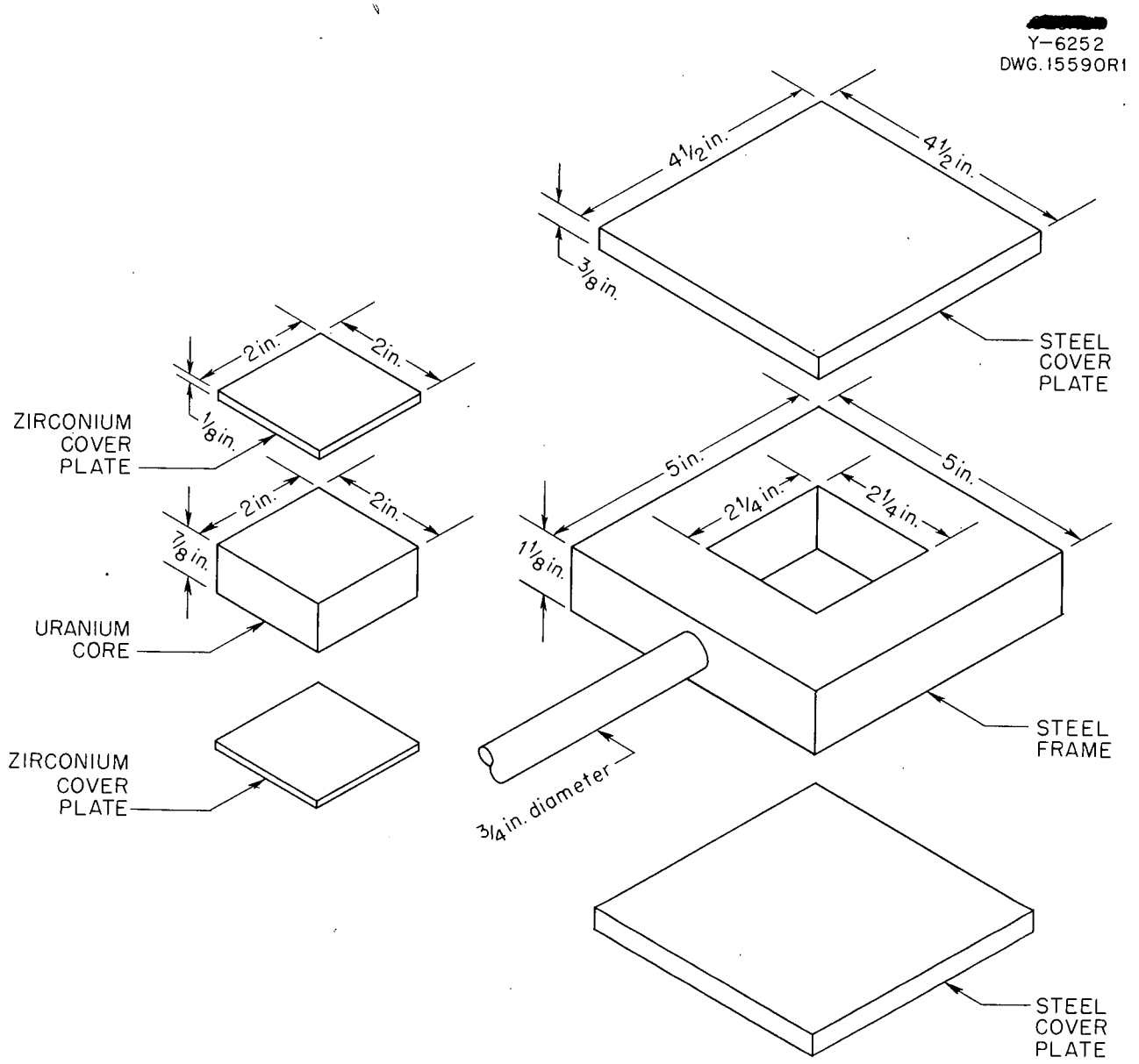


**Fig. 101. Billet Design for Producing Zirconium-Clad Uranium Plates by Utilizing Evacuating Technique.**

redissolve in the opposing zirconium and in time disperse in the surrounding metal. The effects of temperature on outgassing and solution of oxides seem to be as important as the effect on plasticity.

Hot hardness or similar data for the temperature range of interest were not available; however, billets were rolled at temperatures from 1450 to 1900°F without difficulty resulting from differences in plasticity of zirconium and thorium.

Metallographic examination of rolled bonds indicated that diffusion layers between zirconium and thorium

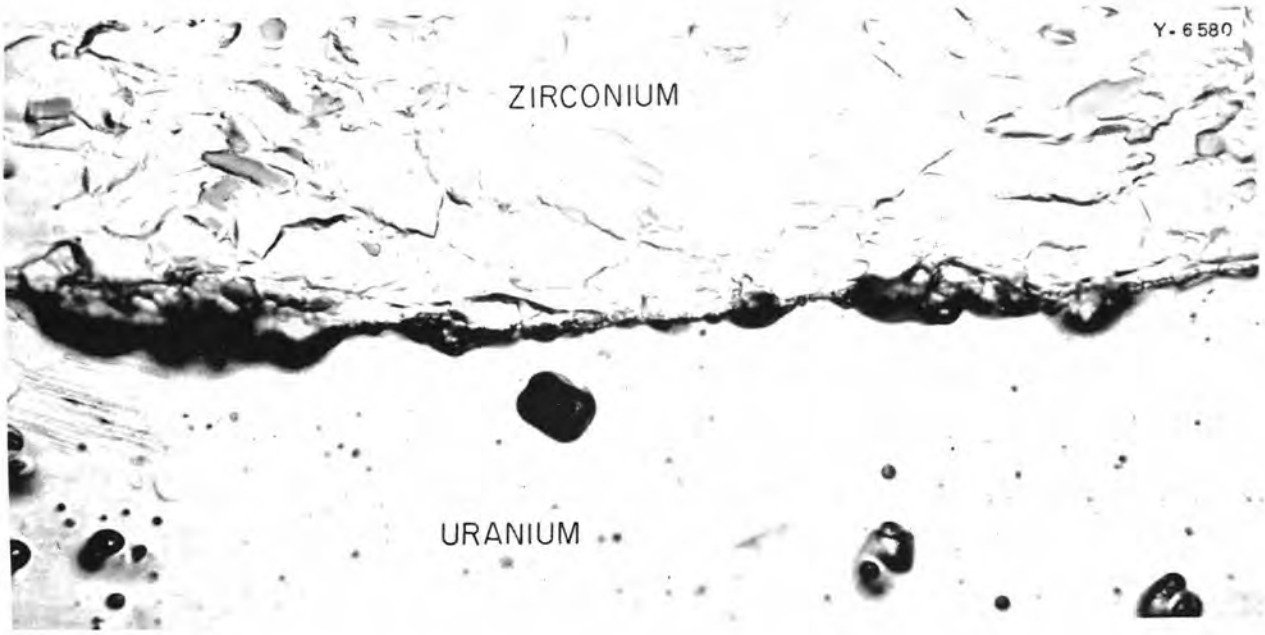


**Fig. 102. Uranium-Zirconium Interface Showing Poor Bonding.** Etched with acetic and perchloric acids. 1000X.

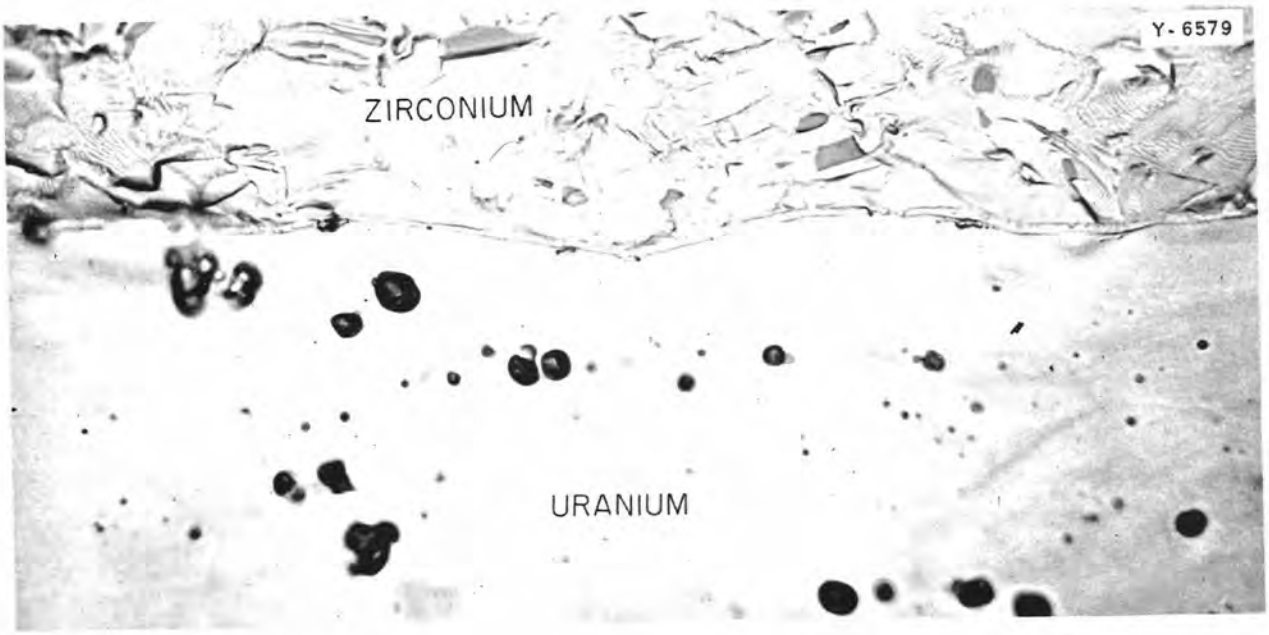


**Fig. 103. Uranium-Zirconium Interface Showing Average Bonding.** Etched with acetic and perchloric acids. 1000X.

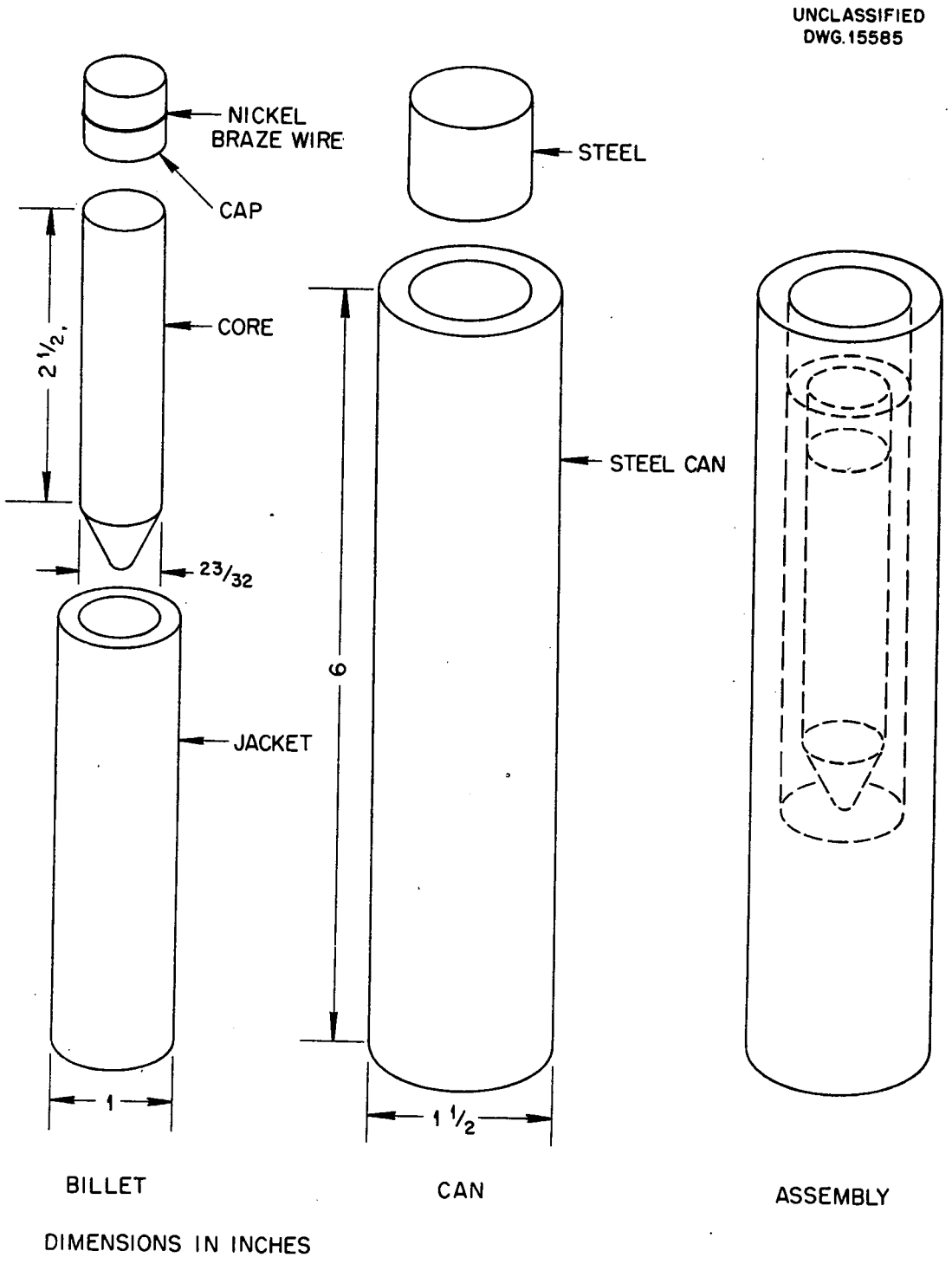


Fig. 104. Cylinder Type of Billet for Roll Cladding.

UNCLASSIFIED
DWG.15586

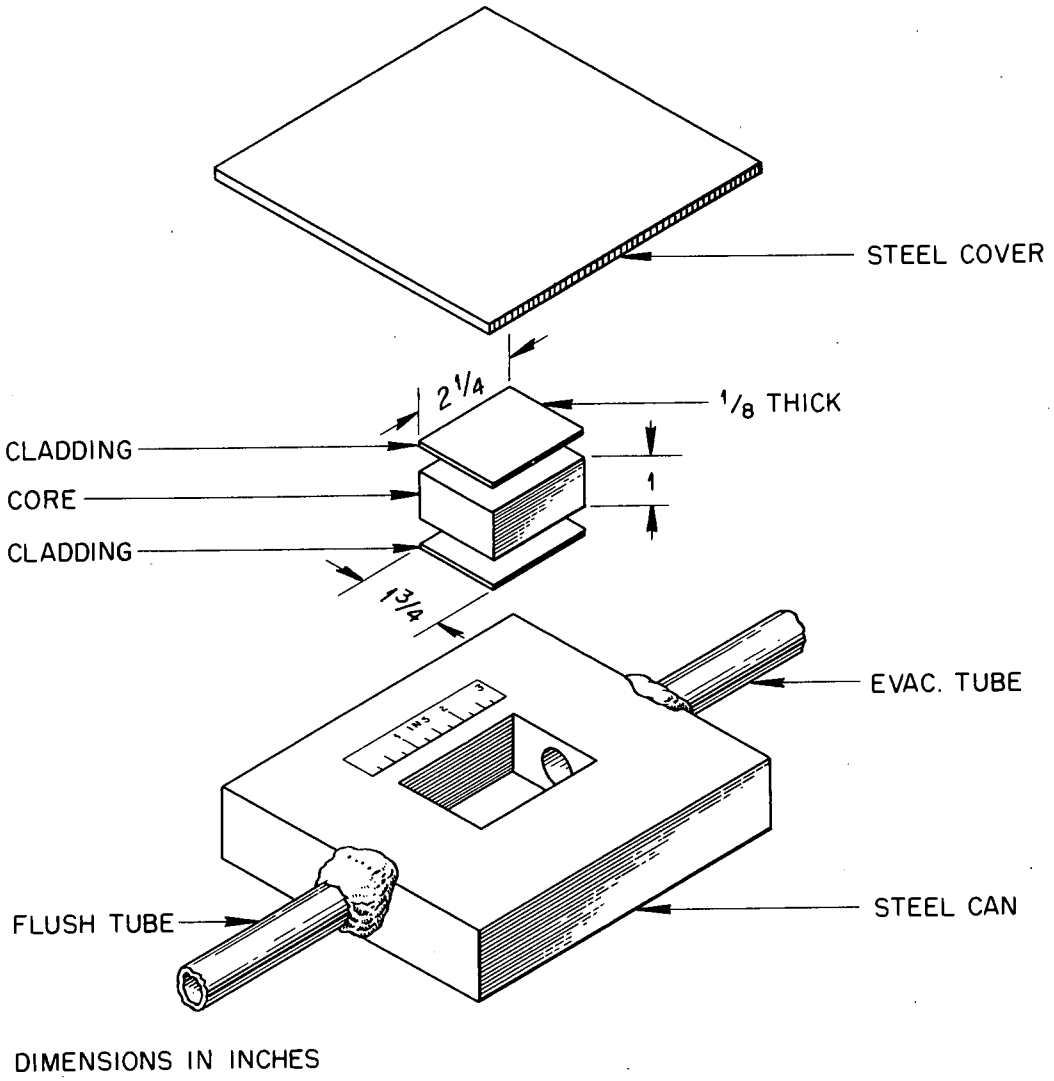


**Fig. 105. Flat Sandwich Type of Billet for Roll Cladding.** Cladding does not extend around edges.

increased with both temperature and time at temperature. The thorium-zirconium phase system shows no compounds, and it is indicated that the presence of diffusion layers would not significantly affect the ductility of clad plates. Samples of the best plates produced in this investigation were bent around a 1/2-in. mandrel and straightened without apparent damage to the bond. At higher temperatures, in the range of 1700°F and higher, very thick diffusion layers were obtained in comparatively short heating times. The sharp increase in the rate of diffusion was thought to be related to the alpha-to-beta phase change in zirconium at about 1650°F.

In addition to the effect of diffusion, high temperatures tend to result in solution of thorium oxide in the zirconium, and with time the oxides disperse to such a degree that, upon reprecipitating, they do not form a plane of weakness at the interface.

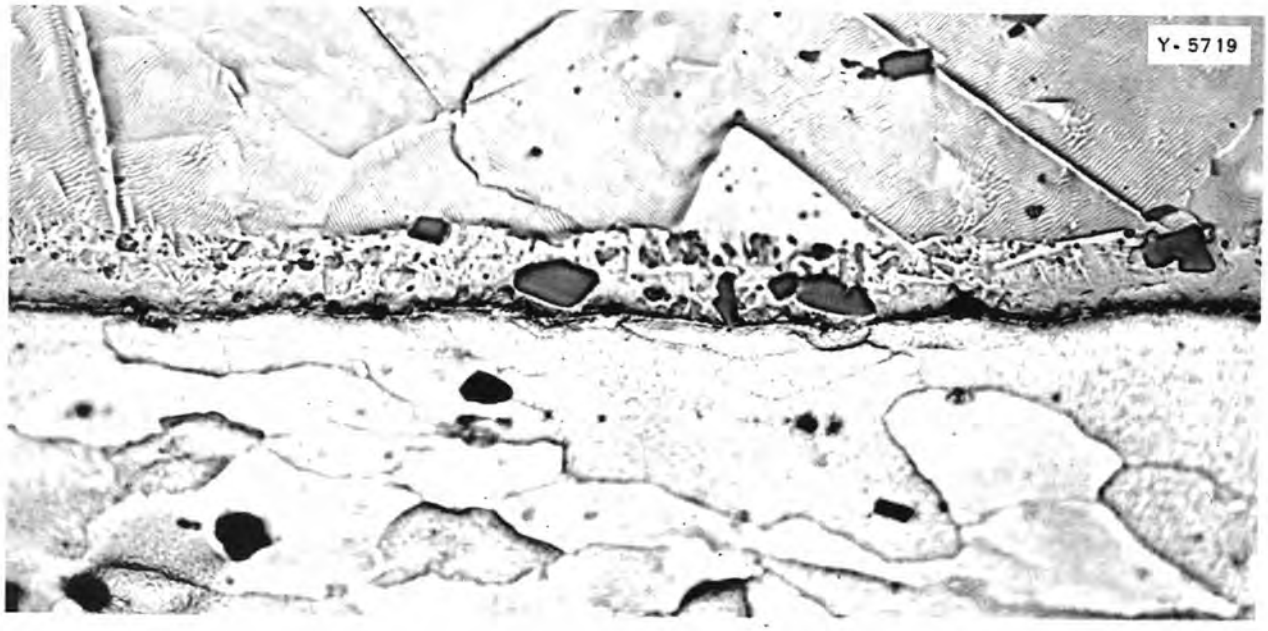


**Fig. 106. Microstructure in the Bond Area of a Plate Rolled from a Billet that Was Simply Evacuated Before Sealing.** Etched with acetic and perchloric acids. 1000X.

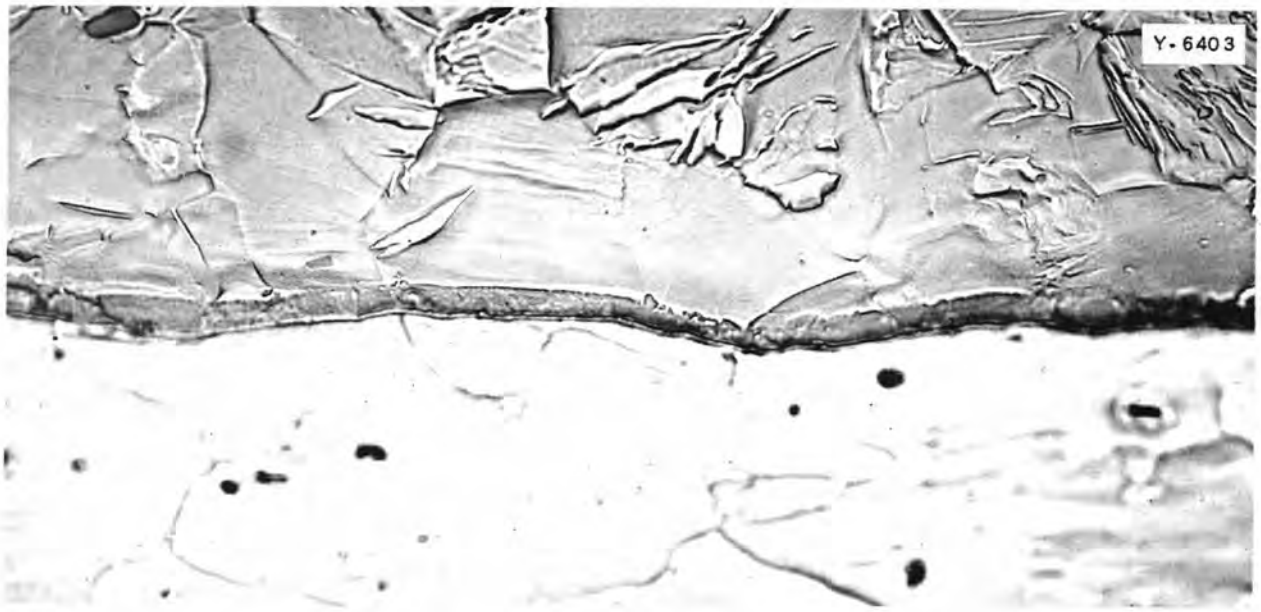


**Fig. 107. Microsturcture in the Bond Area of a Plate Rolled from a Billet that Was Evacuated, Helium Flushed, and Re-evacuated Before Sealing.** Etched with acetic and perchloric acids. 1000X.

Three ideas for utilizing high temperature to enhance bonding were investigated.

1. 1900°F Rolling. Figure 108 shows the bond produced in a plate rolled partially at 1900°F. Tantalum was used as a barrier to prevent formation of a low-melting-point zirconium-iron phase. Tantalum was bonded to zirconium also; however, the lack of bond line voids is notable. The plate shown in Fig. 107 was characterized by the occurrence of oxides at the interface. The photomicrographs shown in Figs. 107 and 108 were obtained from plates made under identical conditions except for rolling temperature. Rolling of zirconium in steel cans above 1650°F is not practical because of the formation of a liquid iron-zirconium eutectic and the attendant hazard.

2. Preheat Billet at 1900°F Briefly (10 min) and Drop Temperature to 1500°F for Rolling. Attempts with this technique resulted in excessive diffusion of iron into the zirconium, and as a result the plate surfaces were badly cracked in rolling.

3. Heat Treat the Finished Plate at 1900°F. This procedure was attempted on plates reduced 15:1 and 30:1. Figure 109 is the macrostructure of a series of plates rolled with a 15:1 reduction and heat treated in vacuum at the times and temperatures indicated. The occurrence of voids and irregular diffusion is noted. Figure 110 shows a similar series of tests made on a plate reduced 30:1 in rolling. The diffusion layer is noted to be more regular and less porous. The regularity and porosity of the diffusion layer seem to be related to time and temperature of heat treatment as well as to the reduction history of the plate. The shorter time and lower temperature give the best results.

**Fig. 108. Microstructure in the Bond Zone of a Plate Rolled at 1900°F.** Etched with acetic and perchloric acids. 1000X.

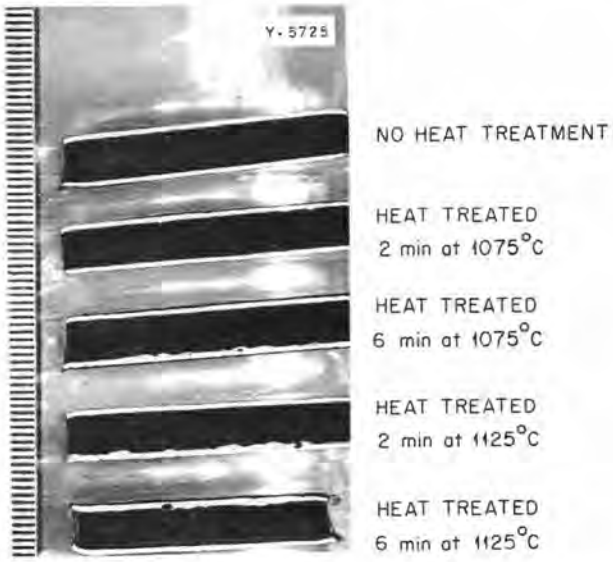


**Fig. 109. Macrophoto Showing Effect of Vacuum Heat Treatments on a Series of Plates Rolled with a Reduction of 15:1.** Unetched. 8X.

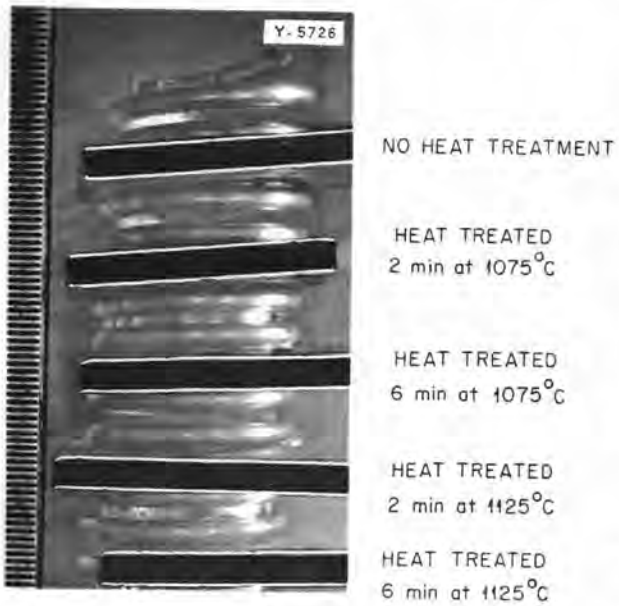


**Fig. 110. Macrophoto Showing Effect of Vacuum Heat Treatment on a Series of Plates Rolled with a Reduction of 30:1.** Unetched. 7X.

The structure produced in a 15:1 reduced plate followed by heat treatment for 2 min at 1965°F is shown in Fig. 111. The original structure of the plate reduced 30:1 is shown in Fig. 112. The structures developed by heat treatment of this plate for 2 min at 1965°F are shown in Fig. 113, and the effect of heat treatment for 6 min at 2055°F is apparent in Fig. 114. It is felt that the results of these tests indicate one feasible method of producing a fairly satisfactory clad plate.

Reduction in rolling has the effect of spreading interface contamination and breaking it into islands that do not obstruct bonding, except intermittently. The employment of high reductions to counteract reoxidation resulting from outgassing in the billet was found to be effective in improving bonds.

The results of this preliminary work indicated that cladding thorium with zirconium was a much more difficult problem than cladding uranium with zirconium. Based on the information gained, an intensive investigation is in progress to produce the necessary bonding. The investigation has been divided into two categories: (1) roll cladding by straightforward procedures and (2) cladding by alternate procedures such as brazing, high-temperature rolling, and high-temperature diffusion.

It is obvious from the preliminary work that some sort of a barrier appearing on the thorium interferes with bonding. Experiments have therefore been designed to observe the effect of heating on oxidation of the core elements at various stages of billet preparation. The billet design currently being used is similar to that shown in Fig. 105 with the exception that the purging tube has been eliminated.

The method of assembling the billet prior to placing under vacuum is as follows:

1. The rectangular thorium core is electropolished in an acetic-perchloric acid solution, rinsed in alcohol, and dried.

2. The zirconium cover plates are sand-blasted, macroetched in a 48% water-50% nitric-2% hydrofluoric acid solution, rinsed in water, and dried.

3. The steel is sand blasted.

4. The steel frame containing the zirconium and thorium core elements is sandwiched between two steel plates. The parts are held in position by two clamps.

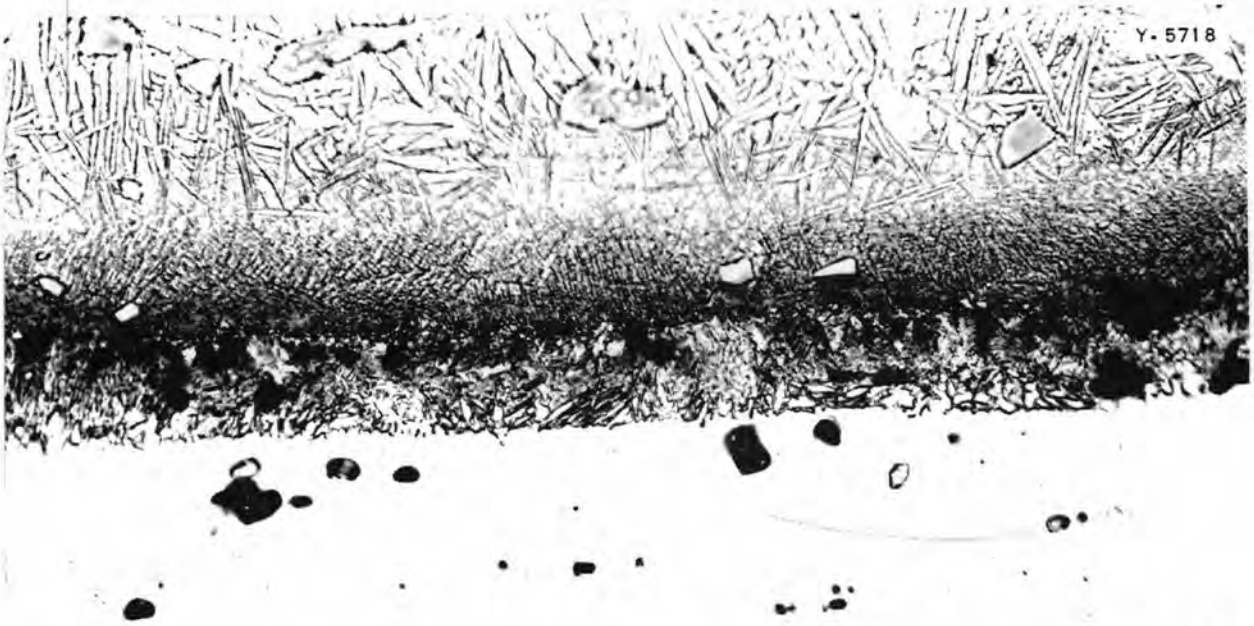


**Fig. 111. Microstructure of the Plate Rolled with a Reduction of 15:1 After Heat Treatment for 2 min at 1075°C in Vacuum.** Etched with acetic and perchloric acids. 1000X.

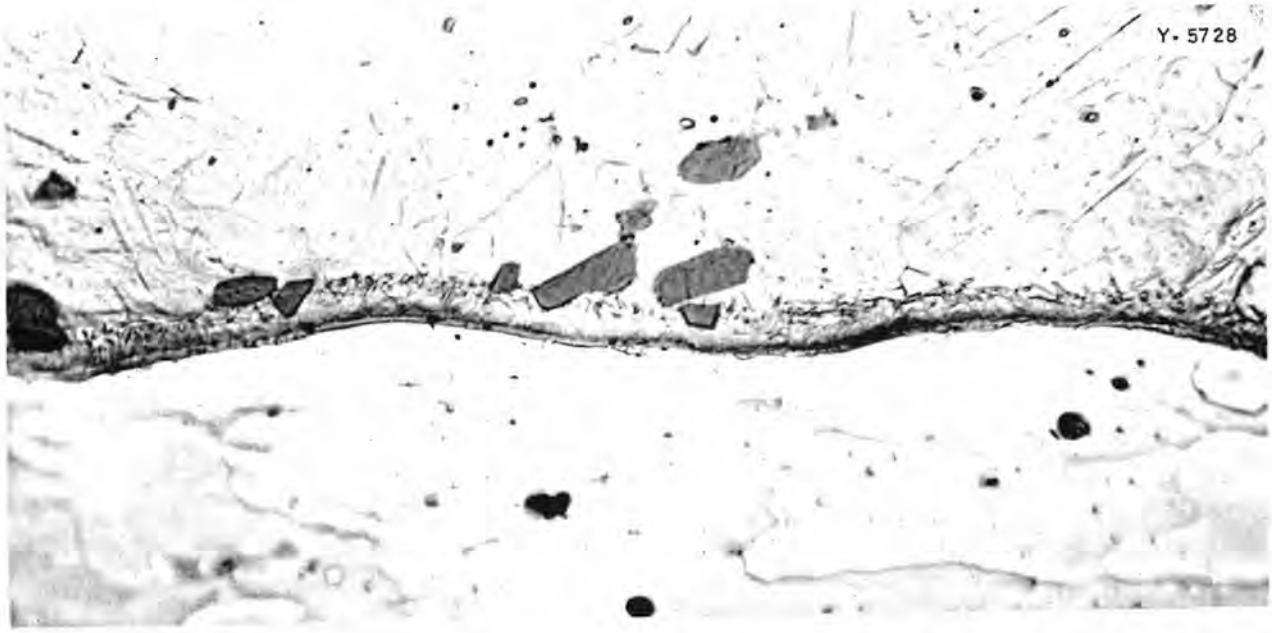


**Fig. 112. Microstructure of the Plate Shown in Fig. 111 Before Heat Treatment.** Etched with acetic and perchloric acids. 1000X.

**Fig. 113. Microstructure of the Plate Rolled with a Reduction of 30:1 After Heat Treatment for 2 min at 1075°C in Vacuum.** Etched with acetic and perchloric acids. 1000X.

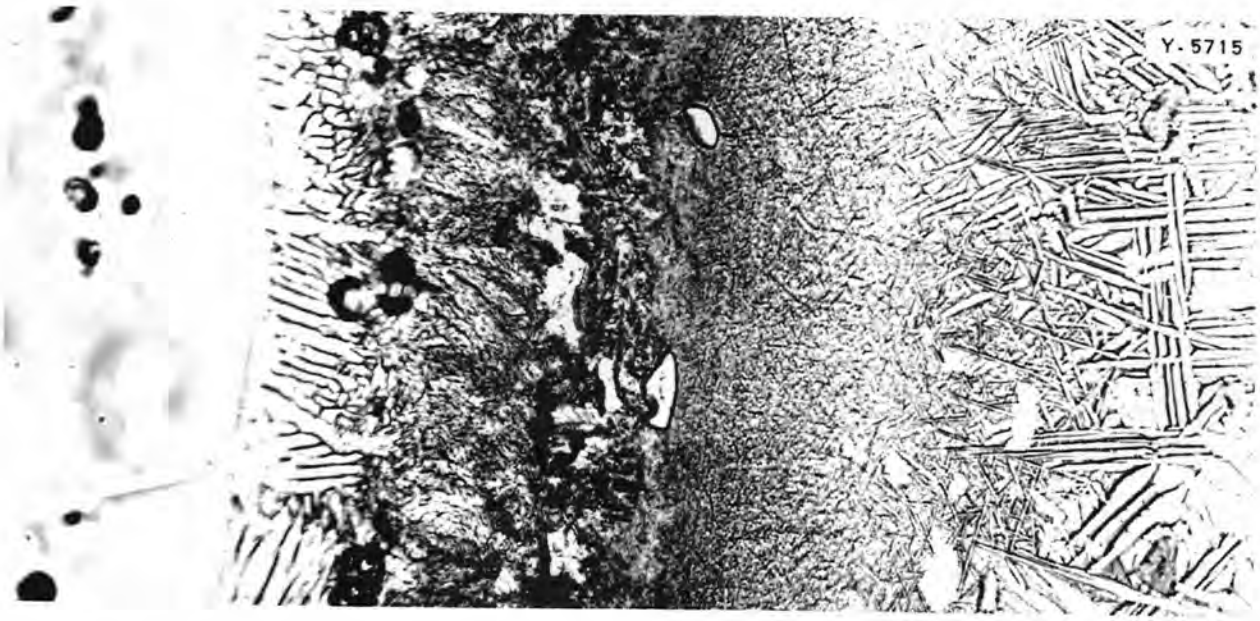


**Fig. 114. Microstructure of the Plate Rolled with a Reduction of 30:1 After Heat Treatment for 6 min at 1125°C in Vacuum.** Etched with acetic and perchloric acids. 1000X.

5. The steel cover plates are welded to the frame while a stream of highly pure helium flows through the evacuating tube to blanket the core elements under an inert atmosphere.

6. After welding, the billet is quenched in water while still under helium pressure.

7. Upon cooling to room temperature the billet is checked for leaks on a Westinghouse leak detector.

8. The billet is placed under vacuum immediately after leak testing.

The effect on the core elements of welding the steel cover plates to the steel frame was observed by welding all but the top cover plate and cooling in dry ice to room temperature while permitting a flow of helium to pass through the evacuating tube. An inspection of the thorium and zirconium revealed that no appreciable oxidation of the core elements occurred during the welding operation, and it is felt that this is a satisfactory procedure for enclosing thorium and zirconium in a steel sheath.

Two types of steel are being investigated. It has been felt that the 0.25% carbon, semikilled, firebox-grade steel may release enough gases during the heating and rolling operations to cause oxidation of the core elements. On the other hand, the 0.04% carbon, titanium-killed, enameling-grade steel (Tinamel) probably contains less gas.

A billet of each type of steel was prepared in the manner described above, evacuated to what appeared to be less than 1 $\mu$ as observed from a Hastings thermocouple gage, and slowly heated to 1000°F for removal of adsorbed gases. After cooling to room temperature, the billets were purged with helium, evacuated again to what appeared to be less than 1 $\mu$, and sealed by hot forging the evacuating tube. The billets were then heated to 1500°F for 1 1/2 hr, cooled to room temperature, and the top cover plate cut away from the billet. A considerable degree of oxidation of the thorium occurred in both billets, with noticeable contamination on the side of the zirconium cover plate adjacent to the thorium core. The oxidation within the titanium-killed steel was somewhat less than that in the semikilled steel, but not to an appreciable extent. A thorough investigation of the vacuum system revealed that the assumption that the vacuum was less than 1 $\mu$ was erroneous, and provisions have been made for more careful measurement of the actual vacuum within the billet.

After observing the results just described and knowing that no oxidation occurred during the welding operation, it was desired to determine the effect on the core elements of heating the billet while under vacuum. A billet was then prepared of Tinamel steel, evacuated to $2 \times 10^{-4}$ mm Hg, and slowly heated to 1000°F. The vacuum was never permitted to exceed $5 \times 10^{-4}$ mm Hg. Heating to the desired temperature consumed 1 hr, and the deflection in vacuum during heating indicated that gases were being released. After cooling to room temperature, the top cover plate was cut away and the results observed. The core had oxidized to some extent but the oxidation was not nearly so severe as that observed in the previous experiments. A slight amount of contamination was also observed on the side of the zirconium cover plate adjacent to the core. The cause of this effect has not been determined, but it is thought that the contamination arises from the thorium or that the vacuum is not quite low enough and permits enough air to remain entrapped at the thorium-zirconium interface to subsequently cause oxidation of the

mating parts. Further investigations are being centered on eliminating the sources of contamination of core elements prior to rolling.

Little work has been done on alternate procedures for obtaining bonding between thorium and zirconium; however, it is felt that within the next two months results will be available.

## EDGE CLOSURE BY WELDING

J. F. Delaney

In the course of conducting experiments on the cladding of thorium and uranium with zirconium by rolling, it was rather difficult to obtain edge bonding with good heat transfer characteristics. Also, the production of a uniformly clad plate in an extra long length was accomplished more easily by rolling large-scale billets in a non-framing type of jacket. This resulted in a double-clad product from which many plates could be sheared but with core material exposed along the ends and lateral edges. The success of such a production method therefore depends largely on the development of reliable techniques for closing the exposed edges.

Work was started to determine the feasibility of closing the exposed edges by welding or brazing. The main requirements of such a weld are that it possess a low neutron-absorption cross section, adequate mechanical properties, good heat transfer, and good resistance to water corrosion. From the start it was evident that the best edge configuration was a groove in which a zirconium weld would be laid. Several methods of edge preparation were tried, and the most successful was found to be an acid etch. The core material is dissolved with 20% HCl from between the cladding to the desired depth, which is approximately 0.010 in. deeper than the diameter of the filler wire. The plates are then cleaned in 50% $HNO_3$ plus 5% HF for 1 minute. The groove formed has a square shape, and there is no preferential attack along the bond line between the cladding and the core. Filler wire of the desired size and composition is placed in the groove and the edges of the cladding are crimped tightly around it at selected points to prevent buckling during welding.

The automatic welding apparatus used in this investigation is shown in Fig. 115. The essential parts are the heliarc welding head, automatic carriage, clamp, fume shield, welding generator, and control equipment. The weld is made by passing the welding torch horizontally along the edge of the clamped plate with no other filler wire added. Direct-current straight polarity is used with a 0.040-in. thoriated-tungsten electrode. Helium gas flow of 10 cfh is generally used.

Results to date have demonstrated that it is possible to obtain a metallurgical weld on both thorium-zirconium and uranium-zirconium plates. Whether such welds meet all the requirements will be determined by a testing program now under way. Thorium-zirconium plates are welded by a pure-zirconium filler wire. A heat range of 30 to 55 watt-min/in. is acceptable for welding plates of 0.065-in. thickness with approximately 0.010-in. zirconium cladding, and using filler wire 0.032 in. in diameter. This range of power input will be narrowed when porosity and diffusion are taken into consideration. A transverse section of a representative weld is shown in Fig. 116.

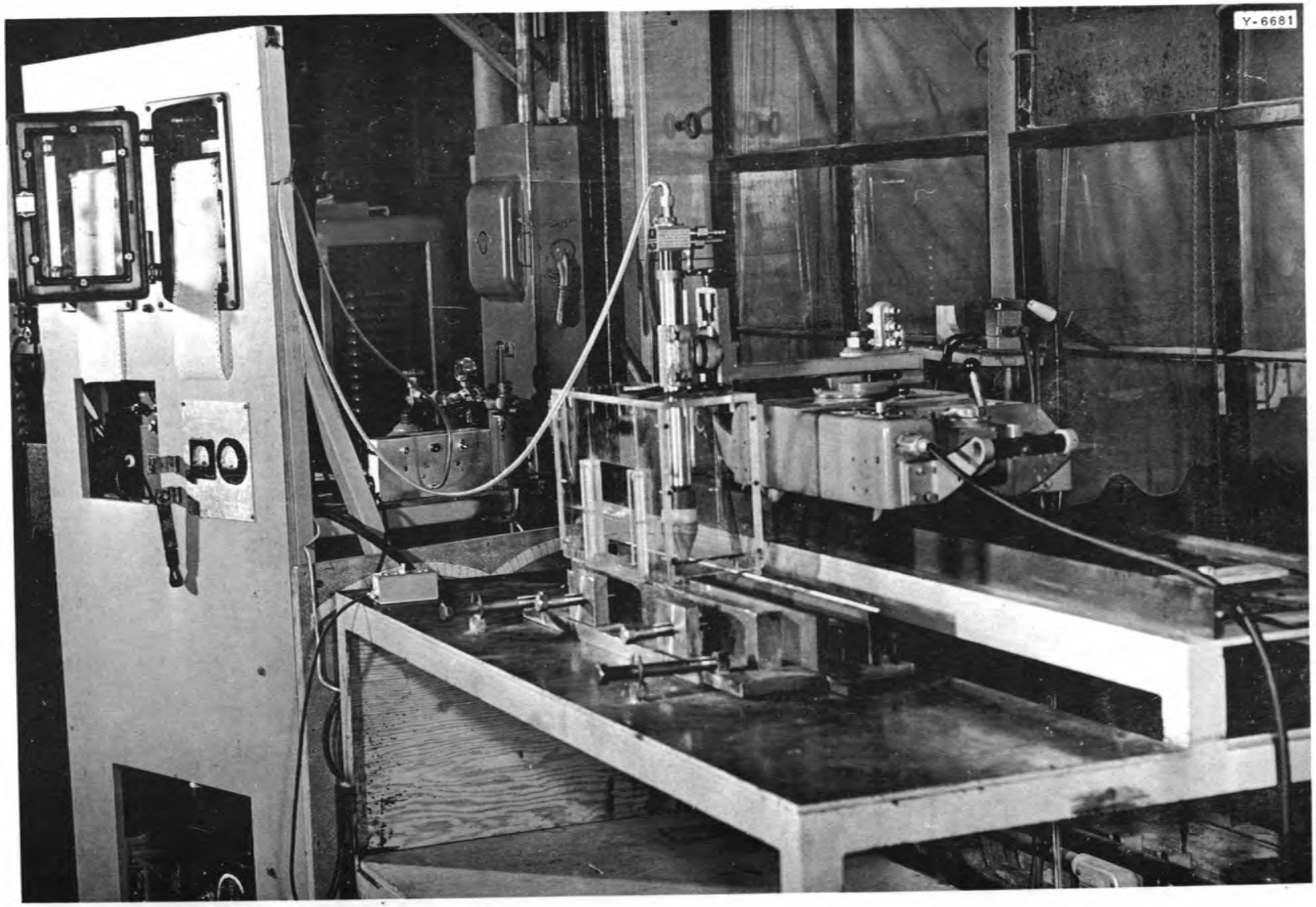


Fig. 115. Welding Apparatus.

Uranium-zirconium plates present a different problem. Uranium melts at a temperature nearly 700°C lower than the melting point of zirconium. If zirconium is used as the filler wire, the solidification after the weld pass will be from the outside inward, with the result shown in Fig. 117. The zirconium weld-metal shell solidifies first and leaves a volume of liquid uranium inside, which, on solidification, shrinks away from the weld metal and leaves a void. In order to achieve the ideal situation of the metal solidifying from the interior outward, a weld metal with a lower solidification temperature than uranium is needed. The zirconium-nickel system has a eutectic point at 15 wt % nickel and 961°C; the solidus line reaches the eutectic line at 1.9% nickel. An alloy of 3% nickel was tried in welding the edges. Three per cent nickel, which would place the alloy in a liquid plus solid phase area above 961°C, proved to be enough to control the direction of the solidification and to fill any shrinkage cavity. Longitudinal and transverse sections of the nickel alloy welds are shown in Figs. 118 and 119. For this type of weld, a power input of 13 to 25 watt-min/in. was used, or approximately half of that needed for good welds with pure-zirconium filler wire. The dimensions of the uranium-zirconium plates are the same as those given for thorium-zirconium plates. The welds with the 3% nickel zirconium filler wire were so promising that they were tried on thorium-zirconium plates. These welds were also quite successful; a section of one is shown in Fig. 120.

The welding heat in all cases improves the bond between the cladding and core and there has been no trouble with heat-affected zones. The plates must be clamped very tightly to prevent

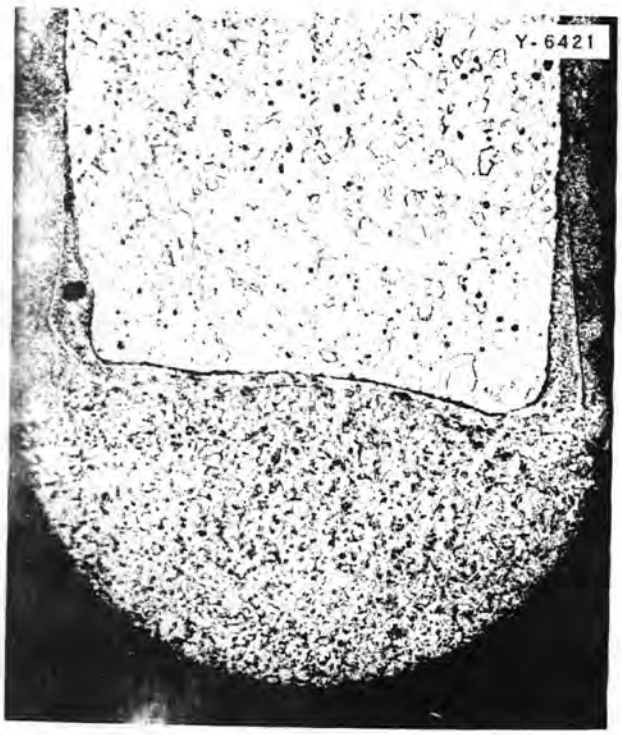


**Fig. 116. Transverse Section of Thorium-Zirconium Plate Welded with Zirconium Filler Wire. 40X.**

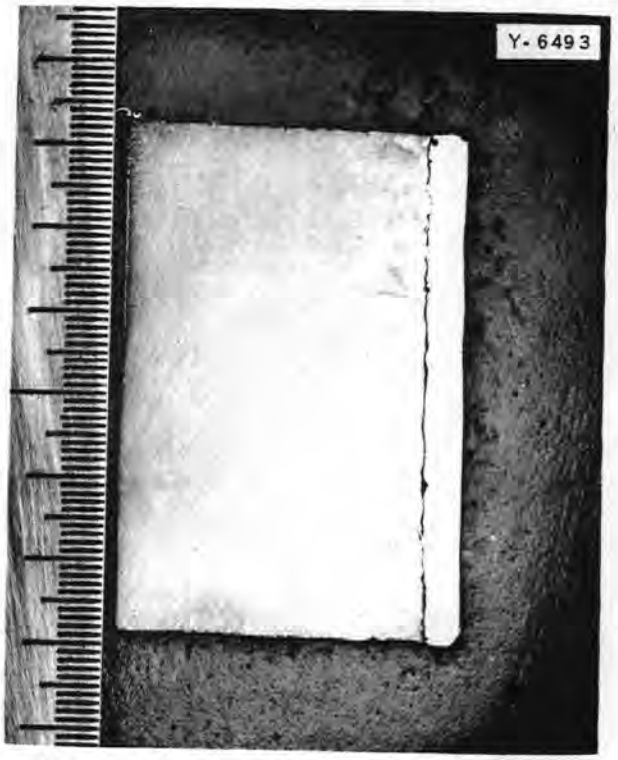


**Fig. 117. Longitudinal Section Through Plate of Uranium-Zirconium Showing Shrinkage Cavity Below Weld. 5X.**

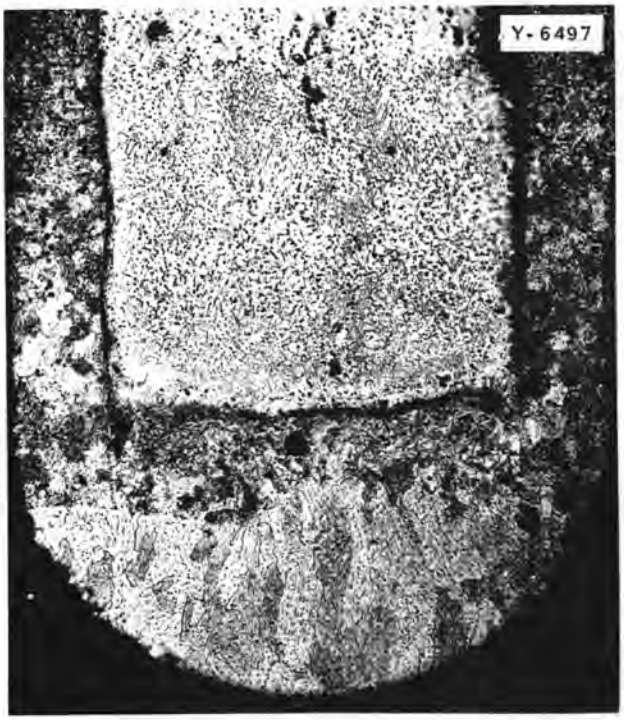


**Fig. 118. Zirconium-3% Nickel Weld on Uranium-Zirconium Plate. 40X.**

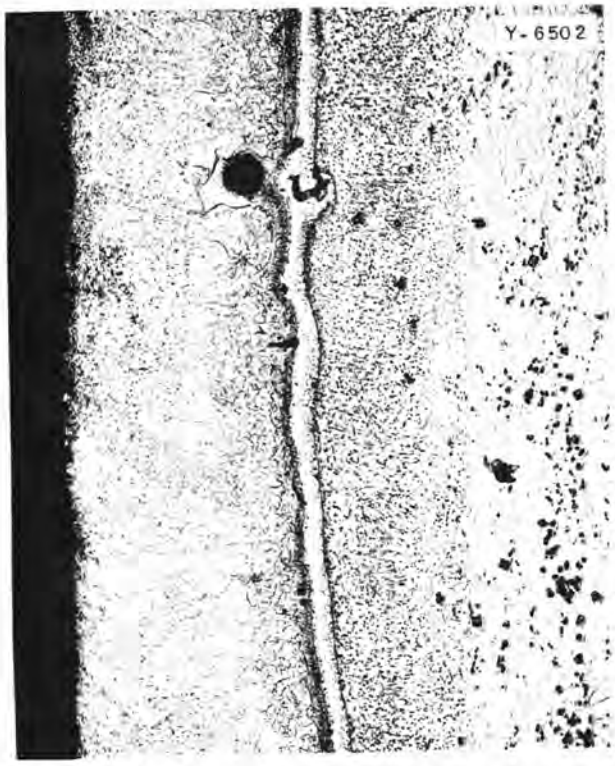


**Fig. 119. Longitudinal Section Through Plate Shown in Fig. 118. 40X.**

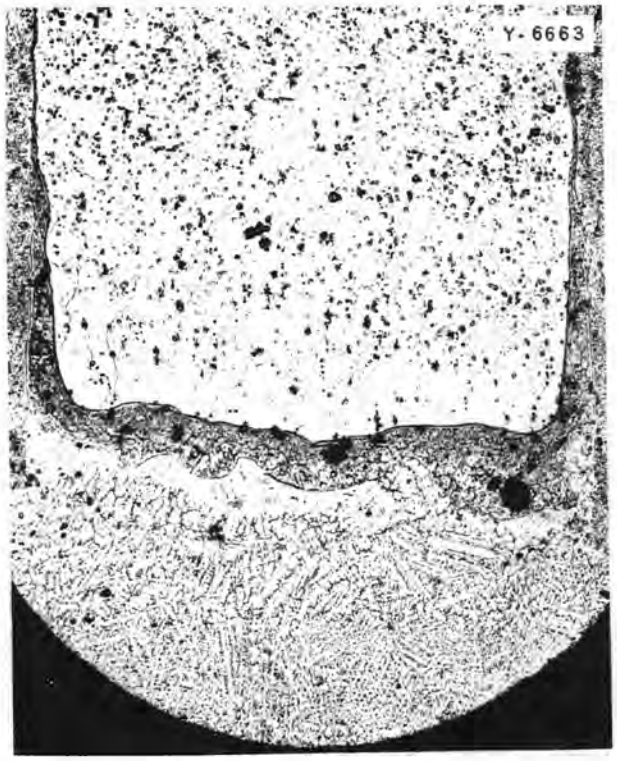


**Fig. 120. Zirconium-3% Nickel Weld on Thorium-Zirconium Plate. 40X.**

buckling. One method of relieving the stresses in the weld is to employ a relatively cold pass of the torch as an anneal.

A major part of the future work will be aimed at reducing the gas porosity that can be seen in most of the welds. The 3% nickel alloy seems to reduce the amount of gas porosity, but this has not been proved. Work is in progress to determine the extent to which the core metal diffuses into the filler metal and the factors that control it.

## CLADDING OF THORIUM WITH ALUMINUM

W. J. Leonard T. W. Fulton

Developmental work on the problem of cladding of thorium with aluminum for production of $U^{233}$ by irradiation

continues. Cladding tests were conducted to evaluate several methods of preparation prior to hot working to obtain a metallurgical bond. The effect of rolling temperature and amount of total reduction were investigated also.

Test samples prepared by the direct method were hot rolled at temperatures of 400, 500, and 600°C. The direct method consists of jacketing a rectangular thorium billet in an aluminum picture frame and covers, evacuating, sealing, and hot rolling. The amount of total reduction in thickness was varied from 12:1 to 20:1. In all cases bonding was achieved.

Bend and chisel tests after rolling indicated that the 400 and 500°C samples could withstand considerable stress with no apparent damage to the bond interface. The 600°C sample, however, fractured on repeated bending and the aluminum cladding could be easily stripped from the thorium. Metallographic examination further supported these initial findings.

Photomicrographs taken at the bond interfaces of samples rolled at 400, 500, and 600°C are shown in Fig. 121. Both the 500 and 600°C samples show the presence of an intermetallic compound. Work is in progress to identify the unknown compound. At least two compounds are known to exist in the thorium-aluminum phase diagram. Results of measurements made to determine the amount of intermetallic compound formed are given in Table 35.

Aluminum-cladding thicknesses in the range 10 to 15 mils have been produced.

Within the range 5:1 to 20:1 reduction, the amount of total reduction apparently is not a critical factor in bonding thorium to aluminum.

Coupons cut from various straight, aluminum-thorium rolled sandwiches were heated at 600°C for 1 hr to simulate the aluminum-silicon brazing operation used on the MTR fuel units. In all cases the bond completely disintegrated because of growth of intermetallic compounds at the metal faces, which indicated that this bond cannot withstand the aluminum-silicon brazing cycle. Another general difficulty experienced was differential flow between the thorium core and aluminum jacket at all rolling temperatures. This resulted in the thorium core breaking through the cladding near the longitudinal ends. The effect was most pronounced at the low rolling temperature.

In an attempt to check the effect of purging jacketed thorium billets with the inert gases helium and argon to remove adsorbed gases, three billets were prepared and rolled at 500°C. Metallurgical results indicated little, if any, beneficial effect from purging with inert gases.

**TABLE 35**

**Thickness of Intermetallic Compound Formed at the Bond Interface of Thorium Clad with Aluminum**

| ROLLING TEMPERATURE (°C) | THICKNESS OF INTERMETALLIC COMPOUND (mils) |
|---|---|
| 400 | None |
| 500 | Average - 2<br>Minimum - too small to resolve |
| 600 | Maximum - 4<br>Average - 3<br>Minimum - too small to resolve |

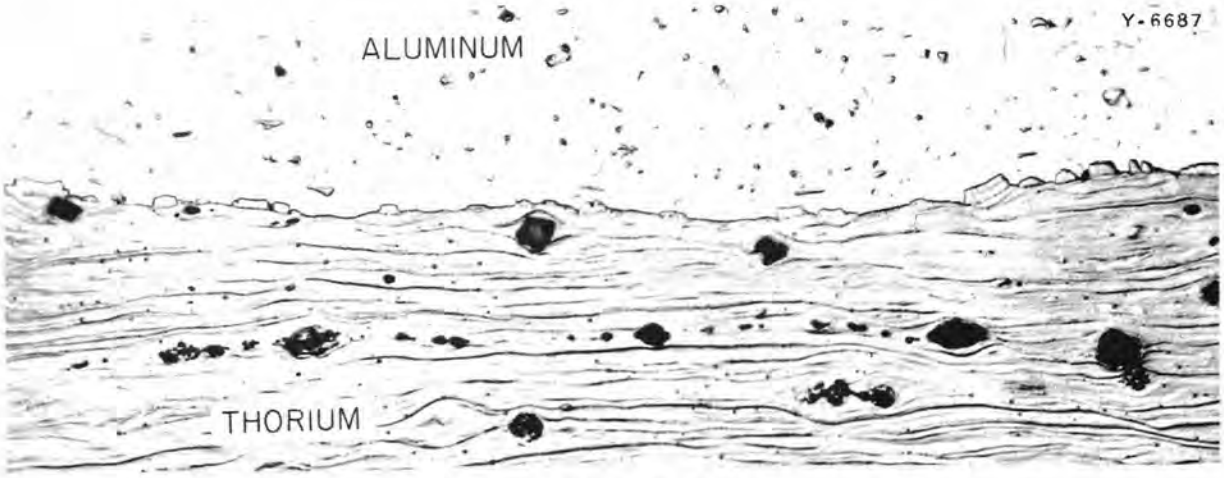


(*a*) Rolled at 400°C

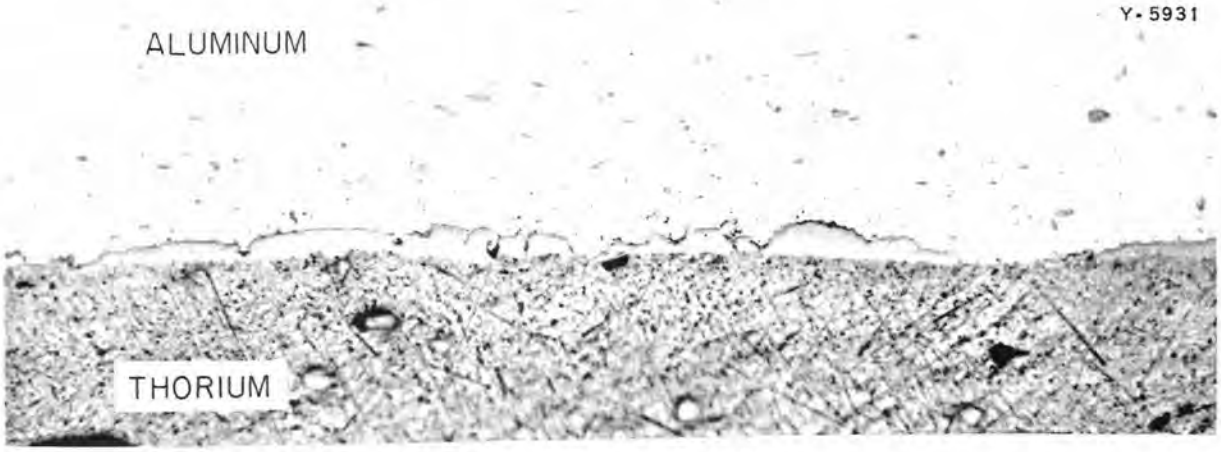


(*b*) Rolled at 500°C

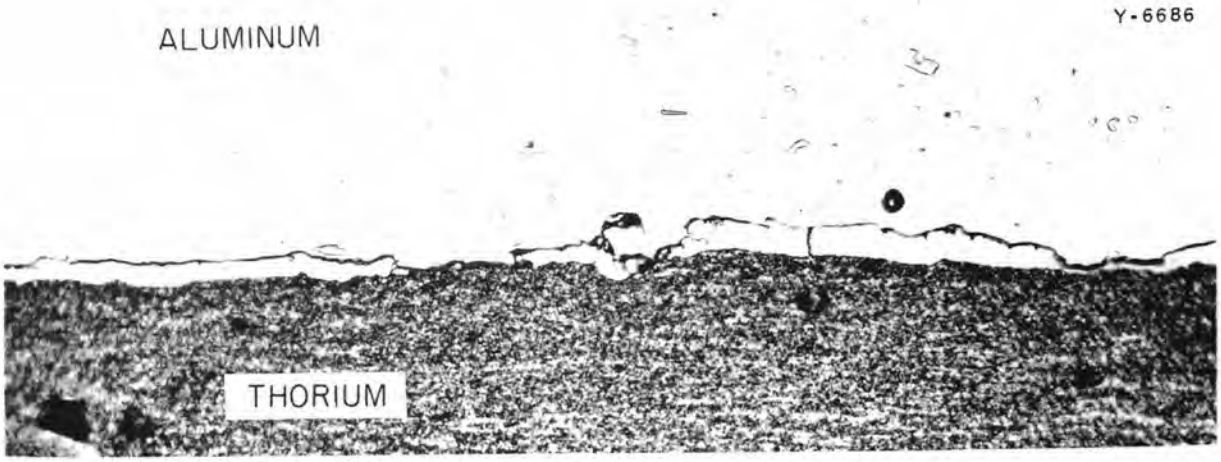


(*c*) Rolled at 600°C

**Fig. 121. Bond Interfaces of Alclad Thorium Rolled at Various Temperatures.** Etched with alcohol and perchloric acid. 1000X.

Work is in progress on the following:

1. using a thin magnesium or aluminum-silicon alloy layer between the aluminum and thorium to act as a diffusion barrier,
2. altering the working or flow characteristics of the two metals by alloying - thorium can be softened by small additions of titanium, whereas aluminum can be hardened by additions of beryllium, magnesium, silicon, etc.,
3. investigating other methods of plate assembly such as mechanical linkage or use of the low-melting (350 to 400°C) aluminum solders.

## CERAMIC PROTECTIVE COATINGS

W. J. Leonard

Ceramics containing enameling agents were studied to evaluate their protection properties as coatings on metals. The ceramics used were of types A-417 and A-418 developed by the Bureau of Standards, or very similar compositions. These ceramics were developed originally as protective coatings for high-temperature-alloy coatings and forgings that were used for jet turbine buckets or blades. They consist essentially of equal parts of BaO, $Cr_2O_3$, and $SiO_2$ with a small addition of CdO or ZrO and a small portion of a vitrifying agent such as $B_2O_3$ or $P_2O_5$ and BeO. $Al_2O_3$ or $Na_2O$ may be substituted or blended in the original compositions if desired.

The coatings were put on type 25-20 stainless steel by the proper preparatory techniques, and the samples were rolled at 1800°F. The coating adhered excellently to the metal, spread and flowed with the metal, and showed no tendency to stick to the rolls or flake off. Zirconium was then successfully coated and rolled with similar results.

Since the preliminary tests indicated the feasibility of hot rolling zirconium, several test samples 9/16 in. thick, 2 in. wide, and 4 in. long were rolled to study the variables of rolling temperature, amount of total reduction, and thickness of coating. In all cases, the reduction per pass was maintained at approximately 20%. Micrographic examination was made of the samples after rolling to determine the amount of diffusion between core and cladding, whether oxides formed in the zirconium, and whether cracks or other discontinuities occurred in the coating.

Results showed that the optimum thickness of coating was approximately 2.5 to 3.0 mils and that the coating was impervious to air penetration when rolled to a reduction of less than 5:1. This reduction ratio is slightly dependent on temperature, being less at the high rolling temperature and slightly more at the lower temperature. Zirconium may be rolled at temperatures from 1200 to 1800°F. Microscopic studies indicate no diffusion into the zirconium by the coating elements or leaks of air through the coating on the flat portion of rolled plate. On the edges the coating flakes off after a few passes, and nitrogen, oxygen, and possibly other gases penetrate to a depth of about 0.030 to 0.040 in. into the zirconium.

Thorium has also been successfully coated with these materials but no quality evaluations have been made.

Twenty-five samples were rolled to 12:1 and 16:1 total reduction at various temperatures with the use of the following standardized procedure: (1) coat with 2.5 to 3.0 mils of the ceramic, (2) roll to total reduction

of 4:1 or slightly less, (3) recoat and roll to final total reduction of 12:1 or 16:1. The rolled plates appeared to be entirely satisfactory. Before use the edges and ends would require trimming and the coating on flat faces would have to be removed.

At present, microscopic studies are being made of the samples by taking hardness transverses into the core from the zirconium surface to detect any possible impurity effects not brought out by etching. Also, methods of removing and cleaning the rolled zirconium plates are being investigated.

## EXPERIMENTAL WELDING OF URANIUM, THORIUM, AND ZIRCONIUM

W. J. Leonard

In conjunction with the cladding program, information was needed on the weldability of certain metals in combination with themselves or with other dissimilar metals. Cursory welding tests were performed to gather some preliminary information, and, in particular, the crack sensitivity of thorium was investigated. Reactor-grade uranium, Ames thorium, and Bureau of Mines arc-melted crystal-bar thorium were used throughout the investigation.

All welding was performed by using a shielded, inert-arc gas-welding torch with a 1/16-in. tungsten electrode in a dry box under a helium (Bureau of Mines grade AA) atmosphere purified by a gas train. The materials to be welded were charged into the box and the box evacuated for a period of at least 16 hr to the best attainable vacuum, which varied from 40 to 100 microns. The system was then continuously flushed with helium through a No. 8 gas cap at a flow rate of 2 to 6 liter/min as measured on a Linde type L 14A flowmeter. After tests inside the box indicated a contamination-free atmosphere, welding was begun. The best electrical control and welding characteristics for use with each different material were determined by experiment.

Butt, fillet, and lap welds were made on thorium plates of known composition in plate sizes of 1/16, 1/8, 3/16, and 1/4 in.; the results were irregular. In general, the small the plate size, the greater the likelihood of obtaining a crack-free weld in the thorium. Larger size thorium welds require a greater "total heat input" (greater number of passes for filling and larger heat input per pass for proper penetration), which in turn appears to be the important factor in producing cracks in thorium welds. Multipass welds of 1/4-in. thorium plate, with and without filler rod, were investigated with more consistent results. These welds showed crack sensitivity under certain welding conditions, and the cracks usually occurred between the base metal and the heat-affected zone. The microstructures of the welds studied in detail showed the usual mode of failure to be in the grain boundaries of the largest grains close to the weld metal, but no difference in grain size, amount of grain boundary constituents, or percentage of impurities could be noted between sound and cracked welds. In general it may be said that single-pass welds of thorium present little or no problem; multipass welds are more likely to crack with each succeeding pass.

Uranium plates 1/8 and 1/4 in. thick were butt welded. Multipass groove welds on 1/4-in. plate were also made. Argon gas atmospheres and alternating-current combinations were tried on uranium but results were not so good as with the use of d-c straight polarity and a helium atmosphere.

Multipass groove welds using filler rod in 1/4-in. plates were made of all possible combinations of thorium, uranium, and zirconium except that no zirconium base plates were welded together nor were two uranium plates welded with thorium or zirconium filler rod. Figure 122 is a photograph of a weld of this type. Figure 123 is a photograph of butt welds of 1/4-in. plates of these metals. None of the welds exhibited crack sensitivity except those for which high heat inputs were necessary to secure a normal penetration in the weld. This condition may happen in welding thorium-to-thorium or thorium-to-zirconium plates with either a thorium or zirconium filler rod unless careful welding control is exercised. The welds in Fig. 122 that cracked had been made with high heat input to secure maximum penetration.

Macrographic and micrographic studies of the uranium-thorium welds show a eutectic present at locations of melting and mixing and also segregation areas of uranium-rich or thorium-rich solutions. These observations are in agreement with the published binary phase diagram. Thorium-zirconium welds show the eutectoid in that system (similar to pearlite in steel). Uranium-zirconium welds show mixtures of alpha uranium in an alpha-zirconium matrix and vice versa.

Micrographic study showed complex phases in welds in which uranium, thorium, and zirconium were mixed in liquid phases. Since the ternary diagram is unknown, no positive identification was attempted. Considerable heterogeneity was present in the weld deposits and adjacent melted areas, and many metastable phases were observed. No intermetallic or brittle compounds were found in any of the welds made.

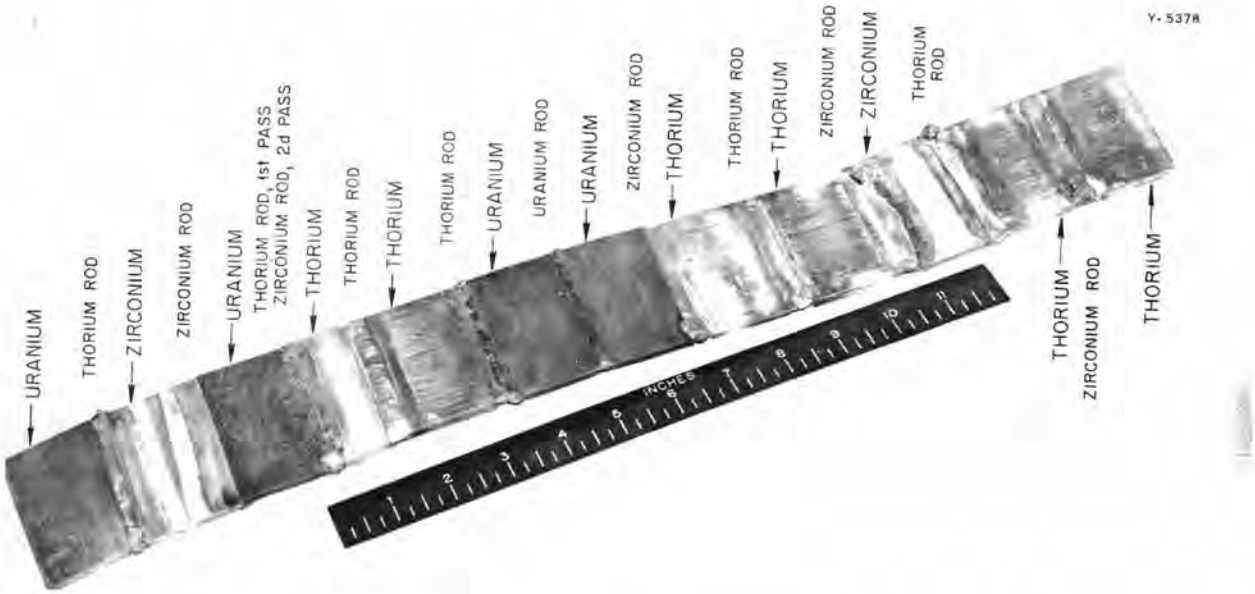


**Fig. 122. Welds of Thorium, Uranium, and Zirconium 1/4-in. Test Plates.**

Y-6634

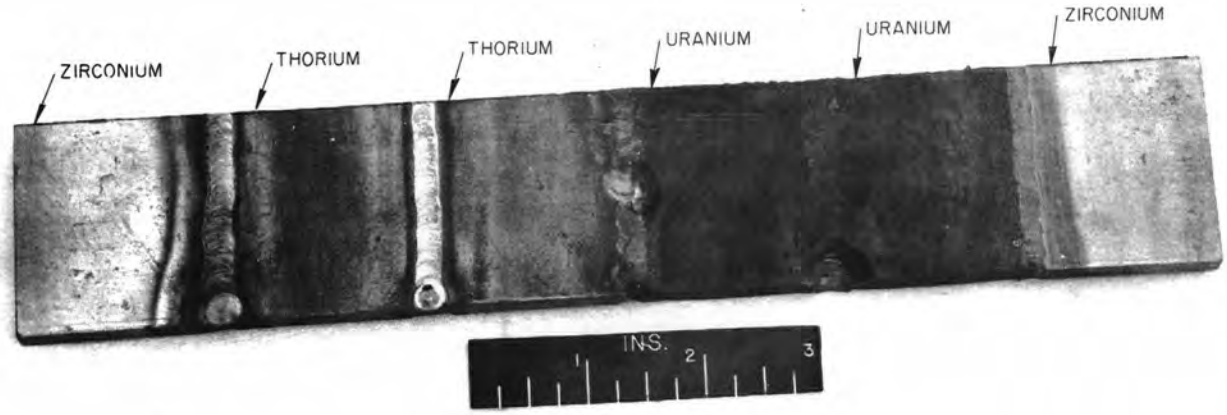


**Fig. 123. Welds of 1/4-in. Test Plates of Thorium, Zirconium, and Uranium.**

# FUEL AND CONTROL ELEMENT FABRICATION

J. E. Cunningham

## MTR FUEL AND CONTROL ROD ELEMENTS

H. J. Wallace G. E. Cooley
E. R. Turnbill

Production work on the fabrication of enriched-uranium fuel and control-rod elements for the Materials Testing Reactor is now progressing at a satisfactory and efficient rate. Measures are being taken to step up production commensurate with the expected increase in demand.

During the quarter several hundred good-quality castings were received from the Aluminum Company of America. These end-box castings were delaying completion of two pile loadings of fuel units on hand. The 356 aluminum castings were required to adapt the fuel assembly to the upper and lower grid sections in the reactor.

Examination revealed that the sand castings were sound and dimensionally correct. As rapidly as possible, castings were attached by welding and the units were rushed through the final machining operation in the shop. New jigs that were designed and constructed to speed up inspection were also available. All units passed dimensional inspection and $U^{235}$ content specifications.

A total of 66 fuel units and 8 shim-safety control rods were crated and shipped to ARCO. The units were packaged in cadmium-containing carriers for shipment - six fuel units or two control rods per container. All shipments were made money waybill via Railway Express, hand-to-hand signature required, and in an amount less than 1 kg of $U^{235}$.

All shipments arrived safely. This is important because the permissable out-of-straightness tolerance on the shim-safety rod is a meager 1 mil/ft or 14 mils on a 14-ft rod. No trouble was experienced in loading the initial set of 23 fuel and 4 control rods into the reactor for start-up.

The remainder of the third and all the fourth pile loading are in various stages of completion. Thirteen fuel and seven uranium sections for shim-safety rods have been brazed and forwarded for final machining. The parts for 16 more units are in the form of uranium-aluminum alloy ingots, cores, clad plates, etc.

Minor adjustments on the component parts and brazing cycle have made it possible to maintain closer tolerance on the water-gap spacing. The nominal 0.117-in. spacing tolerance is now running ±0.006 in., or within, 5% rather than the specified ±0.012 in., or 10%.

An over-all inventory was run on the last 7-kg lot of enriched-uranium metal processed. The account showed a gain of 0.25%, which is a slight decrease over the last batch that ran 0.36% high. These balances are obtained after recovery of all the uranium contained in the dross, graphite crucible, stirring rods, and sampling tools. Although these figures are within the analytical accuracy of ±0.5%, results consistently run high and indicate a bias or constant error. Experimental tests on normal metal are in progress to determine the origin of this slight but disturbing error. Both the analyses by the chemical laboratory

and the method of taking the dip samples are being carefully checked.

A new drying oven capable of drying simultaneously six or more units of lengths up to 6 ft has been purchased and installed. An engraving unit is on order for permanently marking the identification letters and numerals on each assembly. Starting next month, an attempt will be made to process units from raw uranium and aluminum metal into completed assemblies ready for pile operation at the rate of two each working day. With additional manpower, this schedule could be further improved.

### EXPERIMENTAL CP-5 FUEL UNITS

J. N. Hex W. W. Proaps

Developmental work was initiated on the fabrication of a modified MTR fuel unit for the CP-5 reactor at Argonne National Laboratory. The CP-5 fuel unit calls for less active plates of somewhat higher uranium concentration, wider water-gap spacing, and thinner aluminum side plates than are required on the MTR unit.

Three dummy aluminum assemblies were made to determine optimum jig dimensions and to develop a brazing cycle that will yield brazed assemblies well within the CP-5 specified tolerances. Experimental assembly No. 1, designated as P-1-E, was run through the conventional MTR cycle, and inspection revealed that the 0.010 in. of freedom normally allowed between component parts was too much. Also, the wider plate spacing and thinner side plates required a change in the brazing cycle. Units P-2-E and P-3-E were run in a similar manner but with slight adjustments made in jigging and brazing time or temperature. Figure 124 is a photograph of the CP-5 fuel element.

Results of the inspection are shown in Table 36. The figures are based on maximum rather than average deviation at any one point and tend to present a somewhat pessimistic picture, and yet all units, with the possible exception of the first, meet specifications. No trouble is anticipated in fabricating the remaining 16 active elements ordered.

The CP-5 dummy unit, as brazed, weighs 6.53 lb, of which 0.22 lb is eutectic (11.5% Si) aluminum-silicon alloy. Therefore the assembly contains approximately 0.02 lb of silicon metal. Since the design group was concerned about loss in reactivity due to aluminum, it was suggested that the alclad thickness on the active plate be lowered from 20 to 15 or 10 mils. According to J. A. Lane, only about 2 mils is required to stop recoil neutrons.

**Fig. 124. CP-5 Fuel Element.**

TABLE 36

**Inspection Data on the Experimental CP-5 Fuel Units**

| | SPECIFIED DIMENSION | TOLERANCE | EXPERIMENTAL ASSEMBLY | | |
|---|---|---|---|---|---|
| | | | P-1-E | P-2-E | P-3-E |
| Dimensions | | | | | |
| Plate spacing (in.) | 0.154 | ±0.015 or 10% | 0.154 + 0.004 − 0.009 or 6% | 0.154 + 0.004 − 0.006 or 4% | 0.154 + 0.012 or 8% − 0.004 |
| Over-all width (in.) | 2.940 | ±0.016 | 2.940 + 0.000 − 0.005 to 0.012 | 2.940 + 0.000 − 0.007 to 0.011 | 2.940 + 0.000 − 0.007 to 0.013 |
| Vertical center height (in.) | 2.414 | ±0.030 | 2.414 + 0.001 − 0.005 | 2.414 + 0.006 − 0.000 | 2.414 + 0.008 − 0.000 |
| Alignment (in.) | | | 0.040 to 0.050 out of square | Excellent | Slightly out of square |
| Brazing | | | | | |
| Condition of brazed joint | | | Excellent | Excellent | Excellent |
| Distribution of braze metal | | | Good except at one end of space 11-12 | Better | Best |
| Flux removal | | | OK | OK | OK |

In order to more closely meet the target dimensions and facilitate the brazing operation, a few slight alterations on the CP-5 drawings were recommended. All three experimental assemblies and the fabrication record cards were forwarded to ANL for inspection and study.

### LITR FUEL UNITS

In connection with the proposed power increase of the LITR from approximately 1 to 1.5 megawatts, two replacements and five additional fuel assemblies were fabricated according to specifications. Pending approval, three cadmium shim-safety control rods will also be constructed.

### BULK SHIELDING FACILITY FUEL AND CONTROL ELEMENTS

Five assemblies containing a subnormal amount of $U^{235}$ were prepared and forwarded for the Bulk Shielding Facility. These units are needed to complete a matched set of cold elements for making gamma-ray spectra measurements on the ANP divided-shield experiment.

Another special unit that is being assembled will be used for obtaining more reliable data to calculate the heat release per fission of $U^{235}$. The assembly will be constructed in a manner to permit removal or substitution of the central active plate. Besides the removable central plate, another active plate containing several 1 1/4-in.-dia holes will be provided to permit insertion of clad or unclad uranium-aluminum disks prepared from the same heat.

Two of the lead-cadmium alloy (17.5 wt % cadmium) safety rods and one control rod for the Bulk Shielding Facility were fabricated and forwarded.

### FUEL UNITS FOR CHEMICAL PROCESSING

At the request of the American Cyanamid Company at ARCO, 20 normal-uranium MTR fuel elements are being assembled and brazed for use in dissolving and separation studies in the chemical processing plant. To date four units have been completed.

### SERVICE WORK

| | |
|---|---|
| J. H. Irwin | D. E. Rosson |
| L. A. Amburn | G. E. Cooley |
| J. B. Flynn | E. R. Turnbill |

**Rolling of Uranium Plate for UCRL.** The University of California Research Laboratories require approximately 2000 lb of uranium plate for target material, and about 1000 lb has been rolled from bar material furnished by UCRL. The remainder of the required material will be rolled from castings now being made in the melting and casting laboratory.

**Alclad Boral Rolling.** Ninety aluminum-clad boral plates, approximately 1 1/4 by 2 by 2 ft, were rolled to plate material 0.250 in. by 27 in. by 10 ft for the CP-5 reactor at Argonne National Laboratory. The seven small plates remaining on order will be rolled in the near future.

**Preparation of Enriched Foils.** The two lots of enriched foil prepared and shipped to other laboratories included 0.01-in. material furnished to the University of California Research Laboratories and 0.020-in. material furnished to the Brookhaven National Laboratory.

**Preparation of Slugs for Dissolution Work.** The General Electric Company at Hanford was furnished 510 modified "J" slugs, cast from natural uranium and then machined to

tolerance, to be canned for dissolution experiments.

**Thorium Dissolution.** Approximately 30 kg of extruded thorium rod was furnished to the chemical group for dissolution experiments.

**Thorium Research Program.** Approximately 80 thorium alloys were vacuum or arc melted for alloy studies. Thorium plate, rod, and wire were fabricated from Ames cast billets by extrusion, rolling, swaging, and drawing for welding and physical test data.

**ANP Research.** Several brazing alloys were made by arc melting in the small, inert-atmosphere furnace. Chromium alloys were cast and fabricated into rod.

**General.** Installation of the 100-kw, 3000-cycle generator has been completed. The large, Distillation Products, vacuum tilting furnace that is to be operated from this generator will be ready for operation in the near future. The installation of generators and a transformer as the power supply for the large arc furnace will be started soon.